Bacterial Influence on Uranium Oxidation Reduction Reactions: Implications for Environmental Remediation and Isotopic Composition

by

Lisa Maureen Mullen

B.S., Lyman Briggs Physics
Michigan State University (2001)

B.S., Lyman Briggs Microbiology
Michigan State University (2001)

Submitted to the Department of Nuclear Science and Engineering
in Partial Fulfillment of the Requirements for the Degree of
Doctor of Philosophy in Nuclear Engineering

at the

Massachusetts Institute of Technology

February 2007

Signature of Author.....
Department of Nuclear Science and Engineering
1/29/07

Certified by.....
Dr. K. Czerwinski
Professor of Radiochemistry, University of Nevada Las Vegas
Thesis Supervisor

Certified by.....
Dr. M. Polz
Professor of Civil and Environmental Engineering
Thesis Reader

Accepted by.....
Dr. Jeffrey A. Coderre
Chairman, Graduate Thesis Committee

Bacterial Influence on Uranium Oxidation Reduction Reactions: Implications for Environmental Remediation and Isotopic Composition

by

Lisa Maureen Mullen

Submitted to the Department of Nuclear Science and Engineering on 1.29.2007
in Partial Fulfillment of the Requirements for the Degree of
Doctor of Philosophy in Nuclear Science and Engineering

Abstract

The bacterial influence on the chemistry and speciation of uranium has some important impacts on the environment, and can be exploited usefully for the purposes of environmental remediation of uranium waste contamination. It is important to understand both from a scientific and environmental perspective how different types of bacteria can affect the chemistry and speciation of uranium. Analysis of the kinetics of uranium reduction, to determine the influence of external governing factors, can help us to understand the mechanisms of uranium reduction *in vitro* and aid in the design of more effective uranium remediation schemes in the environment. Bacterial reduction kinetics are found to fit well to a first order exponential decay model. Using this model we have determined the dependence of the rate of bacterial uranium reduction on several parameters, including bacterial density and pH.

Understanding the reduction kinetics is also an important step in the determination of the extent of isotopic separation that occurs as a result of the bacterial reduction process. Here, we demonstrate that isotopes of uranium, the heaviest naturally occurring element, are subject to fractionation when uranium serves as a terminal electron acceptor during anaerobic bacterial respiration, resulting in an enrichment of ^{235}U in the reaction product, UO_2.

The manganese oxidizing bacterium *Leptothrix discophora* produces manganese oxides with can both adsorb uranyl and partially oxidize UO_2. Determination of if and how bacteria can influence the oxidation of uranium is important because oxidation will increase the solubility and mobility of uranium in the environment. Although oxidation of UO_2 by biologically precipitated manganese oxides occurs to some degree, reduced uranium remains associated with the manganese oxides in a surface complex and is not significantly mobilized. Taken together, a more complete knowledge of how bacteria can influence the speciation of uranium in the environment will improve not only our fundamental understanding of bacterial interactions with uranium, but also how we can effectively model uranium transport in the environment and our abilities to clean-up uranium contaminated soils and groundwater both cheaply and safely.

Thesis Supervisor: Jeffery Coderre

Title: Associate Professor of Nuclear Science and Engineering

Acknowledgements

Firstly, I'd like to thank the DOE/EMSP Microbial Transformations of TRU and Mixed Wastes project for the funding, it has supported me both at MIT and in my adopted university, UNLV. Secondly, I must acknowledge my advisors on this project, Martin Polz, Jeff Coderre, and of course, Ken Czerwinski who was my principal advisor on this project, even if it didn't always seem so on paper. Without him I would never have gained exposure to such an exciting and dynamic field of research and I would have never had the unique opportunity to finish my graduate studies halfway across the country in the City of Sin. I must of course, also give thanks to the friendship and support that I have received from the members of the Radiochemistry Research group at UNLV, I learned so much from all of you and greatly enjoyed both working and playing with you. I sincerely wish you all the best of luck when the time comes for you to be in my place!

And to my friends from MIT and home, even though I have been far away, your support and friendship were always close at hand, and was instrumental in both my research, writing, and many great memories! I am so glad that I was able to have the opportunity to make such great friends during my studies, such friendships are surely equally as important as this document.

Finally, I must thank my family, this document is solid proof of their love, support and faith in me, because without them, none of this would ever have been possible.

Index

Index of Figures

Index of Tables

1. Thesis Summary

1.1. Abstract

The bacterial influence on the chemistry and speciation of uranium has important impacts on the environment, and can also be exploited for the purposes of environmental remediation of uranium waste contamination. It is important to understand both from a scientific and environmental perspective how different types of bacteria can affect the chemistry and speciation of uranium. Analysis of the kinetics of uranium reduction, to determine the influence of external governing factors, can help us to understand the mechanisms of uranium reduction *in vitro* and aid in the design of more effective uranium remediation schemes in the environment. Not only that, but a better understanding of the reduction kinetics is also an important step in the determination of the extent of isotopic separation that occurs as a result of the bacterial reduction process. Alternately, an understanding of if and how bacteria can influence the oxidation of uranium is important for the opposite reasons. Uraninite (UO_2) is generally considered to be a relatively stable uranium mineral under typical environmental conditions. Oxidation of reduced uranium would increase its solubility and mobility in the environment, making it important to determine what role bacteria may play, either directly or indirectly, in the oxidation of uranium minerals. Taken together, a more complete knowledge of how bacteria can influence the speciation of uranium in the environment will improve not only our fundamental understanding of bacterial interactions with uranium, but also how we can effectively model uranium transport in the environment and our abilities to clean-up soils and groundwater already contaminated with uranium.

1.2. Introduction

Since the onset of the nuclear age, it has become important to understand how uranium behaves in the environment. In the course of extracting this element from the earth and altering it to suit our own purposes, we have changed how uranium interacts in the environment. In the past our poor understanding of the toxicity and mobility of uranium has led to improper storage and contamination of groundwater and soils at numerous sites within the United States. Furthermore, there is an increasing need for the safe and long-term storage of spent nuclear fuel. It is imperative from an environmental standpoint that we fully understand how uranium travels and what impact it can have both chemically and radiologically on the environment, this will help us to adequately reduce the

damage to previously contaminated sites as well as to help to design and model more accurate emplacement schemes, making long-term storage of nuclear waste and spent fuels both safe and reliable.

As a domain, the bacteria are a widely varying and diverse group occupying nearly every niche available in the entire biosphere. Because of their ubiquitous nature bacteria will no doubt play an essential role, either positive or negative, in the migration of uranium in the environment. Understanding how different types of bacteria interact with uranium will be fundamental in our understanding of how this element behaves in the environment.

1.2.1. Research goals and objectives

The primary goal of this work is to contribute to the scientific understanding of how bacteria interact with uranium and to, on a general level, to better understand the mechanisms and factors that govern these interactions with specific attention to bacterial effects on the oxidation-reduction chemistry of uranium. Secondly, another goal of this work is to both improve scientific practice and establish a basis for future studies in this area.

1.2.2. Research tasks

Perform a kinetics analysis study on the reduction of uranium by *Shewanella oneidensis*, utilizing the results to design an experiment to measure the extent of isotopic fraction of uranium during the bacterial reduction process, and to investigate the potential for either direct or indirect bacterial oxidative dissolution of uranium at circumneutral environmental conditions.

1.3. Background

1.3.1. Uranium speciation in the environment.

As an element, uranium can be quite chemically active in the environment. Under typical environmental conditions uranium can be oxidized or reduced, precipitate out of solution, adsorb onto surfaces, form complexes with other molecules, or form colloids that can either inhibit or retard their mobility. And many of these interactions can occur simultaneously. All of these environmental interactions are important in one way or another when considering the fate and transport of uranium throughout the environment.

1.3.2. Uranium oxidation-reduction reactions with bacteria

Bacteria, because of their ubiquitous presence throughout the environment and their tremendous variety of metabolisms and growth conditions, can readily affect the geochemical cycling and transport of metals in the environment. (

Figure 1.1)

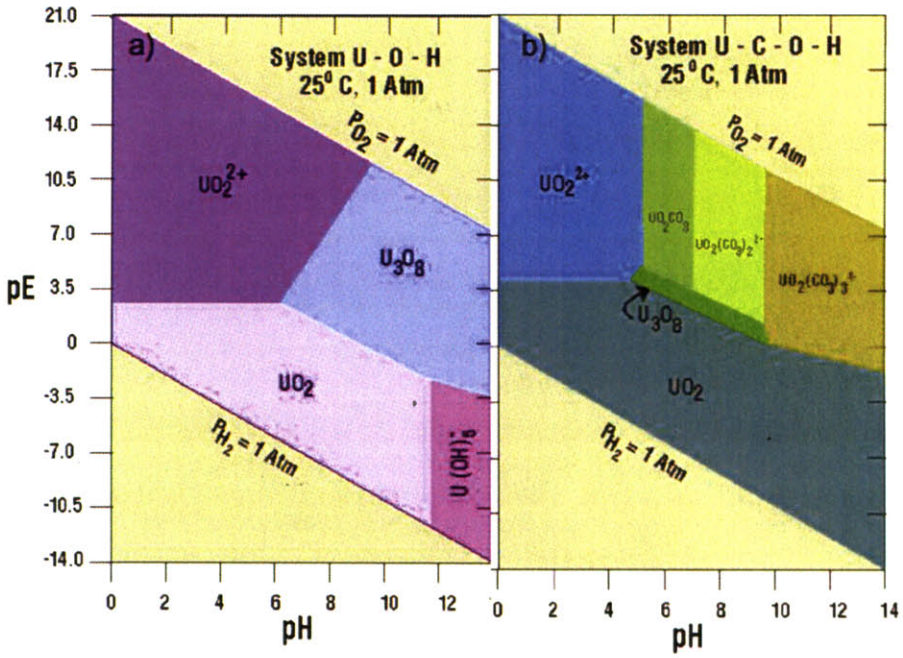

Figure 1.1 A pH/pE Diagram of Fe and U.

Figure 1.1 shows the dominant species of either Fe or U in the presence of carbon, oxygen and hydrogen. Bacteria, as a result of growth or metabolic processes can alter both the pH and the pE of their surrounding environment. It is evident that changes in pH and pE will cause precipitation or dissolution of these elements, and can lead to an increase or decrease in their mobility as a result.

These effects are of particular importance with respect to uranium, a metal that is both radiologically and chemically toxic. Bacteria can interact with uranium directly, by electron transfer to gain energy for metabolism, or indirectly by altering the local environmental chemistry that can, in turn, change the chemistry of uranium. All of the mechanisms mentioned above can affect uranium mobility in the environment.

1.3.2.1. Oxidation reactions

Reduced uranium most often occurs in the environment in a solid-mineral form. Naturally, it is found in uranium containing ores, while, artificially it is often found in spent fuel forms. Oxidation of reduced uranium is considered undesirable because it results in the formation the uranyl (UO_2^{2+}) ion that is more soluble and mobile in the environment than uranium minerals. There are a few types of bacteria known to oxidize uranium. In mill tailings *Thiobacillius ferroxidans*, oxidizes Fe(II) to Fe(III) creating both an acidic environment and Fe(III), both of which enhance oxidative dissolution of uranium containing ores by the following reaction.

$$2FeS_2 + 8O_2 + UO_2 \rightarrow 2Fe^{3+} + UO_2^{2+} + 4SO_4^{2-}$$

This bacteria has also been found to directly catalyze the oxidation of uranium[1]. *T. ferrooxidans* is thought to catalyze the direct oxidation of uranium by the following mechanism:

$$UO_2 + 0.5O_2 + 2H^+ \rightarrow UO_2^{2+} + H_2O$$

Growth of *T. ferrooxidans* solely on the oxidation of uranium has been hypothesized from free energy calculations, but has yet to be determined *in vitro*[1]. Such findings, however, do suggest a pathway for the biological oxidation of uranium in the environment.

1.3.2.2. Reduction reactions

Compared to bacterial oxidation of uranium, much more is known about the process of bacterial uranium reduction. Because this reaction is generally considered desirable by creating an insoluble and less mobile uranium product, and has been suggested[2] and practiced[3] as a mechanism for remediation of uranium contamination, it stands to reason that much more scientific effort has been focused on understanding bacterial reduction. There are several species of bacteria that are now known to directly catalyze the reduction of uranyl[4], most of which are classified as either iron or sulfate reducers and are often capable of reducing several different metals and of utilizing many types of electron donors. For example, the iron-reducing bacterium *Shewanella oneidensis* catalyzes the reduction of uranium in the following manner:

$$H_2 + U(VI)O_2^{2+} \rightarrow 2H^+ + U(IV)O_2.$$

The mechanisms of uranium reduction in iron and sulfate reducing reducing bacteria are not well characterized, but uranium reduction is thought to be mediated by a c-type cytochrome[5].

In the environment, it is microorganisms that are the primary governors of local redox chemistry and thus they can affect changes in actinide oxidation state both directly and indirectly. The mobility of the radionuclides in the environment is largely determined by oxidation state, it is therefore essential to understand how bacteria influence the oxidation and reduction of these elements.

1.3.3. Utilization of bacteria in uranium remediation schemes

At any site that has uranium contamination either in the soil or groundwater, it is imperative that the mobility of uranium be decreased significantly in order to stop the further spread of uranium contamination. Encouraging the development of uranium reducing bacterial populations at the site of uranium contamination is one method which is currently used to decrease the spread of uranium contamination in the environment, and is often more successful at decreasing the amount of uranium present in contaminated groundwater than non-biological remediation schemes[6].

Most sites contaminated with uranium will not naturally have dominant uranium reducing bacterial populations, so the conditions whereby uranium reduction becomes the dominant biological process must be artificially induced. This can be accomplished by adding carbon substrates to induce growth of a succession of bacterial populations that metabolize away all of the products inhibitory to the development of uranium reducing populations (Figure 1.2)[7]. This type of bacterial remediation scheme has been successfully demonstrated in the lab[8] and in the environment[3].

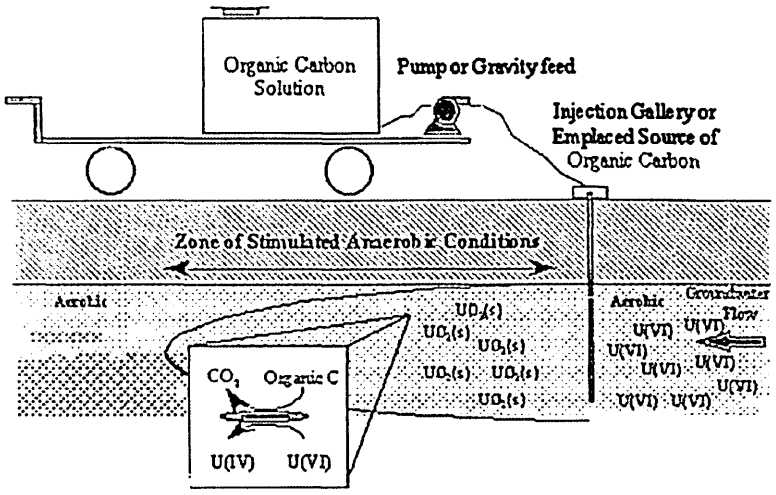

Figure 1.2 A diagram of a typical environmental uranium remediation scheme utilizing natural uranium reducing bacterial populations.

1.3.4. Metal Fractionation Theory in the Environment

There are several elements on the periodic table that have two or more naturally occurring isotopes. Although different isotopes of the same element should behave the same chemically, tiny mass differences between the isotopes cause them to have small differences in reaction kinetics during chemical transformation processes. This kinetic difference is related to the bond energies of the isotopes, with the lighter isotopes having lower bond energies, leading to faster reactivity of the lighter isotope relative to its heavier counterpart. Over time these small kinetic differences can lead to isotopic enrichment of one product relative to another.

There are two fractionation processes that govern chemical reactions, namely, equilibrium and kinetic fractionation. Equilibrium fractionation occurs when the chemical process in question is in equilibrium and the reaction is reversible. In this case the mass difference of the isotopes affects the reaction rate, with the lighter isotope having a slightly faster rate due to its lighter mass. This type of fractionation is dependent upon the variables that affect the chemical reaction rate, like pressure and temperature, and generally the isotope with the larger mass accumulates in the species with the highest oxidation state. Kinetic fractionation on the other hand, occurs when a process is irreversible and governs the fractionation of isotopes during many biological processes including the biological reduction of uranium. In the case of kinetic fractionation mass differences as well as the reaction pathway contribute to the magnitude of fractionation. In

general the chemical bonds of lighter isotopes are more easily broken and react faster than those of heavier isotopes causing the products of the reaction to be enriched in the lighter isotope relative to the substrate. For the case of biological fractionation, it is more energy efficient for bacteria to utilize the lighter isotope the metabolic and chemical reactions they catalyze, thereby enriching reaction products in the lighter isotope. The extent of the fractionation will be dependent on the kinetics of the bacterial reaction. Thus, variables that affect the reaction kinetics such as cell number, pH, electron donor, substrate concentration and availability will also affect the overall fractionation factor.

1.4. Kinetic Modeling of Bacterial Uranium Reduction

Shewanella oneidensis is a widely distributed species of bacteria and is known to utilize several elements such as iron, manganese and sulfur as electron acceptors. In an anoxic environment lacking more electrochemically favorable electron acceptors *S. oneidensis* is shown to reduce uranium, changing its oxidation state from hexavalent to tetravalent, by the following reaction:

$$H_2 + U(VI)O_2^{2+} \rightarrow 2H^+ + U(IV)O_2.$$

Promotion of such a reaction is advantageous, as bacterial reduction of uranium in contaminated waste or groundwater would concentrate the uranium into a more tractable precipitate.

The mechanism of bacterial reduction of uranium must first be well understood before successful bioremediation of this element can be considered a realistic option. Lovley et al.[9] were the first to characterize the bacterial reduction of uranium, and although some of the molecular mechanisms of the reduction have been determined, the extent to which external conditions affect the reduction still remain unclear. Typical environmental influencing factors such as, bacterial density, radionuclide activity, electron donor and pH will all have an influence on the rate of reduction. In order to achieve the most efficient immobilization of uranium in the environment by bacteria, it will be important to quantify and compare these effects on bacterial uranium reduction. Kinetic modeling allows a simple approach for normalization and comparison of multiple data sets of bacterial uranium reduction under different conditions. The model applied for comparison of data sets in this chapter is a modified first order exponential decay curve, and is similar to the model applied for reduction of uranium by SRB by Spear et al. [10] and Liu et. al.[11].

1.4.1. Cell density dependence

In order to determine the effect that bacterial cell concentration had on the rate of uranium reduction, several cell concentrations were

examined and the optimal concentration was found to be approximately $1.3*10^9$ cells/mL. (Figure 1.3) This cell number gave rise to a reduction rate of 0.2 μM U(VI) per hour. The concentration of uranyl acetate (U(VI)) was measured using inductively coupled plasma atomic emission spectroscopy (ICP-AES). Within a period of 72 hours approximately 96% of the original 1.6 mM soluble uranyl acetate was reduced to uraninite, which precipitated out of solution.

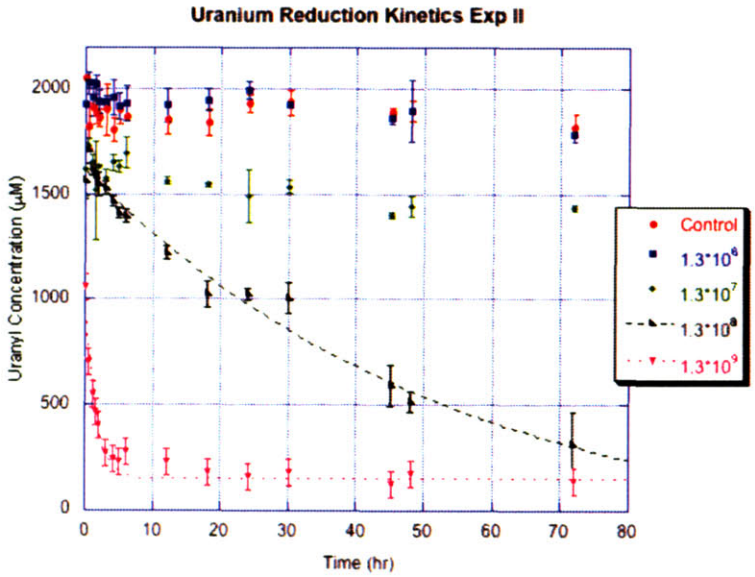

Figure 1.3 Average uranyl reduction over time.

The largest initial reduction rate and the greatest percentage of uranyl reduced in 72 hours occurs for a cell density of $1.3*10^9$ cells/mL. The threshold for significant reduction appears to be about 10^8 cells/mL. The error bars represent one standard deviation in the sample measurement.

Comparison of reduction data from several experiments where the bacterial concentration was known yielded the following relationship between the rate of uranium reduction (k) and the cell density:

$$k=(9.2\pm0.54)*10^{-11}*(\text{cells/mL}) \quad R^2=0.936$$

Fitted to a first-order exponential decal model, the rate of reduction is nearly-linearly dependent upon the density of cells. This is to be expected assuming that the number of uranium reductive sites per cell is approximately the same. This information is important from a remediative perspective in that not only will growth of bacterial biomass need to be stimulated; but that it must exceed a minimum value to occur. It is also important from an *in vitro* perspective

when one is considering optimizing conditions to achieve maximal reduction in a minimal amount of time.

1.4.2. Electron donor dependence

S. oneidensis are known to reduce uranium using two electron donors, H_2 and lactate. Coupling the oxidation of H_2, the reduction of uranium in *Shewanella* is:

$$H_{2(aq)} + UO_2^{2+} \Leftrightarrow 2H^+ + UO_{2(s)}$$

The $\Delta G^{\circ\prime}$ for this reaction is -176.83 kj/mol (Table 4.3). For lactate, *S. oneidensis* couples the oxidation of lactate to CO_2 to the reduction of uranyl:

$$\text{Lactic acid}_{(aq)} + 3H_2O + 6UO_2^{2+} \Leftrightarrow 6UO_{2(s)} + 3CO_{2(aq)} + 12H^+$$

The $\Delta G^{\circ\prime}$ for this reaction is -866.29 kj/mol, thus, the bacteria are, in theory, able to gain more energy from coupling the oxidation of lactate to the reduction of uranium, than they are to the oxidation of H_2.

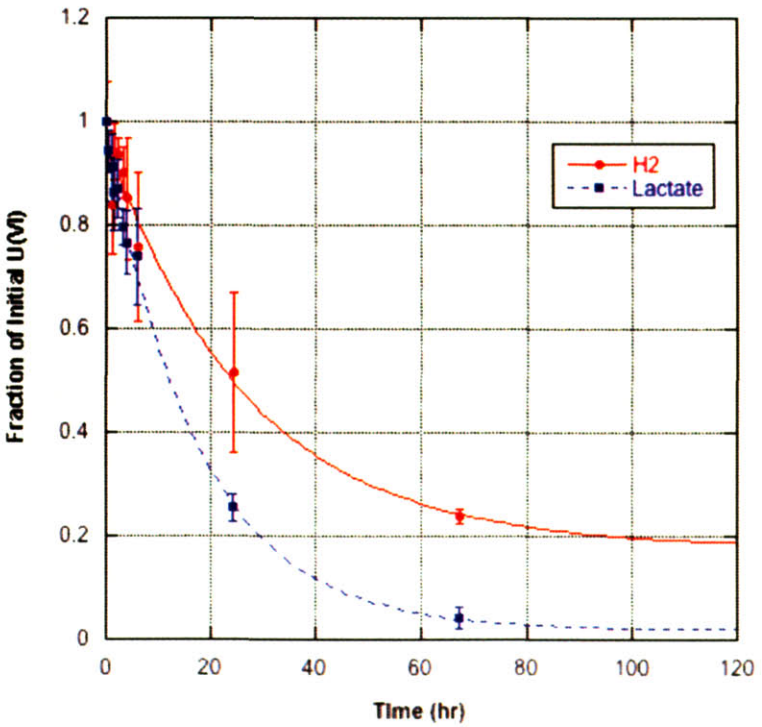

Figure 1.4 Normalized uranium reduction as a function of electron donor. Error bars represent one standard deviation.

Both lactate and H_2 can act as electron donors for the reduction of uranium by *S. oneidensis*, however, the rate of reduction and the overall completeness of the reduction reaction will depend on

which electron donor is available. A comparison of the rates of reduction for other experiments utilizing either H_2 or lactate as the electron donor shows that the rate constants for uranium reduction with lactate are greater than those utilizing H_2. Addition of carbon electron donors (like acetate[3] or lactate) to sites of uranium contamination should yield faster and more complete uranium reduction than H_2. Carbon containing electron donors will act to serve a multiple purposes in the environment, and will encourage the growth of uranium reducing microorganisms as well as to serve as a faster and more efficient electron donor for uranium reduction.

1.4.3. pH Dependence of Uranium Reduction

Although some bacteria can tolerate very low or high proton concentration, many types of bacteria are most viable at circumneutral pH, including *S. oneidensis.* The pH of the environment will have multiple effects on the overall conditions of a system; it can affect the bacterial functionality, as well as dictate the speciation of uranyl and the solubility of UO_2. In order to determine how pH contributes to the bacterial reduction of uranium, the reduction of uranium by *S. oneidensis* was monitored at several pH values.

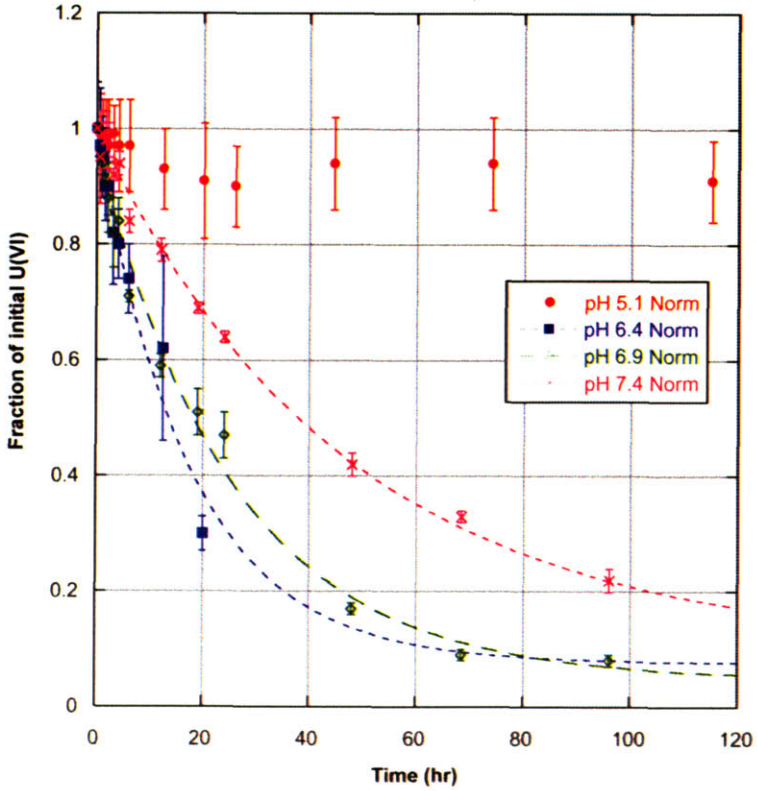

Figure 1.5 Normalized uranium reduction vs. pH. Error bars represent 1 standard deviation.

For the lowest pH (5.1) there is almost no perceivable reduction, at that pH the dominant uranyl species is $UO_2(CO_3)_{(aq)}$. As the pH is increased to 6.4 and 6.9, the rate of reduction increases and more total uranyl is reduced. The rates of reduction are nearly the same for these two pH values. At pH 6.4 the dominant uranyl species is the dicarbonate $UO_2(CO_3)_2^{2-}$, while at pH 6.9 the dicarbonate species and tricarbonate species ($UO_2(CO_3)_3^{4-}$) are in approximately equivalent concentrations. At pH 7.5 the tricarbonate species completely dominates and the rate of reduction is slightly decreased, along with the total amount of uranyl reduced. Although the reduction of uranium is dependent upon the pH, and is optimal at pH 6.4-6.9, small changes in pH of about ±0.5 pH units should still result in the reduction of uranium; larger changes in pH will inhibit uranium reduction most likely due to a decrease in enzyme functionality. In order to achieve maximally effective bacterial uranium reduction in the environment, it will be important to monitor the pH of the carbon substrate media, as well as the pH of the groundwater and effluent.

1.4.4. Conclusion

Here we have demonstrated the effects of some common environmental parameters such as pH, electron donor and cell density have on the bacterial reduction of uranium. It was determined that the rate of reduction fit a first-order exponential decay model and was linearly associated with the density of cells for bacterial concentrations above a minimum density of 1E8 cells/mL. The rate of reduction was also found to be slightly dependent on the electron donor supplied to the bacteria for the reduction with lactate resulting in slightly faster kinetics than H_2. Because environmental remediation strategies usually involve the addition of a carbon substrate, the faster reduction rate seen with lactate as the electron donor will certainly continue to be an effective strategy. It is also clear that the rate of reduction is pH dependent, with pH 6.4-6.9 yielding the fastest reduction kinetics; this could be either due to the reduction enzyme(s) functionality, or to the speciation of the uranium carbonate complexes present in the reduction media. Most likely, a combination of both effects leads to the lack of uranium reduction at pH 5 and the inhibition of reduction at pH 7.4. Bacterial reduction of uranium is an important phenomenon that we can use to help immobilize uranium contamination in the environment. Overall, a fundamental understanding of how external properties affect the mechanism and rate of bacterial uranium reduction should help us to be able to better predict and model how these bacteria will

behave in more complex environments. It should also provide a partial framework for scale-up of bacterial reduction processes *in vitro* for optimizing the rate and production of reduced uranium on a larger-scale.

1.5. Uranium Fractionation by *Shewanella oneidensis*

Despite the high mass of uranium and small relative isotopic mass difference of only ~1%, we hypothesized that biological reduction would lead to fractionation of the two most abundant isotopes ^{238}U and ^{235}U. To establish whether metal-reducing bacteria can fractionate uranium isotopes, we used a highly controlled kinetic approach to obtain precise isotopic ratios of uranium during the bacterial reduction process. In the samples containing live bacteria, the composition of the uranium showed a strong change in isotope ratios with time, which followed opposite trends in the soluble and solid phase, respectively (Table 1.1). While the ratios of $^{235}U/^{238}U$ in solution started to decrease from 0.981 at 0 hours to a minimum of 0.960 at 40 hours, they increased in the solid phase indicating preferential removal of the ^{235}U isotope from solution. No substantial change in isotopic ratios was seen in either of the controls, confirming that biologically active cells are necessary for significant fractionation.

Table 1.1 Solution phase concentration of total uranium and the two isotopes, and the ratio of isotopes at the different time points.

Time (hr)	235/238	[U] (μM)	[^{238}U]	[^{235}U]	f	$\delta^{235}U$
0.0	0.981	1110.792	560.720	550.072	1.000	-18.991
0.5	0.980	1091.913	551.337	540.575	0.983	-19.520
1.0	0.976	966.073	488.928	477.145	0.870	-24.100
1.5	0.979	971.357	490.956	480.401	0.874	-21.500
2.0	0.974	786.367	398.382	387.984	0.708	-26.100
3.0	0.964	768.196	391.045	377.151	0.692	-35.532
4.0	0.965	724.213	368.500	355.713	0.652	-34.700
6.0	0.963	546.520	278.419	268.100	0.492	-37.063
12.0	0.966	108.711	55.310	53.401	0.098	-34.500
18.0	0.962	75.492	38.472	37.020	0.068	-37.745
24.0	0.961	313.560	159.908	153.652	0.282	-39.126
40.0	0.960	98.077	50.028	48.048	0.088	-39.576
52.0	0.961	131.657	67.130	64.527	0.119	-38.776
72.0	0.961	16.961	8.650	8.311	0.015	-39.121
120.0	0.962	36.515	18.616	17.899	0.033	-38.500

A Rayleigh fractionation model[†] was used to determine the fractionation factor (α) for the uranium isotopes to allow comparison with fractionation of other

[†]The Rayleigh model describes a system in which isotope separation occurs under non-equilibrium conditions, i.e., the reactants are removed from the system as the reaction

metals and evaluation of the likelihood of uranium fractionation under natural uranium isotope ratios. Fits from the Rayleigh model resulted in a fractionation factor of $\alpha = 1.029 \pm 0.006$; $R^2 = 0.70$. This result is both surprising and interesting since the value of α is an order of magnitude better than the fractionation factor for the gaseous diffusion process[12]. Although it is an order of magnitude less than gas centrifugation[12], the biological fractionation process occurs at room temperatures and pressures; a distinct advantage over both gas diffusion and centrifugation.

1.6. Studies into the Potential for Uranium Oxidation by Bacteria

There are many other types of bacteria that can interact with uranium other than sulfate and iron reducing microorganisms. Unlike *S. oneidensis*, metal oxidizing bacteria can both inhibit the transport of uranium, by producing metal-oxides capable of uranyl sorption, or mobilize uranium by the process of oxidative dissolution. Although uraninite is generally considered to be a relatively stable uranium mineral under typical environmental conditions, bacteria that are capable of catalyzing uranium oxidation will impact how we understand the effects of long-term storage of UO_2 fuel forms and other UO_2 products (like biologically reduced U) present in the environment. For example, *Leptothrix discophora* produces manganese oxides, which are powerful environmental oxidants that can also adsorb positively charged metal contaminants like uranyl[13], meaning that this microorganism could alter the chemistry of both U(IV) as well as U(VI). Although the properties of uranium reducing bacteria and their impacts on uranium speciation are more well known, it is also important for us to understand the effects that other types of bacteria may have on the chemistry of uranium.

1.6.1. *Leptothrix discophora*

After exploring the properties of a number of Fe and Mn oxidizing bacteria (Fe and Mn are probably the closest chemical analogues of uranium that are used commonly in bacterial respiration), *Leptothrix discophora* was chosen because of its ease of growth in the lab and because the protein it excretes (which oxidizes Mn) might directly oxidize uranium, but also because the bioproduced manganese oxides (BMO) themselves seemed to offer promise that they too might also have an oxidative dissolutive effect on uranium. The initial experiments with the bacterial oxidizing protein(s) were inconclusive, but the differences in the chemistry of reduced uranium, which is highly insoluble and reduced

---

progresses. This is appropriate since the reduction results in an essentially insoluble precipitate so that equilibrium isotope effects are likely insignificant.

manganese, which is readily soluble, suggest that the oxidizing protein produced by *L. discophora* is not capable of any significant uranium oxidation.

1.6.2. Kinetics of BMO formation

In cell free spent media, concentrations of Mn^{2+} (around 400 μM) were inhibitory to oxide formation and high enough concentrations of Mn would prohibit oxide formation altogether. BMO formation was also inhibited at higher Mn concentrations by addition of uranyl, with lower concentrations of uranyl required to inhibit oxidation at higher Mn concentrations (Figure 1.6). The general trend in Figure 1.6 is that increasing the amount of U(VI) present slows down the formation of the MnOx as well as decreases the total amount of oxide formed.

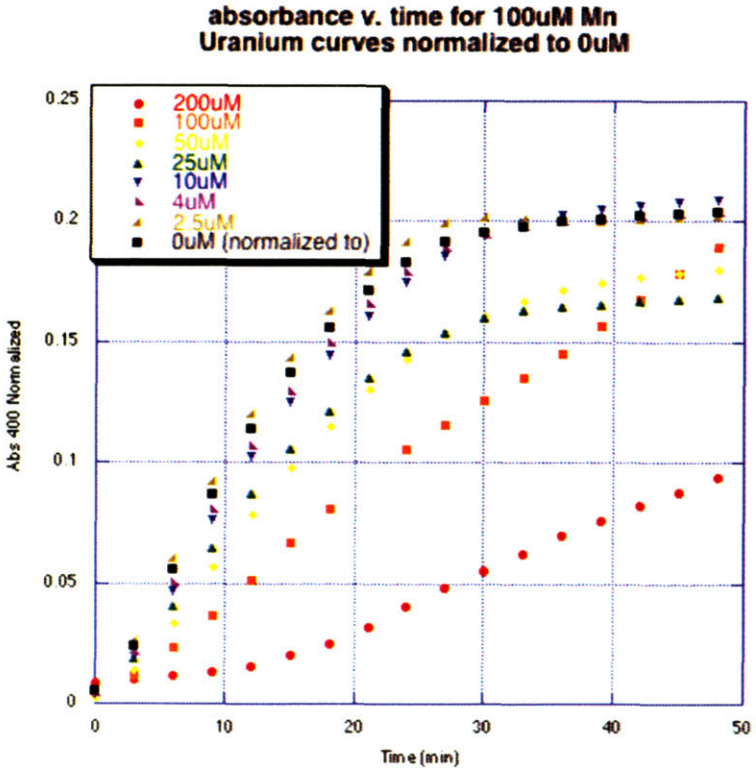

Figure 1.6 Kinetics of manganese oxide formation in spent MSVP media (*L. discophora* grown 96 hours) with 100 μM Mn2+ and varying concentrations of U(VI) (inset).

The interaction of biologically produced manganese oxides and UO_2 were also investigated. The kinetics of BMO formation was also inhibited by the presence of UO_2 (Figure 1.7) as indicated by a slower removal of Mn^{2+} from solution relative to a similar sample

without UO_2. Because the solubility of UO_2 is so low, the inhibitory effect that solid UO_2 has on BMO formation must be different from the inhibitory effects of UO_2^{2+}. Although this effect was not quantified in great detail, adsorption of the MOF to UO_2 could be the reason that manganese oxidation is inhibited in the presence of this solid.

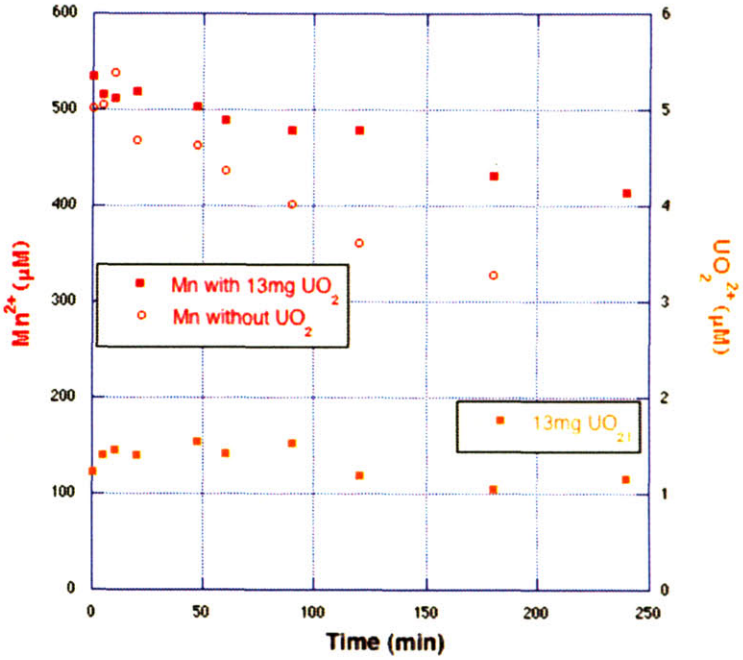

Figure 1.7 Inhibition of BMO formation in the presence of UO_2. Mn^{2+} removal from solution is slower in the presence of UO_2 (closed square) than in the absence of uranium (open circle).

These results show that if growth *L. discophora* could be stimulated in the environment, oxide formation will only occur when contaminant metal concentration is low. This may mean that in highly contaminated areas, decreasing uranium mobility by stimulating metal adsorption to BMO will not be a viable option.

1.6.3. EXAFS study of U(VI) and U(IV) contacted with BMO

Samples of BMO formed in the presence of both uranyl and UO_2 were prepared and analyzed using EXAFS. By this method, it is possible to detect oxidized uranyl adsorbed to the surface of biologically produced manganese oxides based on structural differences between uranium oxidation states. Figure 1.8 shows the uranium EXAFS spectra for a sample where BMO was contacted with 17 mg of UO_2. What is interesting about Figure 1.8 is the small shoulder present on the U(IV) peak, indicating the presence of U(VI) along with U(IV) in the sample.

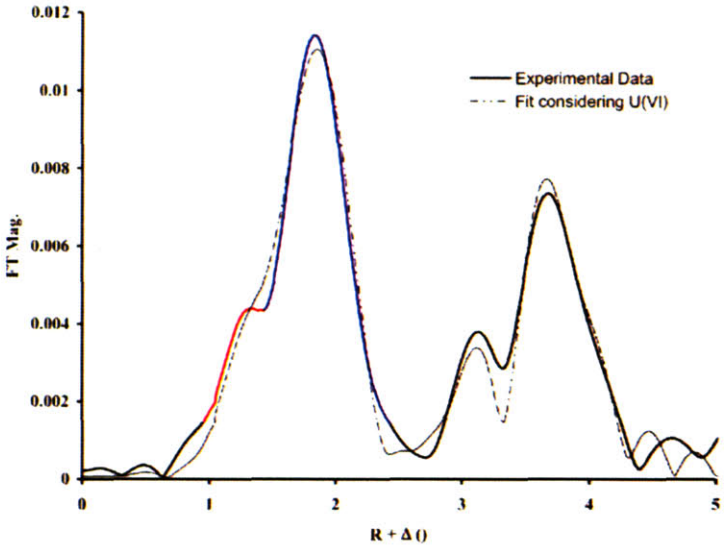

Figure 1.8 The deconvoluted Fourier transform of the uranium EXAFS spectra for a sample where BMO was contacted with 17 mg of UO_2. Both the real data and the experimental fit are shown. The dominant peak here (blue) is due to UO_2 because the measured sample contained both BMO and UO_2, however, the shoulder of this peak (red) is an indication of the presence of U(VI).

Because of their negative surface charge and high surface area, manganese minerals are known to be good absorptive agents for contaminant metals like Cu, Pb, Hg, Pu, and U[14]. Figure 1.9 shows the deconvoluted fourier transform of the uranium EXAFS spectra in which BMO were precipitate in the presence of 20μM UO_2^{2+}. Both the real data and the experimental fit are shown. The first large peak is indicative of a U(VI)-oxygen double bond, while the second, smaller peak is due to an association of U(VI) with the MnOx surface.

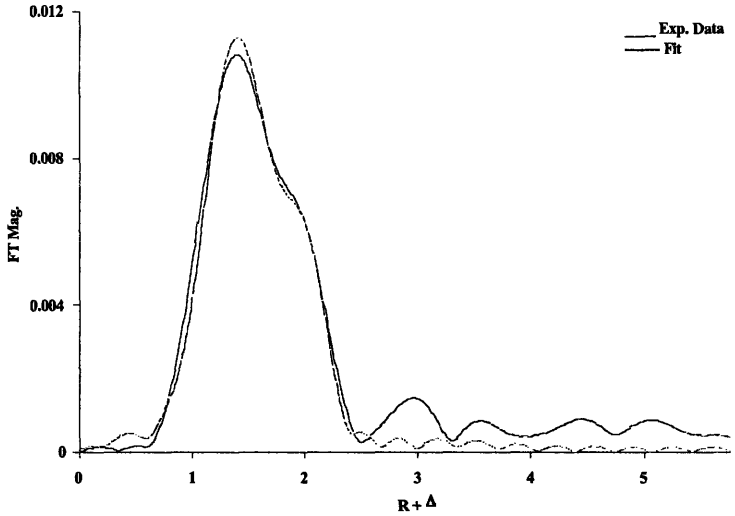

Figure 1.9 The deconvoluted Fourier transform of the uranium EXAFS spectra for a sample where Mn^{2+} was bioprecipitated in the presence of 20 μM U(VI).

From the concentration of uranium used and analogy with literature, MnO_2 can present the pseudo-tunnel structure. These data are in good agreement with previous findings by Webb et al.[15] who showed similar uranium speciation for samples complexed with manganese oxides produced by spores of *Bacillus sp.*

Investigation into the catalysis of uranium oxidation by *L. discophora*, showed that the MOF produced by the bacteria alone does not appreciably lead to UO_2 oxidation over a short period of time. Not only that but, although EXAFS results suggest the production of some U(VI), BMO precipitation in the presence of UO_2 does not lead to measurable uranium mobilization. However, manganese oxides of biological origin can adsorb uranyl at micromolar concentrations and oxides of biological origin already present in the environment will most likely serve to impede the transport of uranium.

1.7. Conclusion

Here we have described the effects that conditions such as cellular density, electron donor, and pH have on kinetics of uranium reduction by *S. oneidensis*. This information can help us to better understand how to optimize uranium reduction not only on the benchtop, but also for environmental remediatory efforts. Optimal reduction conditions may also provide an initial framework to better study the isotopic separation effects that have been shown to occur during the process of bacterial reduction of uranium. Bacterial fractionation of uranium has never before been described, and exploitation of this effect could be useful in both geochemistry and for potential uranium enrichment scenarios.

It was also apparent that although bacterial oxidation of uranium is energetically possible, that, from the species explored here, there is relatively little bacterial interaction with reduced uranium. Although unsurprising, this information offers further support that reduced uranium in the form of UO_2 should be relatively stable in the environment, and that no new assumptions about bacterial oxidative dissolution of UO_2 need to be made at this time.

We are only just beginning to scratch the surface when it comes to our understanding of how microorganisms affect the geochemical cycling and transport of metals in the environment. Uranium and other radionuclides are of special importance because of current contamination with these metals, but also because of plans to emplace large quantities of nuclear waste in the Earth. It is our responsibility to understand the impact that the will have, not only on the environment but for us as well both in the immediate future and in the long term. The efforts described here emphasize that the study of model systems *in vitro* can give us insights into the redox interactions between bacteria and uranium that can be applied to environmental remediation schemes as well as to provide some framework for future improvements to uranium speciation and transport models.

1.8. References

[1] **DiSpirito, A. A., O. H. Tuovinen.** (1982) Kinetics of Uranous Ion and Ferrous Iron Oxidation by *Thiobacillus ferrooxidans*. Arch. Microbiol. **133:**33-37.

[2] **Lovley, D.R., E. J. P. Phillips, Y. A. Gorby, E. R. Landa.** (1991) Microbial Reduction of Uranium. Nature. 350:413-415.

[3] **Anderson, R. T., et al.** (2003) Stimulating the *In Situ* Activity of *Geobacter* Species to Remove Uranium from the Groundwater of a Uranium-Contaminated Aquifer. Appl. Environ. Microbiol. **69:** 5884-5891.

[4] **Lovley, D. R.** (1993) Dissimilatory Metal Reduction. Annu. Rev. Microbiol. **47:**263-290.

[5] **Lovley, D. R., P. K. Widman, J. C. Woodward, E. J. Phillips.** (1993) Reduction of Uranium by Cytochrome c_3 of *Desulfovibrio vulgaris*. Appl. Environ. Microbiol. **59:**3572-3576.

[6] **Abedoulas, A., W. Lutze, H. E. Nuttal.** (1996) Uranium Contamination in the Subsurface: Characterization and Remediation. Uranium: Mineralogy, Geochemistry and the Environment. Mineralogical Society of America, Washington D.C..

[7] **Anderson, R. T., D. R. Lovley.** 2002. Microbial interactions with Uranium: An Environmental Perspective. Interactions of Microorganisms with Radionuclides. Elsevier Science Ltd.

[8] **Barton, L. L., K. Choudhury, B. M. Thomson, K. Steenhoudt, A. R. Groffman.** (1996) Bacterial Reduction of Uranium: The First Step of *In Situ* Immobilization of Uranium. Rad. Waste. Manage. Environ. Rest.

[9] **Lovley, P. K. Widman, J. C. Woodward, E. J. P. Phillips.** (1993) Reduction of Uranium by Cytochrome c3 of *Desulfovibrio vulgaris*. Appl. Environ. Microbiol. **59:**3572-3576.

[10] **Spear, J. L., L. A. Figueroa, B. D. Honeyman.** (2000) Modeling Reduction of Uranium Under Variable Sulfate Concentrations by Sulfate Reducing Bacteria. Appl. Environ. Microbiol. **66:**3711-3721.

[11] **Liu, C., Y. A. Gorby, J. M. Zachara, J. K. Fredrickson, C. F. Brown.** (2002) Reduction Kinetics of Fe(III), Co(III), U(VI), Cr(VI), and Tc(VII) in Cultures of Dissimilatory Metal-Reducing Bacteria. Biotechnol. Bioeng. **80:**637-649.

[12] **Benedict, M., T. H. Pigford, H. W. Levi** (1981) Nuclear Chemical Engineering 2nd Ed. McGraw Hill Ltd. NY NY. 8.

[13] **Banfield, J. F, K. H. Nealson eds.** (1997) Bacterially Mediated Mineral Formation; Insights into Manganese (II) Oxidation from Molecular Genetic and Biochemical Studies. Geomicrobiology; Interactions Between Microbes and Minerals. Mineralogical Society, Washington, D. C. **36:**225-266.

[14] **Tebo, B. M. et al.** (2004) Biogenic Manganese Oxides: Properties and Mechanisms of Formation. Annu. Rev. Earth. Planet. Sci. **32:**287-328.

[15] **Webb, S. M., J. R. Bargar, B. M. Tebo.** (2005) Determination of Uranyl Incorporation into Biogenic Manganese Oxides Using X-ray Absorption Spectroscopy and Scattering. Phys. Scr. **T115:** 949-952.

2. Introduction

Microorganisms are ubiquitous throughout the environment and play an important role in the redox cycling of many metals, of these, uranium is of both economic interest and environmental concern. It is an element that has been and most likely will be fundamental to power production in the United States and across the globe. However, our increasing global reliance on nuclear power does not come without an environmental cost; there are many sites throughout the USA and the world that are contaminated with uranium and other radionuclides, making a scheme for the safe geological disposal of nuclear waste of the utmost importance if we are to continue to rely on nuclear power. Uranium and spent nuclear fuel is both chemically and radiologically toxic, and great care must be taken in the consideration of how and where it can be stored effectively and safely for long periods of time. In order to do that, we must not only understand the fundamental chemistry of uranium, but also the slew of complex speciation and transport mechanisms that take place in the environment both biologically and chemically. Bacteria affect the speciation and transport of uranium in the environment in several different ways, sorption to bacterial membranes, by production of extracellular metal-complexing molecules, by altering the local environmental chemistry, or by coupling metal reduction or oxidation to cellular energy generation. It is the greater understanding of how bacteria can affect the chemistry of uranium that will be an important fundamental tool in our approach to cleanup of radionuclide contamination and the way in which waste will be managed in the future.

Compared to what little was known about the impact that uranium would have on the environment when it was first utilized for commercial nuclear power production, our understanding has increased dramatically. However, even as our understanding increases, it becomes more evident that the chemistry, speciation and transport of uranium in the environment is governed by a series of complex processes. In order to achieve a complete understanding of the complex mechanisms that govern uranium chemistry in the environment, we must first break them down and examine each process individually.

Environmental remediation of uranium contamination most often focuses on first inhibiting the mobility of uranium in the environment, to limit the area of contamination, followed by the removal of uranium from the site of contamination. Interactions that play a role in the mobility of uranium are, precipitation, dissolution, sorption, desorption, and association with chelating ligands, however, it is the oxidation state of uranium that is a primary factor in its environmental mobility. Of the two commonly occurring oxidation states of uranium, U(IV) is less mobile in the environment, while U(VI) is more mobile and is the dominant oxidation state of most of the uranium released into the environment.

It has long been known that bacteria can influence the oxidation state of metals, and that bacteria can directly catalyze both the oxidation and reduction uranium. The bacterial reduction of U(VI) to U(IV) offers a potentially low-cost and secondary-waste free mechanism for inhibiting the spread of uranium in the environment. Although the bacterial oxidation of uranium will tend to increase its environmental mobility in the

environment, making it an unfavorable interaction to encourage from a remediatory standpoint, it will nonetheless be important to understand to what extent bacterial oxidation could influence the mobility of uranium in the environment. This thesis will thus focus on the factors that can influence the extent of bacterial uranium reduction in both the laboratory and the environment as well as to explore the potential for bacterial oxidative mobilization of uranium in the environment.

2.1. Project Overview

2.1.1. Problem description

It has been established that bacteria are capable of altering the speciation and transport of uranium, by several interactions both indirectly and directly. However, the chemical, kinetic, and molecular mechanisms of these interactions have yet to be investigated in detail. For example, what are the factors that lead to the greatest and most efficient reduction of uranium? This thesis aims to determine some of the important influencing chemical factors in the kinetics of bacterial uranium reduction and to determine the potential for bacterial influence on the oxidation of uranium, about which relatively little is known, with the purpose of better understanding these interactions both under controlled and environmental conditions.

2.1.2. Research goals and objectives

The research goals of this thesis are to answer the following questions: What influences the kinetics of uranium reduction by *Shewanella*? What are the optimum conditions to achieve the fastest and most complete uranium reduction? Does the reduction of uranium by bacteria lead to significant isotopic separation? How can bacteria influence the oxidation of uranium either directly or indirectly, and if so, is this a significant process in the environment? What impact might bacterial oxidation of uranium have? And to unite the answers to those questions into a more thorough picture of how bacteria interact with uranium and how such interactions can affect the speciation and transport of uranium in the environment.

2.1.3. Research task list

In order to achieve the goals described in the previous section, a series of tasks were undertaken. Tasks 1 and 2 relate to the reduction of uranium by *S. oneidensis*, while Task 3 considers both

indirect and direct influence that oxidizing bacteria might have on uranium.

Task 1: Characterize and describe some factors that influence the reduction of uranium *in vitro* by the bacterium *S. oneidensis*.

- 1a: Determine the relationship between the density of bacteria and the rate of reduction. Additionally, this information will be used to determine the optimal cellular density for further reduction experiments *in vitro*.
- 1b: From reduction experiments with different enrichments of uranium, determine if there is a relationship between the reduction of uranium and the total activity of the system.
- 1c: Compare the rate of uranium reduction when *S. oneidensis* utilizes two different electron donors, lactate and H_2.
- 1d: Model the speciation of uranium in the reduction media and determine the effects that uranium speciation and pH have on the uranium reduction rate.

Task 2: Utilizing optimal uranium reduction conditions determined is task 1a; measure the isotopic ratio of a 1:1 $^{235}U/^{238}U$ mixture of uranium during the bacterial reduction process and asses the extent of microbial isotopic separation during uranium reduction.

Task 3: Characterize and describe the effects the metal oxidizing microorganisms have on uranium.

- 3a: Asses the growth of a putative iron-oxidizing microorganism on media containing UO_2 and determine how this organism can effect the oxidation of uranium.
- 3b: Asses the direct oxidation of uranium by cell free spent media containing manganese oxidizing factors produced by *L. discophora*.
- 3c: Asses the extent of indirect oxidation of uranium by manganese oxides produced by *L. discophora*. Determine by EXAFS, the speciation of uranium that has been contacted with these oxides.
- 3d: Explore the interactions between uranyl and manganese oxides of biological origin. Determine the effects that uranyl has on manganese oxide formation and the speciation of uranium associated with the manganese oxide surface.

2.2. Thesis Overview

This thesis is presented in 11 sections. The first chapter is a summary of the important points of the thesis. The second chapter introduces the work, chapters 3-6 provide the background information regarding the sources of and environmental chemistry of uranium and other actinides, the bacterial influence on uranium redox chemistry, and the theory and premise of bacterial isotopic fractionation. Chapter 7 describes a majority of the analytical and experimental techniques used in this work. The body of the thesis is divided into chapters based on a series of experiments, as follows:

Chapter 8 – Kinetic Modeling of Bacterial Uranium Reduction

Chapter 9 – Bacterial Fractionation of Uranium Isotopes

Chapter 10 – Interactions of Metal Oxidizing Bacteria with Uranium

The conclusion, chapter 11, discusses future experiments and the contribution that the efforts herein have made to understanding the mechanisms and environmental influences of bacterial interactions with uranium. There are also three appendices, one for each chapter in the body of the thesis, which contain a more detailed description of experimental methods along with additional supportive information.

3. Uranium Speciation in the Environment

The biological, geological and chemical behavior of uranium will dictate its speciation and mobility and therefore its impact on both humans and the environment. Uranium is unique in that it is the heaviest naturally occurring radionuclide and can be both chemically and radiologically toxic. Unlike many of its natural heavy radionuclide counterparts, uranium is known to be both biologically and geologically active in numerous complex environments. Not only that, but its continued processing, refinement and storage is of the utmost importance for the future of nuclear power in this country and elsewhere. These properties make the study of the mobility of uranium in the environment both important and complex.

3.1. Environmental Sources of Uranium

Uranium is found ubiquitously throughout the ecosphere with over 200 different uranium-containing minerals identified. However, because of our increased interest in the mining and enrichment of uranium for nuclear power, much of this uranium has become distributed throughout the environment in new forms and in high local concentrations. Uranium mining, fuel production, research efforts, and spent fuel all represent sources of uranium introduced into the environment by mankind.

3.1.1. Uranium Mining and Mill Tailings Sites

While the largest deposits of uranium ore are located outside of the United States, the U.S. has, since the advent of nuclear technology, made an effort to mine uranium from sites within the United States[1]. The three methods of uranium mining employed at these sites are: *in situ* leach mining, traditional ore removal, and recovery of uranium from acid leaching of mill tailings. While there are fewer mines open today, uranium mining and former mine sites represent a source of release of uranium into the environment.

3.1.1.1. *In Situ* Leach Mining

There are currently about ten mines licensed for leach mining in the U.S. and they supply about 85% of the U.S.'s uranium, and makes up about 16% of the worlds total uranium production[2]. *In situ* leach mining, or ISL, is a method by which a lixiviant is injected directly into and dissolving the ore. The leachate is collected downstream of the injection point. (Figure 3.1) ISL mining only works when the ore is located in porous rock (like sandstone) surrounded by layers of non or poorly porous rock, to

prevent the leachate from migration into the surrounding environment. The makeup of the rock at most U.S. mining sites is such that an alkaline lixiviant (oxygen and sodium bicarbonate) is used to extract the uranium as soluble uranyl tricarbonate ($UO_2(CO_3)_3^{4-}$).

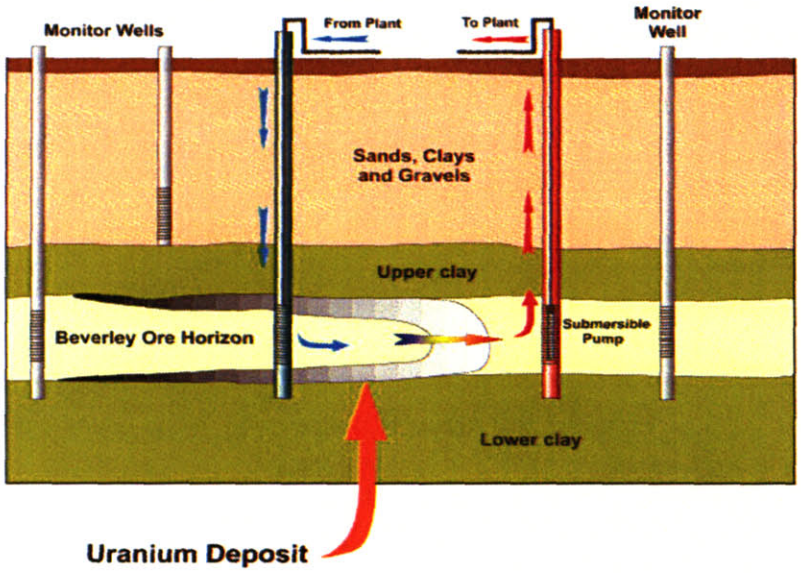

Figure 3.1 In situ leach mining at the Beverly uranium mine in Australia[2].

Some of the advantages to ISL are that it is cheaper and safer for workers because it does not generate harmful dust or significant quantities of radon gas. But as with all mining, there are also potential environmental hazards associated with this type of operation. Mine sites must be carefully chosen and monitored to ensure that all of the leachate is recovered, but pumps can become clogged and leachate can leak out through explorative boreholes. The production lifetime of a typical ISL well field is usually less than three years[3]. Upon closing of the mine, the quality of the groundwater is mandated to be restored to its original state, but due to the nature of leach mining, this is often takes several years to achieve.

3.1.1.2. Traditional Ore Removal

When the environmental conditions aren't conducive to ISL, or where uranium ore deposits are prevalent, traditional mining techniques can be employed. If the ore is near the surface, it can be removed by open pit mining, which is done by drilling and blasting away the surface rocks to expose the uranium ore. The hazard in this case is commonly from dust and particulates, either

spreading over large areas around the mine, or by endangering miners through the lung. Water is used to limit production of dust as much as possible.

If the ore is too far from the surface to be mined by open pit methods, it can be removed by drilling and tunneling underground. This method reduces the amount of dust as well as the amounts of waste rock produced, however, underground tunnels greatly increase the exposure risk for miners to radon gas.

Both of these mining schemes generally represent less of an environmental uranium contamination hazard than ISL mining techniques; but because traditional ore mining poses a much greater exposure risk to workers, and because the current need for uranium is not overwhelming, traditional uranium ore mining is no longer the primary method of uranium ore recovery being utilized today[4].

3.1.1.3. Acid Leaching of Mill Tailings

Waste rock from uranium mining often contains dilute, but significant amounts of uranium. This uranium can be recovered by acidic heap leaching. This is a process that is similar to ISL, but in this case the lixivant (usually sulfuric acid) is allowed to percolate through a pile of discarded ore. The leachate can then be collected and the uranium recovered. (Figure 3.2)

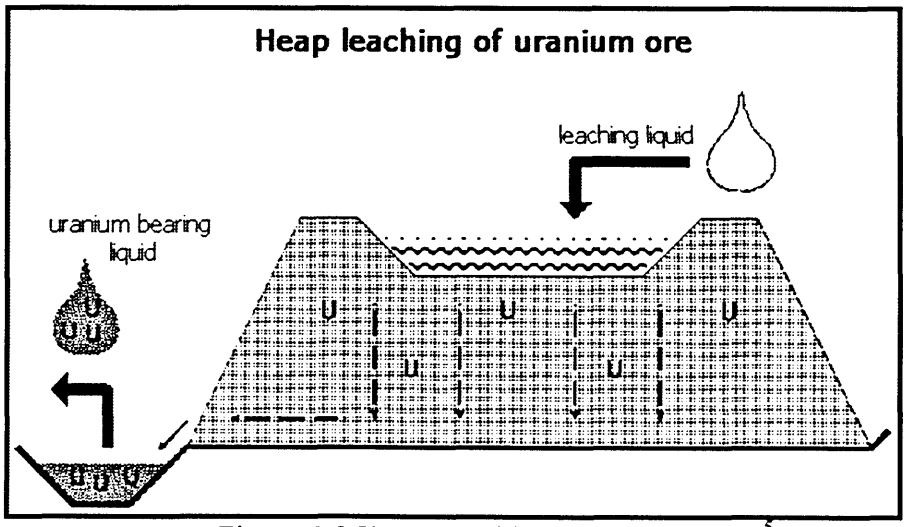

Figure 3.2 Heap Leaching of Uranium Ore[5].

The nature of heap leaching, however, is such that uranium release into the environment is quite common, which is why this practice is no longer used in the United States[6]. However, there are still many sites throughout the United States that have uranium contamination because of previous heap leaching efforts. In 1978

Congress enacted the Uranium Mill Tailings Radiation Control Act (UMTRCA) to ensure the proper precautions with the future mining of uranium ore as well as to provide for the proper remediation of contamination prevalent at many of the uranium mining sites in the US. In 1995, the UMTRCA was expanded to include the remediation of both soils and groundwater.

3.1.2. Spent Nuclear Fuel

As fossil and alternative fuels become more scarce and costly, Americans will have to rely more heavily on nuclear resources for their power. This means that there is and will be an increased need for the environmental storage of spent nuclear fuel and other highly radioactive wastes. Currently, Yucca Mountain is slated to be the nations only permanent high-level waste repository.

Prior to its lifetime in a reactor nuclear fuel consists mostly of uranium dioxide, but after being spent in the core of a nuclear reactor will contain many more elements. (Table 3.1)

After spending approximately 10 years in a spent fuel pool to account for decay of a majority of the short-lived fission products such as ^{90}Sr and ^{137}Cs, it is then stored temporarily at one of six major storage facilities in the United States. Temporary storage methods are designed to shield the public from the harmful effects of radiation, but are not designed to withstand the elements for many thousands of years. The current plan is to transfer the spent fuel into a permanent long-term storage facility that has been engineered to withstand the elements for many thousands of years and to inhibit as much as possible the transport of radionuclides out of the boundaries of the site. The Department of Energy has chosen the Yucca Mountain site in southern Nevada for its long-term storage facility. If the site is licensed, then emplacement of spent fuel into the site should begin in 2017. Spent fuel and other highly radioactive waste slated for long-term storage in Yucca Mountain will be placed in casks and emplaced into the site robotically.

Table 3.1 Elemental Constituents in Uranium Fuel Discharged from a PWR. Quantities are expressed per metric ton of uranium in the fresh fuel charged to the reactor. Average fuel exposure=33 MWd/kg. Average specific power = 30 MW/mg. 150 days after discharge.[7]

	g/Mg	Ci/Mg	W/Mg
Actinides			
Uranium	9.54×10^{5}	4.05	4.18×10^{-2}
Neptunium	7.49×10^{2}	1.81×10^{1}	5.20×10^{-2}
Plutonium	9.03×10^{3}	1.08×10^{5}	1.52×10^{2}
Americium	1.40×10^{2}	1.88×10^{2}	6.11
Curium	4.70×10^{1}	1.89×10^{4}	6.90×10^{2}
Subtotal	9.64×10^{5}	1.27×10^{5}	8.48×10^{2}
Fission products			
Tritium	7.17×10^{-2}	6.90×10^{2}	2.45×10^{-2}
Selenium	4.87×10^{1}	3.96×10^{-1}	1.50×10^{-4}
Bromine	1.38×10^{1}	0	0
Krypton	3.60×10^{2}	1.10×10^{4}	6.85×10^{1}
Rubidium	3.23×10^{2}	1.90×10^{2}	0
Strontium	8.68×10^{2}	1.74×10^{5}	4.50×10^{2}
Yttrium	4.53×10^{2}	2.38×10^{5}	1.05×10^{3}
Zirconium	3.42×10^{3}	2.77×10^{5}	1.45×10^{3}
Niobium	1.16×10^{1}	5.21×10^{5}	2.50×10^{3}
Molybdenum	3.09×10^{3}	0	0
Technetium	7.52×10^{2}	1.43×10^{1}	9.67×10^{-3}
Ruthenium	1.90×10^{3}	4.99×10^{5}	3.13×10^{2}
Rhodium	3.19×10^{2}	4.99×10^{5}	3.99×10^{3}
Palladium	8.49×10^{2}	0	0
Silver	4.21×10^{1}	2.75×10^{3}	4.16×10^{1}
Cadmium	4.75×10^{1}	5.95×10^{1}	2.13×10^{-1}
Indium	1.09	3.57×10^{-1}	1.04×10^{-3}
Tin	3.28×10^{1}	3.85×10^{4}	1.56×10^{2}
Antimony	1.36×10^{1}	7.96×10^{3}	2.74×10^{1}
Tellurium	4.85×10^{2}	1.34×10^{4}	1.66×10^{1}
Iodine	2.12×10^{2}	2.22	8.98×10^{-3}
Xenon	4.87×10^{3}	3.12	3.04×10^{-3}
Cesium	2.40×10^{3}	3.21×10^{5}	2.42×10^{3}
Barium	1.20×10^{3}	1.00×10^{5}	3.93×10^{2}
Lanthanum	1.14×10^{3}	4.92×10^{2}	8.16
Cerium	2.47×10^{3}	8.27×10^{5}	7.87×10^{2}
Praseodymium	1.09×10^{3}	7.71×10^{5}	5.73×10^{3}
Neodymium	3.51×10^{3}	9.47×10^{1}	2.65×10^{-1}
Promethium	1.10×10^{2}	1.00×10^{5}	9.17×10^{1}
Samarium	6.96×10^{2}	1.25×10^{3}	2.18
Europium	1.26×10^{2}	1.35×10^{4}	7.19×10^{1}
Gadolinium	6.29×10^{1}	2.32×10^{1}	3.34×10^{-2}
Terbium	1.25	3.02×10^{2}	2.54
Dysprosium	6.28×10^{-1}	0	0
Subtotal	3.09×10^{4}	4.18×10^{6}	1.96×10^{4}
Total	9.95×10^{5}	4.31×10^{6}	2.04×10^{4}

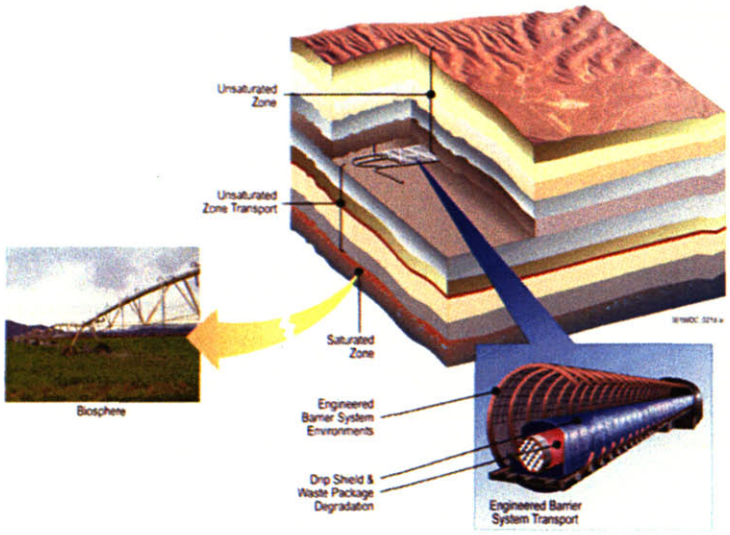

Figure 3.3 Geography of the Yucca Mountain Site[8].

The location of the site, the fuel form, and cask and dripshield are all designed to impede the dissolution and transport of radionuclides away from the site and into the environment. (Figure 3.3) Current models predict that there will be no significant radionuclide intrusion into the environment for many thousands of years. However, the geochemistry of the Yucca Mtn. makes it a dry oxidizing environment, and although the plan is to emplace the waste above the water table, the conditions of the repository site are such that the reduced fuel will eventually (on geological time scales) end up as the more mobile UO_2^{2+}. Thus, it is of utmost importance that we fully understand the dissolution, speciation and transport of radionuclides in the environment around the site.

There are also three licensed low-level waste repositories in the USA as well as the Waste Isolation Pilot Plant (WIPP) for transuranic waste storage. Because of the precautions taken in waste storage and monitoring these sites do not present an immediate environmental concern, but it is still important to understand what the risk is for environmental (and subsequently, human) contamination is, in order to better design storage and monitoring and to be ready to take any actions necessary upon accidental release.

3.1.3. High-Level Waste Storage Facilities

The Department of Energy stores its high level waste in tanks at the West Valley, New York; Savannah River, South Carolina; and

Hanford, Washington sites. This waste consists primarily of liquid wastes associated with reprocessing.[9] This waste is a proverbial "thorn in the side" for the DOE because it is difficult waste to deal with. In fact, many of the tanks at the Hanford site are leaking, at the Savannah River site the liquid waste there is slated for removal and vitrification for permanent disposal, but neither of these tasks will be an easy effort. Some of the tanks that are leaking at the Hanford site are as large as 1 M gallons and as of 2004 only 50% of the contaminated soil at the Hanford site had been cleaned up[10]. At the Savannah River site, there are a number of large tanks where sludge formed from reprocessing waste has become a recalcitrant problem. The speciation and composition of the sludge is largely unknown and much of it has been in the tanks since before strict nuclide accounting measures were put in place. It is because of these and other high-level waste storage sites that a permanent storage facility is important. It is imperative that waste be removed from these sites as soon as it becomes scientifically possible to prevent any further environmental contamination.

3.1.3.1. Savannah River

Waste at the Savannah River Site (SRS) stems from the large-scale chemical separation of plutonium and uranium and is stored in 51 underground tanks. The volume of waste is estimated to be 36.4 Mgal with a total activity of 426 MCi[9]. The tank waste consists primarily of three phases:, saltcake, sludge, and a basic liquid supernatant, which makes up a majority of both the volume (48%) and activity (49%) of waste. Much of the current radioactivity in the waste originates from short-lived radionuclides such as ^{137}Cs and ^{90}Sr which have half-lives on the order of 30 years. The radionuclides that pose the greatest long term risk are ^{14}C, ^{79}Se, ^{99}Tc, ^{129}I, ^{126}Sn, and ^{237}Np because of both their activity and environmental mobility[11]. The plan for long-term management and disposal of waste at SRS is to vitrify sludge-waste, and to separate the highly active radionuclides from the low-activity radionuclides in the remaining salt-waste, followed by vitrification of the high-activity waste and immobilization of the low-activity waste with grout and subsequent storage in concrete vaults. Once all of the waste is removed from the tanks, they will be sealed with cement and capped.

3.1.3.2. Hanford

Waste at the Hanford Site in Washington state originates from plutonium production, extraction, and processing, with a total of 177 tanks compromising 54 Mgal and 193 MCi. 149 of the earliest

construction tanks are considered to be past their designed lifetimes and 67 of these tanks have leaked approximately 1 Mgal of waste[10]. The composition of the waste at the Hanford site is similar to SRS in that is consists of basic supernate, sludge and saltcake, however a larger variety of waste was processed at this site relative to SRS, so there is more variation in the nuclide inventory at Hanford. Also, while the overall inventory of the tank waste can be determined from process conditions and bookkeeping, the radionuclide inventory in individual tanks is less well known[12]. The plan for waste processing and disposal at Hanford involves retrieval of all of the tank waste, separation and removal of highly active waste, followed by vitrification for long-term storage.

3.2. Environmental Chemistry of Uranium

As an element, uranium can be quite chemically active in environment. Under typical environmental conditions uranium can be oxidized or reduced, precipitate out of solution, adsorb onto surfaces, form complexes with other molecules, or form colloids that can either inhibit or retard their mobility. Many of these interactions can occur simultaneously, but all of these interactions are important in one way or another when considering the fate and transport of uranium throughout the environment.

3.2.1. Oxidation-Reduction Reactions

Under typical environmental conditions, uranium can be found in one of two oxidation states: U(IV) and U(VI), the most common of which is U(VI), usually present as the uranyl ion (UO_2^{2+}). In the environment, the oxidation state of uranium plays an important role in its mobility; in the tetravalent state, uranium is typically found as a solid whereas hexavalent uranium is readily soluble and more mobile. There are many factors that can affect the oxidation state of uranium in the environment, such as the presence of other metals, microbial metabolism, metabolic byproducts, and ultimately pH and pE. Figure 3.4 shows a pE/pH diagram for two simple uranium systems and illustrates how changes in pE and pH can lead to alteration of uranium's oxidation state.

Environmental factors that can alter either the pE or pH will ultimately affect the oxidation state of uranium. Acid production as a result of microbial metabolism is a good example of such an effect; and leads to the oxidative dissolution of uranium minerals in mill tailings. Microorganisms can also directly catalyze the reduction of uranium. Conversely, uranium can be directly oxidized by reduced iron and manganese minerals (Table 4.2).

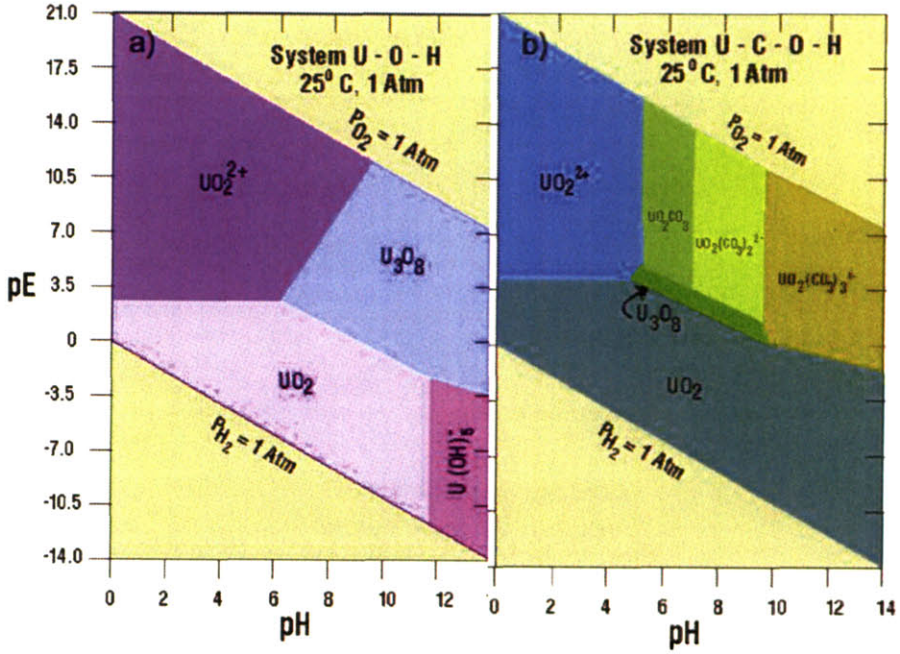

Figure 3.4 Two uranium pE/pH diagrams. Each block represents the most common species at each pE and pH . a) showing the U-O-H system only b) showing the U-C-O-H system. Just the addition of carbon to the system adds three other species.

3.2.2. Precipitation

Precipitation of uranium in the environment will occur when a given species of uranium exceeds its solubility limit. Precipitation reactions will impede the transport of uranium in the environment, and such reactions central to most uranium remediation schemes. Precipitation is also one of the mechanisms of formation of uranium mineral deposits. For uranium there is a marked solubility difference dependent upon the oxidation state, with the tetravalent state having significantly lower solubility limits than the hexavalent state (Table 3.2).

Table 3.2 Solubility Products of Actinide Oxides/hydroxides. Values are given as log K^0_{sp} at 25°C[13].

	U	Np	Pu	Am
$AnO_2OH_{(am)}$		-8.7	-9.0	-8.7
$AnO_2(OH)_{2(s)}$	-22.8	-22.5	-22.5	
$AnO_3 \cdot 2H_2O_{(cr)}$	-23.2			
$An(OH)_{3(am)}$			-26.2	-25.1
$An(OH)_{4(am)}$	-54.5	-56.7	-58.5	
$AnO_{2(cr)}$	-60.9	-63.7	-64.0	-65.4

3.2.3. Complexation

The most environmentally significant species of uranium that forms aqueous complexes is U(VI). Tetravalent uranium does not tend to form soluble complexes under typical environmental conditions, and so will not be discussed here. Counter to precipitation, complexation of uranium will tend to increase its solubility and lead to greater migration of uranium in the environment.

3.2.3.1. Inorganic Ligands

Common inorganic ligands found in aqueous environments are: hydroxide, carbonate, phosphate, sulfate, nitrate and chloride. Of these, hydroxide and carbonate are among the most significant ligands, both because of their affinity for uranyl and their prevalence in the environment; other ligands like phosphate and sulfate can become important in certain environments where they are found in relatively high concentrations. Figure 3.5 shows the percentage of uranyl carbonate and hydroxyl complexes in an aqueous environment as a function of pH at differing partial pressures of CO_2. At atmospheric CO_2 concentrations and at low pH the system is dominated by uncomplexed uranyl, while between pH 5 and ~6.5 the uranyl hydroxide complex dominates, and above pH ~6.5 the uranyl-hydroxyl carbonate complex is the most common species. Figure 3.6 shows the percentage of total uranyl species, including any precipitates as a function of pH and partial pressure of CO_2. At atmospheric CO_2 concentrations, schoepite ($UO_3 \cdot nH_2O$) precipitates between pH 5 and 8, and is the dominant form of uranyl. The total solubility of uranium is governed by the concentration of both the free ion and the concentrations of the complexed species, thus, the presence of complexing ligands will lead to an overall increase in the total solubility (and therefore mobility) of uranium.

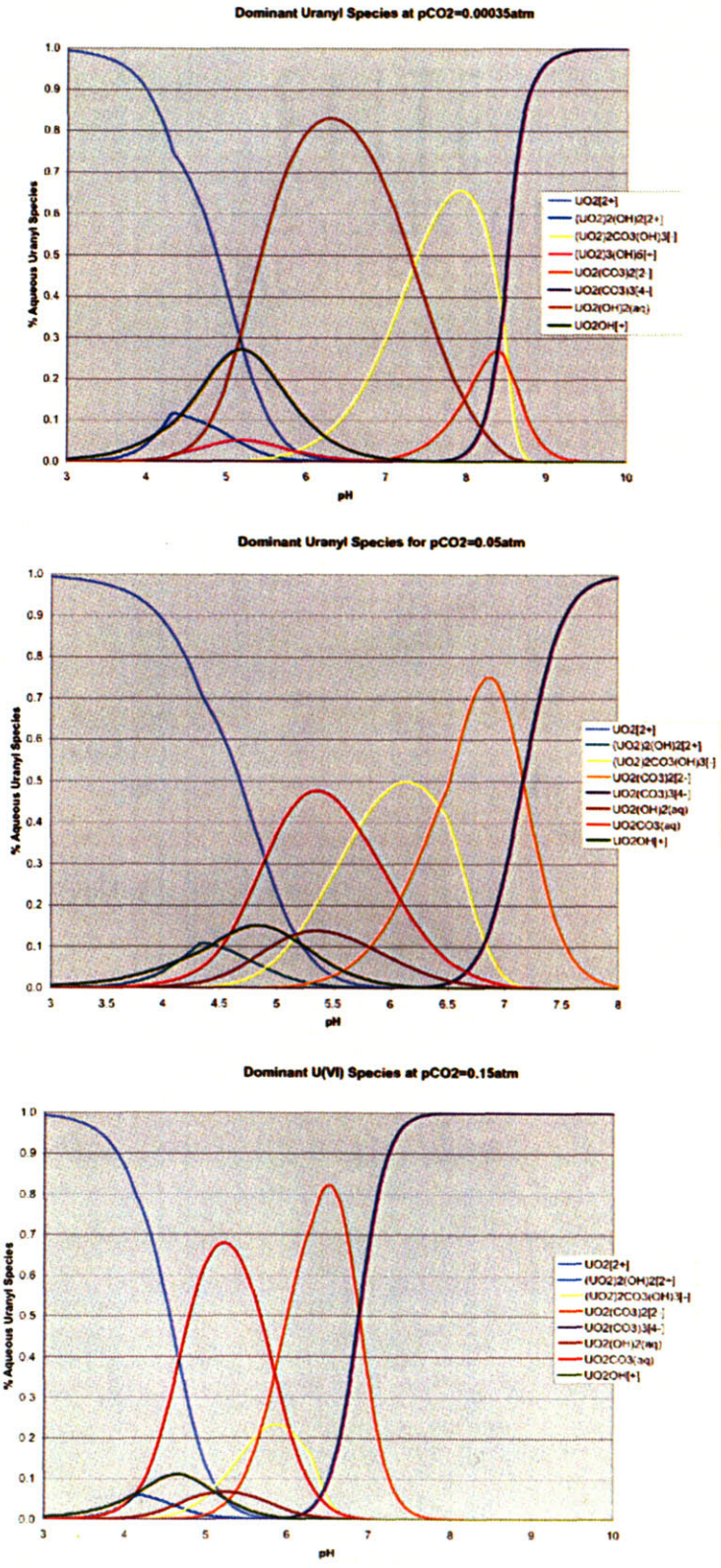

Figure 3.5 Aqueous U(VI) species at T=25°C, pCO2=0.00035, 0.05 and 0.15 atm, U=25 μM.

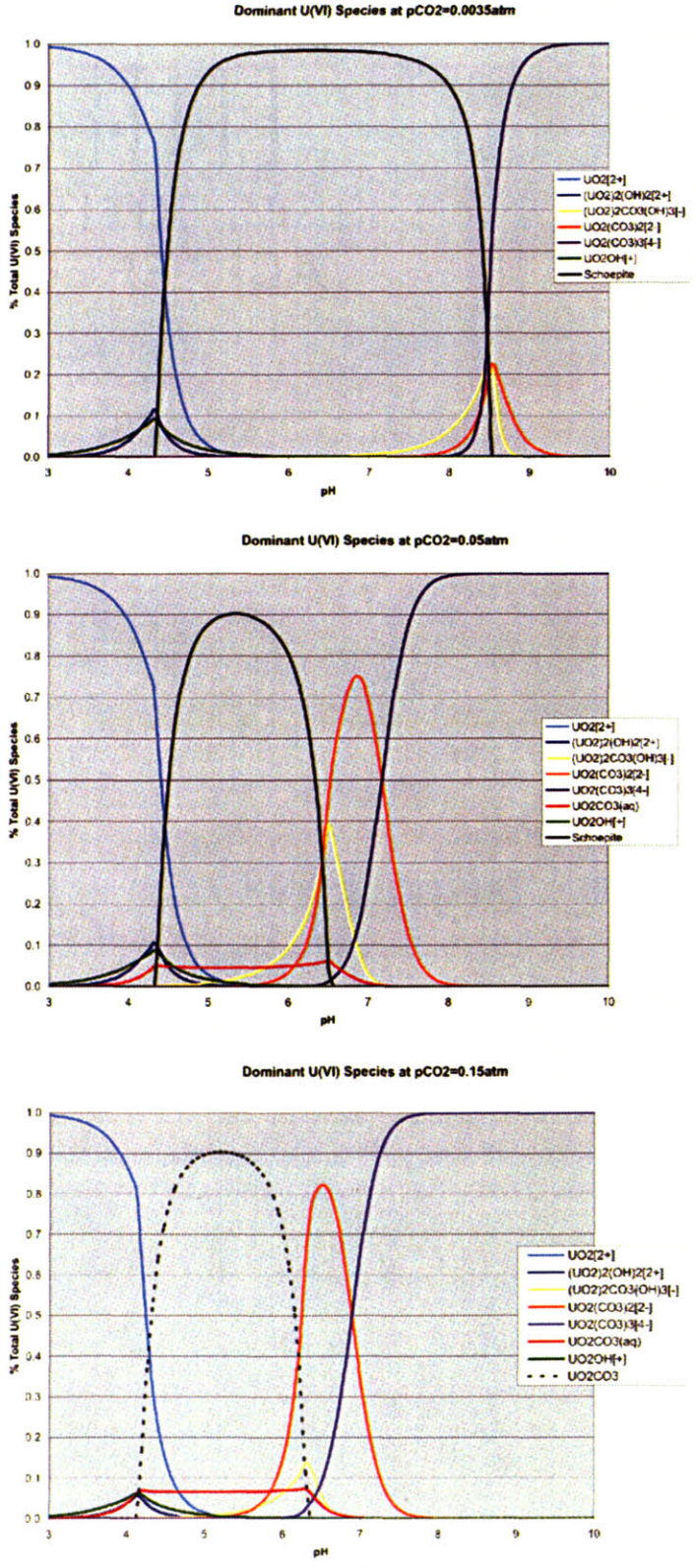

Figure 3.6 Total U(VI) species at T=25°C, pCO2=0.00035, 0.05 and 0.15 atm, U=25 μM.

3.2.3.2. Organic Ligands

In certain situations, such as soils and in fuel reprocessing wastes, organic ligands can also play a role in the complexation of uranium. Humic acids comprise a majority of the organic material present in the near surface environment. They are high molecular weight compounds with an undefined structure, large numbers of functional groups and are resistant to metabolic degradation. The humic acids are classified into three groups according to their aqueous solubility: Humic acid is soluble in dilute alkaline solutions, Fulvic acid is soluble at most pH's, and Humin, which is generally insoluble. Complexation of uranyl to solid humic acids will tend to immobilize it, while association with soluble humic acids can lead to an increased mobility of uranium in the environment, but unlike humic complexation with other metals, uranium does not become reduced upon association with humic acids (on laboratory time scales)[14]. Table 3.3 gives stability constants for the formation of some common trivalent actinide-humic acid complexes. In some instances, uranyl complexation with humic acids has been known to compete favorably with inorganic ligands[15,16] (Figure 3.7). The interactions of uranyl with humic acids in the environment should not be overlooked, as the type and concentration of humic acid present can readily affect the mobility of uranium in the environment.

Table 3.3 Results from complexation studies of trivalent actinides with different humic acids (I=0.1 M)[14].

Humic Substance	pH	Loading Capacity	Log K (mol/L)	Log β (L/mol)
Aldrich HA	6.0	0.815±0.023	5.85±0.23	6.42±0.14
Bradford HA	5.0	0.190±0.002	4.36±0.66	6.41±0.70
Bradford HA	5.5	0.400±0.005	5.05±0.50	6.41±0.35
Bradford HA	6.0	0.650±0.012	5.45±0.30	6.29±0.34
Gohy-573 HA	3.0	0.076±0.002	4.17±0.26	6.10±0.12
Gohy-573 HA	4.0	0.234±0.018	5.07±0.59	6.08±0.21
Gohy-573 HA	5.0	0.458±0.019	5.55±0.42	6.26±0.33
Gohy-573 HA	6.0	0.622±0.005	5.25±0.43	6.32±0.24

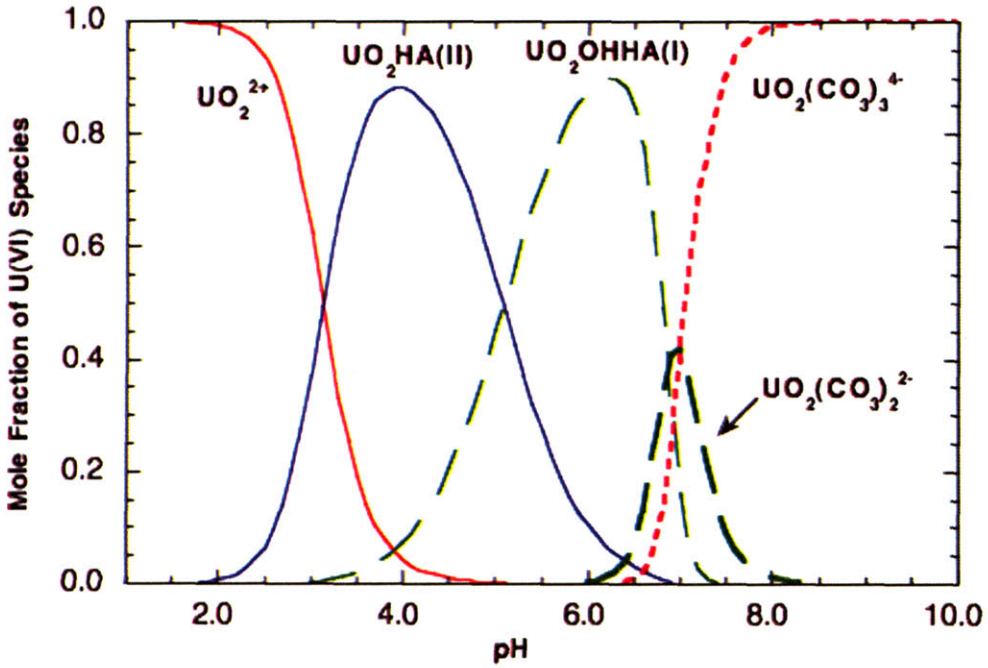

Figure 3.7 Calculated uranium species distribution at 1% CO_2 partial pressure. At this concentration of CO_2 uranyl-humic complexes dominate between pH 3.5 and 6.5.[16]

There are several other organic ligands that can play an important role in uranium complexation and mobility if they are readily present in the environment. Siderophores are large chelating molecules produced by bacteria to scavenge metals in nutrient poor environments and often contain anionic hydroxamate or catecholate functional groups that will form strong soluble complexes with uranyl. The siderophores Desferrioaxamine B (DFO) and enterobactin have been shown to solubilize both hydrous plutonium oxide and uraninite[17]. In the range of pH 3-10, there are three dominant U(VI)-DFO complexes whose stability constants are given in Table 3.4. Such high stability constants indicate that the uranyl-siderophore complexes are relatively strong, and as such can play a role in the complexation of U(VI) even at low concentrations.

Table 3.4 Stability Constants of Uranium-DFO at I=0.1 M[18].

Species	Log β
UO_2DFOH_2	22.93±0.04
UO_2DFOH	17.12±0.35
UOOHDFOH	22.76±0.34

Other organic ligands of import include those used in reprocessing, which also form strong soluble complexes with uranyl and will tend to keep uranyl in solution when stored together in the environment. While these organic ligands are not found ubiquitously throughout the environment, they can lead to mobilization of uranium under certain circumstances.

3.2.4. Sorption

Uranyl migration in groundwater and soils can be retarded by sorption to minerals and solids present in the environment. Some common sorptive surfaces include iron and manganese minerals as well as clays, which form reactive surfaces that the uranyl can bind to. This binding can be either covalent and typically irreversible, or electrostatic and more reversible. Overall, the degree or sorption will depend both on the availability of uranyl as well as the surface area of the sorbant. Minerals having a greater surface area and therefore, more available binding sites will have a greater potential to bind uranium. Sorption of uranium to hydroxyapatite minerals to form a permeable reactive barrier has been suggested as a possible mechanism for remediation of uranium in the environment[19].

3.2.5. Colloid Formation

Colloids are small agglomerates of molecules that can range in size from 1 nm to 1 μm. There are four major groups of colloids commonly found in the environment. Silicate colloids originating from silicon-bearing minerals like quartz; secondary mineral colloids which are made up of oxides, hydroxides, and carbonates of minerals like iron and manganese; organic colloids comprised of humic acids; and biological colloids such as bacteria, yeast and fungi. Uranyl can both adsorb to the surfaces of colloids as is the case with U(VI) sorption to phosphate groups on a bacterial surface, as well as form colloid-complexes on its own, like polymeric uranyl carbonate species that can form at high uranyl concentrations or high ionic strength[20]. Colloid complexes can both magnify and inhibit uranium transport in the environment, depending on environmental conditions and the nature of the colloid. For example, radionuclide transport by colloids can occur faster than groundwater flow due to hydrodynamic chromatography, the exclusion of larger colloids from small pores which water can enter. At Los Alamos National Laboratory both

Pu and Am were detected on colloids over a kilometer from the source term[21], much further away from the source than had been predicted. In contrast, free radionuclide sorption to biomass can inhibit its transport. Overall, the complete role that colloid formation plays in actinide migration in the environment in not yet fully understood.

3.3. Conclusion

The chemistry, speciation and mobility of uranium in the environment is a complex and a unique problem. Before successful remediation can be accomplished and before highly radioactive waste forms can be safely stored almost indefinitely in the environment, it is important for us to understand not only the specific nature of the environment but also how these conditions will affect the mobility of uranium. Oxidation-reduction, precipitation, complexation, sorption, and colloid formation must all be taken into account when developing a model to asses the potential transport of uranium in the environment, and can then be applied to the real environmental scenarios involving the cleanup of radioactive waste contamination and the long-term storage of spent fuel and highly radioactive waste.

3.4. References

[1] Uranium Location Database Compilation. (2006). EPA Document ID 402-R-05-009.

[2] http://www.world-nuclear.org/info/inf27.htm

[3] **Szymanski, W. N.** (1994) Uranium In Situ Leach Mining in the United States. Uranium Industry Annual 1993. Energy Information Administration. Washington, D.C. ix-xxv. DOE/EIA-0478(93).

[4] http://en.wikipedia.org/wiki/Uranium_mining#Open_pit

[5] http://www.agroeco.nl/~wise/439-440/image/leaching.gif

[6] http://www.nrc.gov/materials/fuel-cycle-fac/ur-milling.html

[7] **Benedict, M., T. H. Pigford, H. W. Levi** (1981) Nuclear Chemical Engineering 2nd Ed. McGraw Hill Ltd. NY NY. 8.

[8] http://www.goldsim.com/images/Yucca2.gif

[9] Tank Waste Retrieval, Processing and On-site Disposal at Three Department of Energy Sites: Final Report. (2006) http://www.nap.edu/catalog.11618.html. 13-33.

[10] Department of Energy, Richland Office FY04 progress report. http://www.hanford.gov/rl/uploadfiles/10025_pie.pdf

[11] **Cook, J.R.** (2005) Estimated All Pathways and Inadvertent Intruder Doses from Saltstone Disposal Using Updated Salt Waste Compositions. Revision 0. Aiken, S.C., Westinghouse Savannah River Company.

[12] **Honeyman, B.** (2005) Understanding of Hanford Tank Wastes. Presentation to the Committee on the Management of Certain Radioactive Waste Streams Stored in Tanks at Three Department of Energy Sites. Richland, Wa.

[13] **Fanghanel, T., V. Neck.** (2002) Aquatic Chemistry and Solubility Phenomena of Actinide Oxides/Hydroxides. Pure. Appl. Chem. **74:**1895-1907.
[14] **Kim, J. I., K. R. Czerwinski.** (1996) Complexation of Metal Ions with Humic Acid: Metal Ion Charge Neutralization Model. Radiochim. Acta. **73:**5-10.
[15] **Shanbahg, P.M., G. R. Choppin.** (1981). Binding of Uranyl by Humic Acid. J. Inorg. Nucl. Chem. **43:**3369-3372.
[16] **Zeh, P., K.R. Czerwinski, J.I. Kim** (1997) Speciation of Uranium in Gorleben Groundwaters. Radiochim. Acta. **76**: 37-44.
[17] **Brainard, J. R., B. A. Strietelmeier, P. H. Smith, P. J. Langston-Unkefer, M. E. Barr, R. R. Ryan.** (1992) Actinide Binding and Solubilization by Microbial Siderophores. Radiochim. Acta. **58/59**: 357-363.
[18] **Mullen, L., C. Gong, K. Czerwinski.** Complexation of Uranium(VI) with the Siderophore Desferrioaxamine B. in press.
[19] **Fuller, C. C., J. R. Bargar, J. A. Davis, J. Piana.** (2002). Mechanisms of Uranium Interactions with Hydroxyapatite: Implications for Groundwater Remediation. Enviorn. Sci. Tech. **36:**158-165.
[20] **Clark, D. L., D. E. Hobart, M. P. Neu.** (1995). Actinide Carbonate Complexes and Their Importance in Actinide Environmental Chemistry. Chem. Rev. **95:**25-48.
[21] **Nelson, D.M., and K.A. Orlandini.** (1986) Source effects of metal movement in groundwater. Argonne National Laboratory Report ANL 86-15.

4. Actinide Oxidation-Reduction Reactions With Bacteria

The actinide elements have extremely rich oxidation-reduction chemistry. Figure 4.1 shows the Frost diagrams* for U, Np, and Pu, and illustrates the number of oxidation states, several of the species for each element, as well as the most thermodynamically stable oxidation state. For the actinides U, Np, and Pu in particular, a number of different redox states are accessible in both the solution and solid phase. This redox behavior is of paramount importance because oxidation state is one of the primary dictators of environmental mobility. And, in the environment, bacteria are one of the primary dictators of redox chemistry. Uranium is the heaviest naturally occurring element for which bacterial redox reactions are known and bacteria are thought to have played a role in the deposition of some uranium ores[1]. Bacteria also can catalyze the oxidation and/or reduction of the radionuclides technetium, plutonium, and neptunium.

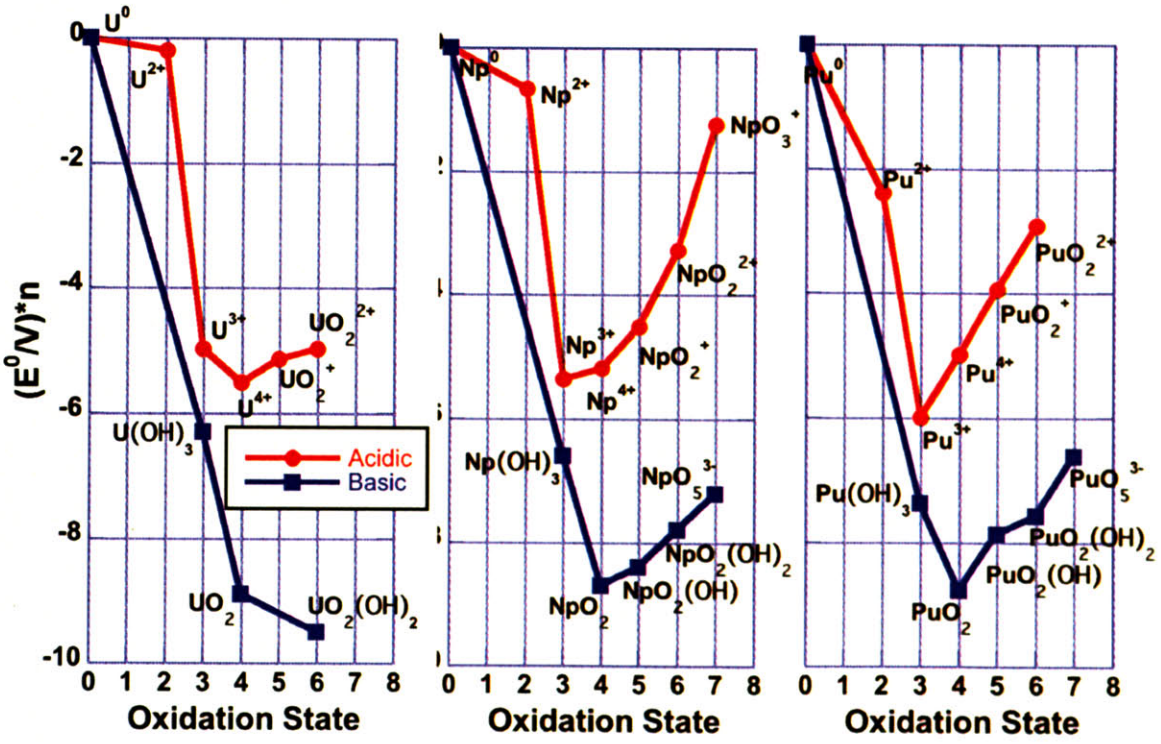

Figure 4.1 Frost Diagram for U, Np and Pu.

* A Frost diagram plots the relative free energy of a given species vs. its oxidation state. The most thermodynamically stable species will appear at the lowest relative free energy. Species on an outward curve will tend to disproportionate, while those on the inward curves tend not to disproportionate. Species located on the upper left side are reducing agents, while those on the upper right are oxidizing agents.

4.1. The Importance of Metal Redox by Bacteria in the Environment

Bacteria play an important role in the catalysis of many oxidation-reduction reactions in the environment, from the reduction of gaseous hydrogen to the oxidation of uranium and nearly all of the elements in between. Such reactions drive the geochemical cycling of many of the Earth's metals, releasing them from their mineral traps and subsequently making them available to higher organisms. Bacteria, because of their ubiquitous presence throughout the environment and their tremendous variety of metabolisms and growth conditions, can readily affect the geochemical cycling and transport of metals in the environment. These effects are of particular importance with respect to uranium, a metal that has both radiological and chemical properties. Bacteria can affect uranium, and other radionuclides, by all of the mechanisms mentioned above. This in turn can greatly influence that metals' mobility in the environment. Bacteria can interact with uranium directly, by electron transfer to gain energy for metabolism, or indirectly by altering the local environmental chemistry that can impact uranium speciation. Recently, it has been established that bacteria may play a larger role in the geochemical cycling of metals than abiotic redox reactions[2]. Furthermore, bacterial metal respiration is thought to be the first and oldest metabolic pathway.

4.2. Bacterial Oxidation of Uranium

Oxidation of uranium can be energetically favored in some environments, although it is often difficult to achieve oxidation both kinetically and biologically due to the crystallinity and insolubility of most mineral forms of reduced uranium. Reduced uranium most often occurs in the environment in a solid-mineral form as UO_2 and is also the chemical form of nuclear fuel[3]. Oxidation of reduced uranium increases solubility and mobility as it results in the formation the uranyl (UO_2^{2+}) ion. There are a few known mechanisms for both indirect and direct biological oxidation of uranium.

4.2.1. Indirect Oxidation

A large portion of uranium oxidation occurs in mill tailings piles, such mineral-rich acidic environments facilitate the growth of chemolithotrophic microorganisms that couple the fixation of carbon dioxide to the oxidation of iron and sulfur. Chemolithotrophic bacteria commonly found in mill tailings piles are: *Thiobacillus thiooxidans, Thiobacillus ferrooxidans*, and *Leptospirillum ferrooxidans*.

Table 4.1 Iron and Sulfur Oxidation Mechanisms. 1) *Thiobacillus sp.;* 2) *T. ferrooxidans* and *L. ferrooxidans*; 3) Fe^{3+} product from (2)[4] 4) the overall reaction.

$2S^0_{(s)} + 3O_2 + 2H_2O \rightarrow 2H_2SO_{4\,(aq)}$	(1)
$2FeS_{2\,(s)} + 7O_2 + 2H_2O \rightarrow 2FeSO_{4\,(aq)} + 2H_2SO_{4\,(aq)}$	(1)
$4FeSO_{4\,(aq)} + O_2 + 2H_2SO_{4\,(aq)} \rightarrow 2Fe_2(SO_4)_{3\,(aq)} + 2H_2O$	(2)
$FeS_{2(s)} + 14Fe^{3+}_{(aq)} + 8H_2O \rightarrow 15Fe^{2+}_{(aq)} + 2SO_4^{2-}{}_{(aq)} + 16H^+$	(3)
$2S^0_{(s)} + 3FeS_{2\,(s)} + 2FeSO_{4\,(aq)} + 14Fe^{3+} + 11O_2 + 10H_2O \Rightarrow$ $2H_2SO_{4\,(aq)} + 2Fe_2(SO_4)_{3\,(aq)}\ 15Fe^{2+}_{(aq)} + 2SO_4^{2-}{}_{(aq)} + 16H^+$	(4)

The end products of the metabolism of these microorganisms are Fe(III) and H_2SO_4. (Table 4.1) The decrease in pH resulting from the production of H^+ during this process can dissolve mineralized U(IV), the resulting U^{4+} can then be oxidized to the mobile UO_2^{2+} by Fe(III) as demonstrated by the reduction half reactions under acidic conditions (Table 4.2). The overall reaction leads to the eventual release of U(VI) into the environment.

Table 4.2 Selected Standard Reduction Potentials[5].

Half Reaction	E^0(V)
$Mn^{3+} + e^- \Leftrightarrow Mn^{2+}$	1.560
$Pu^{4+} + e^- \Leftrightarrow Pu^{3+}$	1.006
$PuO_2^{2+} + 4H^+ + 2e^- \Leftrightarrow Pu^{4+} + 2H_2O$	1.000
$Fe^{3+} + e^- \Leftrightarrow Fe^{2+}$	0.771
$NpO_2^{2+} + 4H^+ + e^- \Leftrightarrow Np^{4+} + 2H_2O$	0.567
$UO_2^{2+} + 4H^+ + 2e^- \Leftrightarrow U^{4+} + 2H_2O$	0.273
$S_{(s)} + 2H^+ + 2e^- \Leftrightarrow H_2S_{(aq)}$	0.144
$TcO_4^- + 2H_2O + 3e^- \Leftrightarrow TcO_{2(s)} + 4OH^-$	-0.366

In fact, these reactions were encouraged in uranium mining as a way to recover uranium from poor grade ores until it was determined that not all of the released uranium could be solubilized; and many uranium mill tailings sites still represent an ongoing source of uranium contamination (§ 3.1.1.3).

Fungi, which often release organic acids (citric and oxalic acid are the most common), can also, in theory, catalyze the indirect oxidative leaching of uranium because they acidify the local environment as well as complex U^{4+}. The fungal species *Aspergillus* and *Penicillum* are known to produce citric acid in concentrations as high as 600 mM[6]. Although uranium complexation with fungal organic acids has not been directly studied as it has been demonstrated for other toxic metals like Cd,

Zn, Ni, Pb and Cu[7], it is likely that these bioproduced organic acids will have similar effects on uranium as their chemical counterparts, particularly those elements with complexation chemistry similar to uranium.

4.2.2. Direct Oxidation

Direct oxidation of uranium has not been widely studied. The investigation of bacteria capable of oxidizing hard acid metals chemically similar to uranium such as Fe and Mn indicates that there might be more than one bacterial species that directly catalyzes the oxidation of uranium. (§ 9) To date, the only bacteria known to directly catalyze the oxidation of uranium is *Thiobacillus ferrooxidans*[8]. *T. ferrooxidans* is thought to catalyze the direct oxidation of uranium by the following mechanism:

$$UO_2 + 0.5O_2 + 2H^+ \rightarrow UO_2^{2+} + H_2O$$

In pure cultures *T. ferrooxidans* was found to oxidize uranium at a rate of 0.077 μM U^{4+} oxidized/min/mg protein[8]. Growth of *T. ferrooxidans* solely on the oxidation of uranium has been hypothesized from free energy calculations, but has yet to be determined *in vitro*[9]. Such findings, however, do suggest a mechanism for direct uranium oxidation in the environment, although it is most likely that in mill tailings piles the total oxidation of uranium will be due to a combination of both direct and indirect microbial processes.

4.3. Bacterial Reduction of Uranium

Compared to bacterial oxidation of uranium, much more is known about the process of bacterial uranium reduction. As this reaction is generally considered favorable for environmental remediation by creating an insoluble and less mobile uranium product, and has been suggested[10] and practiced[11] as a mechanism for remediation of uranium contamination, it stands to reason that much more scientific effort has been focused on understanding bacterial uranium reduction. There are several species of bacteria that are now known to directly catalyze the reduction of uranyl[12], most of which are classified as either iron or sulfate reducers and are often capable of reducing several different metals and of utilizing many types of electron donors.

4.3.1. Indirect Reduction

While biological reduction of uranium is primarily a direct process, there are a few instances of indirect uranium reduction. Microbially produced humic acids are known to reduce Fe(III)[13] and other metals. Humic acids are also known to complex U(VI)[14]

although they do not reduce uranium on laboratory time scales[15]. It is thought that in the environment, humic acids will be reduced first by contact with Fe(III) before reduction of U(VI) can occur[16], and some uranium ore deposits are associated with organic material, where deposition is thought to occur via complexation followed by reduction[17].

In marine sediments and sedimentary rock, uranium deposits are often associated with sulfide minerals. This association led to the previous assumption that abiotic sulfide reduction was the primary factor in the deposition of uranium in marine sediments[18]. In these environments bacterial sulfate reduction is the source of the sulfide. Abiotic sulfide reduction of uranium has been demonstrated *in vitro* at environmentally high levels of uranium (>3 mg/l)[1], however in the environment low levels of uranium persist even in the presence of sulfide. Not only that, but it has more recently been established that sulfate reducing bacteria can also directly catalyze the reduction of uranium. (§ 4.3.2) Although sulfide reduction of uranium is energetically possible (Table 4.2), these recent developments have led to the assumption that uranium reduction in the environment is considered to be almost wholly a biologically catalyzed process[16].

4.3.2. Direct Reduction

Iron and sulfate reducing bacteria are the two main types of bacteria known to directly catalyze the reduction of uranium[†].

4.3.2.1. Sulfate Reducing Bacteria

Sulfate reducing bacteria (SRB) are dominant in sulfate rich anaerobic environments like marine sediments. As a group, SRB couple the oxidation of organic compounds to the reduction of sulfate to sulfide. (Table 4.3) There are several species of sulfate reducing bacteria known to catalyze the reduction of uranium, but a majority falls into either the genus *Desulfotomaculum* or *Desulfovibrio*. *Desulfotomaculum* reduce sulfate by the following mechanism (although it can grow on other organic compounds like lactate and valerate):

$$2CH_3CH_2CH_2COO^- + SO_4^{2-} \rightarrow 4CH_3COO^- + HS^- + H^+$$

[†] While mesophillic, neutrophillic iron and sulfate reducing bacteria are not the two sole groups of bacteria known to reduce uranium, they do represent the most environmentally significant portion of uranium reducing bacteria.

The $\Delta G^{\circ\prime}$ for this reaction is -28 kj/mol[19] other electron donors will yield slightly different values of $\Delta G^{\circ\prime}$. A similar mechanism for uranium reduction is as follows:

$$CH_3CH_2CH_2COO^- + UO_2^{2+} + 2H_2O \rightarrow 2CH_3COO^- + UO_2 + 5H^+$$

The $\Delta G^{\circ\prime}$ for this reaction is -130 kj/mol! This organism has also been reported to be able to couple the reduction of uranium to cellular growth at a rate of approximately $5.14*10^6$ cells/day[19], although if true, is the only known SRB to do so.

Collectively, much more is known about the reductive mechanisms of the more widely studied *Desulfovibrio sp.*, which are abundant in the environment, easy to culture in the laboratory and many of its species' genomes have been fully sequenced[20]. Experiments by Lovley[21] showed that a c_3 type cytochrome is involved in the direct reduction of uranium by *D. vulgaris*. Soluble cell extracts lost their uranium reducing abilities when passed over a cation exchange column designed to remove cytochrome c_3. Uranium reduction was restored upon re-addition of cytochrome c_3 eluent to the soluble cell extracts. This organism was not capable of growth using U(VI) as the sole electron acceptor. The c_3 type cytochromes in *Desulfovibrio sp.* had been previously shown to act as intermediates in the electron shuttling of various sulfur compounds. The c_3 type cytochrome in *Desulfovibrio* is a small tetra-heme enzyme with a low redox potential and is located in the periplasmic space of the organism. Consistent with this location was the finding that whole cell fractions of *D. vulgaris* precipitated U(IV) at the cell surface. Discovery of an enzyme in the reduction pathway of uranium is an important piece of the puzzle for biological uranium reduction. In the future it could be possible to isolate the gene(s) in this pathway and transform other organisms with uranium reductive capabilities, or to screen for organisms with the potential for enhanced uranium reduction capabilities. It has also been suggested that cytochrome c_3 could be mass-produced and utilized in a fixed-enzyme bioreactor for cell free reduction of uranium[21].

Table 4.3 Energetics of selected microbial metabolic redox couples.

Reaction	$\Delta G^{\circ\prime}$ (kj/mol)	Ref
$2CH_3CH_2CH_2COO^- + SO_4^{2-} \rightarrow 4CH_3COO^- + HS^- + H^+$	-28	19
$CH_3CH_2CH_2COO^- + UO_2^{2+} + 2H_2O \rightarrow 2CH_3COO^- + UO_2 + 5H^+$	-130	19
$H_2 + UO_2^{2+} \rightarrow 2H^+ + UO_2$	-79.6	
Lactic $acid_{(aq)} + 0.5\ SO_4^{2-} + H^+ \Leftrightarrow$ Acetic $acid_{(aq)} + 0.5H_2S_{(aq)} + CO_{2(aq)} + H_2O$ (*Desulfotomaculum*)	-86.6	22
Butanoic $acid_{(aq)} + 1.5\ SO_4^{2-} + 3H^+ \Leftrightarrow$ Acetic $acid_{(aq)} + 1.5H_2S_{(aq)} + 2CO_{2(aq)} + 2H_2O$ (*Desulfotomaculum*)	-66.51	22
$H_{2(aq)} + UO_2^{2+} \Leftrightarrow 2H^+ +$ $Uraninite_{(s)}$ (*Shewanella oneidensis*)	-176.83	22
$Uraninite_{(s)} + 0.5O_{2(aq)} + 2H^+ \Leftrightarrow UO_2^{2+} + H_2O$	-86.35	22
Acetic $acid_{(aq)} + 2H_2O + 4UO_2^{2+} \Leftrightarrow 4Uraninite_{(s)} + 2CO_{2(aq)} + 8H^+$ (*Geobacter metallireducens*)	-537.53	22
Lactic $acid_{(aq)} + 3H_2O + 6UO_2^{2+} \Leftrightarrow 6Uraninite_{(s)} + 3CO_{2(aq)} + 12H^+$ (*Shewanella oneidensis*)	-866.29	22
$S_{(s)} + 6Fe^{3+} + 4H_2O \Leftrightarrow HSO_4^- + 6Fe^{2+} + 7H^+$ (*Thiobacillus ferrooxidans*)	-523.28	22
$H_{2(aq)} + 2Fe^{3+} \Leftrightarrow 2Fe^{2+} + 2H^+$ (*Geobacter sulfurreducens*)	-246.16	22
$2FeS_{(s)} + 7.55O_{2(aq)} + H_2O \Leftrightarrow 2Fe^{3+} + 4\ SO_4^{2-} + 2H^+$ (*Thiobacillus ferrooxidans*)	-2658.64	22

4.3.2.2. Iron Reducing Bacteria

The second group of bacteria known to directly catalyze the reduction of uranyl to uraninite are the iron-reducing bacteria. Of this group, members of the genus *Geobacter*, and several *Shewanella* species including *S. oneidensis* and *S. alga*, have been shown to reduce uranium. Coupling the oxidation of H_2, the overall reduction of uranium in *Shewanella* is:

$$H_2 + UO_2^{2+} \rightarrow 2H^+ + UO_2$$

The $\Delta G^{\circ\prime}$ for this reaction is -176.83 kj/mol (Table 4.3). Several of the iron-reducing bacteria can also couple the reduction of uranium to the incomplete oxidation of organic carbon compounds like lactate, albeit with a greater $\Delta G^{\circ\prime}$. Both *Geobacter* and *Shewanella* can utilize the energy gained from uranium reduction for growth[23], a fact which distinguishes them from the SRB.

The mechanisms of uranium reduction in iron reducing bacteria are less well known than in SRB, but uranium reduction is also thought to be mediated by a c-type cytochrome. Whole cells of *G. sulfurreducens* were treated with a protease to destroy any protein activity on the outer membrane. Treatment with the protease did not result in a decrease in uranium reduction however[24], leading the authors to conclude that in *G. sulfurreducens* uranium reduction is mediated by an intracellular electron transfer. This is

further supported by transmission electron microscopy images showing UO_2 localization within the cell membrane.

In both types of bacteria the uranium reduction pathways appear at least in part to be separate from the more common pathways of iron and sulfur reduction. Although the reasons as to why these bacteria developed independent pathways remains unclear, both reduction of uranium by sulfate and iron-reducing bacteria offers a potentially cheap, effective, and environmentally effective means of immobilizing uranium contamination. Furthermore, uranium can prove to be a useful probe in examining metal reduction by bacteria.

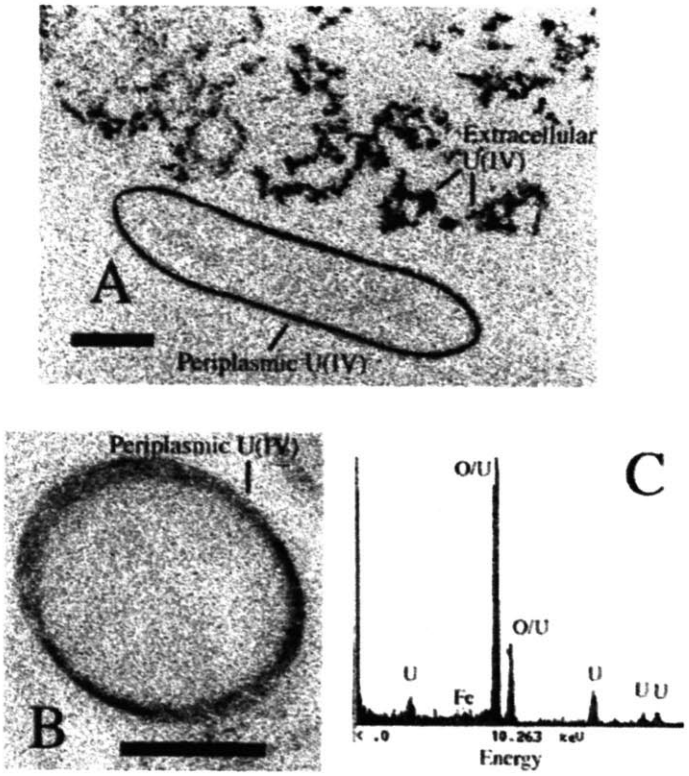

Figure 4.2 TEM's showing U(IV) precipitate formed by *G. sulfurreducens*. A) periplasmic vs extracellular U(IV) B) a detail of periplasmic U(IV) Bar=0.5 μm C) Energy Dispersive X-Ray Spectrum of the U(IV) precipitate[24]

4.4. Microbial Interactions with other Radionuclides

Besides uranium, several species of microorganisms are known to directly affect the oxidation state of other radionuclides such as technetium, plutonium, and neptunium. These interactions are interesting not only from an environmental standpoint, because bacteria might also help us to immobilize these radionuclides as well, but also from an evolutionary standpoint, because it is unique that microorganisms have the capabilities to chemically interact with anthropogenic

elements. Furthermore, the redox routes expressed through bacterial reduction may prove useful in manipulating these radionuclides in separation schemes.

4.4.1. Technetium

Technetium is present in the environment as a result of contamination due to weapons testing, nuclear fuel (re)processing, and radioactive waste storage. Technetium is of particular environmental concern because of its long half life ($t_{1/2}$ ^{99}Tc=0.214 My) and high solubility as the pertechnetate species (TcO_4^-). Although technetium has complex redox chemistry, the predominant species in the environment will be Tc(VII) and Tc(IV), with the pertechnetate forming Tc(VII) the most common in oxygenated environments. (Figure 4.3)

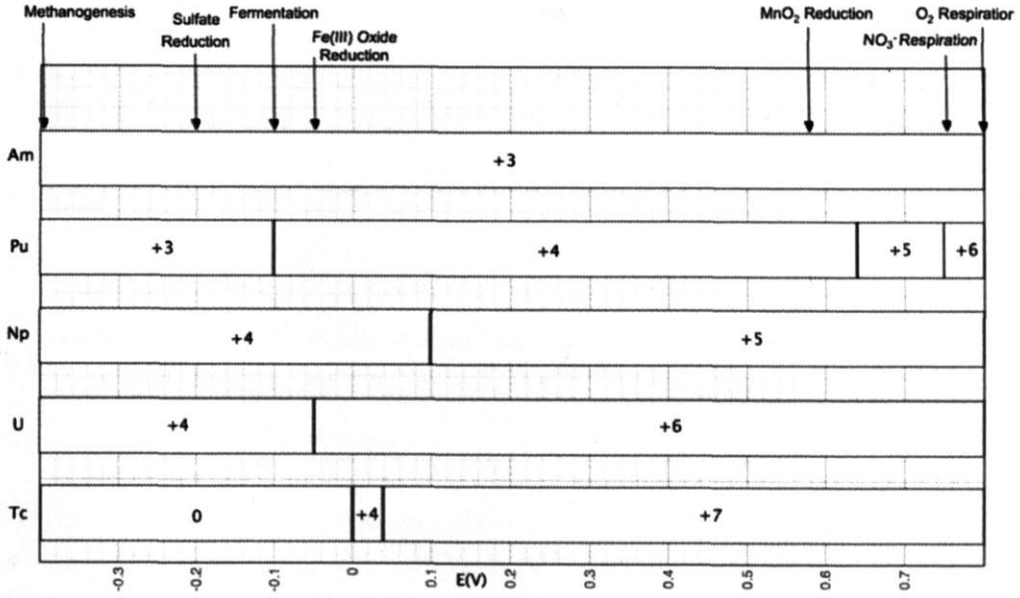

Figure 4.3 Expected dominant oxidation states of the selected actinides and technetium as a function of standard reduction potential at pH 7. Arrows at show the expected redox potentials associated with common microbial electron-acceptor couples. (Adapted from Banaszak et al[25])

There are several species of bacteria known to reduce Tc(VII), of these, *Shewanella*, *Geobacter*, *Desulfovibrio*, and *Escherichia coli*, are amongst the most commonly studied[24]. In these bacteria, Tc reduction is either solely dependent on H_2 as an electron donor, or the reduction proceeds much slower when organic carbon is used as an electron donor. With hydrogen as an electron donor, the reduction of Tc proceeds as follows:

$$TcO_4^- + H_2 + H^+ \rightarrow TcO_2 \bullet nH_2O_{(s)} + H_2O$$

Reduction of Tc in these bacteria is also thought to be mediated by a periplasmic hydrogenase complex. TEM images similar to Figure 4.2 show TcO_2 precipitates in the periplasmic space[26]. The determination of the enzymatic mechanism for Tc reduction also provides a means of screening for natural mutants in the environment capable of enhanced Tc immobilization.

Technetium may also be reduced indirectly by Fe(II) generated as a result of bacterial (in this case *Geobacter sulfurreducens*) Fe(III) reduction[26] (Figure 4.4). Both reactions can occur simultaneously in the environment, however direct Tc reduction by bacteria occurs much faster than abiotic reduction. It is also energetically possible for U(IV) to reduce Tc(VII). (Table 4.2)

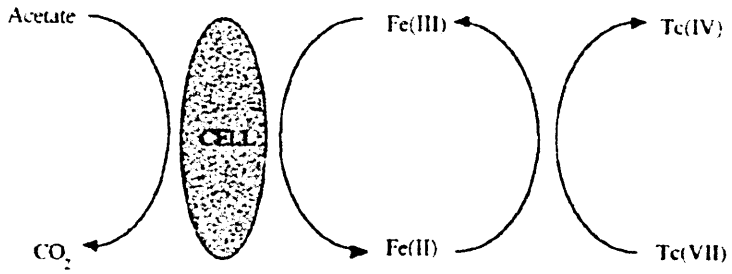

Figure 4.4 The proposed mechanism of indirect biological Tc(VII) reduction[24].

This could potentially allow the co-precipitation of U(IV) and Tc(IV), where bacteria directly reduce U(VI) to U(IV) followed by abiotic reduction if Tc(VII) by U(IV). In a co-precipitation study using *G. sulfurreducens*, the U(VI) reduction rate was similar with and without Tc(VII) while 90% of the total 1 mM U(VI) was reduced concomitantly with 94% of the 50 μM Tc(VII)[24]. Such co-precipitation might provide a mechanism for remediation of both uranium and technetium, which often occur together in radioactive waste and contaminated sites.

4.4.2. Plutonium

Like technetium, plutonium also has a complex environmental behavior; and because it is both radiologically and chemically toxic it is also crucial to understand the speciation and mobility of plutonium in the environment. In the environment, plutonium can be found in oxidation states from III to VI, can hydrolyze, form complexes, precipitate and adsorb to surfaces. At circumneutral pH under oxic conditions Pu(IV)/(V) are the most common, while under anoxic conditions, Pu(III)/(IV) will tend to dominate (Figure 4.3).

Rusin et al. used two *Bacillus* strains to show that plutonium reduction can be directly mediated by iron-reducing bacteria[27]. Over 90% of the initial (0.4-1.6 μM) hydrous PuO_2 was solubilized to Pu(III) over a period of 6-7 days. This degree of solubilization, however, was only achieved in the presence of a chelating agent, NTA (nitrolotriacetic acid). Cell suspensions lacking NTA only solubilized about 45% of PuO_2 and cell free suspensions with and without NTA only solubilized about 4.5% and 1.3% of the total plutonium, respectively. Thus, the reductive solubilization was attributed to the *Bacillus*, albeit with significant enhancement in the presence of NTA. Although the exact mechanism of the microbial dissolution of PuO_2 was unclear, the authors speculated that initially, the reduction forms a Pu(III)-NTA complex which over time abiotically reoxidizes to form a soluble Pu(IV)-NTA complex. They further suggest that Pu(III) complexation with NTA may stabilize the Pu(III) and/or prevent adsorption to the soluble species to the PuO_2 solid surface.

Direct bacterial reduction of Pu(V) and Pu(VI) has also been observed in the iron-reducing bacteria *S. oneidensis*, *S. putrefaciens*, and *G. metallireducens*[28]. Reduction of Pu was observed by measuring disappearance of soluble plutonium species using liquid scintillation counting and optical spectroscopy. Although some slow abiotic reduction of Pu(VI) and speciation changes were observed, a majority of the plutonium reduction was attributed to direct microbial reduction.

Bacterial oxidation of plutonium is energetically possible for Pu(III) and Pu(IV) when the redox couples of Pu are compared to those of bacterial oxidation of Fe(II) and Mn(II). (Table 4.2) Although such interactions are theoretically possible, they have not been demonstrated *in vitro*.

Due to the complex aqueous chemistry of plutonium, there are also multiple pathways by which plutonium reduction or oxidation occurs indirectly as a result of microbial metabolism. For example, because the Pu(IV) complex is the most stable (Figure 4.1), Pu(III), Pu(V), and Pu(VI) exposure to the siderophore DFB (desferrioxamine B) resulted in the formation of the Pu(IV)-DFB complex[29]. Other indirect Pu reduction mechanisms include reduction of Pu by humic acids, and reductive dissolution of Pu(IV) by bacterially produced Fe(II) and Mn(II).

4.4.3. Neptunium and Americium

Comparatively less is known about biological interactions of Neptunium and transplutonium elements. However, some inferences can be made about the effects that microorganisms might have on the heavier actinides based upon their environmental chemistry and what is known about bacterial interactions with Tc, U and Pu.

Neptunium and Americium can exist in oxidation states from III to VI, but in the environment, their common oxidation states are V and III respectively (Figure 4.3). Although Americium is not truly redox active under typical environmental conditions, bacteria may still affect Am mobility indirectly. In the absence of complexing agents at circumneutral pH, the actinyl species are the most soluble, followed by the trivalent state, with the tetravalent state being the least soluble. Neptunium and Americium will also form stable complexes with several ligands of biological origin, including OH-, CO_3^{2-}, SO_4^{2-}, PO_4^{3-}, with the strength of the complex being in general the greatest for the tetravalent state, followed by the trivalent, hexavalent, then pentavalent.

Based on the E^0 of the half-reaction, it is conceivable that microorganisms will be able to reduce Np(V) to Np(IV). (Table 4.2) Indeed, there are a few studies that have demonstrated this. Banaszak et al.[30], found that pure and mixed cultures of sulfate-reducing bacteria were able to reduce Np(V) and precipitate Np(IV). *S. putrefaciens* has also been shown to reduce Np(V) to Np(IV), the soluble Np(IV) was then precipitated by phosphate produced by a *Citrobacter sp*[31]. It is also possible that Np(V) may be reduced indirectly by bacterially produced Fe(II) and Mn(II).

4.5. Conclusion

In the environment, it is microorganisms that are the primary governors of local redox chemistry and thusly they can affect changes in actinide (and technetium) oxidation state both directly and indirectly. The mobility of the radionuclides in the environment is largely determined by oxidation state, and, excluding americium, there are at least two oxidation states for all of the common actinides and technetium under environmental conditions, as well as several chemical species for each oxidation state, giving these elements a diverse and complicated redox chemistry. In order to properly determine and/or model the speciation and mobility of a particular radionuclide in the environment it will therefore be essential to understand how bacteria influence the oxidation and reduction of these elements.

4.6. References

[1] **Mohaghegi, A., D. M. Updegraff, M. B. Goldhaber.** (1985) The Role of Sulfate Reducing Bacteria in the Deposition of Sedimentary Uranium Ores. Geomicrobiol. J. **4:**153-173

[2] **Madsen, E. L.** (1998) Epistemology of Environmental Microbiology. Env Sci Tech. **32:** 429-439.

[3] **Benedict, M., T. H. Pigford, H. W. Levi** (1981) Nuclear Chemical Engineering 2nd Ed. McGraw Hill Ltd. NY NY. 8.

[4] **Keith-Roach, M. J., F. R. Livens eds.** (2002) Microbial Interactions with Metals/Radionuclides: The Basis of Bioremediation. Interactions of Microorganisms with Radionuclides. Elsevier Science Ltd, Oxford UK. 179-203.

[5] **Harris, D. C.** (1995) Quantitative Chemical Analysis 4th Ed. W. H. Freeman and Co. NY NY. AP32-AP41.

[6] **Poole, R. K. ed.,** (1999) Fungal Production of Citric and Oxalic Acid: Importance in Metal Speciation, Physiology and Biogeochemical Processes. Advances in Microbial Physiology. Academic Press, San Diego, Ca. **41:** 47-79.

[7] **Poole, R. K. ed.,** (1999) Fungal Production of Citric and Oxalic Acid: Importance in Metal Speciation, Physiology and Biogeochemical Processes. Advances in Microbial Physiology. Academic Press, San Diego, Ca. **41:** 47-79.

[8] **DiSpirito, A. A., O. H. Tuovinen.** (1982) Kinetics of Uranous Ion and Ferrous Iron Oxidation by *Thiobacillus ferrooxidans*. Arch. Microbiol. **133:**33-37.

[9] **DiSpirito, A. A., O. H. Tuovinen.** (1982) Uranous Oxidation and Carbon Dioxide Fixation by *Thiobacillus ferrooxidans*. Arch. Microbiol. **133:**28-32.

[10] **Lovley, D.R., E. J. P. Phillips, Y. A. Gorby, E. R. Landa.** (1991) Microbial Reduction of Uranium. Nature. 350:413-415.

[11] **Anderson, R. T., et al.** (2003) Stimulating the *In Situ* Activity of *Geobacter* Species to Remove Uranium from the Groundwater of a Uranium-Contaminated Aquifer. Appl. Environ. Microbiol. **69:** 5884-5891.

[12] **Lovley, D. R.** (1993) Dissimilatory Metal Reduction. Annu. Rev. Microbiol. **47:**263-290.

[13] **Nevin, K. P., D. R. Lovley.** (2000) Potential for Nonenzymatic Reduction of Fe(III) During Microbial Oxidation of Organic Matter Coupled to Fe(III) Reduction. Env. Sci. Technol. **34:**2472-2478.

[14] **Shanbahg, P.M., G. R. Choppin.** (1981) Binding of Uranyl by Humic Acid. J. Inorg. Nucl. Chem. **43:**3369-3372.

[15] **Wood, S.A.** (1996) The Role of Humic Substances in the Transport and Fixation of Metals of Economic Interest (Au, Pt, Pd, U, V). Ore. Geol. Rev. **11:**1-31.

[16] **Finneran, K. T., R. T. Anderson, K. P. Nevin, D. R. Lovley.** (2002) Potential for Bioremediation of Uranium-Contaminated Aquifers with Microbial U(VI) Reduction. Soil. Sed. Contam. **11:**339-357.

[17] **Nakashima, S., J. R. Disnar, A. Perruchot.** (1999) Precipitation Kinetics of Uranium by Sedimentary Organic Matter Under Diagenetic and Hydrothermal Conditions. Econ. Geol. **94:**993-1006.

[18] **Jensen, M. L.,** (1958) Sulfur Isotopes and the Origin of Sandstone-Type Uranium Deposits. Econ. Geol. **53:**598-616.

[19] **Tebo, B. M., A. B. Obraztsova.** (1998) Sulfate-reducing Bacterium Grows with Cr(VI), U(VI), Mn(IV), and Fe(III) as Electron Acceptors. FEMS Microbiol. Lett. **162:**193-198.

[20] **Copeland, A. et al.,** (2005) Complete sequence of *Desulfovibrio desulfuricans G20.* US DOE Joint Genome Institute. Genbank ID: CP000112.

[21] **Lovley, D. R., P. K. Widman, J. C. Woodward, E. J. Phillips.** (1993) Reduction of Uranium by Cytochrome c_3 of *Desulfovibrio vulgaris.* Appl. Environ. Microbiol. **59:**3572-3576.

[22] **Amend, J. P., E. L. Shock.** (2001) Energetics of Overall Metabolic Reactions of Thermophillic and Hyperthermophillic Archea and Bacteria. FEMS Microbiol. Rev. **25:**175-243.

[23] **Lovley, D. R., E. J. P. Phillips, Y. A. Gorby, E. R. Landa.** (1991) Microbial Reduction of Uranium. Nature. **350:**413-415.

[24] **Llyod, J. R. et al.** (2002) Reduction of Actinides and Fission Products by Fe(III) Reducing Bacteria. Geomicrobiol. J. **19:**103-120.

[25] **Banaszak, J. E., B. E. Rittmann, D. T. Reed.** (1999) Subsurface interactions of actinide species and microorganisms: Implications for the bioremediation of actinide-organic mixtures. J. Radioanal. Nuc. Chem. **241:**385-435.

[26] **Lloyd, J. R., V. A. Sole, C. V. G. Van Praagh, D. R. Lovley.** (2000) Direct and Fe(II)-Mediated Reduction of Technetium by Fe(III)-Reducing Bacteria. Appl. Environ. Microbiol. **66:**3743-3749.

[27] **Rusin, P. A., et al.,** (1994) Solubilization of Plutonium Hydrous Oxide by Iron-Reducing Bacteria. Environ. Sci Technol. **28:**1686-1690.

[28] **Neu, M. P., G. A. Icopini, H. Boukhalifa.** (2005) Plutonium Speciation Affected by Environmental Bacteria. Raciochim. Acta. **93:**705-714.

[29] Ruggerio 2000 paper...

[30] **Banaszak, J. E., D. T. Reed, B. E. Rittmann.** (1999) Reduction and Precipitation of Neptunium(V) by Sulfate-Reducing Bacteria. Migration 1999 Conference Proceedings, Lake Tahoe Nv.

[31] **Lloyd, J. R., P. Yong, L. E. Macaskie.** (2000) Biological Reduction and Removal of Np(V) by Two Microorganisms. Environ. Sci. Technol. **34:**1297-1301

5. Utilization of Bacteria for Radionuclide Remediation

Many of the physical and chemical properties of bacteria make them ideal candidates for use as tools in our efforts to immobilize and remove harmful radionuclides from the environment. The variety and nature of bacterial interactions with radionuclides can potentially allow us to tailor a remediation scheme to both the specific nature of the site as well as to the radionuclide present.

5.1. Suggested Methods

Bacteria can interact with radionuclides in the environment in a variety of ways, both actively via mechanisms like direct reduction and passively, for example, by biosorption. The mechanisms of interaction will be dependent on the local chemistry of the environment, the types of bacteria present, and the speciation of the radionuclide in question. Not only that, but several active and passive interactions may occur simultaneously. Because the design of a remediation scheme must take into account all of these factors, it is important to understand how each interaction can contribute to the extent of radionuclide immobilization or removal.

5.1.1. Passive Methods

Passive radionuclide immobilization can occur when bacteria sequester these metals through adsorption and mineralization.

5.1.1.1. Biosorption

Adsorption occurs through complexation of the radionuclide to bacterial biomass. In gram negative bacteria, the outer cell membrane is composed of polysaccharide, glycoprotein, lipopolysaccharide, and protein groups, generally creating an overall net negative charge at the cell surface[1] (Figure 5.1). The negative charge attracts cations that can then adsorb to hydroxyl, carboxylate, and phosphate functional groups. The benefit to radionuclide adsorption by biomass is that it is a not necessarily a species specific interaction, nor does it require living biomass.

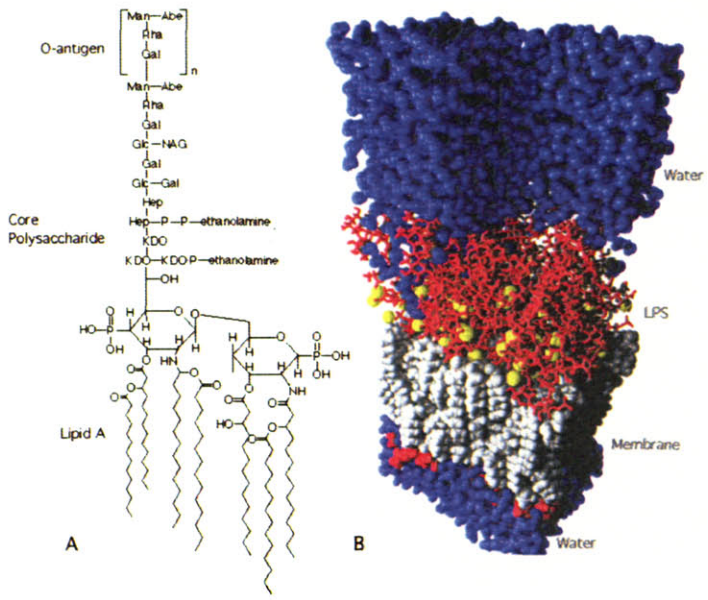

Figure 5.1 (A) a chemical structure of lipopolysaccharide. (B) a molecular model of the membrane from *Pseudomonas aeruginosa*[1].

Dead biomass can be advantageous because radiotoxic (or metal toxic) effects need not be taken into consideration. It has been suggested that spent brewers yeast might provide a cost effective matrix for biomass sorption because it is essentially a waste product from another process[2]. There are however, several drawbacks to biosorption. Contaminated waste-streams often contain high radionuclide concentrations, which can lead to saturation of bacterial sorption sites. On a per mass basis, biomass sorption is a relatively inefficient process compared to other immobilization mechanisms because the ratio of sorbed radionuclide to biomass is small. Not only that but, biomass sorption will only be effective for cationic species, and although many of the radionuclides in the environment will be present as cations, pertechnetate (TcO_4^-) is one anion of significance in many radionuclide containing waste-streams. In order to effectively adsorb technetium to biomass it would first need to be reduced to TcO_2.

In a typical biosorption remediation scheme, bacterial biomass is first adhered onto a polymeric inert support matrix. Some common materials used for support matrices are polymers like alginate, polyacrylamine, polysulfone, silica gel, cellulose, and glutaraldehyde[3].

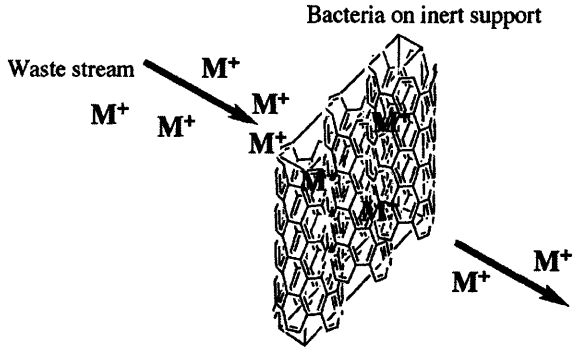

Figure 5.2 Schematic of metal adsorbtion by bacterial biomass.

The radionuclide containing waste-stream is then passed through the biomass. Figure 5.2 shows how metals might be removed from a waste stream by adsorption to bacterial biomass. This type of sorption is a reversible process, providing ony a semi-permanent option. Radionuclides immobilized on biomass must eventually be removed from the environment for further processing (i.e. combustion) to prevent remobilization. Attempts to engineer more efficient sorptive biomass have been successful for non-radioactive toxic metals[4], though these techniques have not been applied to radioactive elements. While biosorption remains an inefficient process for radionuclide immobilization, it is an inexpensive alternative that has the potential for engineered improvement in order to enhance radionuclide specificity and can easily be applied to larger-scale operations.

5.1.1.2. Biomineralization

Biomineralization is the precipitation of solid-minerals from solution using biological processes or materials. Passive biomineralization can be catalyzed by the bacterial surface serving as a nucleation site for mineral precipitation, by excretion of precipitating ligands like carbonate, phosphate, sulfide, or organic ligands, by indirect release of these ligands from surrounding minerals through direct metabolic action, by changing the local pH, or through a combination of any of these mechanisms. When bacteria act as solely a nucleation site for mineralization living biomass is not always necessary, but production of precipitating ligands is usually necessitated by metabolically active cells. In all cases, however, the extent of radionuclide biomineralization will be dependent upon factors that affect the solubility product of the metal such as, the local environmental chemistry, radionuclide concentration and speciation.

Perhaps one of the most commonly studied and most effective methods of radionuclide immobilization is by enzymatic phosphate

production. For example, *Citrobacter sp.* produces extracellular inorganic phosphate using a membrane-bound phosphatase enzyme. This enzyme catalyzes the production of phosphate by cleavage of the phosphate group from an organic phosphate donor (often glycerol-2-phosphate), causing metal phosphate precipitation on and around the cell surface.

Immobilization of U(VI), Am(III), Pu(IV), and Th(IV) by phosphate precipitation by *Citrobacter* has been demonstrated, with 100% maximum removal being obtained for uranium and americium[5]. Uranium removal in a flow through bioreactor by phosphate precipitation has also been demonstrated[6]. Here, *Citrobacter* was grown in a foam matrix, placed in a column-type flow through bioreactor and challenged with U(VI).

The immobilization of uranium as a uranyl phosphate precipitate was dependent upon the flow rate through the reactor, with slower flow rates leading to greater U(VI) removal, phosphatase production, biomass surface area and temperature. Although not directly addressed in this paper, uranium biomineralization will also be dependent on pH. Barring introduction of acid, chelating agents or phosphate consuming sources, actinide-phosphate precipitates should also be relatively stable for long periods of time in the environment. While the process of radionuclide immobilization and remediation by phosphate precipitation is a relatively simple and effective for removal of cationic actinide species (especially uranium), achieving the right bioreactor parameters for optimal radionuclide removal is more difficult in practice. However, such systems do offer promise for inexpensive and efficient radionuclide removal if they can be developed further.

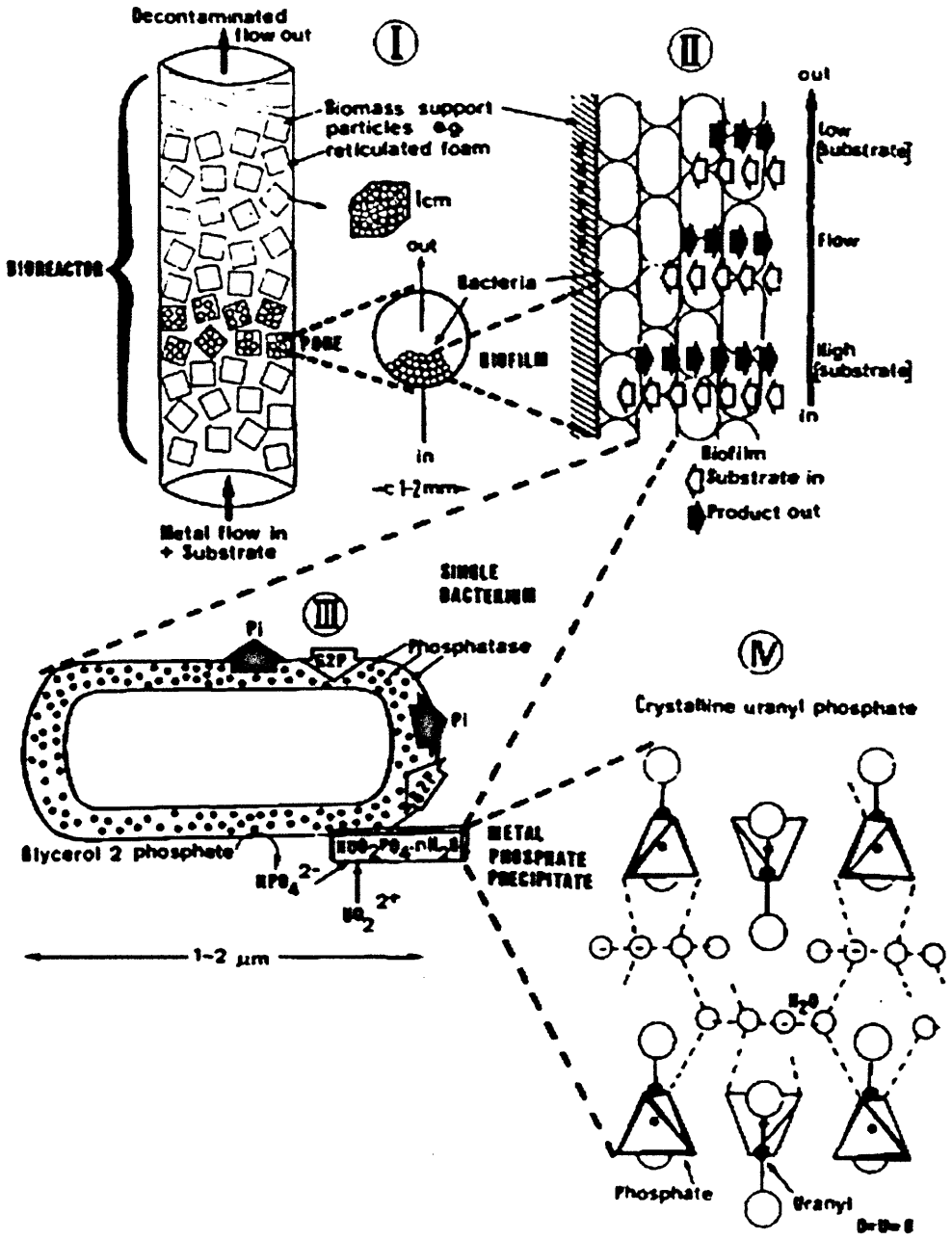

Figure 5.3 Schematic of the biofilm reactor used for metal-phosphate precipitation. I) Bacteria are immobilized on foam cubes in a flow-through column. II) Formation of a biofilm on the foam support surface. Substrate and metal diffuse into the film; products diffuse out. III) Events at a single bacterium, phosphatase cleaves G2P to release phosphate, which combines with the metal to for cell-bound metal phosphate. IV) Structure of uranyl phosphate produced by bacteria[6].

5.1.2. Active Methods

Active radionuclide immobilization can occur when bacteria precipitate metal oxides, or degrade chelating agents. Both of these mechanisms of actinide immobilization require living biomass.

5.1.2.1. Direct Microbial Reduction

Perhaps the most commonly suggested method of active bioremediation scheme is harnessing the uranium (as well as other radionuclides) reducing capabilities of iron and sulfate reducing bacteria (§ 4.3). Direct immobilization of uranium by bacteria has the potential to be an effective means of radionuclide remediation in the environment and has been demonstrated both on a laboratory scale and in the environment (§5.2, 5.3).

5.1.2.2. Degradation of Chelating Agents

Radionuclide decontamination of solid surfaces and structures often involves the copious use of chelating agents, the most common of which are, citrate ($C_3H_5O(COO)_3^{3-}$), NTA (nitrilotriacetate) and EDTA (ethylenediaminetetraacetic acid). (Figure 5.4) Of these, citrate and NTA

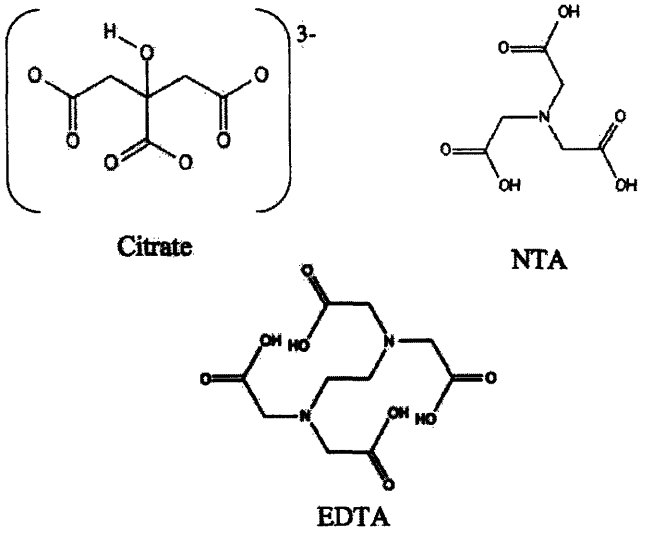

Figure 5.4 Chemical structures of commonly used remediatory chelating agents.

are readily degraded by bacteria. For example, uranyl-citrate is not easily accessed by uranium-reducing microorganisms, based on the strength and size of the complex. Bacterial decomposition of NTA and citrate chelating agents should release the radionuclides complexed to them. This can either decrease the solubility product, allowing for precipitation, or free them up for microbial reduction.

5.1.3. Bacterial Influence on Radionuclide Mobilization

Besides indirectly affecting changes in the local soil and groundwater chemistry, bacteria can also directly mobilize radionuclide minerals.

5.1.3.1. Reduction of Iron and Manganese Minerals

Uranyl readily adsorbs to many types of iron and manganese minerals; and inhibits its transport in the groundwater. Also, metals from nuclear fuel cycle and electroplating waste are often coprecipitated with ferric iron[7]. There are, however, many types of bacteria capable of reductive dissolution of iron and manganese-bearing mineral solids. In this case, the microbial reduction will solubilize the minerals, releasing any sorbed radionuclides into the surrounding environment. Ribet et al.[8] found that samples taken from the Nickel Rim mill tailings site in Ontario, Canada contained not only secondary Fe(III)-(oxy)hydroxide minerals formed due to the oxidation of sulfide, but that these minerals contained large amounts of coprecipitated or adsorbed contaminant minerals such as Ni, Cu, Pb, Cr, and several others. Extraction of these metals was done in two phases, the water-soluble and reducible (ie secondary mineral) phase. The authors found that more contaminant metal was present in the reducible phase, and their results showed that large amounts of contaminant metals could be released by reductive dissolution of secondary mineral phases; the authors calculated 13 tons of Ni and 15 tons of Cr for the Nickel Rim site. In the oxidized zone of the mill tailings, >80% of Fe, Ni, Cu, Cr, and Co could be released by reductive dissolution. While release of uranium was not studied at this site, the release of uranyl sorbed onto secondary iron minerals by reductive dissolution should be similar to the results presented by Ribet et al. for several other contaminant metals.

5.1.3.2. Production of Chelating Agents

As previously described in §4.2.1 some species of fungi produce natural radionuclide chelating agents such as citric and oxalic

acids. Although uranium complexation with fungal organic acids has not been directly studied as it has been for other toxic metals like Cd, Zn, Ni, Pb and Cu[9]. It is also likely that these bioproduced organic acids will have similar effects on uranium as their chemical counterparts. Uranium forms a citrate complex that is not readily biodegradable, with both the citrate and uranium being unavailable to bacteria that might degrade either. However, exposure to light can decompose the uranyl-citrate complex[7].

5.2. Applications *Ex Situ*

There have been several *ex situ* remediatory efforts designed to explore the effectiveness of different treatment schemes for the immobilization and removal of uranium contamination. *Ex situ* experiments can better emulate specific environmental conditions in a more controlled laboratory setting. One such effort took place at UMTRA site at Shiprock, New Mexico.

The Shiprock site was contaminated with uranium from a nearby mill tailings site, and was designated for remediation by the UMTRA. Uranium-bearing water leaches from the tailings pile into the floodplain and can make its way into the nearby San Juan River. Remediation efforts are focused on immobilization and removal of uranium from the floodplain. The purpose of the Shiprock experiment was to determine what types of additives could best stimulate the maximum reduction of uranium by bacteria.

For the experiment[10], two floodplain sites were sampled at two different times of the year (October and April). Sediment from these sites was drawn from below the water table and stored under a N_2 atmosphere to maintain anaerobic sediment conditions. Groundwater from these sites was also sampled.

An 80 g anaerobic sediment sample was added to 20 g of groundwater in an N_2 atmosphere, 2 mM of different carbon sources (acetate, lactate, formate, benzoate, and glucose) were then added to stimulate bacterial reduction of uranium. Soluble uranium in the groundwater was rapidly removed in samples amended with acetate and glucose, while there was no significant removal of uranium in samples with lactate, formate, and benzoate. Acetate amended samples at both sites showed Fe(III) and U(VI) reduction occurring concurrently over a period of 37 days, with no initial depletion of sulfate. There was little or no abiotic removal of uranium in any of the samples. Thus, the authors concluded that iron-reducing bacteria were responsible for the immobilization of uranium in the groundwater, and that addition of electron donors, like acetate, could stimulate the growth of these bacteria and subsequent reduction of uranium.

5.3. Applications *In Situ*

The ultimate goal of *in vitro* and *ex situ* research is to apply what has been learned to the immobilization and removal of uranium contamination from actual environmental sites. Bacterial reduction of uranium has been demonstrated in the

environment and various endeavours are currently underway to improve our understanding of this process in natural systems.

Anderson et al[11] determined the potential feasibility of uranium removal from a contaminated aquifer in Rifle, Co. The Rifle contamination stemmed from an ore processing facility and several large mill tailings piles leached uranium into the soil and groundwater. The groundwater eventually ends up in an aquifer that drains into the Colorado River.

A series of injection wells (6.1 m depth 3.2 cm diameter) and observation wells were drilled into a 384 m^2 area (Figure 5.5). Injection wells were placed perpendicular to the direction of the groundwater flow, with three injection points positioned at three depths below saturation. Groundwater collected upstream of the site was amended with 100 mM Na-acetate and introduced into the injection wells at a rate of approximately 2 mL/min from June to October 2002. A series of observation wells were placed such that they corresponded to roughly 4, 9, and 18 days of groundwater flow. Control wells were placed upstream of the injection wells.

Groundwater samples were collected at regular intervals during the course of the experiment and monitored for U(VI), bromide, nitrate, sulfate, sulfide, acetate, and iron concentration. Filtered groundwater samples were also used for 16s ribosomal DNA analysis in order to determine the community structure and dominant microbial populations present in the groundwater over the course of the experiment.

After beginning injection of acetate to stimulate the growth of iron-reducing bacteria, soluble uranium concentrations began to decrease after 9 days. After 50 days soluble uranium had decreased in all 15 monitoring wells and was below the UMTRA designated limit of 0.18 μM in five of the monitoring wells. During this time uranium reduction was concurrent with Fe(II) production, while sulfate concentrations remained relatively constant. After 50 days the soluble uranium concentration began to rise along with a decrease in Fe(II) and a decrease in sulfate concentrations.

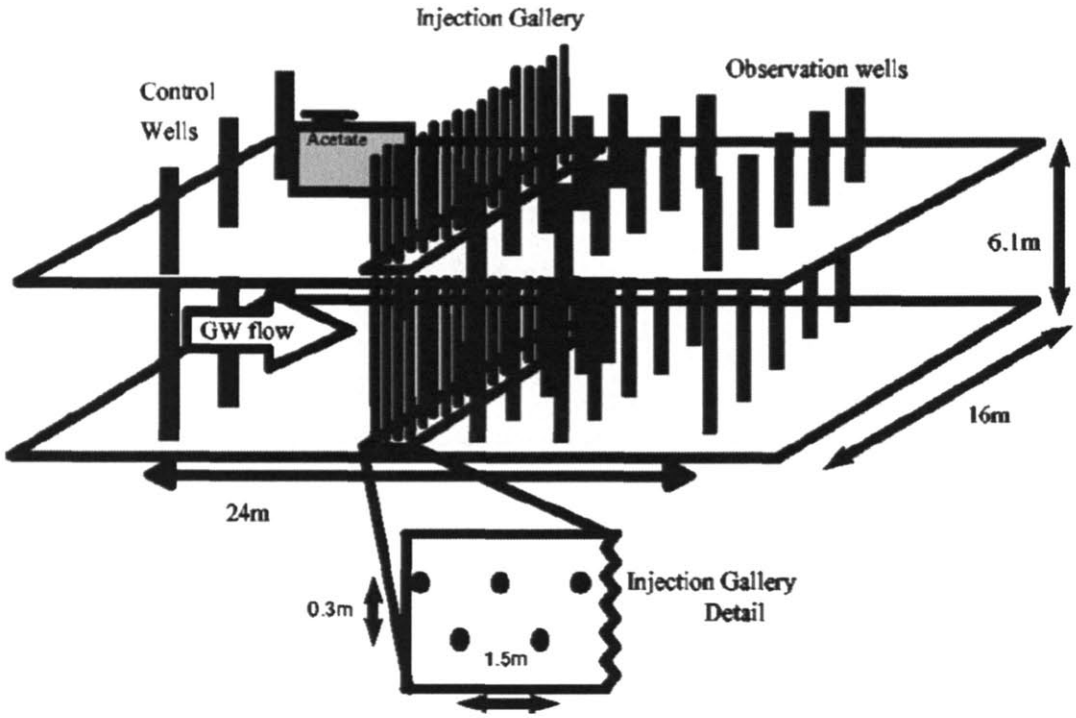

Figure 5.5 Concept and layout of the in situ test plot installed at the Old Rifle UMTRA site in Rifle, Co[11].

Microbial 16s ribosomal DNA analysis indicated dominance of microorganisms in the family *Geobacteraceae* after addition of acetate. After 17 days *Geobacteraceae* made up 89% of the microbial community and remained the dominant microbial community for the first half of the experiment. After about 50 days sulfate reducing microorganisms, namely members of the *Desulfobacteraceae*, began to dominate.

The results of this experiment demonstrated that *in situ* bioremediation of uranium is possible. Acetate addition to the groundwater stimulated the growth of iron-reducing microorganisms, causing the concurrent reduction of both uranium and iron, and in some sites uranium was immobilized to below prescribed limits. It was also apparent that the period of iron-reduction was only semi-permanent, and that after approximately two months sulfate reduction became the dominant microbial process. This occurs because as the iron is depleted locally, iron reducing microorganisms can no longer out-compete sulfate reducing bacteria for the available acetate. As sulfate reduction begins to dominate, uranium reduction either slowed down, stopped altogether, or in some cases, resolubilized. Although some species of sulfate-reducing microorganisms have been shown to reduce U(VI), they usually require lactate or hydrogen, rather than acetate, to serve as the electron donor. The authors concluded that injection of acetate was successful for the stimulation of bacterial iron and uranyl reduction, but that further study was necessary to maintain *Geobacteracae* as the dominant microbial population in the long-term.

Stimulation of bacterial reduction at this site required relatively few steps, due to the nature of the groundwater and sediment, which was anaerobic, iron-bearing, and free of significant quantities of nitrate that can inhibit the reduction of uranium. Nitrate is inhibitory to the reduction of uranium because the reduction of nitrate yields more energy for the bacteria, meaning that they will use nitrate preferentially over uranium. If nitrate is present, it should be possible to first stimulate a nitrate-reducing microbial population to remove the nitrate, and then allow for the subsequent dominance of iron-reducing bacterial populations. Although each site of uranium contamination will be unique, this experiment demonstrates that it is indeed possible to achieve uranium bioremediation in the environment.

5.4. The Future of Actinide Decontamination and Immobilization with Bacteria

There will always be a concern for the safe environmental disposal of nuclear waste, and there are many sites throughout the United States and the rest of the world contaminated with radionuclides from past activities that will require ongoing attention. We are only just beginning to be able to model and understand the complex interactions these elements have in the environment and our understanding will only improve in the future. Current research efforts to understand how to best encourage the bacterial immobilization of uranium have been successful both in controlled laboratory experiments as well as in the environment. Strict bioreduction, however, is not the only method available, and there have been many other proposed methods of radionuclide immobilization for nuclear wastes. Some other proposed methods include[5]: biosorption onto inert biomass, actinide precipitation with biophosphate; citric acid-actinide chelation to desorb actinides from soil followed by photodegredation of citric acid for controlled release and recovery of the actinides[7], bicarbonate-actinide complexation to remove actinides from the soil followed by reductive precipitation to remove the actinides from the bicarbonate waste stream, and abiotic actinide precipitation catalyzed by reactive barriers (like Fe^0)[12]. The common thread between many of these proposed ideas is that they are multi-step processes often employing actinide solubilization followed by controlled biotreatment of the waste stream. One example of such a process is given by Francis[7]; solids contaminated with uranium and other metals are treated with citric acid, which extracts the metals from the solids due to the formation of metal-citrate complexes (Figure 5.6). The resulting metal-citrate complexed waste-stream is then passed through a bioreactor, where some metal-citrate complexes are degraded by *Pseudomonas flourescens*. The metal released by this degradation will adsorb to bacterial biomass and can be removed from the bioreactor. The waste stream containing uranyl-citrate complexes not degraded in the bioreactor is then exposed to sunlight, where the uranyl-citrate complexes are photodegraded, resulting in the precipitation of UO_3. This process was found to extract ~85% of the contaminant uranium as well as other metals like Cr and Th. The nature of the process is such that it can be easily scaled up, requires little in

the way of expensive or environmentally toxic reagents, and produces no additional waste, while concentrating contaminant metals like uranium.

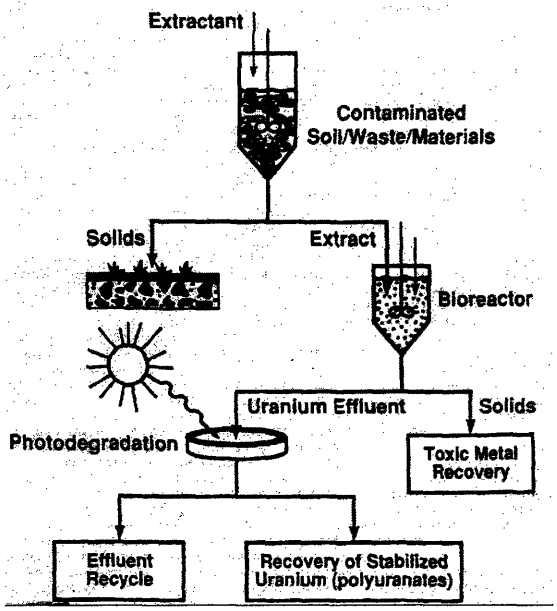

Figure 5.6 Removal and recovery of contaminant metals from solid waste as proposed by Francis[7].

A combined chemical and biological treatment approach would be more flexible and be easier to adapt to each site's specific contaminants and soil and groundwater chemistry. The treatment scheme proposed in Figure 5.6 offers not only a less-expensive and environmentally sound solution to the removal and recovery of metal and radionuclide contaminated solid wastes; but each step could be tailored by combining ligands, bacteria, concentration and degradation steps to meet the specific needs of the contamination or the site itself. Successful environmental remediation of radionuclides will most likely require a flexible treatment approach like the one proposed above that combines multiple biological and chemical efforts with minimal expense and damage to the environment. Future research is not only needed in the fundamental aspects of of actinide speciation and migration in the environment, but is also required in the environment at the sites of radionuclide contamination themselves so that we may combine both fundamental and remediation experiments for a better understanding of radionuclide immobilization and removal from the environment.

5.5. References

[1] **Paustian, T.** (1999) Microbiology and Baceteriology: The World of Microbes. Section 2-25 The cell wall surrounds and holds in the microbe. http://www.bact.wisc.edu/Microtextbook/index.php?module=Book&func=displayarticle&art_id=60

[2] **Riordan, C., M. Bustard, R. Putt, A. P. McHale.** (1997) Removal of Uranium from Solution Using Residual Brewery Yeast: Combined Biosorption and Bioprecipitation. Biotechnol. Lett. **19:**385-387.

[3] **Brar, S. K. et al.** (2006) Bioremediation of Hazardous Wastes – A Review. Pract. Periodical of Haz., Toxic, and Radioactive Waste Mgmt. **10:**59-72.

[4] **Valls M., S. Atrian, V. De Lorenzo, L. A. Fernandez.** (2000) Engineering a Mouse Metallothionen on the Cell Surface of *Ralstonia eutrophia* CH34 for Immobilization of Heavy Metals in Soil. Nat. Biotechnol. **18:**661-665.

[5] **Banaszak, J. E., B. E. Rittmann, D. T. Reed.** (1999) Subsurface interactions of actinide species and microorganisms: Implications for the bioremediation of actinide-organic mixtures. J. Radioanal. Nuc. Chem. **241:**385-435.

[6] **Macaskie, L. E., R. M. Empson, F. Lin, M. R. Tolley**. (1995) Enzymatically-Mediated Uranium Accumulation and Uranium Recovery Using; a *Citrobacter* sp. Immobilised as a Biofilm Within a Plug-Flow Reactor. J . Chem. Tech. Biotechnol. **63:**1-16.

[7] **Francis, A. J.,** (1994) Microbial Transformations of Radioactive Wastes and Environmental Restoration Through Bioremediation. J. Alloys. Compd. **213:** 226-231.

[8] **Ribet, I., C. J. Ptacek, D. W. Blowes, J. L. Jambor.** (1995) The Potential for Metal Release by Reductive Dissolution of Weathered Mine Tailings. J. Contam. Hydrol. **17:**239-273.

[9] **Poole, R. K. ed.,** (1999) Fungal Production of Citric and Oxalic Acid: Importance in Metal Speciation, Physiology and Biogeochemical Processes. Advances in Microbial Physiology. Academic Press, San Diego, Ca. **41:** 47-79.

[10] **Finneran, K. T., R. T. Anderson, K. P. Nevin, D. R. Lovley.** (2002) Potential for Bioremediation of Uranium-Contaminated Aquifers with Microbial U(VI) Reduction. Soil. Sed. Contam. **11:**339-357.

[11] **Anderson, R. T., et al.** (2003) Stimulating the In Situ Activity of *Geobacter* Species to Remove Uranium from the Groundwater of a Uranium-Contaminated Aquifer. Appl. Envion. Microbiol. **69:**5884-5891.

[12] **Morrison, S. J., P. S. Mushovic, P. L. Neisen.** (2006) Early Breakthrough of Molybdenum and Uranium in a Permeable Reactive Barrier. Environ. Sci. Technol. **40:**2018-2024.

6. Metal Fractionation in the Environment

Many of the elements on the periodic table have at least two stable isotopes present in the environment. Partitioning of stable isotopes in the environment provides a lasting signature of reaction rates and mechanisms based on the isotopic differences. By determining stable isotope ratios of various elements we can measure the age of rocks and fossils, ancient climate, and rates of metabolic reactions[1]. While these natural processes are important from a scientific point of view, the same principles underlying the separation of isotopes in the environment can be applied to the separation of radioactive isotopes for the purposes of research and medicine, as well as for the enrichment of heavy elements like uranium for nuclear fuel production.

6.1. General Theory of Isotopic Separation

One would expect that different isotopes of the same atom would behave the same when undergoing chemical interactions, due to the fact that all chemical reactions and processes occur through interaction between the electron clouds of an atom, not its nucleus. This is not entirely the case however, as the nuclear properties of an atom effect its electrical properties in small and subtle ways[2]. In fact, although isotopic separation is highly dependent on classically macroscopic properties like temperature and pressure; it is an entirely quantum mechanical process.

Classically, the kinetic energy of an atom is:

$$E = \frac{1}{2}mv^2 \qquad \text{Equation 6.1}$$

On a quantum mechanical level however, the energy of an atom can only be described by discreet energy levels[†]

$$E = (n + \frac{1}{2})h\nu \quad \text{where n = 0, 1, 2, ...} \qquad \text{Equation 6.2}$$

By applying Hooke's Law[‡], the energy for a diatomic molecule made up of atoms A and B becomes:

$$E_n = \hbar\left(\sqrt{\frac{k}{\mu}}\right)\left(n + \frac{1}{2}\right) \text{ where } \mu \text{ is the reduced mass } \frac{M_A M_B}{M_A + M_B} \qquad \text{Equation 6.3}$$

Replacing atom A by its heavier isotopic counterpart A′ will be such that:

[†] this stems from the Heisenberg Uncertainty Principle: $\Delta x \Delta p \geq h$

[‡] Hooke's Law describing the vibrational frequency of a harmonically oscillating spring: $\nu = 1/2\pi\sqrt{(k/\mu)}$. The quantum mechanical low energy states of a diatomic molecule can be approximated well using this model.

$$\mu' > \mu$$
$$\nu' < \nu$$
$$E_n' < E_n$$

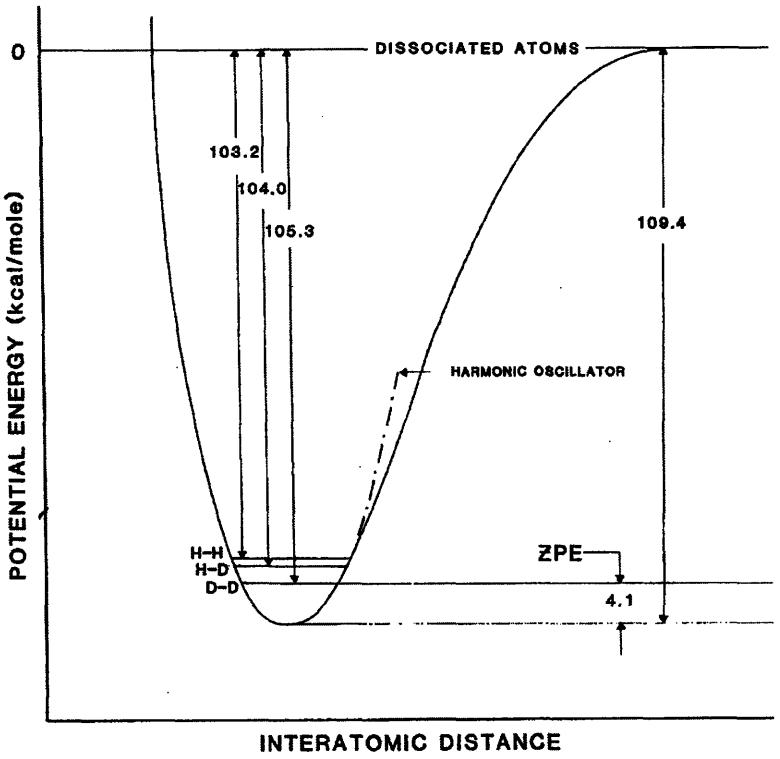

Figure 6.1 A Potential energy diagram illustrating the differing Zero Point Energies (n=0) for H-H, H-D, and D-D gas.[3]

These small energy differences are several orders of magnitude smaller than those associated with bond energies of chemical reactions, but can have noticeable effects for isotopes with large percent mass differences and under certain circumstances. Figure 6.1 illustrates these energy differences for the simple diatomic system of hydrogen, deuterium and a mixed hydrogen-deuterium gas, and although it is an idealistic model, the same basic principles also apply to liquids and larger molecules. These small differences in vibrational energy (although they are the greatest for hydrogen and deuterium relative to any other isotopes) have implications on reactions and are what lead to molecular isotopic separation.

There are two processes that govern the isotopic separation of chemical reactions, namely, equilibrium and kinetic fractionation. Equilibrium fractionation occurs when the chemical process in question is in equilibrium and the reaction is reversible. In this case the mass difference of the isotopes affects the reaction rate, with the lighter isotope having a slightly faster rate due to its lighter mass. Equilibrium fractionation is thus dependent upon the variables that affect the

balance of equilibrium in a system, like pressure and temperature. Generally the isotope with the larger mass accumulates in the heaviest species or in the highest oxidation state. Kinetic fractionation on the other hand, occurs when a process is irreversible. In the case of kinetic fractionation both mass difference and reaction pathway will contribute to the magnitude of fractionation. In general the chemical bonds of lighter isotopes are more easily broken and react faster than those of heavier isotopes causing the products of the reaction to be enriched in the lighter isotope relative to the substrate.

6.2. Nomenclature for Isotopic Separation

For many geological and environmental samples, isotopic ratios are reported relative to a set standard isotopic ratio. This relative difference is known as the δ value and is defined as[4]:

$$\delta_x = \left(\frac{R_x - R_{std}}{R_{std}} \right) 10^3 \qquad \text{Equation 6.4}$$

By convention, isotopic ratios are expressed as the value of the less abundant isotope relative to the more common one. Differences in δ values are expressed in per mil (‰) quantities.

Interpretation of the δ values, leads to another common convention of expressing isotopic differences, namely the fractionation factor. The isotopic fractionation factor between two components of a chemical reaction is defined as[4]:

$$\alpha_{A \to B} = \frac{R_A}{R_B} \qquad \text{Equation 6.5}$$

In terms of δ notation this expression becomes:

$$\alpha_{A \to B} = \frac{1000 + \delta_A}{1000 + \delta_B} \qquad \text{Equation 6.6}$$

For systems where reactants are chemically or physically separated from the products, and for which α does not change during the progress of the reaction, the Rayleigh[◊] approximations apply[5]. Rayleigh separation processes dominate in natural systems; biological fractionation, for example, is a Rayleigh-type of process.

The Rayleigh equations can be derived as follows:

For a reaction involving isotopes A and A' (where A' is the heavier isotope) one can say that:

[◊] These equations are named for Lord Rayleigh, who derived them for fractional distillation of mixed liquids.

$\partial A = k_A A$ and $\partial A' = k_{A'} A'$ where k_x is the rate constant Equation 6.7

If the isotopes are randomly distributed throughout the reaction space (as is generally the case), then the fractionation factor α is related to the rate of the reaction by[6]:

$$\alpha = \frac{k_{A'}}{k_A} \text{ then } \frac{\partial A'}{\partial A} = \alpha \frac{A'}{A} \text{ and } \frac{\partial A'}{A'} = \alpha \frac{\partial A}{A} \quad \text{Equation 6.8}$$

Integrating these equations we get:

$$\frac{A'}{A'_o} = \left(\frac{A}{A_o}\right)^{\alpha} \text{ and } \left(\frac{A'}{A'_o}\right)\left(\frac{A_o}{A}\right) = \left(\frac{A}{A_o}\right)^{\alpha-1} \quad \text{Equation 6.9}$$

For most light elements A»A' so that:

$$\frac{A}{A_o} \cong \frac{A + A'}{A_o + A'_o} = f \quad \text{Equation 6.10}$$

letting

$$R = \frac{A'}{A} \text{ and } R_o = \frac{A'_o}{A_o} \quad \text{Equation 6.11}$$

we get the Rayleigh equation:

$$\frac{R}{R_o} = f^{\alpha-1} \quad \text{Equation 6.12}$$

By substitution, we can also express this equation in terms of δ notation:

$$\delta = 1000(f^{\alpha-1} - 1) \quad \text{Equation 6.13}$$

This same derivation can be applied for other instances (i.e. when A is not much greater than A') yielding similar forms of the Rayleigh equation, however, the form of the Rayleigh equation as given above is the most common in literature.

6.3. Abiotic Isotopic Separation Processes

There are six light isotopes that are primarily studied in isotopic separation processes. They are H, C, O, N, S and Si, due mainly to their prevalence (both total and isotopic) and the relatively large isotopic mass differences. While there are numerous abiotic processes involving the separation of the isotopes of these, and other "heavier" elements like Se, only a few pertinent examples will be discussed here.

6.3.1. $^{16}O/^{18}O$ ratios in water evaporation

A classic example of an abiotic kinetic fractionation process is the evaporation of water in an open system such as a lake or the ocean. For the case of $H_2{}^{16}O$ and $H_2{}^{18}O$, the lighter $H_2{}^{16}O$ is slightly

favored as it undergoes evaporation. Thus as lake or seawater evaporates the body of water tends to become enriched in $H_2{}^{18}O$, and the vapor in $H_2{}^{16}O$. (Figure 6.2) This is a kinetic process, due to vapor dilution in the atmosphere and climate change, evaporation in an open system is almost never a reversible reaction. This process is interesting from a climatologists' perspective since global oxygen fractionation due to evaporation and condensation is a temperature dependent process, one can infer much about climate temperature of the present and early earth from the isotopic ratios of water frozen in ice cores or in sediments.

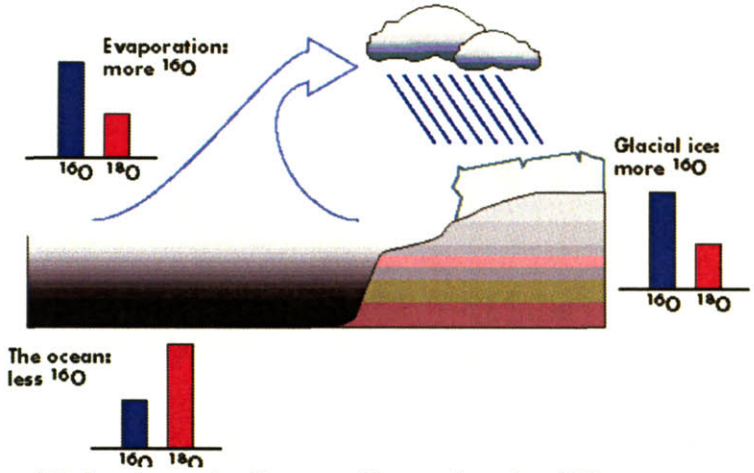

Figure 6.2 A schematic diagram illustrating the differences on oxygen isotope ratio concentration due to climate[7].

6.3.2. Carbon Isotope Fractionation During Equilibrium Processes

At equilibrium, when two molecules are in competition for the same isotopes, the molecule with the greatest difference in Zero Point Energies, and therefore stronger bonds, will become enriched in the heavier isotope. For example, exchange reactions occur between many of the carbon species in the atmosphere, groundwater and in minerals. An example of a carbon exchange reaction is:

$$H^{13}CO_3^- + {}^{12}CO_2 \Leftrightarrow H^{12}CO_3^- + {}^{13}CO_2$$

This type of exchange reaction will occur with any two carbon species in equilibrium. The ^{13}C sequestration in different carbon species will trend as follows[8]: $CO_{2(aq)} < CO_{2(g)} < CO_3^{2-} < HCO_3^- < CaCO_{3(calcite)} < CaCO_{3(aragonite)}$. Zhang et al.[9] reported calculated equilibrium fractionation values for the isotopic exchange values of several carbon species. By measuring the $\delta^{13}C$ of dissolved inorganic carbon (DIC) in groundwater, it is often possible to trace the source of carbon as it moves through the aquifer. Typically,

DIC sources are acidic dissolution of carbonate and silicate bearing minerals (by carbonic or other acids) and dissolution of soil CO_2[10]. If the isotopic ratios of the original carbonate minerals are known, then, by measuring the $\delta^{13}C$ of the groundwater, it is possible to determine the contribution of each source of DIC to the groundwater[11] for a greater understanding of the environmental processes that govern the equilibrium in an aquifer.

6.4. Biological Isotope Separation Processes

Because all biological systems incorporate many if not all of the isotopically interesting light elements, it is not surprising then that metabolic processes lead to isotopic separation. Metabolic fractionation is almost always a kinetic process, meaning that the reaction pathway and therefore the type of metabolism will have an impact on the degree of fractionation in a system. This is an interesting property that has been used to infer microbial production of ores[12], determine food chain patterns[13], and even to infer the possibility of ancient life on Mars[14]. Metabolic fractionation has been observed for nearly all of the light elements, and many of the metabolically active lighter metals, such as Fe[15,16], up to heavier metals like Te[17].

6.4.1. Metabolic Carbon Sequestration

All organisms utilize carbon for energy and cellular construction, and the pathway of carbon isotopes can be traced throughout the carbon cycle. Carbon dioxide is fixed by plants and phytoplankton, which are then consumed up the food chain by animals, and finally fungi and bacteria degrade the carbon waste back into CO_2. (Figure 6.3) As carbon is incorporated into and up the food chain, the more complex carbon molecules will tend to become enriched in ^{13}C. $^{13}C/^{12}C$ ratios can provide much information on both the carbon uptake pathway as well as the environmental uptake conditions in past and present environments. For example, a study by Londry and Des Marais[23] found that the extent of carbon fractionation in the cell biomass of several species of SRB was dependent upon the enzymatic pathway and carbon substrate that the microorganism used for growth. The greatest fractionation was observed with CO_2 as the sole source of carbon, yielding α values in bacterial biomass as high as 1.03, while they observed minimal carbon fractionation when the organisms were grown with acetate or lactate as the carbon source. Thus, carbon isotopic ratios of SRB samples from the environment can be used to infer the type of substrate used for growth by these microorganisms.

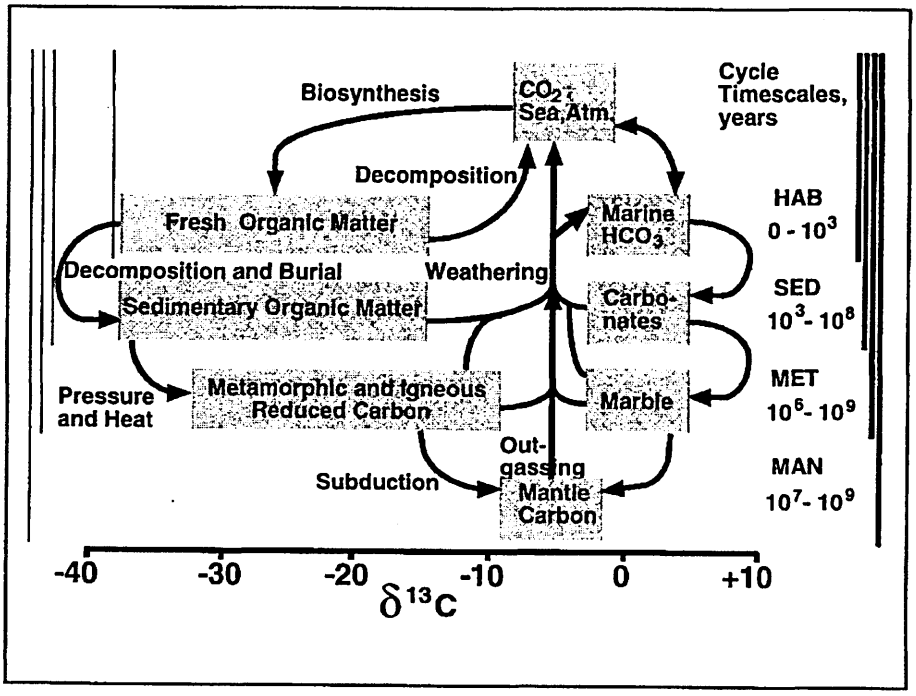

Figure 6.3 Biogeochemical Carbon Cycle, showing principal C reservoirs (boxes) in the mantle, crust, oceans, and atmosphere, and showing processes (arrows) that unite these reservoirs. The range of each of these reservoir boxes along the horizontal axis gives an estimate of $\delta^{13}C$ values most typical of each reservoir.[18].

6.4.2. Isotopic Fractionation of Metals During Microbial Metabolism

While all microorganisms incorporate the light elements H, C, N and O and alter their chemistry in some manner, leading to fractionation, there are many species of microorganisms that gain energy for metabolism by oxidation or reduction of transition metals and semi-metals. These redox processes often involve several enzymes and lead to physical and/or chemical separation of the reduced and oxidized metals. Although heavier elements necessarily have a less significant isotopic mass difference, Rayleigh type redox processes often lead to noticeable isotopic separations. Bacteria have been shown to isotopically separate Mg[19], Fe[15,16], Hg[20], and Te[17] during oxidation-reduction processes. (Table 6.1) As expected, non-redox active elements, like Ca, show little fractionation in the environment[21]. The fractionation factors associated with bacterial metal fractionation can be used as "signatures" for the determination microbial influence on the deposition of ore deposits[12], as evidence for early life on earth[22], and even to speculate the possibility of life on Mars[14]. Not only

that, but because Rayleigh fractionations are reaction pathway dependent, the extent of fractionation may also provide clues to some of the mechanisms of bacterial redox reactions, as is can for determination of bacterial metabolic pathways[23].

Table 6.1 Fractionation factors for biologically associated intermediate element isotopic fractionation. Values selected from literature, negative sigma* values indicate samples that are isotopically lighter than the original material to which they were compared.

Element	Source	ε (‰)	δ	Reference
Ca	vertebrate bone		0.49– -2.88	21
^{56}Fe	Shewanella alga reduction of Fe(III)-Fe(II)		-1.6 – -0.87	15
	uptake into ferroxidan protein	-0.68		24
	bacterial dissolution of horneblend	0.8		16
^{65}Cu	yeast uptake of Cu-proteins	-1.6 – -2.13		24
^{68}Zn	yeast uptake of Cu-Zn proteins	2.1		24
$^{76/80}$Se	Se(VI) reduction by bacteria in marine sediment	-2.7±0.3		25
	Se(IV) reduction by bacteria in marine sediment	-5.6±0.5		25
	Se(VI) reduction by pure bacterial culture	-1.1 – -8.4		26
	Se(IV) reduction by pure bacterial culture	-8 – -9.4		26
$^{122/130}$Te	Bacterial reduction of TeO32-	6±0.5		17
$^{198/202}$Hg	Bacterial reduction of Hg(II)	6±0.5		20

6.5. Conclusion

It is fortunate that the subtle differences imparted to isotopes by their quantum mechanical properties can be detected and harnessed. Isotopic separation is an important key in our understanding of many environmental processes; globally and microscopically, allowing us to measure ancient global temperatures, to determine the age of rocks, fossils, and even aquifers; by tracing carbon, nitrogen and oxygen ratios, we can follow the path of these elements within individual organisms and throughout the food chain, it has even allowed us to infer possible life on Mars! It is interesting that we can use isotopic fractionation mechanisms to give us information on both molecular (i.e. carbon uptake) and global processes like ocean evaporation and precipitation. Not only that, but because many fractionation processes such as rock and glacier formation occurred many thousands of years ago without any significant change, the isotopic ratios in these phenomena provide us insight about the formation of these systems in the early

* $\varepsilon = \delta_{product} - \delta_{reactant}$

Earth. With the greater precision mass discrimination techniques like MC-ICP-MS have offered us, it is now easier than ever to measure isotopic differences, giving us ever more powerful tools for understanding geological and metabolic processes. The measurement of isotopic ratios and fractionation is a unique and powerful tool that can be used to provide a broad range of information, and will continue to be an important too for understanding both geological and biological processes in the environment.

6.6. References

[1] **Valley J. W., D. R. Cole, eds.** (2001) Reviews in Mineralogy and Geochemistry: Stable Isotope Geochemistry. **43**.

[2] **Valley J. W., D. R. Cole, eds.** (2001) Equilibrium Oxygen, Hydrogen and Carbon Isotope Fractionation Factors Applicable to Geologic Systems: Reviews in Mineralogy and Geochemistry: Stable Isotope Geochemistry. **43:**3-6.

[3] **Valley, J. W., H. P. Taylor, J. R. O'Neil eds.** (1986) Theoretical and Experimental Aspects of Isotopic Fractionation. Reviews in Mineralogy: Stable Isotopes in High Temperature Geological Processes. **16:**1-40.

[4] **Hoefs, J.** (1997) Stable Isotope Geochemistry. Springer-Verlag, Berlin. 7-8.

[5] **Kendall, C., J. J. McDonnel eds,** (1998) Isotope Tracers in Catchment Hydrology. Elesevier, N.Y.. 60-70.

[6] **Ishida, T.** (2002) Isotope Effect and Isotope Separation: A Chemist's View. J. Nuc. Sci. Technol. **39:** 407-412.

[7] http://www.wwnorton.com/college/anthro/bioanth/ch12/O-isotope2.gif

[8] **Peters, K. E., C. C. Walters, J. M. Moldowan.** (2005). The Biomarker Guide Second Edition, I. Biomarkers and Isotopes in the Environment and Human History. P.138-139.

[9] **Zhang, J., P. D. Quay, D. O. Wilbur**. (1995). Carbon Isotope Fractionation During Gas-Water Exchange and Dissolution of CO_2. Geochim. Cosmichim. Acta. **59:**107-114.

[10] Resources on Isotopes: Carbon. http://wwwrcamnl.wr.usgs.gov/isoig/period/c_iig.html

[11] **Kharaka, Y.K. , A.S. Maest eds.** (1992). Tracing watershed weathering reactions with $\delta^{13}C$. Water- Rock Interaction, Proceedings of the 7th International Symposium, Park City, Utah, 13-18 July 1993, Balkema, Rotterdam, pp. 569-572.

[12] **Konhauser et al.** (2002) Could bacteria have formed the Precambrian banded iron formations? *Geology*. **30:**1079-1082.

[13] **Lajtha, K., R. H. Michener eds.** (1994) Tracing the Diets of Fossil Animals Using Stable Isotopes. Stable Isotopes in Ecology and Environmental Science. 63-92.

[14] **McKay, D. S., et al.** (1996). Search for Past Life on Mars: Possible Relic Biogenic Activity in Martian Meteorite ALH84001. Science. **273:**924-930.

[15] **Beard, B. L., C. M. Johnson, L. Cox, H. Sun, K. H. Nealson, C. Aguilar.** (1999) Iron Isotope Biosignatures. Science. **285:**1889-1892.

[16] **Brantley, S. L., L. Liermann, T. D. Bullen.** (2001) Fractionation of Fe Isotopes by Soil Microbes and Organic Acids. Geology. **29:**535-538.

[17] **Smithers, R. M., H. R. Krouse.** (1967) Tellurium Isotope Fractionation Study. Can. J. Chem. **46:**583-591.

[18] **Valley J. W., D. R. Cole, eds.** (2001) Isotopic Evolution of the Biogeochemical Carbon Cycle During the Precambrian. Reviews in Mineralogy and Geochemistry: Stable Isotope Geochemistry. **43:**555.

[19] **Carder, E. A., A. Galy, J. A. McKenzie, C. Vasconcelos, H. Elderfield.** (2005) Magnesium Isotopic Evidence for Widespread Microbial Dolomite Precipitation in the Geological Record. American Geophysical Union Fall Meeting.

[20] **Kritee, K., B. Klaue, J. D. Blum, T. Barkay.** (2004) Mercury Stable Isotope Fractionation During Bacterial Reduction Of Hg(II) to Hg^0. 7^{th} International Conference on Mercury as a Global Pollutant. Ljubljana, Slovenia. (poster). http://aesop.rutgers.edu/~barkay/Goldschmidt05Final.ppt

[21]. **Johnson, T. M.** (2004) A Review of Mass-Dependent Fractionation of Selenium Isotopes and Implications for Other Heavy Stable Isotopes. Chem. Geol. **204:**201-214.

[22] **Schidlowski, M.** (1988) A 3,800-Million-Year Isotopic Record of Life from Carbon in Sedimentary Rocks. Nature. **333:**313-318.

[23] **Londry K. L., D. J. Des Marais.** (2003) Stable Carbon Isotope Fractionation by Sulfate-Reducing Bacteria. Appl. Env. Microbiol. **69:**2942.

[24] **Zhu, X. K., et al.** (2002) Mass Fractionation Processes of Transition Metal Isotopes. Earth. Planet. Sci. Lett. **200:**47-62.

[25] **Ellis, A. S., T. M. Johnson, M. J. Herbel, T. D. Bullen.** (2003) Stable Isotope Fractionation of Selenium by Natural Microbial Consortia. Chem. Geol. **195:**119-129.

[26] **Herbel, M. J., T. M. Johnson, R. S. Oremland, T. D. Bullen.** (2000) Fractionation of Selenium Isotopes During Bacterial Respriatory Reduction of Selenium Oxyanions. Geochim. Cosmichim. Acta. **64:**3701-3709.

7. Analytical Techniques

A variety of analytical techniques were used to both determine the concentration and speciation of elements and isotopes of interest, as well as to determine growth rates and properties of the microorganisms studied here. Techniques utilized included Inductively Coupled Plasma Atomic Emission Spectroscopy (ICP-AES), Inductively Coupled Plasma Mass Spectroscopy (ICP-MS), UV-Visible Spectroscopy (UV/VIS), Light microscopy, Transmission Electron Microscopy (TEM), Extended X-Ray Absorption Fine Structure Spectroscopy (EXAFS), X-Ray Absorption Near Edge Spectroscopy (XANES) and X-Ray Diffraction (XRD).

7.1. ICP-AES Procedure

Samples containing dissolved metals of interest in a 0.1 M HNO_3 acid matrix were measured for metal concentration using Inductively Coupled Atomic Emission Spectroscopy (ICP-AES). Typically the working range for this instrument is 1 μM to 1 mM metal and the minimum sample volume for a statistically accurate measurement is about 3 mL.

7.1.1. Principle of ICP-AES

ICP-AES works by excitation of ionized atoms in an argon plasma. As the atoms de-excite they emit a characteristic wavelength that can then be detected. Figure 7.1 shows the detection limits of selected elements for commonly used characteristic wavelengths[1]. There are two parts to elemental detection with ICP-AES, ionization of the sample in an argon plasma followed by spectrophotometric detection of the characteristic wavelengths of the element or elements in question.

Element	Line (nm)	LOD (µg/L)
Ag	328.068	2.1
Al	167.078	0.07
As	189.042	7.4
B	249.678	1.6
Ba	455.403	0.08
Be	223.061	6.4
Br	154.065	25
Ca	396.847	0.04
Cd	226.502	0.3
Cl	134.724	102
Co	228.616	0.7
Cr	267.716	0.78
Cu	324.754	1.5
Fe	259.94	0.8
Ga	141.444	2.8
Ge	164.917	3.2
Hg	184.95	2.1
I	142.549	48
In	158.583	0.5
K	766.491	2.3

Element	Line (nm)	LOD (µg/L)
Li	670.784	0.03
Mg	279.553	0.02
Mn	257.61	0.1
Mo	202.03	1.1
Na	589.592	0.4
Ni	231.604	0.7
P	177.495	3.6
Pb	220.353	3.1
Pt	177.708	4.6
S	180.731	7.3
Sb	231.147	0.9
Se	196.069	8.9
Si	251.611	3
Sn	189.991	1.4
Sr	407.771	0.03
Te	214.281	8.5
Tl	190.864	3.6
V	311.071	1.1
Zn	213.856	0.2

Figure 7.1 Detection limits and commonly used wavelengths for selected elements.

The argon plasma is formed and maintained my means of a magnetic field generated by a water-cooled radio frequency generator coil around a torch through which the argon gas flows. (Figure 7.2) As the R.F field is activated, the gas becomes electrically conductive and ignites the argon plasma. The shape and stability of the argon plasma are maintained by the magnetic field and a countercurrent flow of cooling argon gas. As long as there is adequate gas flow and a stable magnetic field the argon plasma can be maintained for several hours.

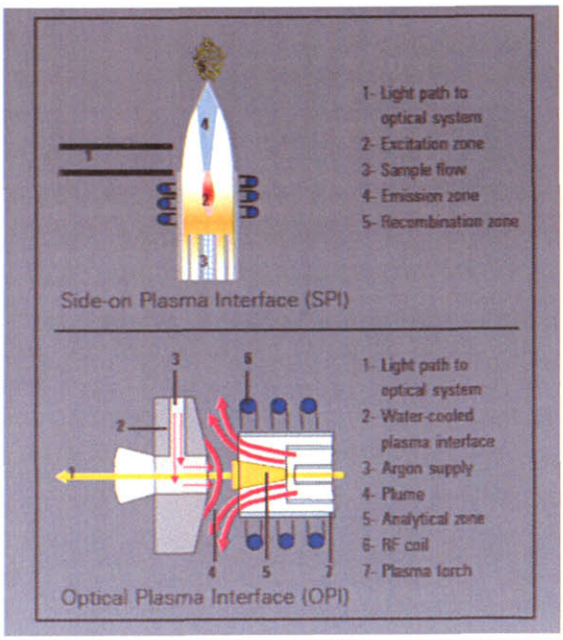

Figure 7.2 A schematic diagram of the ICP-AES torch and plasma interface[1].

Liquid samples introduced into the instrument are first aerosolized by means of a nebulizer. These fine particles of sample are then introduced into the argon plasma where they become dried, atomized and eventually ionized as they collide with the argon atoms in the plasma and become excited, emitting characteristic photons as they de-excite.

The emitted light then passes through a grating, separating the light into its component wavelengths. As the light spreads out it is intensified by means of a photomultiplier tube and the intensity of the characteristic wavelength of interest is measured. (Figure 7.3)

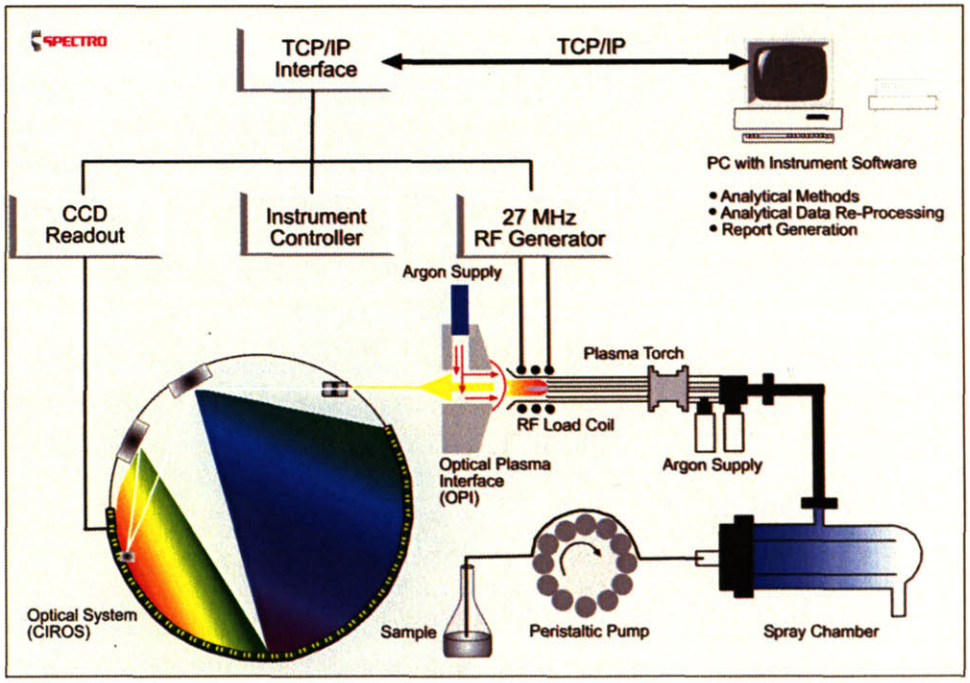

Figure 7.3 A diagram of the optics system of an ICP-AES[1].

By comparing the intensity of the desired characteristic wavelength to those of standards with known elemental concentration (usually prepared from an ICP-AES standard solution) it is possible to accurately determine the concentration of any desired element in your sample.

The detection limits of the instrument are dependent upon both the signal to noise ratio as well as the chosen characteristic wavelength for the element in question but are on the order of 1 μM to 1 mM. Minimal sample volume for accurate measurement is typically approximately 3 mL, samples are generally dissolved in 0.1 M or 1% HNO_3 to prevent sorption to tubing.

7.1.2. Standard Preparation

The limitations of ICP-AES require that all measured samples be compared against standards of known concentration. This is due to both the variance of the instrument from run to run as well as variance in the detection efficiency of the instrument optics. Therefore, the preparation of high quality standards is essential for accurate concentration determination. Standards must be diluted in the same matrix as the samples, although they need not be in the same oxidation state or chemical form as the argon plasma ionizes and strips away any chemical differences before measurement. The dilution matrix is typically 0.1 M HNO_3[†] since. the solubility of most metal ions are the same in this solution regardless of oxidation state.

For the highest accuracy standards are prepared to match the predicted concentrations of the samples and samples must always be within the concentration range of the standards for accurate calibration. Generally seven standards are utilized. Standards are prepared from ICP-AES standard solutions (Uranium: Inorganic Ventures Cat. # CGU1-1 Lot # X-U01061 Manganese: Ricca Chemical Co. Cat. # PMN1KN-100 Lot # 3501012).

A linear regression fit of counts per second versus standard concentration is accepted if the R^2 value is greater than 0.996. Standard preparations not meeting this criterion are rejected and remade.

7.1.3. General Procedure

During the progress of this thesis, two different ICP-AES instruments were used; the Spectro Analytical Instruments Spectroflame and the Spectro Analytical Instruments Ciros Vision (Model # FEC12), however, the same general startup and analysis procedures apply to both instruments.

Prior to instrument start-up, samples are filtered through a 0.45 μm pore size filter, with a diameter of either 25 mm or 13 mm depending on the size of the sample and the amount of suspended particulates. All samples must be filtered prior to analysis to prevent clogging and sample mixing in the instrument's tubing. In most cases samples are above the detection limits of the instrument and do not have enough volume for a good quality measurement

[†] It is important to ensure that the element(s) of interest is soluble in 0.1 M HNO_3. If not it is possible to use other acids, dIH_2O, and even organics as matricies as long as the standards are prepared accordingly. All of the elements discussed in this thesis are diluted in a HNO_3 acid matrix.

and are diluted in 0.1 M HNO_3 to dilute and acidify the sample. Typical sample volumes for ICP-AES are on the order of 3-5 mL.

A gas flow of argon is established and the instrument is flushed with Ar for several minutes to remove any contaminant gasses from the torch and gas lines. The argon plasma is then ignited according to the internal instrument protocol and allowed to equilibrate for a minimum of 15 minutes. The sample introduction tubing is then flushed for a minimum of 5 minutes with 1-5% HNO_3 to clean and remove any possible contaminants sorbed onto the tubing.

The nebulizer flow rate is optimized by maximizing the signal-to-noise ratio of a 1 ppm Mn solution at λ=257.611 nm. The optics are then aligned to a reprofiling solution (SCP Science Catalog # 140-128-201). Typical instrument operating parameters are given in Table 7.1. The peak shape and line intensity are then verified for the measured wavelengths of the elements in question to verify proper alignment of the optics and low background which are both good indicators that the instrument is operating properly. Standards prepared according to § 7.1.2 are then measured, a linear regression is applied, if the R^2 value is greater than 0.996 then the regression is accepted and the samples are subsequently measured. Two check standards are measured approximately every 10 samples to ensure proper instrument functioning, and a standard calibration is completed approximately every 20 samples to account for any signal drift in the instrument. A final calibration is performed at the end of each sample run. When the autosampler is used (Spectro Analytical Instruments Type 76060017) a 60 second rinse (either DIH_2O or 0.1 M HNO_3) was performed between samples.

Table 7.1 ICP-AES Typical operating conditions.

Plasma Power	1400 W
Coolant flow rate	14 L/min
Auxiliary flow rate	1.2 L/min
Nebulizer flow rate	0.95 L/min

After sample measurement is completed, the sample introduction tubing is flushed again with 1-5% HNO_3 for a minimum of 5 minutes. The plasma is then turned off following the internal instrument shutdown protocol and the instrument is put on standby.

7.2. ICP-MS Procedure

Samples below ICP-AES detection limits were measured using ICP-MS. Samples for which isotopic discrimination was necessary were measured using MC-ICP-MS.

7.2.1. Quadrupole ICP-MS

This instrument is the Perkin Elmer SCIEX Elan DRC Plus. (Figure 7.4) This type of instrumental analysis utilizes the same underlying principles as ICP-AES but differs in how the samples themselves are detected. Samples are aerosolized and injected into an argon plasma, where they are ionized in the plasma. (Figure 7.5)

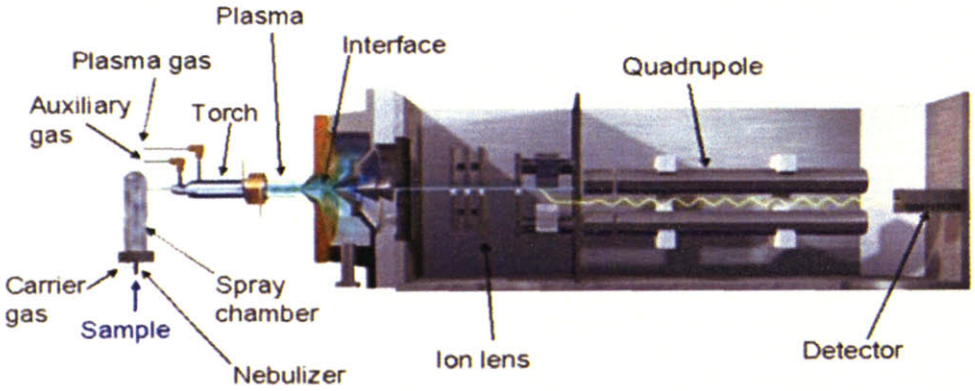

Figure 7.4 A Diagram of an ICP-MS[2].

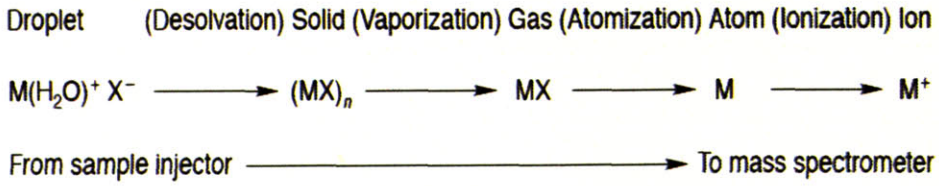

Figure 7.5 Sample progression within the plasma[3].

The gaseous ionized sample passes through a series of focusing cones and then into ion optics, which, through a series of voltage differentials separates out the positively charged ions from electrons and other small neutral particles, the ion optics also refocus and homogenize the ion beam as it passes from ~2 Torr to $\sim 10^{-6}$ Torr. These positively charged ions then pass through a quadrupole mass analyzer. The quadrupole consists of four hyperbolic rods; a direct current is applied to two rods in one plane, and a radio frequency is applied perpendicularly to the other two. The correct rf-dc frequency creates a specific negative charge

on the quadrupole rods allowing the ions of interest to pass through to the detectors, while other heavier or lighter ions are ejected from the quadrupole. (Figure 7.6) If there is more than one ion of interest, this process is repeated, tuning the rf-dc voltage to the specific frequency corresponding to each particular ion of interest. After passing through the quadrupole the ions strike a dynode, setting off a chain reaction creating electrons and generating a signal, the intensity of which is related to the concentration of the ion of interest.

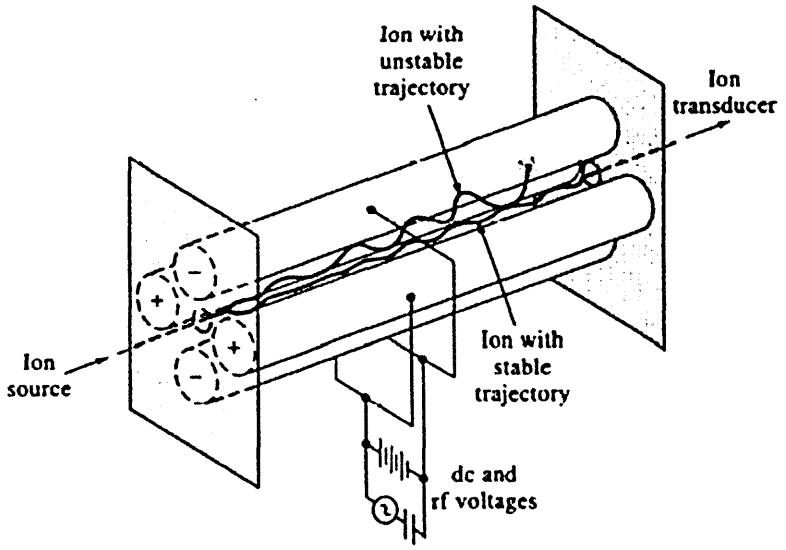

Figure 7.6 The Quadrupole[4].

7.2.2. Double focusing multicollector ICP-MS

A second ICP-MS (VG-Axiom Thermo Electron Corp.) has a different set of mass analyzers and detectors that are optimal for isotopic mass discrimination. (Figure 7.7) After the sample is ionized in the argon plasma, the ions are accelerated in the ion optics to a few kilovolts and then pass into the mass analyzer. In the mass analyzer the ions then pass through an electromagnet where the magnetic field focuses the ions with respect to their angle of flight. They then pass into an Electrostatic Analyzer (ESA) that again focuses the ion beam, this time with respect to mass and charge. If the ESA and the magnetic field are equal in magnitude but opposite in directionality, this will have the effect of double focusing the beam of ions, which is then directed at the detector creating a signal. Although this process is slower than alternating the rf/dc voltages of a quadrupole (400-500 ms for a mass scan vs. about 100 ms for a quadrupole) it has the advantages of having a much higher resolution, capable of resolving peaks only a few hundredths of a mass unit apart, as well as capabilities for high precision measurements of very dilute samples.

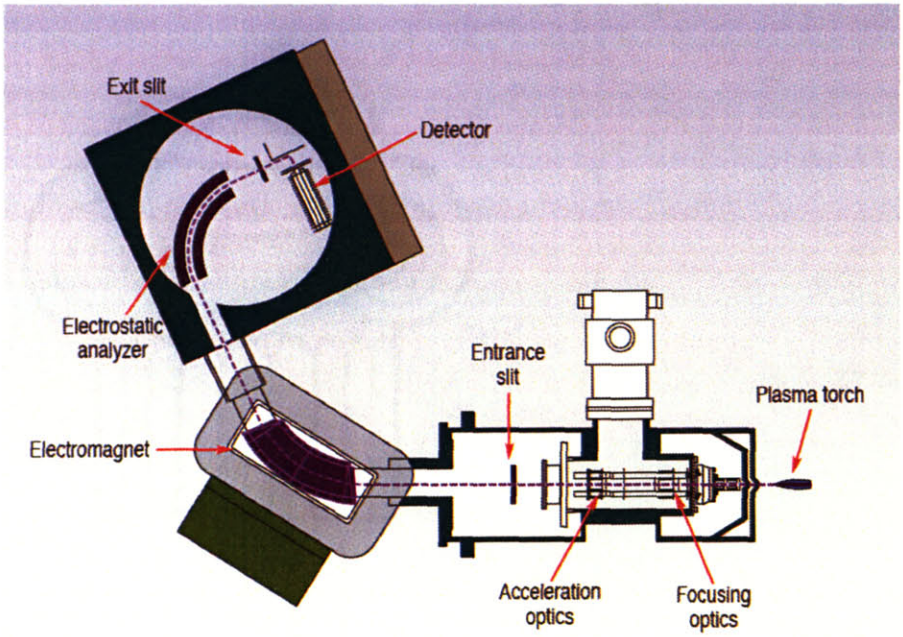

Figure 7.7 A schematic of double focusing magnetic sector ICP-MS[5].

The VG-Axiom also has multiple detectors, known as a multicollector, or MC-ICP-MS. The multiple collector design is ideal for fast isotopic ratio discrimination because it allows for collection and measurement of multiple ion signals simultaneously.

7.2.3. Standard Preparation

For concentration determination with ICP-MS all measured samples must be compared against standards of known concentration. The preparation of high quality standards is essential for accurate concentration determination. It is crucial that standards be diluted in the same matrix as the samples, although they need not be in the same oxidation state or chemical form as long as the fundamental behavior of the element is the same in the matrix regardless of oxidation state. The dilution matrix is typically 0.1 M HNO_3.

For the highest accuracy standards are prepared to match the predicted concentrations of the samples and samples must always be within the concentration range of the standards for accurate calibration. Also, because of the degree of sensitivity of analysis of ICP-MS, standards are prepared by serial dilution. Generally seven standards are utilized. Standards for concentration analysis are prepared from a 1,000 ppm Uranium ICP-AES standard (Inorganic Ventures Cat. # CGU1-1).

7.2.4. General procedure

Prior to instrument start-up, samples are filtered through a 0.45 μm pore size filter, with a diameter of either 25 mm or 13 mm depending on the size of the sample and the amount of suspended particulates. All samples must be filtered prior to analysis to prevent clogging and sample mixing in the instrument's tubing. In most cases samples are above the detection limits of the instrument and do not have enough volume for a good quality measurement and so are diluted in 0.1 M HNO_3 to dilute and acidify the sample. Typical sample volumes for ICP-MS are on the order of 15-30 mL.

The start-up procedure for both ICP-MS instruments is similar to ICP-AES, once the plasma is lit, the system is allowed to equilibrate for 30-45 minutes and the instrument tubing is flushed with 1-5% HNO_3. The instruments' detectors are then aligned using a standard solution (1 ppb each of Ba, Be, Ce, Co, In, Pb, Mg in a 2% HNO_3 matrix) and the machine is optimized for peak shape, low background, and sensitivity of detection. Once all of these parameters are optimized, the standards and samples can be run. For most samples 10-20 sweeps of the quadrupole per reading is adequate. If many elements are to be analyzed, this number can be lowered to reduce run time and total sample volume uptake. If the sample contains only one element of interest, 20 sweeps of the quadrupole per reading is not too time-consuming and gives minimal error in the measurement. To further ensure accuracy, three readings are done for each sample. For the Elan ICP-MS Standards prepared according to § 7.2.3 are then measured, a linear regression is applied, if the R^2 value is greater than 0.996 then the regression is accepted and the samples are subsequently measured. Standards are calibrated at the beginning of a run and every 40-50 samples after that. Check standards are run approximately every 10 samples. For the Axiom ICP-MS samples are run in the pattern sample-standard-sample. (See Ch 9 Appendix for more details).

After sample measurement is completed, the sample introduction tubing is flushed again with 1-5% HNO_3 for a minimum of 5 minutes plasma is then turned off following the internal instrument shutdown protocol and the instrument is put on standby.

7.3. Uv-Visible Spectroscopy

Uv-Visible Spectroscopy (UV/VIS) is a simple yet important method for probing molecular structure, concentration, as well as sample density. In this thesis UV/VIS is employed to determine uranium concentration, protein concentration, manganese oxide concentration and formation kinetics and microbial cell density.

7.3.1. Principles of UV/VIS

The Cary 6000i (Varian Inc. Part #: Cary 6000i) consists of two light sources, a tungsten lamp emitting visible light, and a deuterium lamp emitting ultra-violet light. The light passes through a pre-grating slit to reduce the amount of scattered light, it then travels through a diffraction grating where it is split into its component wavelengths. The diffracted light then enters a second slit which acts as a monochromator. By altering the angle of the diffraction grating with respect to the second slit, it is possible to scan through the entire UV/VIS spectrum with only a very narrow wavelength of light passing through the sample at a given time. The light passing through the sample is absorbed by a photodiode and the absorbance recorded. (Figure 7.8)

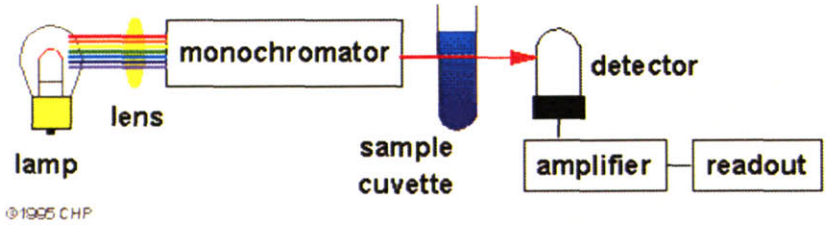

Figure 7.8 A schematic diagram of a UV/VIS[6].

As the monochromatic light passes through the sample, the intensity of the light decreases, and certain molecules absorb different wavelengths of light according to their chemical properties. Beer's Law (Eqn. 7.1) states that the absorbance of any given sample will be proportional to the concentration and the path length of light traveling through the sample.

$$A(\lambda) = \alpha(\lambda)lc \qquad \text{Equation 7.1}$$

Where A is the absorbance, l is the path length of the cuvette, c is the concentration of the sample, and α is the molar absorptivity; which is a chemical property, related to how strongly the sample absorbs light at a given wavelength.

Light of specific wavelengths will have just the right amount of energy to excite a molecule's outer electrons, which become promoted to an excited state. These photons are absorbed and do not make it to the detector. The wavelength(s) of light absorbed by any given molecule are related to the energy needed to cause electronic transitions within the atoms of the sample.

Although not strictly related to the probing of molecular structure, UV/VIS is also useful for determining the optical density of samples containing suspended particulate matter. The suspended particles in a liquid cause the light passing through the sample to

scatter, with the amount of scattering being related to the density of suspended particles in the sample.

7.3.2. Procedures

7.3.2.1. Determination of Uranium Concentration with UV/VIS

At high concentrations (approximately 1 mM or greater), the uranyl ion (UO_2^{2+}) is visible in solution and absorbs light between 400 and 450 nm. The exact peak shape will be dependent upon factors such as pH, ionic strength, and complexing agent.

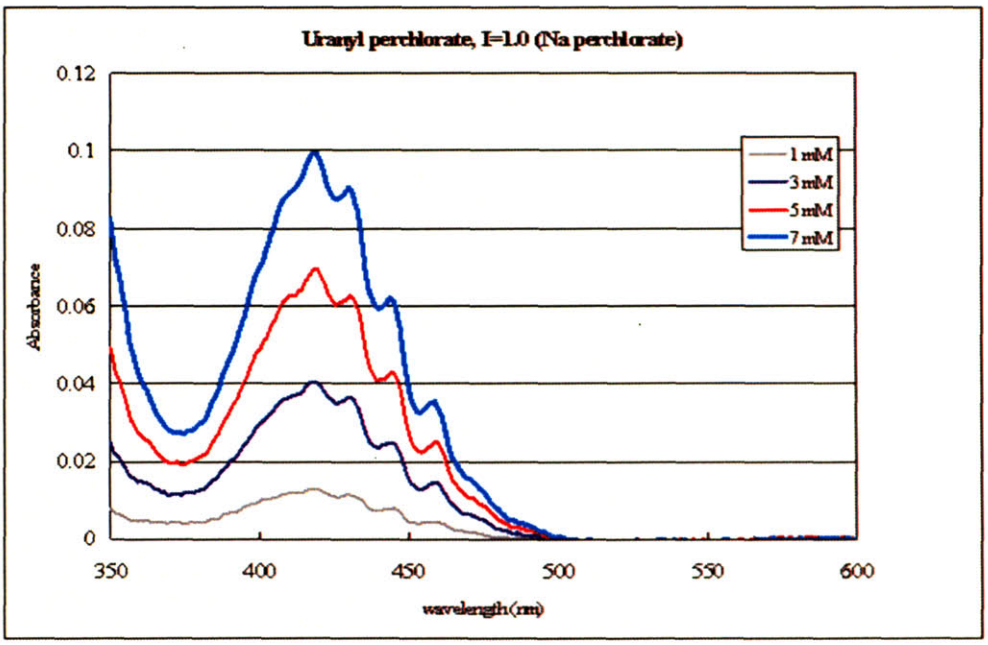

Figure 7.9 Absorption spectra of varying concentrations of uranyl perchlorate at I=1.0 and pH =4[7].

An indicator dye is necessitated if the desired uranium concentration is below 1 mM. Dyes in the Arsenazo family are known for their particularly strong complexation of uranium and broad pH working range. Arsenazo III forms complexes with both U(VI) and U(IV). When the dye is complexed to uranium a double peak structure can be seen with UV/VIS, peaks are usually around 610 and 650 nm (although precise peak location will depend on pH and metal concentration) and forms a blue-purple complex. Free uncomplexed arsenazo is dark pink in color and shows only one peak (at about 530 nm) in the absorbance spectra because the molecule is symmetrical (Figure 7.10). Because of the stability of the arsenazo III-U complex, the complexation reaction is essentially instantaneous and the absorbance change is detectable at concentrations of uranium as low as a few μM. (Figure 7.11).

The shape of the absorbance spectra is dependent upon pH, since the stability of the complex is also dependent upon pH. For uranium, the arsenazo III complex is more stable at lower pH's, yielding the largest absorbance at 650 nm for pH 2.2 (Figure 7.12).

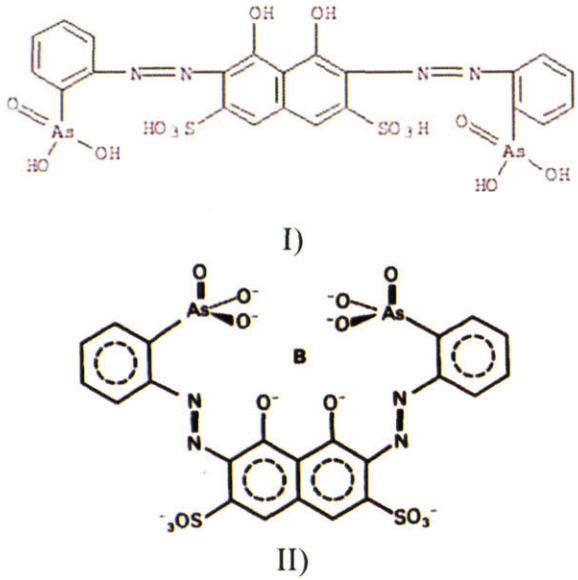

Figure 7.10 I) Structure of uncomplexed Arsenazo III II) Complexed arsenazo III[8], the metal cation is indicated by **B**.

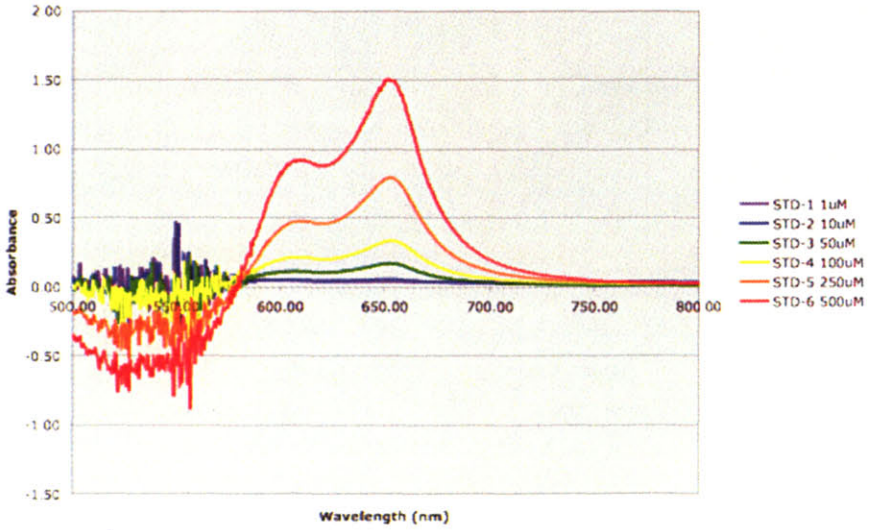

Figure 7.11 Absorbance of arsenazo III -U complexes at varying concentrations of uranium.

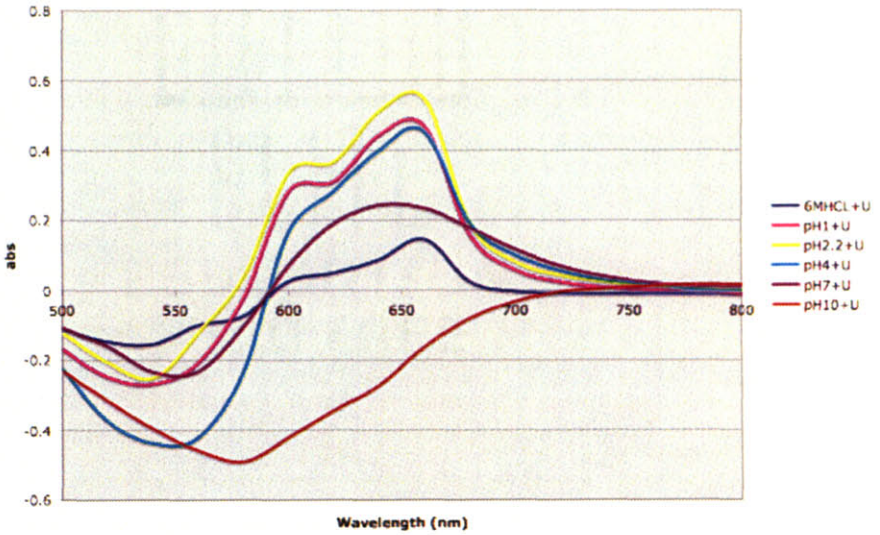

Figure 7.12 Absorbance spectra of 20 μM arsenazo III complexed with 2.5 μM uranium at various pH, normalized to uncomplexed arsenazo III.

Colormetric determination of uranium, while not as precise as measurement with ICP-AES is beneficial because it is much quicker and can be done with sample volumes as little as 20 μL.

Samples and standards for determination of UO_2^{2+} are prepared by addition of pH 2 buffer, 2 mM stock solution Arsenazo III, and sample in a 7.25:1.25:1 ratio (determined by experimental analysis) respectively. At pH 2, the complexation between the uranyl and the arsenazo is maximized; while the 1.25:1 ratio of arsenazo dye to uranium provides an excess of indicator dye, ensuring that all of the uranium in a sample is complexed. Standards are prepared from a 1,000 ppb U ICP-AES standard (Inorganic Ventures Cat. # CGU1-1) in the estimated range of uranium concentration, and a linear or quadratic regression is fit to the 5 times averaged absorbance maximum at λ=653 nm. R^2 values below 0.996 are rejected.

Generally an identical set of standards is prepared and run concurrently with samples to ensure proper machine functioning and standard preparation. If multiple samples are to be measured the 96 well plate reading UV/VIS is used (Cary 50 Varian inc Product # 0010086900). This instrument allows for fast readings of up to 96 samples at a time and requires very little sample volume (200 μL total, 20 μL sample). The absorbance is measured at λ=653 nm 5 times per sample and samples are run in triplicate for a better statistical average on the measurement. Concentration of the sample is then determined by applying the average absorbance to the line of best fit for the standards.

7.3.2.2. Determination of Protein Concentration

Like uranium, protein of high concentrations (typically greater than 0.1 mg/mL) can be measured directly with UV/VIS, typically at λ=280 nm. Some disadvantages of this method are that it requires special cuvettes or 96 well plates designed to be UV blind at lower wavelengths. Direct measurement can only be quantitative if the sample is reasonably pure and if you know the extinction coefficient. The extinction coefficient is related to how well a sample absorbs light; for proteins this is primarily dependent upon the amount of tryptophan and tyrosine residues. The advantages of direct measurement are that it is a non-destructive technique that leaves the same sample available for other analyses.

For lower concentrations of proteins or samples that contain several different types of proteins, a colormetric assay is usually more useful. The Lowry Protein Assay[9] (Pierce Biosciences Product #23240) is one of the most commonly used protein assays and was primarily the one used to determine protein concentration in this thesis.

The Lowry Method works as follows: in an alkaline solution Cu^{2+} forms a complex with the protein or proteins of interest. The protein-Cu complex is then added to the Folin-phenol reagent containing phosphotungstric acid and phosphomolybdic acid. The tungsten and molybdenum complexes are reduced, resulting in a blue color with an absorbance maximum at λ=750 nm. (Figure 7.13) Protein concentration in an unknown can then be determined by comparing the absorbance at λ=750 nm to those of a standard solution prepared from a 2 mg/mL Bovine Serum Albumin (BSA) (Pierce biosciences Product #23210).

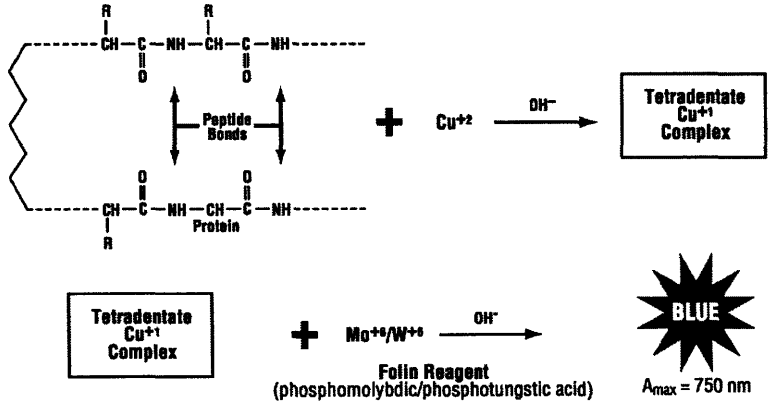

Figure 7.13 Mechanism of Protein Determination by the Lowry Method[10].

7.3.2.3. Kinetics of Manganese Oxide Formation

The formation of Manganese Oxides by an extracellular protein(s) produced by *Leptothrix discophora* can be measured using UV/VIS. While the UV/VIS does not probe the structure of the oxide itself, it is useful in measuring the formation of the particulate oxide. As the oxide forms it increases light scattering within the sample, and, due to the even distribution of both the Mn^{2+} and the oxidizing protein, the manganese oxide forms evenly throughout the sample in the cuvette. There is no distinct absorbance peak for the manganese oxide, but there is an absorbance maximum at λ~400 nm. By taking a number of spectra of the oxide over time, it is possible to establish its formation kinetics. The absorbance of an unknown sample can also be compared to the absorbance of several Mn^{2+} standards that have been oxidized in the same protein solution in order to determine approximate MnOx concentration.

7.3.2.4. Optical Density for Cell Mass Approximation

As bacteria grow in solution, the optical density of the media increases in relation to the number of bacteria. While there is no distinct absorbance maximum, the optical density is typically measured at λ=600 nm[11]. Absorbance at this wavelength increases as a function cell density up to a maximum of about 2. By comparing optical density with known cell numbers it is possible to determine the approximate number of cells in solution based on their optical density. This method, however, cannot distinguish between viable and non-viable cells, nor is it sensitive to small changes in cell number and is thus only useful as a quick "order of magnitude" approximation. For *Leptothrix discophora*, it was determined experimentally that an optical density of 0.4 absorbance units or greater was an indication of growth significant enough to elicit manganese oxidation.

7.4. Cell Enumeration

7.4.1. Cell Counting Using the DAPI method

7.4.1.1. Properties of the DAPI Stain

DAPI or 4',6-diamidino-2-phenylindole (Pierce Biosciences Cat. # 46190, CAS # 28718-90-3), is a fluorescent dye commonly used in cellular staining. Its structure (Figure 7.14) is such that it readily

binds with DNA. When it is bound to DNA DAPI will fluoresce, absorbing photons at 358 nm and emitting light at 461 nm[12].

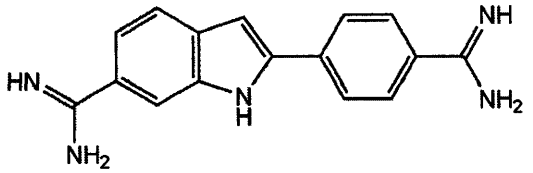

Figure 7.14 The Chemical Structure of DAPI, 4',6-diamidino-2-phenylindole.

7.4.1.2. Method of Cell Counting with DAPI

Cells are usually killed first in a solution of 10% formaldehyde (although this is not strictly necessary) and serially diluted by several orders of magnitude in autoclaved DIH_2O; 1 mL or 900 μL of these cells are then filtered through a 25 mm diameter 0.2 μm pore size Isopore polycarbonate membrane black filter (Millipore Cat # GTBP02500) either by vacuum filtration or using a Swinnex (Millipore Cat. # SX00 025 00) syringe filter unit. The black filter allows for better contrast under the microscope, and the small pore size will stop the bacteria on the filter. The pipette tip and Eppendorf tubes are then rinsed with approximately 1 mL DIH_2O to ensure that all cells are removed for staining. 200 μL of DAPI working solution is then added (50 μg/mL) and is contacted with the cells for approximately 10 minutes. The filters are then placed on glass slides for microscopic analysis.

Most bacterial cells will be visible at a magnification of 1000X (100X lens, 10X objective), and cells stained with DAPI will be visible on a microscope with a fluorescent light source and the appropriate filter (Olympus Model # BX51TRF). The number of bacterial cells in the miscoscope's field of vision is related to both the total number of cells in the original filtered solution and the area of the filter (415.5 mm^2). By counting the number of cells visible in several fields, it is possible to obtain an average number of cells per field, and thus, per filter. The total number of cells in the original sample can then be calculated using the total volume filtered and the dilution factor. As a rule of thumb, dilutions with greater than 300 cells/field or less than 50 cells/field are prone to a greater statistical variation and so are not utilized. Cells are either counted manually using a counter and gridded reticle, or with the cell counting program CellStats[13]. The DAPI staining method is a quick and relatively simple way to accurately determine cell numbers.

7.4.2. Cell Counting Using the Dilution Plating Method

This cell counting method is based on the theory that a single colony will develop on solid media for every viable bacterium in a sample. Thus, it is possible to count the number of colonies growing on an agar plate and relate them back to the total number of viable cells in the original sample. A series of serial dilutions is done on the unknown sample, then a specific volume of each of these dilutions is added to a plate (or several, for better statistics) containing solid media that the bacteria will grown on. These plates are incubated at the appropriate temperature until colonies are large enough to be counted. Based on experience, approximately 30-300 colonies/plate are considered countable. (Figure 7.15) By applying the dilution factor, the volume applied to the plate and the number of colonies per plate, it is possible to estimate the number of bacteria in the original sample.

$$\text{cells/mL} = \frac{\text{(Average \# of Colonies) * (Dillution Factor)}}{\text{Volume plated}} \qquad \text{Equation 7.2}$$

While this method is simple, and requires little in the way of specialized equipment, it can often present an underestimate of the cells in a specific sample, especially in the case of environmental samples where there may be multiple species of bacteria present, each with different growth needs. It can also take several days to obtain a cell number estimate.

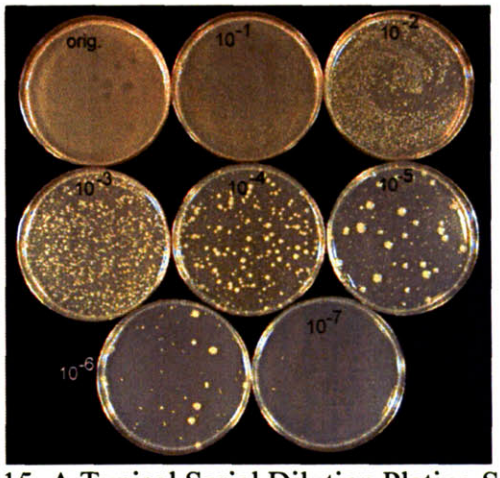

Figure 7.15 A Typical Serial Dilution Plating Scheme[14].

7.5. Cell Visualization by Microscopy

7.5.1. Principles of Optical Microscopy

A simple microscope consists of a light source and a lens or series of lenses. Magnification is achieved by bringing an object into the focal point of the lens. (Figure 7.16)

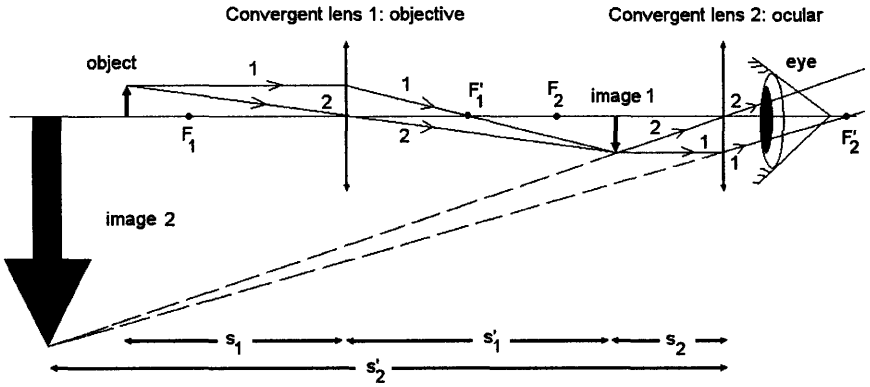

Figure 7.16 A Conceptual Diagram of Magnification by Lenses[15].

The degree of magnification will be limited by the thickness of the sample, the wavelength of the light source, and the manufacture of the lens or lenses. The resolution of a microscope is defined as the minimum distance between two objects such that they appear distinct, and has an inverse relationship between the wavelength of light and the Numerical Aperture of the lens or lenses. For most simple optical microscopes the maximum resolution obtainable is on the order of 0.2 μm, which is good enough to view most whole bacteria, but generally not detailed enough to determine other structural properties.

7.5.2. Preparation of Cells for Optical Microscopy

Because bacterial cells are generally optically clear, addition of a contrast agent is needed to visualize cells under a microscope. There are a number of contrast agents available that allow one to stain particular types of cells or to stain certain parts of cells, but they are all typically either colored or fluorescent dyes.

7.5.2.1. The Gram Stain

A good example of a commonly used colored dying scheme is the Gram Stain[16]. It is used to distinguish Gram positive cells from Gram negative cells. Gram positive cells have a thick outer cell wall made of peptidoglycan while gram negative cells have only a

thin layer of peptidoglycan separating their outer cell wall from their inner cell membrane. (Figure 7.17)

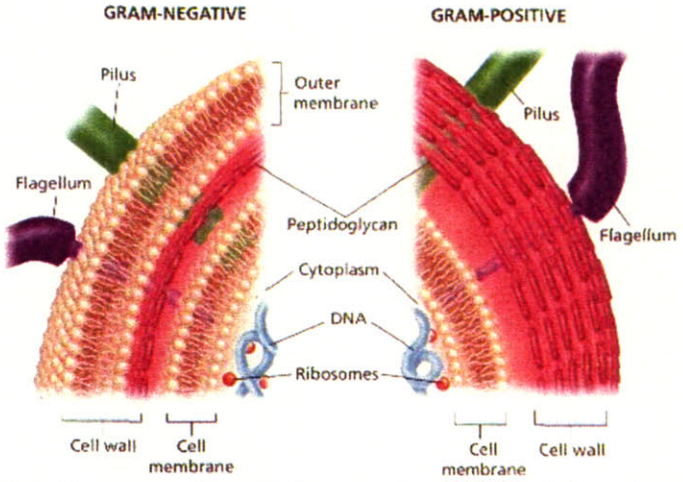

Figure 7.17 A diagram of the differences in cell physiology between gram positive and negative cells[17].

Bacterial cells are first fixed to a glass slide by heating under a flame. A purple dye known as Crystal Violet (CAS #548-62-9) is then added to the fixed cells, the Crystal Violet ubiquitously binds to the cell walls of all types of cells. The excess dye is rinsed away with water and an iodine solution (1% iodine 2% potassium iodide in water) is added to aid in fixing the Crystal Violet. After the excess iodine is rinsed away, a decolorizing solution (3:1 ethanol and acetone) is added. This solution will dissolve the lipids in the cell wall of gram negative bacteria and remove the Crystal Violet dye adhered to the thin layer of peptidoglycan underneath. A second dye, Basic Fuschin (Cas # 632-99-5) is added which colorizes the gram negative cells pink. In this way, gram positive cells appear purple and gram negative cells appear pink under a microscope. While the Gram stain is often used as one of the methods of assessing the physiology of unknown bacteria, for the purposes of this thesis it is used primarily as a positive test for monocultural or uncontaminated bacterial growth.

7.5.2.2. Florescent Dyes

There are many types of commercially available florescent dyes available for the purposes of cell staining, and they can be as specific as fluorescently tagged antibodies or nonspecific, like DAPI. For the purposes of this thesis, DAPI was the only florescent dye utilized and how it works for staining and cell enumeration is described in §7.4.1.

7.5.3. Principles of Transmission Electron Microscopy

Transmission Electron Microscopy, or TEM, is based on the same fundamental physics as optical microscopy. By using electrons, which have a shorter wavelength than optical photons, it is possible to greatly increase the resolution. Modern electron microscopes have resolving power of fractions of an angstrom, making TEM a powerful tool for probing structural details of bacteria.

An electron gun at the top of the TEM emits a stream of electrons that travel through a vacuum and are focused by a magnetic field into a very narrow beam, which is then focused onto a thin sample. Electrons are either attenuated, scattered or pass though the sample. Electrons passing through the sample are detected on a screen, forming an image. The TEM (Figure 7.18) (Tecnai Model # G² F30 S-TWIN TEM) has a point resolving power of 2 Å, and can magnify up to 1000k x.

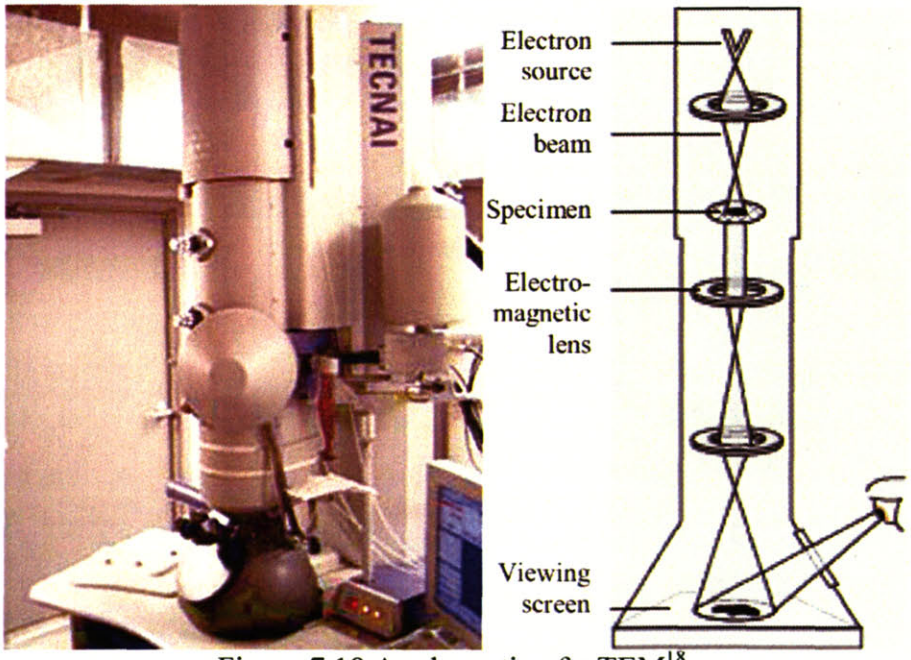

Figure 7.18 A schematic of a TEM[18].

7.5.4. Sample Preparation for TEM

Biological samples for TEM are first fixed in a mixture of 4 to 1 freshly prepared formaldehyde and biological grade gluteraldehyde in phosphate buffer. They are then postfixed in a phosphate buffered solution of 1% osmium tetroxide (CAS#20816-12-0). The process of fixation coagulates a cell's proteins making it rigid so that it can withstand further processing. The samples are then gradually dehydrated in solutions of increasing concentrations of

ethanol, followed by acetone. The dehydration step replaces the water in the sample with –OH groups, this must be done to prevent the destruction of the sample under vacuum. The water is replaced gradually so that as much of the cellular structure can be preserved as possible. The fixed and dehydrated sample is then encased in a resin that provides structural support for the sample when it is sliced thinly. In order to allow electrons to pass through the sample, TEM samples must be extremely thin (70-100 μm). An ultramicrotome (Leica EM U6rt) fitted with a sharp diamond knife is used to slice the samples, which are then mounted on support grids (Electron Microscopy Sciences Cat. #030519) so that they can be handled. Once the samples are sliced, they must be post-stained in order to create contrast. Sample grids are placed in a 7.5% solution of uranyl acetate, rinsed, then placed in a solution of 134 mM lead citrate[19]. The heavy metals bind to the cellular components and provide contrast by attenuating the electrons.

7.6. X-ray Absorption Fine Structure

X-ray absorption fine structure, or XAFS, is a powerful tool that can be used to probe molecular properties such as elemental makeup, coordination number, and bond distances. Because XAFS only probes local structure, long-range order of samples is not required (unlike in XRD, described in §7.7). Solids, liquids and gasses can be analyzed using XAFS.

XAFS requires a bright source of x-rays, which are usually produced in a synchrotron. (Figure 7.19) To produce these x-rays, electrons are first emitted from a cathode and then accelerated to 450 MeV in alternating electric fields by a linear accelerator. They are then injected into a booster synchrotron and accelerated to 7 GeV by switching electrical fields, the path and integrity of the electron beam is maintained by a series of bending and focusing electromagnets. From there, they then travel into a large electron storage ring where they are maintained by several more electromagnets. Photons emanating tangentially from the storage ring are collected by a series of beam-lines where the actual experiments take place.

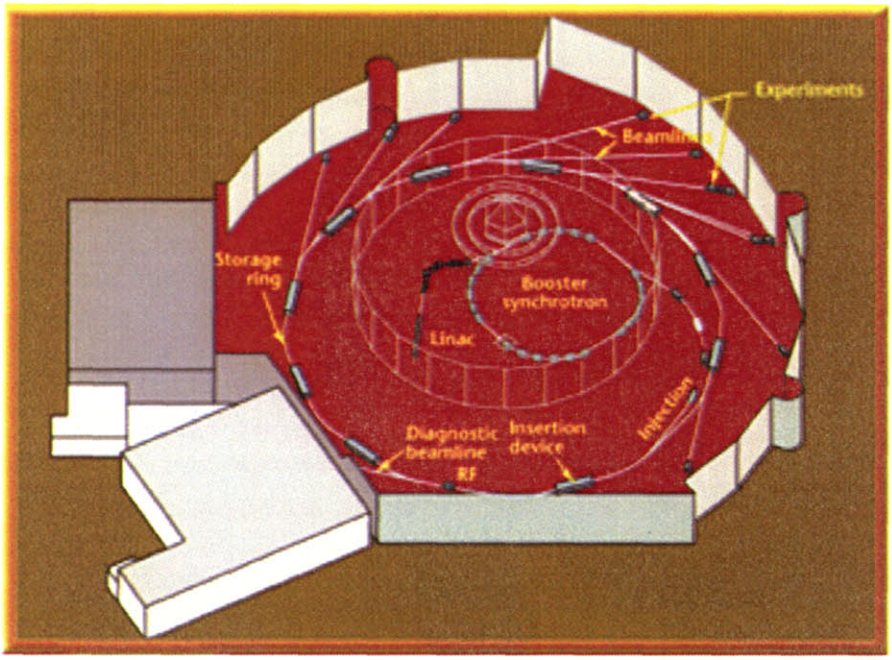

Figure 7.19 A diagram of the Advanced Light Source Synchrotron[20].

For uranium XAFS, the x-rays pass through a monochromator tuned to the uranium L_{III} edge (17,166 eV). The relative intensity of the incident to transmitted x-rays is measured to give the XAFS spectra (Figure 7.20), which is commonly divided into two regions x-ray absorption near edge structure (XANES) and extended x-ray absorption fine structure (EXAFS).

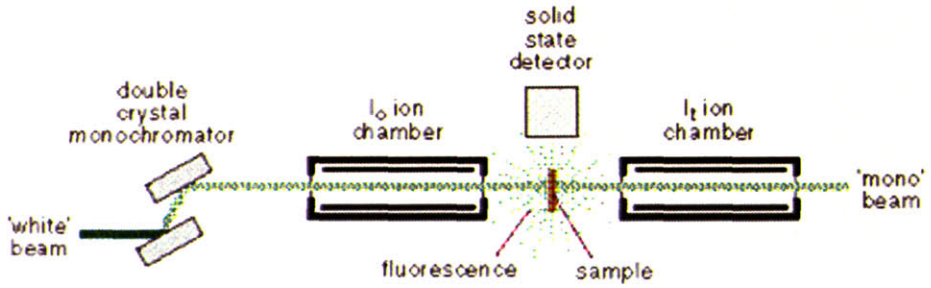

Figure 7.20 A schematic of an XAFS detector.

7.6.1. XANES

The XANES region of the XAFS spectra is the region just before and about 40 eV after the absorption edge. In this region the incident photons are absorbed completely, causing a core photoelectron to be ejected, this is known as the photoelectric effect. (Figure 7.21) The XANES spectrum gives information about chemical bonds, site symmetry, and oxidation state.

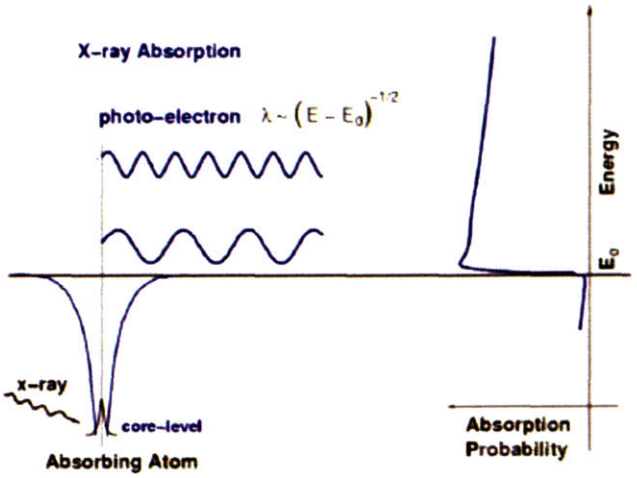

Figure 7.21 The photoelectric effect[21].

7.6.2. EXAFS

Further from the absorption edge, the resulting photoelectrons are scattered by neighboring atoms. This creates patterns of interference that are either destructive or constructive (depending on the wavelength of the photoelectron) and leads to oscillations in the XAFS spectra in the EXAFS region. (Figure 7.22) The EXAFS spectrum provides information about the coordination number, distance, and atomic number of the atoms' nearest neighbors.

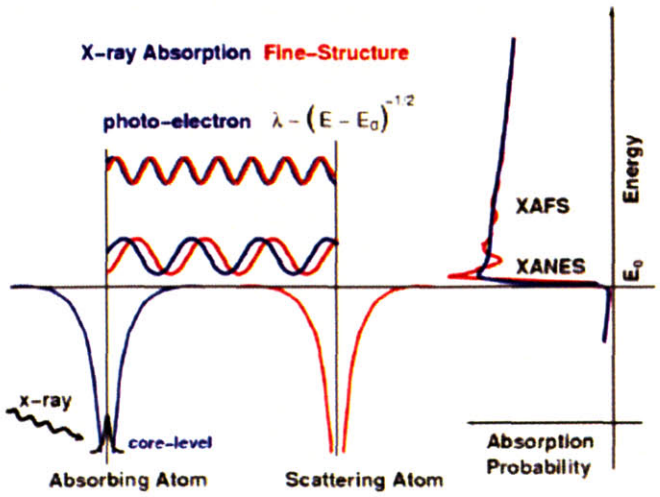

Figure 7.22 X-ray absorption interference leading to spectral oscillations in the EXAFS region[21].

7.6.3. Sample Preparation

Liquid radionuclide-containing samples are prepared by adding liquid of interest to a 1.5 mL polypropylene tube (the material is

relatively transparent to x-rays). The tube is then sealed with epoxy and further heat sealed in two layers of plastic to prevent sample leakage. The triply contained sample can then be mounted on an aluminum cartridge for examination by EXAFS.

Solid samples are diluted to 1-5% uranium with boronitride powder, which is x-ray transparent, and mixed thoroughly. Approximately 10 mg of the sample-boronitride mix is then packed into a small cut-away in a Teflon holder. A piece of kapton tape is applied over the sample to keep it in place and sealed with an o-ring. A thin piece of plastic is then applied over the Teflon holder and screwed into place with aluminum mounting brackets. These brackets serve to contain the sample as well as to keep it in place in the beam's sample changer.

7.7. X-Ray Diffraction

7.7.1. Principles of X-Ray Diffraction

X-Ray Diffraction (XRD) is a tool used to probe a materials crystal structure and lattice distance. The principle of XRD relies entirely on Braggs law which states that:

$$n\lambda = 2d\sin\theta \qquad \text{Equation 7.3}$$

where n is an integer, λ is the wavelength of the x-ray, d is the lattice parameter, and θ is one-half the diffraction angle. (Figure 7.23)

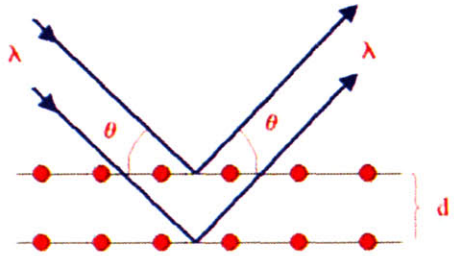

Figure 7.23 Bragg's Law.

A coherent source of x-rays is generated by striking a metal (usually copper) with high-energy electrons. The x-rays pass through a monochromator and a slit such that a coherent parallel beam of radiation is directed at the sample. The beam is then rotated at an angle θ with respect to the sample. The interaction of the x-ray beam with the sample creates secondary radiation that is diffracted in relation to the crystalline lattice parameters of the

sample. These secondary beams usually interfere destructively with one another unless the conditions of Bragg's Law are met, in which case they interfere constructively creating a narrow peak of high intensity. The resulting peak pattern (with intensity on the y-axis and 2θ on the x-axis) is unique and samples can be identified by pattern matching with a library of known peak patterns. XRD is an important tool used to determine crystal structure and lattice parameters of both inorganic and organic crystals.

7.7.2. Sample Preparation for XRD

The Pan Analytical Xpert Pro (# PW3040-PRO) is a powder diffractometer, and thus samples must be both crystalline and in powder form. Samples are ground to uniformity using a mortar and pestle. A slurry is created by adding methanol to the ground sample that is then spread evenly and thinly on a single crystal silicon wafer (this type of support backing prevents interference) and mounted in a bracket (Pan Analytical Part # PW1811/27) that fits into the XRD sample holder. For more precise lattice parameter determination, a standard (such as LaB_6) can be used to align pattern shifts.

7.8. References

---

[1] Spectro Analytical Instruments Ciros Vision ICP-AES Brocure.
[2] http://cp.chem.agilent.com/cag/other/icp-ms.jpg
[3] **Thomas, R.** (2001) Beginner's Guide to ICP-MS Part III: The Plasma Source. Spectroscopy. **16(6):**26-30.
[4] **Thomas, R.** (2001) Beginner's Guide to ICP-MS Part VI – The Mass Analyzer. Spectroscopy. **16(10):**44-48.
[5] **Thomas, R.** (2001) Beginner's Guide to ICP-MS Part VII – Mass Separation Devices – Double Focusing Magnetic Sector Technology. Spectroscopy. **16(11):**22-27.
[6] http://elchem.kaist.ac.kr/vt/chem-ed/spec/uv-vis/graphics/uv-vis-1.gif
[7] **Gong, C.** (2006) Personal correspondence.
[8] **Miller, C. J., J. R. Del Mastro.** (1994) The Use of Selective Extraction Chromatographic Columns as an Alternative to Solvent Extraction for the Separation of Uranium Followed by the Use of Arsenazo III as a Colormetric Reagent for Uranium Determination. INEL http://www.osti.gov/bridge/servlets/purl/10183134-g0un6c/webviewable/10183134.pdf.
[9] **Lowry, O.H., et al.** (1951.) Protein Measurement with the Folin Phenol Reagent. J. Biol. Chem. **193**:265-275.
[10] Pierce Protein Assay Technical Handbook. http://www.piercenet.com/files/1601325%20ProteinAssay.pdf

[11] **Madigan, M. T., J. M. Martinko, J. Parker eds.** (2003) Brock Biology of Microorganisms 10th ed. 148.
[12] http://en.wikipedia.org/wiki/DAPI
[13] **Selinummi, J., S Hautaniemi.** (2004) CellStats. http://www.cs.tut.fi/sgn/csb/cellstats/
[14] http://biology.uwsp.edu/faculty/TBarta/dilPlating/DilutionSeries.html
[15] http://en.wikipedia.org/wiki/Image:Microscope_diag.PNG
[16] **Gram, HC.** (1884) Über die isolierte Färbung der Schizomyceten in Schnitt- und Trockenpräparaten. Fortschritte der Medizin **2:**185-89.
[17] http://www.biologycorner.com/resources/gram_bacteria.jpg
[18] http://nobelprize.org/educational_games/physics/microscopes/tem/index.html
[19] **Hayat, M. A.** (2000) Principles and Techniques of Electron Microscopy: Biological Applications. 299, 342-343.
[20] Advanced Light Source, http://www-als.lbl.gov/als/quickguide/viewstouse.pdf
[21] **Newville, M.** (2004) Fundamentals of XAFS. Consortium for Advanced Radiation Sources. University of Chicago. Chicago, Il.

8. Kinetic Modeling of Bacterial Uranium Reduction

8.1. Abstract

The rate of bacterial uranium reduction by *Shewanella oneidensis* was examined under a number of conditions in order to determine the effect that external factors such as bacterial density, radionuclide activity, electron donor, and pH had on the rate of uranium reduction. It was determined that the rate of reduction fit a first-order exponential decay model with a near-linear association with the density of cells for bacterial concentrations above a minimum threshold density of 1E8 cells/mL, with an optimal cellular density to rate ratio for *in vitro* studies of 1E9 cells/mL. The total uranium solution activity is found to be generally uncorrelated with the reduction rate, although a somewhat faster rate of reduction was observed in samples with greater overall activity. The rate of reduction is slightly dependent on the type of electron donor utilized by the bacteria, and it was found that utilization of lactate as an electron donor for uranium reduction resulted in a rate of reduction that was 34% faster than when compared to H_2. Reduction is also found to be pH dependent, with pH 6.4-6.9 yielding the fastest reduction kinetics. The pH effects both reductive enzyme(s) functionality and uranium speciation dependence, where large changes in pH outside of the optimal pH 6.4-6.9 range lead to no uranium reduction, but smaller changes in pH lead to a decrease in rate associated with the complexation constant of the dominant uranyl carbonate species. Kinetic modeling of uranium reduction should help us to be able to better predict and model how uranium will behave *in situ*, as well as also providing a framework for optimizing bacterial reduction processes *in vitro*.

8.2. Introduction

Mining of uranium ores involves solublizing any uranium present in crushed rock removed from a mine and leaching it out under either acidic or basic conditions. Basic conditions are often utilized in the US for *in situ* leach mining of uranium ores, while acidic conditions are often used for heap leaching of ore and mill tailings piles (§ 3.1.1). Only one to five pounds of uranium can be extracted from every ton of ore, and up until the late 1970's excess tailings could be discarded or stored without governmental regulation. This resulted in the contamination of 24 sites in the United States[1] and most likely many more throughout the world. Cleanup efforts at these sites have consisted mainly of removal of contaminated soil from the site or securing the soil onsite to prevent any further spread of uranium; both of which are often costly and large-scale processes[1]. Bioremediation of soils contaminated with other heavy metals such as chromium, and mercury[2] has been shown in many cases to be a useful and more efficient process than traditional chemical or electric methods of treatment; it has also been

suggested[3] and practiced[4] as a mechanism for remediation of uranium contamination. There are several species of bacteria that are now known to directly catalyze the reduction of uranyl[5], most of which are classified as either iron or sulfate reducers and can be capable of reducing several different metals and inorganic compounds (such as sulfate or nitrate), and of utilizing many types of electron donors. Bioremediation often involves a microbially facilitated change in oxidation state of the target metal to reduce either the mobility or toxicity of the element. Exploitation of a naturally occurring process for cleanup of metal contaminated soils generally causes less stress on the environment than other methods[6], requires less human management, and is often significantly more cost-effective than synthetic chemical treatment schemes[7].

The metal reducing soil bacterium *S. oneidensis* is known to metabolize several different metals including uranium[8]. In an anoxic environment *S. oneidensis* will reduce soluble uranium(VI) to uranium(IV), which is insoluble at a wide range of pH. Uranium in its insoluble form is much less mobile and reactive in soil and groundwater, thus microbially mediated reduction of uranium would help to sequester uranium at the site of contamination.

The mechanism of bacterial reduction of uranium must first be well understood before successful bioremediation of this element can be considered a realistic option. Lovley et al.[9] were the first to characterize the bacterial reduction of uranium, and although some of the molecular mechanisms of the reduction have been determined, the extent to which external conditions affect the reduction still remain unclear. Typical environmental influencing factors such as, bacterial density, radionuclide activity, electron donor and pH will all have an influence on the rate of reduction. In order to achieve the most efficient immobilization of uranium in the environment by bacteria, it will be important to quantify and compare these effects on bacterial uranium reduction. Kinetic modeling allows a simple approach for normalization and comparison of multiple data sets of bacterial uranium reduction under different conditions. The model applied for comparison of data sets in this chapter is a modified first order exponential decay curve, and is similar to the model applied for reduction of uranium by SRB by Spear et al. [10] and Liu et. al.[11], with the exception that an additional constant, $[U_f]$ is added to our model in order to better describe the final non-zero concentration of uranium. Data are fit to the model as follows:

$$[U(t)]=[U_0]\, e^{-kt} + [U_f] \qquad \text{Equation 8.1}$$

where $[U_0]$ and $[U_f]$ are the initial and final concentrations of uranyl, respectively*.

* if $[U_0] >> [U_f]$, otherwise the initial uranium concentration will be equal to $[U_0]+[U_f]$.

8.3. Materials and Methods

Shewanella oneidensis MR-1 is grown aerobically approximately 24 hours at room temperature in Tryptic Soy Broth (TSB). Cells are then concentrated by centrifugation and washed thoroughly with $NaHCO_3$ (1-2.5 g/L) buffer. A small sub-sample of cells are stained with DAPI (4',6-Diamidino-2-phenylindole) and counted under a microscope for accurate determination of cell number (§7.4.1). The cells are then diluted to the appropriate final concentration of approximately 1*E9 cells/mL (unless otherwise specified), two negative controls are also prepared, cells killed in 10% formaldehyde and one containing no cells. Cells are then transferred into sterile anaerobic bicarbonate buffered freshwater medium (unless otherwise specified) as described by Kuai et al.[12], with the following exceptions; phosphate was removed to prevent uranyl precipitation, the carbon source and electron donor was 5 mM lactate, and the electron acceptor was ~2 mM uranium. The cells do not grow in this media but remain metabolically active. At several time points three 1 mL samples are removed from each of the batch experiments and the control into 1.5 mL Eppendorf tubes containing 0.1 mL formaldehyde. The samples are then removed from the anaerobic environment and frozen until analysis. Individual samples are filtered (0.2 μM pore size) to remove any uraninite and cellular material and diluted with 0.1 M HNO_3. The concentration of uranyl present in each sample was measured using ICP-AES (§7.1) or determined photometrically with Arsenazo III (§7.3.21). Data are fit to the first order model (Eqn 8.1).

A more detailed explanation of the methods is provided in the chapter 8 appendix.

8.4. Cell Density Dependence

Understanding reduction kinetics as a function of cell density will help to determine the mechanism as well as some of the primary operating conditions for this reaction. The experimental procedure given in §8.3 is followed except that multiple batches with differing cellular densities ranging from 10^6-10^{10} cells/mL are compared. Here we show that *S. onedensis* reduces uranium with first order kinetics as previously demonstrated by Spear et al. for *Desulfovibrio* and *Clostridium* [13,14], and that the first order reduction rate constant k is dependent upon cell density.

8.4.1. Results

Each of the cell aliquots, with the exception of the batches with less than ~10^7 cells/mL, were shown to facilitate the reduction of U(VI) to U(IV) as evidenced by a reduction in the uranyl present in the media over time (Figure 8.1) and the accumulation of a brown-black precipitate determined from previous experiments to be uraninite by XRD[15]. Those batches containing less than ~10^7 cells/mL did not differ significantly in uranyl reduction from the controls. All of the batches containing cells showed an immediate

drop in uranyl concentration that increased roughly with cell density, which is attributed to uranyl sorption onto the cellular biomass (see appendix for further details). Results also indicate that the reduction reaction occurs only in live cells, those killed with heat, formaldehyde or inhibited by cyanide and molybdate[16] did not exhibit significant uranyl reduction, only an initial sorption indicated by a drop in uranyl concentration within the first 30 minutes without further reduction over time (Figure 8.2).

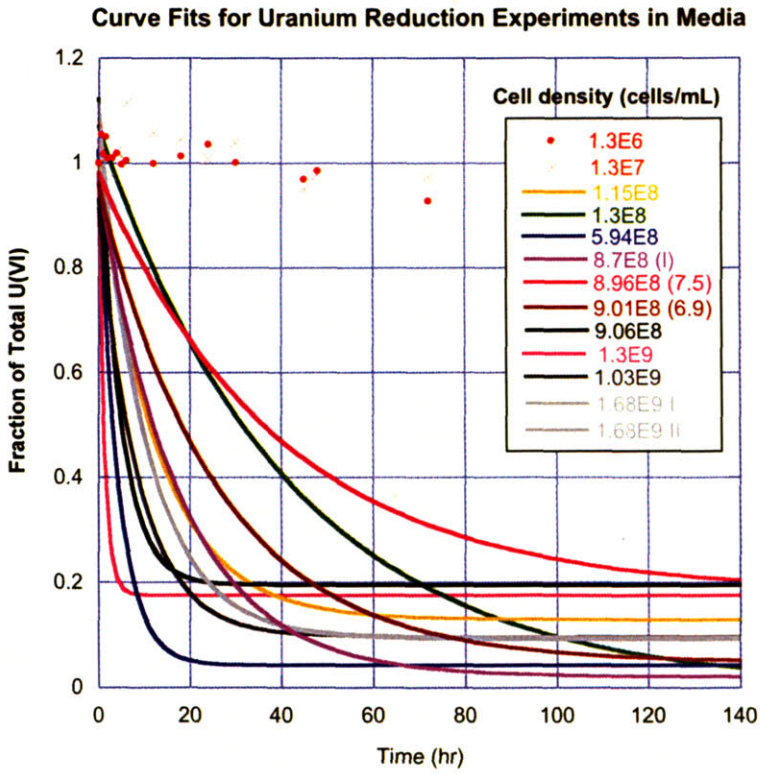

Figure 8.1 Normalized uranyl Reduction vs time
Data are normalized with respect to initial uranyl concentration.

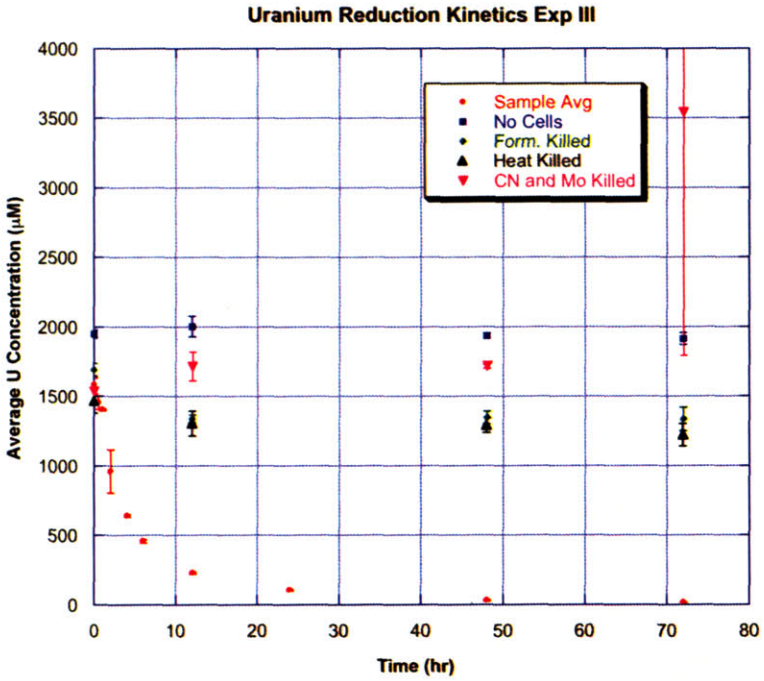

Figure 8.2 Absence of uranium reduction by *S. oneidensis* in the presence of different inhibitors. Error bars represent 1 standard deviation from triplicate samples. The method of killing the cells had no significant effect on the uranium concentration or reduction.

Figure 8.1 shows the normalized reduction of uranium over time for several differing cell concentrations. Uranium concentrations are normalized to the value of $[U(VI)]_{t=0}$, because although initial uranium was added consistently to concentration of approximately 2 mM, there were differences in the measured initial values of uranium throughout the course of several experiments. In order to determine the optimal cell density for uranium reduction by *S. oneidensis* there are two important constants to factor in, the initial reduction rate k, and the total amount of uranium reduced, or $[U_f]$, both of which are accounted for in the decay-fit model. Figure 8.3 gives a comparison of reduction rate constant k for several cell concentrations, and although not completely linear, the results indicate that the rate of uranium reduction is related to the density of bacteria present. The total amount of uranium reduced $[U_f]$ seems to be less well correlated, although uranium reduction by most cell densities reached ~90% during the time of the experiment, roughly 70-120 hours. These data show that the total amount of uranyl reduced may be dependent on more system variables than just bacterial density.

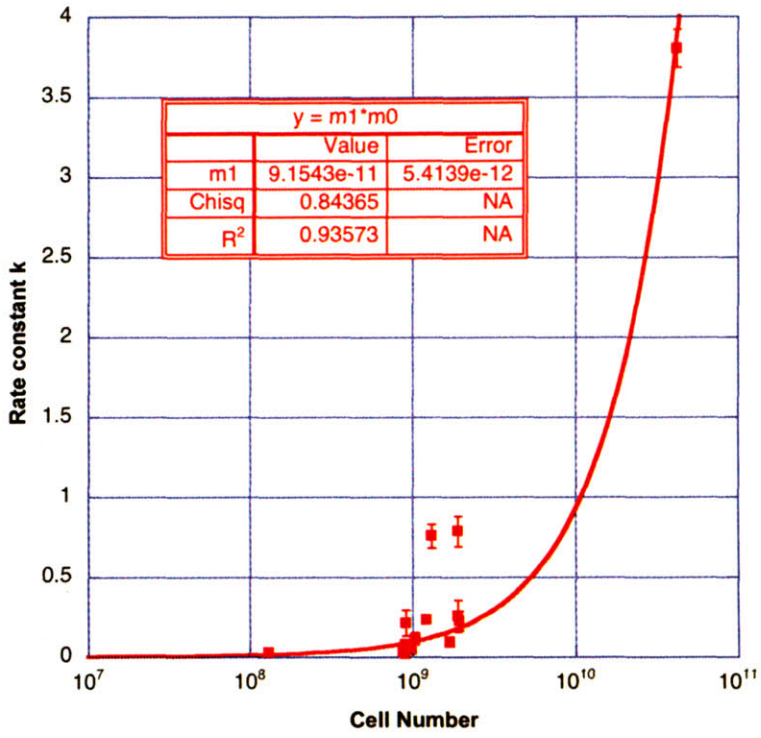

Figure 8.3 Reduction rate constant (k) as a function of cell number, the solid line indicates a linear fit of $y = (9.154E\text{-}11 \pm 5.41E\text{-}12)*X$ with an R^2 of 0.936.

8.4.2. Discussion

There are several features of the cell density dependence of uranium reduction that are of interest, namely the instantaneous initial drop in uranium concentration, the total amount of uranyl reduced and the reduction rate, k.

The initial sorption of uranyl should be dependent on initial uranium concentration as well as cell number. The total sorption will be a function of the cell density because the number of cells/mL will be related to the number of surface binding sites for uranyl sorption (Figure 8.4).

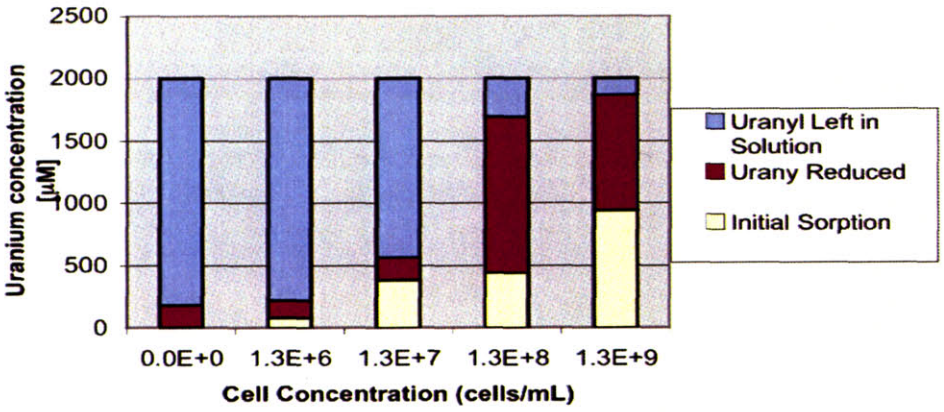

Figure 8.4 Reductive capacity, illustrating both the total uranium reduced as well as the initial uranium sorption.

Sorption is a fast reaction step, occurring within the short amount of time that it takes to add the uranyl, and then to subsequently remove the samples. Although biosorption processes like these will have the immediate effect of reducing the free uranyl concentration in the environment where these bacteria are present, it is not a long-term solution since the sorption process is often reversible. Changes in the local environment could lead to desorption of the uranyl from bacterial biomass. Not only that, but once all of the binding sites on a cell have been filled, there can be no further binding of uranyl without the adding more biomass. So although the adsorption step is related to the density of bacteria, more overall uranium can be removed from the solution by fewer cells if active reduction also occurs.

After the initial drop in uranyl concentration due to sorption, the metabolically active cells will reduce uranium. From Figure 8.3 the rate constant k, is linearly associated with the density of cells by:

$$k=(9.2\pm0.54)*10^{-11}*(\text{cells/mL}) \quad R^2=0.936$$

When data are grouped according to electron donor (either H_2 or lactate) the rate constants become (see § 8.6):

$$k_{H_2}=(9.1\pm0.74)*10^{-11}*(\text{cells/mL}) \quad R^2=0.961$$
$$k_{lac}=(6.7\pm0.34)*10^{-10}*(\text{cells/mL}) \quad R^2=0.180^{\dagger}$$

† the lack of correlation for this fit is likely due to the fact that there cell number only varied from 1.3E8 to 1.68E9 cells/mL

A majority of the bacterial reduction experiments were performed at cell concentrations of approximately 1E9 cells/mL, with only one reduction curve for the cell concentrations ranging from 10^6 - 10^8, and 10^{10} cells/mL. In order to obtain a more statistically accurate interpretation of the rate of uranium reduction as a function of cell density that is not dominated by its endpoints, a more thorough examination of cell concentrations in the range of 10^7-10^{10} is necessitated. However, both the experimental data and the fit model both indicate that there will be no significant uranium reduction below a certain threshold value of about 10^8 cells/mL. Such a threshold could be due to either: the detection limits of the instrument (for ICP-AES they are on the order of 1 μM, but due to dilution, will be about 5 μM for the actual samples) making changes in uranium concentration of 5 μM or less out of the range of detection. For a 100 mL batch sample this would mean that ~0.1 mg of UO_2 must be produced before it can accurately be detected by ICP-AES. Also, for cell densities lower than 10^8 cells/mL the time required to achieve a change in uranium concentration of 5 μM using the estimated rate constant k of 9.2E-11, is on the order of 225 days, much longer than the 120 experimental hours. The apparent minimal threshold for uranium reduction could also be because a certain minimum concentration of U(VI) needs to be reduced to U(VI) before the solubility limit of uraninite is exceeded, causing precipitation. At pH 7, the solubility of U^{4+}/UO_2 is: $K_{sp}{}^{11}=10^{-26.7}$. Typically, for uranium reduction to occur in the environment microbial communities of uranium reducing bacteria must be stimulated to grow[3,17]. Holmes et al.[3], found that the density of *Geobacter sp.* at the site of uranium contamination in Shiprock, NM increased about three orders of magnitude to 10^6 cells/g of soil after 10 days of acetate injection. At this bacterial density there was a decrease in uranyl concurrent with the growth of the *Geobacter sp.*, during the time of this experiment, which was over a period of 40 days. Thus, although uranium reduction was observed at a lower cell density than estimated here, the duration of the experiment was much longer. This data implies that, even under optimal reducing conditions (ie anoxygenic, nitrate-free, abundance of electron donor), a minimal bacterial density must be achieved before significant uranium reduction will take place, and that the threshold density may be different for bacteria found in the environment versus under laboratory conditions.

The total amount of uranium reduced varied in these experiments from less than 1% (for cell concentrations of 1.3E6 and 1.3E7) to nearly 100% (for cell concentration of 4.1E10), and did not seem to correlate directly to cell concentrations ranging from $1.3e^8$ to $1.9e^9$ as is apparent from Figure 8.5, however, for cell densities of

$>10^9$ there was less than 25% of the initial uranyl remaining in solution.

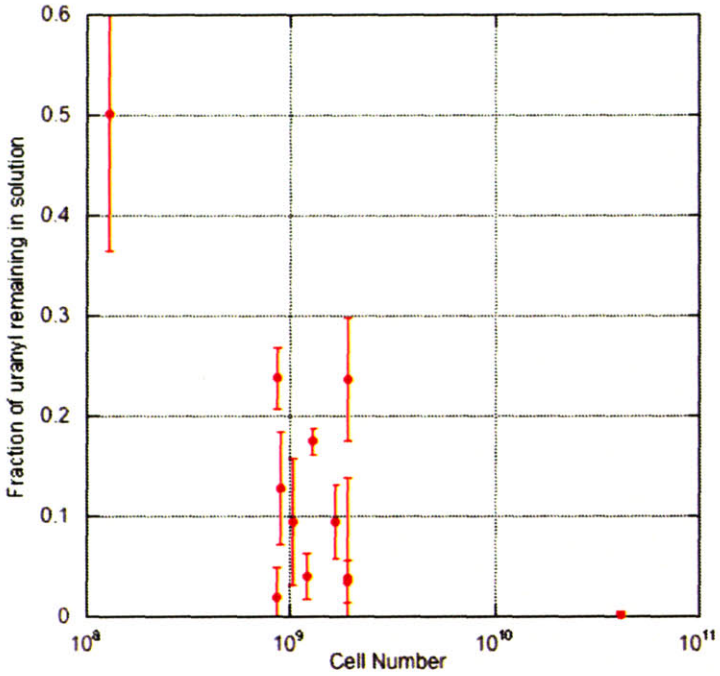

Figure 8.5 Fraction of remaining uranyl vs. cellular density (cells/mL).

This lack of direct correlation between the cell density and the amount of free uranyl could indicate that the total uranyl reduced in the course of the experiment is related to properties other than just the bacterial density. Organic ligands that form moderate to strong complexes with uranium have been shown to slow down and even prevent the reduction of uranium by *S. oneidensis*[18]. Calcium in millimolar concentrations has also been shown to be inhibitory to uranium reduction[19] however, these conditions are not met in the uranium reduction media used in these experiments. The release of organic phosphate after long periods of incubation due to cell death and lysis also does not play a significant role in uranium complexation because no late-drop in uranium concentration was observed in control samples. However, cells harvested from rich media after longer periods of time (late log phase) might remain viable in solution for shorter periods of time, leaving behind more unreduced uranyl than cells harvested earlier which may remain metabolically active for longer.

Overall the kinetics behave as expected with respect to the cellular density of *S. oneidensis*. The initial sorption is related to the biomass concentration, whether living or dead, but this fast-step is independent of the overall rate of reduction in live cells. Fitted to a first-order exponential decal model, the rate of reduction is nearly-

linearly dependent upon the density of cells. This is to be expected assuming that the number of uranium reductive sites per cell is approximately the same. This information is important from a remediative perspective in that not only will growth of bacterial biomass need to be stimulated; but that it must exceed a minimum value to occur. It is also important from an *in vitro* perspective when one is considering optimizing conditions to achieve maximal reduction in a minimal amount of time.

8.5. Activity Dependence of Uranium Reduction

Dose is necessarily a concern when considering the harmful effects of radioactive waste. For uranium bio-reduction to be an effective option either *in vitro* or *in situ*, it will be important to consider the effects that radiation dose might have on the bacteria and their subsequent ability to reduce uranium. Here we compare the activity from 50%, 25% enriched, and depleted uranium to the rate of uranium reduction by *S. oneidensis*.

8.5.1. Results

A comparison was made for several experiments involving 50% enriched uranium (2.94E-4 Ci/mol), 25% enriched uranium (1.87E-4 Ci/mol) and depleted uranium (8.05E-5 Ci/mol) in order to determine if the increased activity due to significant uranium enrichment had any effect on the rate of uranium reduction. Figure 8.6 shows the rate of uranium reduction normalized to a cellular density of 1.68E9 using Eqn 8.1 versus the total activity in the sample. Surprisingly, this data suggests that, if anything, the increase in activity due to enrichment results in a faster rate of uranium reduction, however, more detailed information is necessary in order to determine if this effect is real or not.

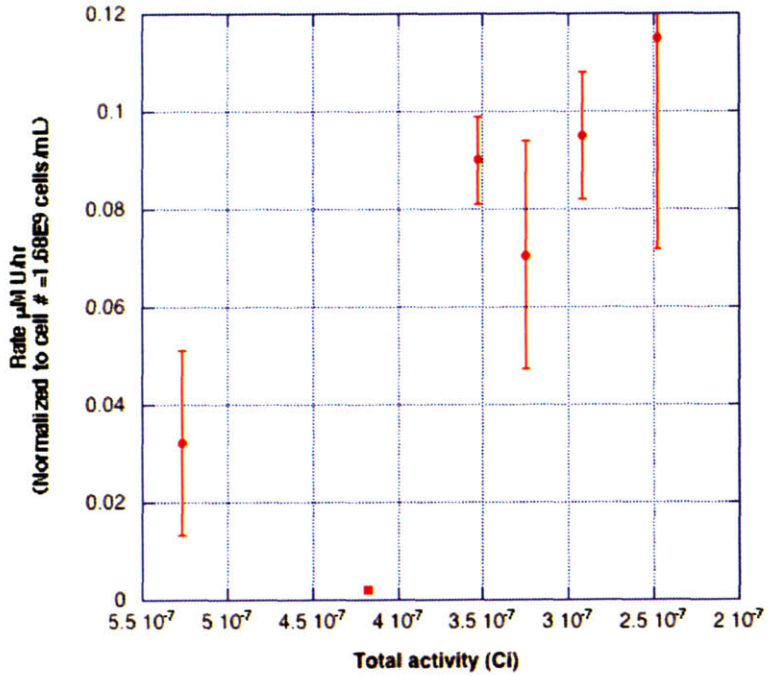

Figure 8.6 Normalized rate (using Eqn. 8.1) vs. total activity for selected experiments.

8.6. Electron Donor Dependence

S. oneidensis are known to reduce uranium using at least two electron donors, H_2 and lactate. Coupling the oxidation of H_2, the reduction of uranium in *Shewanella* is:

$$H_{2(aq)} + UO_2^{2+} \Leftrightarrow 2H^+ + UO_{2(s)}$$

The $\Delta G^{\circ\prime}$ for this reaction is -79.6 kj/mol[11]. For lactate, *S. oneidensis* couples the oxidation of lactate to acetate to the reduction of uranyl:

$$Lactate_{(aq)} + 2H_2O + 2UO_2^{2+} \Leftrightarrow 2UO_{2(s)} + Acetate_{(aq)} + HCO_3^- + 5H^+$$

The $\Delta G^{\circ\prime}$ for this reaction is -80.61 kj/mol[11], thus, the bacteria are, in theory, able to gain slightly more energy from coupling the oxidation of lactate to the reduction of uranium, than they are to the oxidation of H_2. However, the values of $\Delta G^{\circ\prime}$ are for the standard conditions of: 1 molar concentration, 25°C, and pressure of 1 atmosphere. While the temperatures and pressure of bacterial reduction are similar to standard values, typically, the concentrations are orders of magnitude lower (in the mM-µM[17] range). Meaning that the $\Delta G^{\circ\prime}$ values cannot be considered strict indicators of the energy bacteria can gain from a certain electron donor in the environment under non-standard conditions[20].

Most uranium bioreduction schemes involve the injection of a carbon substrate such as acetate[17] into the soil, to encourage the removal of nitrate and the growth of bacteria capable of reducing uranium. Injection of a liquid media containing

carbon is much easier to achieve than the injection of a gas like H_2 into the groundwater, not only that, but *S. oneidensis* can use the carbon in lactate for both growth and energy, rather than H_2 for which they can only utilize for energy.

8.6.1. Results

Here we compare the rates of reduction between *S. oneidensis* utilizing either H_2 or lactate as the electron donor for uranium reduction. Cells of *S. oneidensis* at a final concentration of 8.7E8 are placed in an anaerobic chamber containing 3:5:92 H_2:CO_2:N_2, approximately 2 mM U(VI), and either a phosphate-free lactate media[12], or 15 mM HEPES. Figure 8.7 shows the electron donor dependent reduction of uranium under these conditions.

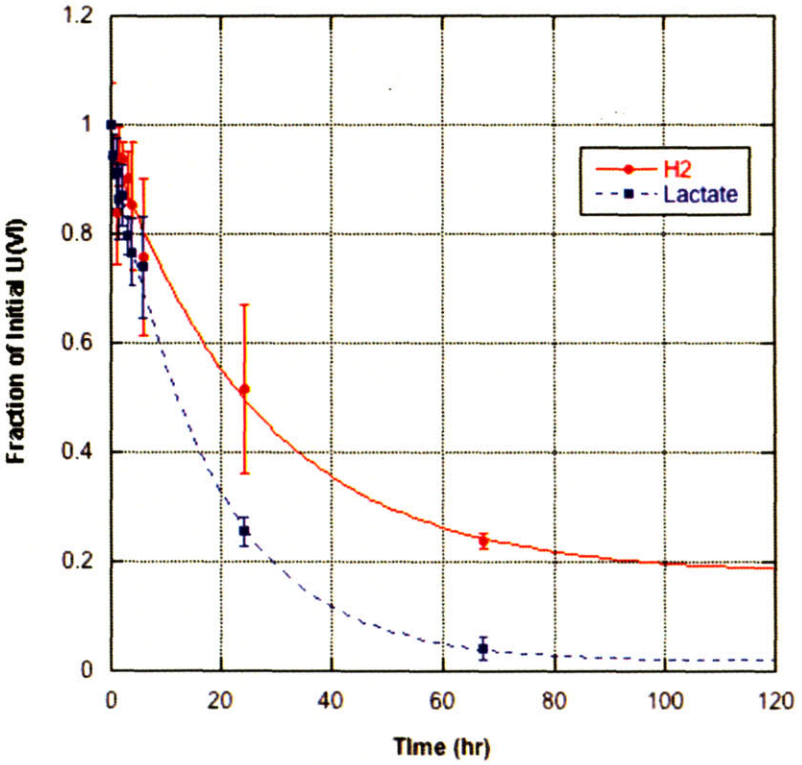

Figure 8.7 Normalized uranium reduction as a function of electron donor. Error bars represent one standard deviation.

With H_2 as the electron donor, the reduction of uranium can be modeled by:

$$[U(VI)_t / U(VI)_{t=0}]_{H_2} = (0.179 \pm 0.085) + (0.780 \pm 0.080)\exp\left[(-0.037 \pm 0.01)t\right]$$

With lactate as the electron donor the reduction is

$$[U(VI)_t / U(VI)_{t=0}]_{lac} = (0.019 \pm 0.031) + (0.950 \pm 0.030)\exp\left[(-0.057 \pm 0.01)t\right]$$

With the R^2 values for both fits being 0.971 and 0.995, respectively.

For the same reaction conditions, the use of lactate results in a uranium reduction rate that is 34% faster, and proceeds to 96% completion in 70 hours. With hydrogen on the other hand, the reduction only reaches 76% completion during the duration of the experiment.

8.6.2. Discussion

Both lactate and H_2 can act as electron donors for the reduction of uranium by *S. oneidensis*, however, the rate of reduction and the overall completeness of the reduction reaction will depend on which electron donor is available. A comparison of the rates of reduction for other experiments utilizing either H_2 or lactate as the electron donor also shows that the rate constants for uranium reduction with lactate are greater than those utilizing H_2. Figure 8.8 is the same as Figure 8.3 except that experiments are differentiated on the basis of electron donor.

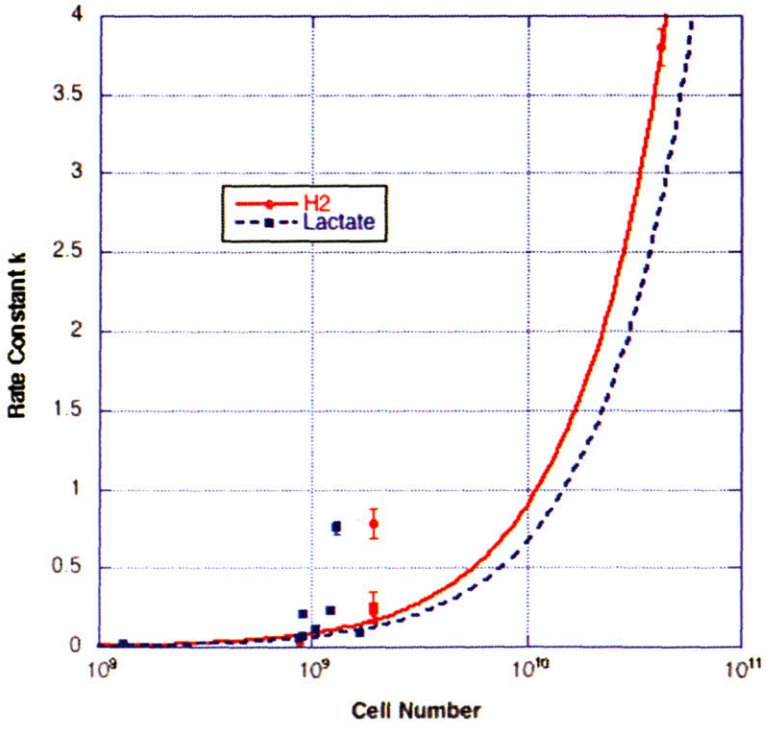

Figure 8.8 The rate constant k as a function of electron donor and cell number. The line represents a linear fit of k.

In another study, Liu et al.[11] found that H_2 serving as the electron donor for uranium bioreduction resulted in faster reduction kinetics than for lactate. In their study however, they used significantly more H_2 than in the experiment performed here (about 37% vs. 3%). The differences in rate of electron donor use in this case are then attributed to H_2 being in a rate-limiting, but more environmentally relevant concentration for this experiment. The concentration of lactate was comparable to Liu et al. (10 mM vs. 5 mM, both being in excess). In the case of Liu et al., the difference in rate for the two electron donors is due to diffusion. When both electron donors are in excess; because of its small size, hydrogen will diffuse through cellular membrane much faster than lactate. For the data presented here, hydrogen is not in excess, so the rate of reduction in this case is limited by the substrate availability, rather than the rate of substrate diffusion. Although these results are unsurprising, amending uranium contaminated sites with carbon electron donors (like acetate[17] or lactate) should yield faster and more complete uranium reduction than H_2. Carbon containing electron donors will act to serve a multiple purposes in the environment, and will encourage the growth of uranium reducing microorganisms as well as to serve as a faster and more efficient electron donor for uranium reduction.

8.7. pH Dependence of Uranium Reduction

The pH of the environment will have multiple effects on the overall conditions of a system; it can affect the bacterial functionality, as well as dictate the speciation of uranyl and the solubility of UO_2. It is thus important to understand how pH can contribute to the bacterial reduction of uranium.

Although some bacteria can tolerate very low or high proton concentration, many types of bacteria are most viable at circumneutral pH, including *S. oneidensis.* The pH can alter the dominant functional groups exhibited by proteins and enzymes that could be responsible for the adsorption and reduction of uranyl. Haas et. al[21]. determined that U(VI) sorption to *S. oneidensis* was dominated by carboxyl, phosphoryl, and amine groups with pK_a values of 5.16, 7.22, 10.04 respectively, that the overall surface charge was atypically positive below pH 7.5, and that optimal U(VI) sorption occurred around pH 5 (Figure 8.9). However, sorption to the bacterial surface only tells half of the story; the reduction rate will also be dependent upon the functionality of the enzymes responsible for uranium reduction and how those enzymes can sterically interact with the dominant uranium species as a function of pH. In general, enzymes have an optimal stereochemical functionality at a certain pH; changes in pH will alter the hydrogen bonds responsible for the shape of the enzyme, and hence, its functionality. Thus, for *S. oneidensis* while U(VI) sorption may be greatest at pH 5, the rate of uranium reduction may be higher at pH 7.0, where the growth of *S. oneidensis* is most favorable[21].

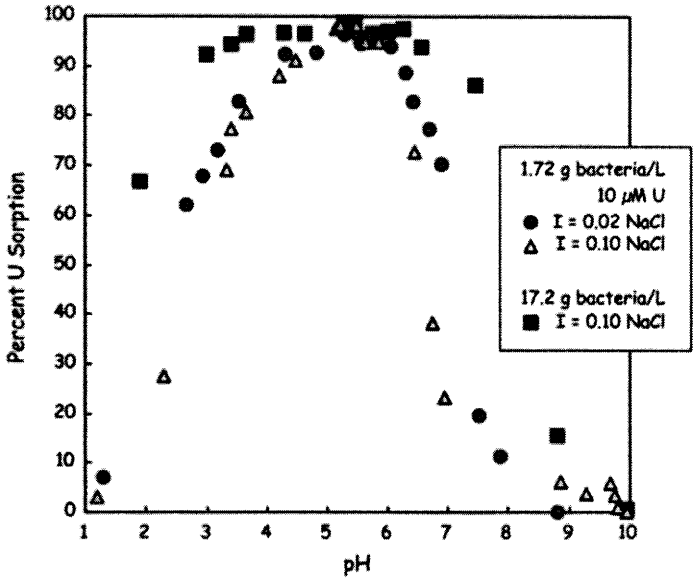

Figure 8.9 Uranium sorption data from Haas et al.[21] showing uranium sorption (10 μM) onto *S. oneidensis* after 12 hours as a function of pH.

The pH will also play a role in the speciation of uranyl. Figure 8.10 shows the dominant U(VI) species as a function of pH in lactate media and was calculated using the speciation algorithm JCHESS[22] using the chess.tdb database, which is a CHESS-formatted version of EQ3/6 (V.8-R.6)[23]. For the pH range 5-8 and pCO_2 of 0.05 atm, uranyl carbonate complexes are the most abundant, but the number of carbonates surrounding the uranyl and the overall charge of the complex will vary with solution carbonate concentration and pH.

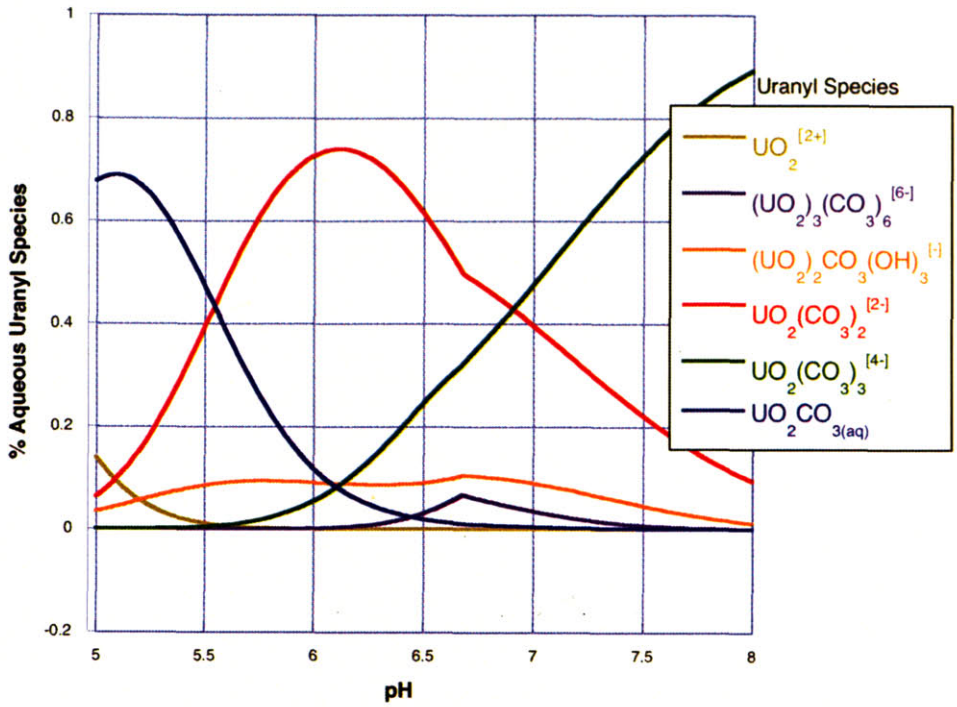

Figure 8.10 Dominant U(VI) species in lactate media at pCO_2=0.05 atm as a function of pH.

8.7.1. Results

Cells were separated into batches containing lactate media at several pH's at a final cell concentration of ~$1E^9$. Three pH's were chosen to correspond to each dominant uranyl species as shown in Figure 8.10, and the fourth pH (6.9) was chosen where the dicarbonate and tricarbonate uranyl species are in equal concentrations. They were 5.1±0.10, 6.4±0.14, 6.9±0.04 and 7.4±0.11. The pH was monitored throughout the course of the experiment and adjusted, if necessary, to maintain as best as possible a constant pH. Figure 8.11 shows the rate of uranium reduction at the aforementioned pH values.

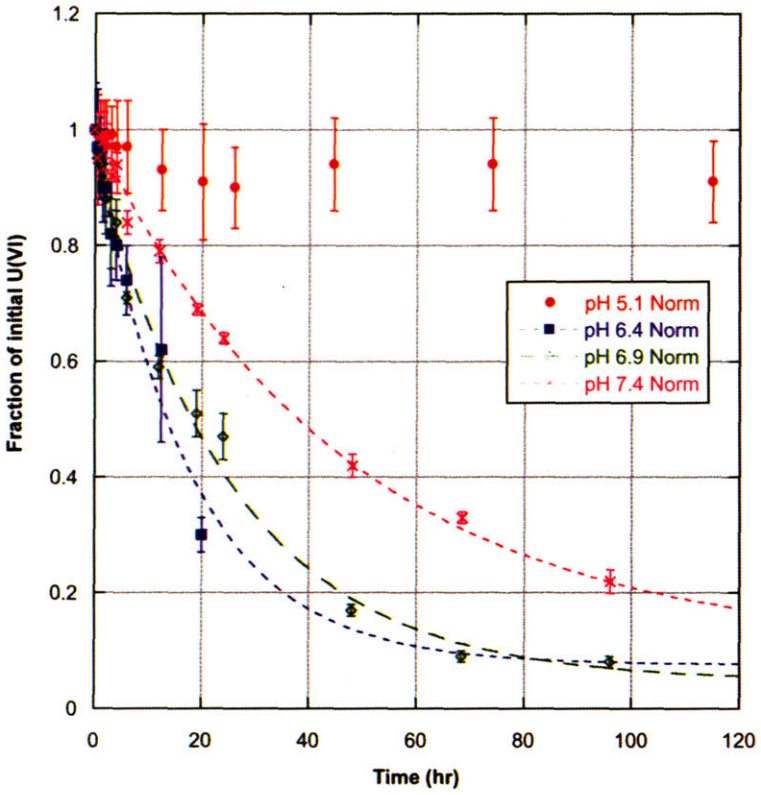

Figure 8.11 Normalized uranium reduction vs. pH. Error bars represent 1 standard deviation. Note that for pH 6.4 time points exceeding 24 hours were removed in order to model the reduction, Figure 8.13 presents the entire data set.

Table 8.1 gives the values for the constants used in the first order reduction fit, because pH 5.1 exhibited little change in the uranyl concentration, it could not be fit well using this model.

Table 8.1 Fitted reduction rate constants.

$$[U(VI)]/[U(VI)_i]=[U(VI)_f]/[U(VI)_i]+[U(VI)_i]/[U(VI)_I]*\exp(-k*t)$$

pH	$[U(VI)_f]/[U(VI)_i]$	$[U(VI)_f]/[U(VI)_i]$ Error	$[U(VI)_i]/[U(VI)_I]$	$[U(VI)_i]/[U(VI)_I]$ Error	k (per hr)	k (per hr) Error	R^2
5.1	--	--	--	--	--	--	--
6.4	0.076	0.327	1.385	0.311	0.056	0.033	0.958
6.9	0.047	0.025	0.911	0.026	0.039	0.003	0.992
7.4	0.104	0.031	0.888	0.029	0.021	0.002	0.996

Figure 8.12 gives the controls for the data in Figure 8.11. With the exception of the pH 6.4 control, none of the controls were observed to reduce uranium, and the data shows that the uranium concentration in these samples remained relatively constant.

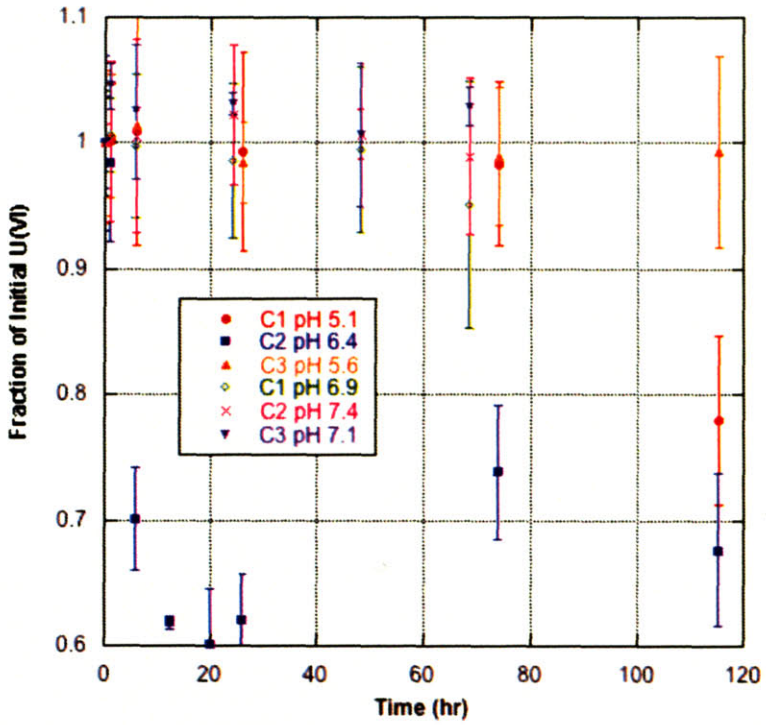

Figure 8.12 Normalized Controls for the reduction of uranium as a function of pH. Error bars represent 1 standard deviation.

For the lowest pH (5.1) there is almost no perceivable reduction, at the pH the dominant uranyl species is $UO_2(CO_3)_{(aq)}$. As the pH is increased to 6.1 and 6.9, the rate of reduction increases and more total uranyl is reduced. The rates of reduction are nearly the same for these two pH values (Table 8.1). At pH 6.4 the dominant uranyl species is the dicarbonate $UO_2(CO_3)_2^{2-}$, while at pH 6.9 the dicarbonate species and tricarbonate species ($UO_2(CO_3)_3^{4-}$) are in approximately equivalent concentrations. At pH 7.5 the tricarbonate species completely dominates and the rate of reduction is slightly decreased, along with the total amount of uranyl reduced.

It should also be pointed out that there were slightly anomalous results for both the sample and its corresponding formaldehyde killed control at pH 6.4. Firstly, uranium reduction was observed in the control, and secondly, after 24 hours the uranium concentration in both the sample and the control began to increase. Figure 8.13 shows the data for sample and control at pH 6.4. For all other pH values no reduction was observed in the control samples, nor did it occur in any other of the formaldehyde-killed control samples for other uranyl reduction experiments, thus in this case the reduction observed in the control was attributed to improperly killing the control cells before the experiment. This is further evidenced by the similar reduction kinetics of both the

sample and supposed control. Their similarity suggests that a large portion of control cells exposed to formaldehyde remained metabolically active during the experiment and behaved as a sample rather than a proper control.

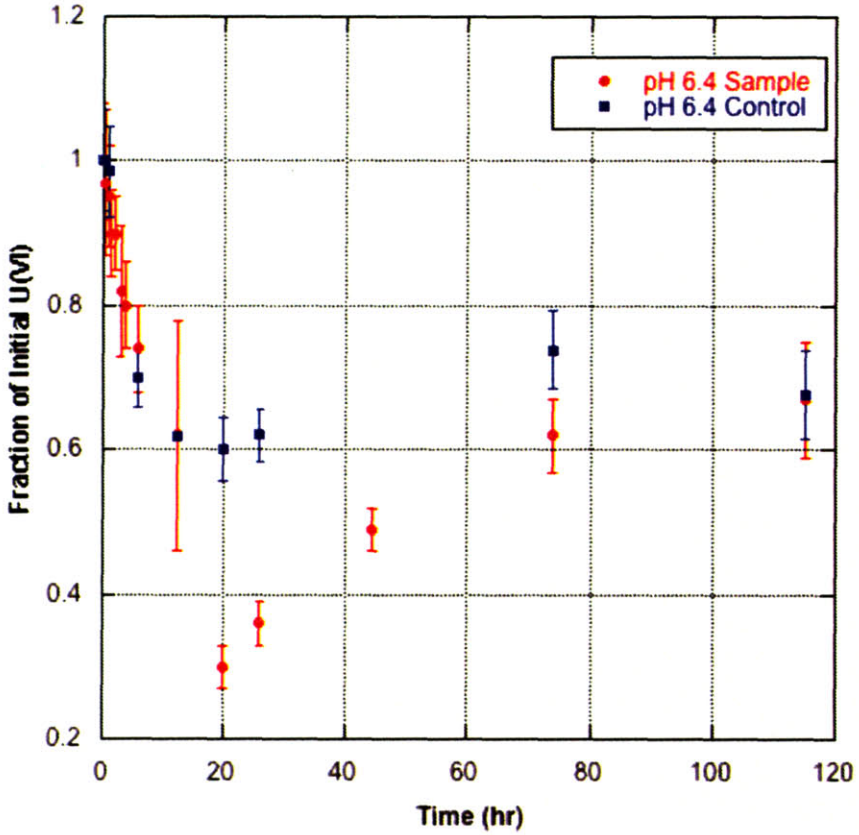

Figure 8.13 Sample and Control data for pH=6.4. Error bars indicate 1 standard deviation.

It is apparent that at pH 6.4 (Figure 8.13) there was some resolubilization of uranium in the sample. At that pH dissolution of UO_2 in carbonate may occur, but on a scale of several weeks[24] rather than hours. Dissolution of the precipitate was observed, as evidenced by a return of the sample to a yellow color, which may mean that the precipitate formed during this experiment was a less stable form of reduced uranium. The dissolution of the precipitate occurred only after 24 hours, and is most likely a chemical process not related to the metabolic dependent reduction of uranium by bacteria, meaning that the initial reductions kinetics can still be fit, analyzed and interpreted. For the samples at pH 6.9 and 7.4, the precipitate was much darker and more indicative of UO_2.

8.7.2. Discussion

Regardless of the anomalous data for pH 6.4, the rate of uranium reduction by *S. oneidensis* is dependent upon the pH of the uranium-bearing media. It is clear that there is an optimal pH for reduction between about 6.4 and 6.9, in this pH range the reduction proceeds the fastest and results in the reduction of about 95% of the initial uranyl. Almost no reduction was observed for pH 5.1, where the speciation of uranyl is an uncharged aqueous mono carbonate complex. However, even though not as fast or as efficient, reduction was still observed at pH 7.5. It is interesting that the least reduction was observed at pH 5.1, the same pH that Haas et al.[21] found to adsorb the largest fraction of uranium[‡]. This is an indication that although the pH affects the sorption of uranyl to the cell surface, that the subsequent reduction of uranium is affected differently by the pH. Plotting the reduction rate (k) vs. pH (and the complexation constants for the uranyl carbonate species) yields a linear relationship for pH 6.4-7.4 (Figure 8.14). The viability of *S. oneidensis* is not significantly affected for any of the pH values studied here during the first 8 hours; growth of *S. oneidensis* is observed even after 29 hours at each pH. (see the chapter 8 appendix for further information) Thus, at least for the initial 24 hours where a majority of uranium reduction occurs, the cells do not lose a significant portion of their ability to divide, regardless of the pH. The pH, however, may still affect the stereochemistry and functionality of the proteins expressed on the cell surface, some of which are responsible for reduction of uranium. Most likely, the pH effects both the functionality of the uranium reducing enzyme(s) as well as their ability to overcome the increasing complexation of uranyl as the pH is increased. At pH 5.1 the functionality of the enzyme(s) responsible for uranium reduction must be drastically impaired, because there is no observed reduction even though the sorption of uranium is maximal and the uranium-carbonate complex is at its weakest.

[‡] Although Haas et al. had 1% CO_2, where uranyl-hydroxide complexes also exist in a larger fraction, whereas at 5% CO_2 (Figure 8.10), uranyl hydroxide complexes make up less than 0.1% of the dominant uranium complexes.

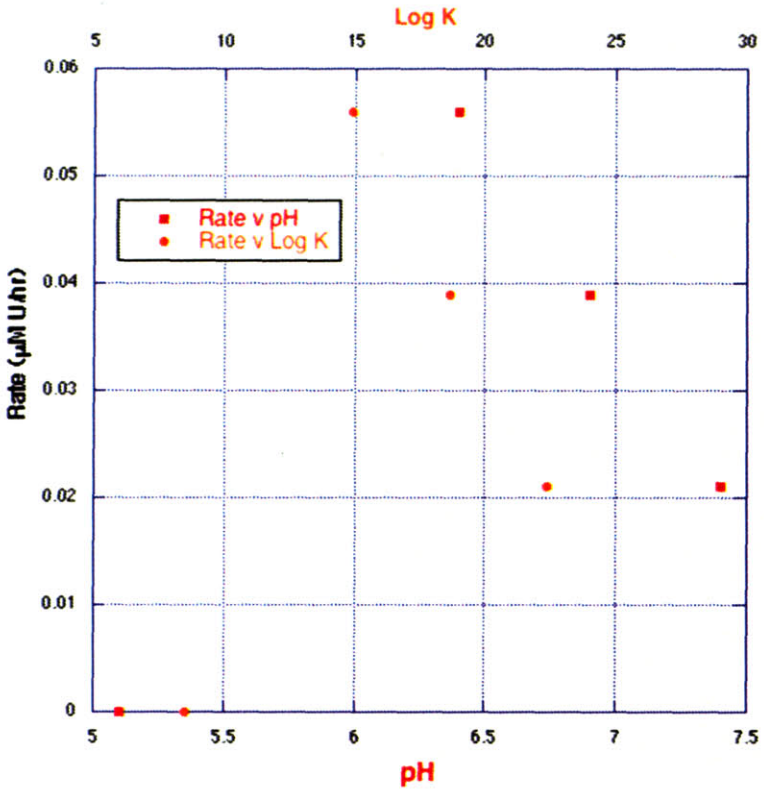

Figure 8.14 Reduction rate vs pH and the log K of the dominant uranium species (for pH 6.9 where the di and tri carbonate species are in approximately equal concentrations, the log K's were averaged).

Although the reduction of uranium is dependent upon the pH, and is optimal at pH 6.4-6.9, small changes in pH of about ±0.5 pH units should still result in the reduction of uranium, while larger changes in pH will inhibit uranium reduction most likely due to a decrease in enzyme functionality. In order to achieve maximally effective bacterial uranium reduction in the environment, it will be important to monitor the pH of the carbon substrate media, as well as the pH of the groundwater and effluent. Fortunately, it should be relatively easy to monitor and alter the pH of the groundwater to keep it within the circumneutral range for optimal uranium reduction. In order to determine the impact of uranyl-carbonate complexation effects on uranium reduction, a similar experiment could be carried out in a carbonate-free environment.

8.8. Conclusion

Here we have demonstrated the effects of some common environmental parameters such as pH, electron donor and cell density have on the bacterial reduction of uranium. It was determined that the rate of reduction fit a first-order exponential decay model and was linearly associated with the density of cells for bacterial concentrations above a minimum density of 1E8 cells/mL. These results suggest that there is a minimum cell density threshold necessary for bacterial immobilization of uranium in the environment, although it may be lower for soil populations, as indicated by Holmes et al.[3]. It was also determined that the optimal cellular density to rate ratio was on the order of 1E9 cells/mL, this density gave rise to a quick and nearly complete reduction of uranium in approximately 24 hours, which is ideal for *in vitro* study of uranium reduction. The rate of reduction was also found to be slightly dependent on the electron donor supplied to the bacteria for the reduction with lactate resulting in slightly faster kinetics than H_2. Because environmental remediation strategies usually involve the addition of a carbon substrate, the faster reduction rate seen with lactate as the electron donor will certainly continue to be an effective strategy. However, both electron donors result in uranium reduction, so further studies can also be carried out in carbon-free medium if necessary. It is also clear that the rate of reduction is pH dependent, with pH 6.4-6.9 yielding the fastest reduction kinetics. This could be either due to the reduction enzyme(s) functionality, or to the speciation of the uranium carbonate complexes present in the reduction media. Most likely, a combination of both effects leads to the lack of uranium reduction at pH 5 and the inhibition of reduction at pH 7.4. Sites contaminated with uranium are often acidic (due to acidic leaching of mill tailings), so highly acidic conditions must first be addressed in the environment before sulfate-reducing bacteria like *S. oneidensis* can be encouraged to reduce uranium effectively, however, it is evident that small changes to the optimal pH, although slower, will still result in uranium reduction.

Bacterial reduction of uranium is an important phenomenon that we can use to help immobilize uranium contamination in the environment. Overall, a fundamental understanding of how external properties affect the mechanism and rate of bacterial uranium reduction should help us to be able to better predict and model how these bacteria will behave in more complex environments. It should also provide a partial framework for scale-up of bacterial reduction processes *in vitro* for optimizing the rate and production of reduced uranium on a larger-scale.

8.9. References

---

[1] UMTRA Uranium Mill Tailings Remedial Action Project: End-of-Project Report (U.S. Department of Energy Environmental Restoration Division, Albuquerque, NM, 1999) p. 7-8.

[2] **Lovley, D. R., J. R. Lloyd.** (2000) Microbes With a Mettle for Bioremediation. Nat. Biotechnol. **18:** 600-601

[3] **Lovley, D.R., E. J. P. Phillips, Y. A. Gorby, E. R. Landa.** (1991) Microbial Reduction of Uranium. Nature. 350:413-415.

[4] **Holmes, D. E., K. T. Finneran, R. A. O'Neil, D. R. Lovley.** (2002) Enrichment of Members of the Family *Geobacteraceae* Associated with Stimulation of Dissimilatory Metal Reduction in Uranium-Contaminated Aquifer Sediments. Appl. Environ. Microbiol. **68:** 2300-2306.

[5] **Lovley, D. R.** (1993) Dissimilatory Metal Reduction. Annu. Rev. Microbiol. **47:**263-290.

[6] **Francis, A. J.,** (1994) Microbial Transformations of Radioactive Wastes and Environmental Restoration Through Bioremediation. J. Alloys. Compd. **213:** 226-231.

[7] **Banaszak, J. E., B. E. Rittmann, D. T. Reed.** (1999) Subsurface interactions of actinide species and microorganisms: Implications for the bioremediation of actinide-organic mixtures. J. Radioanal. Nuc. Chem. **241:**385-435.

[8] **Lovley, D.R., E. J. P. Phillips, Y. A. Gorby, E. R. Landa.** (1991) Microbial Reduction of Uranium. Nature. **350:**413-415.

[9] **Lovley, P. K. Widman, J. C. Woodward, E. J. P. Phillips.** (1993) Reduction of Uranium by Cytochrome c3 of *Desulfovibrio vulgaris*. Appl. Environ. Microbiol. **59:**3572-3576.

[10] **Spear, J. L., L. A. Figueroa, B. D. Honeyman.** (2000) Modeling Reduction of Uranium Under Variable Sulfate Concentrations by Sulfate Reducing Bacteria. Appl. Environ. Microbiol. **66:**3711-3721.

[11] **Liu, C., Y. A. Gorby, J. M. Zachara, J. K. Fredrickson, C. F. Brown.** (2002) Reduction Kinetics of Fe(III), Co(III), U(VI), Cr(VI), and Tc(VII) in Cultures of Dissimilatory Metal-Reducing Bacteria. Biotechnol. Bioeng. **80:**637-649.

[12] **Kuai, L., A. A. Nair, M. F. Polz.** (2001) Rapid and Simple Method for the Most-Probable-Number Estimation of Arsenic-Reducing Bacteria. Appl. Environ. Microbiol. **67:**3168-3173.

[13] **Spear, J. L., L. A. Figueroa, B. D. Honeyman.** (1999) Modeling the Removal of Uranium U(VI) from Aqueous Solutions in the Presence of Sulfate Reducing Bacteria. Environ. Sci. and Technol. **33:**2667-2675.

[14] **Spear, J. L., L. A. Figueroa, B. D. Honeyman.** (2000) Modeling Reduction of Uranium Under Variable Sulfate Concentrations by Sulfate Reducing Bacteria. Appl. Environ. Microbiol. **66:**3711-3721.

[15] **Lewis, M.** (2000) M.S. The Behavior or Uranium in the Environment: Bacterial Reduction of an Aqueous Uranium Species Thesis, Massachusetts Institute of Technology.

[16] **Lovley, D. R.** (1993) Dissimilatory Metal Reduction. Annu. Rev. Microbiol. **47:**263-290.
[17] **Anderson, R. T., et al.** (2003) Stimulating the *In Situ* Activity of *Geobacter* Species to Remove Uranium from the Groundwater of a Uranium-Contaminated Aquifer. Appl. Environ. Microbiol. **69:** 5884-5891.
[18] **Haas, J. R., A. Northup.** (2004) Effects of Aqueous Complexation on Reductive Precipitation of Uranium by *Shewanella putrefaciens*. Geochem. Trans. **5:**41-48.
[19] **Brooks, S. C., et al..** (2003) Inhibition of Bacterial U(VI) Reduction by Calcium. Environ. Sci. Technol. **37:**1850-1858.
[20] **Amend, J. P., E. L. Shock.** (2001) Energetics of Overall Metabolic Reactions of Thermophillic and Hyperthermophillic Archea and Bacteria. FEMS Microbiol. Rev. **25:**187-190.
[21] **Haas, J. R., T. J. Dichristina, R. Wade Jr..** (2001) Thermodynamics of U(VI) sorption onto *Shewanella putrefaciens*. Chem. Geol. **180:**33-54.
[22] **van der Lee, J., L. De Windt.** (2000) JCHESS v. 2.5. CIG-École des Mines de Paris.
[23] **Wolery, T.** (1992) Eq3/6: A Software Package Designed for Geochemical Modelling of Aqueous Systems: A Package Overview and Installation Guide (Version 7). (UCL-MA-110662 PT I ed.). Lawrence Livermore National Laboratory.
[24] **Anderson, V. K.** (2002) The Effect of Carbonate Concentration on Uranium Oxide Dissolution Kinetics. M.S. Thesis, Massachusetts Institute of Technology.

9. Bacterial Fractionation of Uranium Isotopes

9.1. Abstract

To date, biological fractionation has only been observed for low to intermediate mass elements. Here, we demonstrate that isotopes of uranium, the heaviest naturally occurring element, are subject to fractionation when uranium serves as a terminal electron acceptor during anaerobic bacterial respiration. Batch cultures of the metal-reducing bacterium *Shewanella oneidensis* MR-1 were exposed to soluble uranyl [$U(VI)O_2^{2+}$] ions containing the isotopes ^{235}U and ^{238}U in a ~1:1 ratio. Reduction resulted in precipitation of solid uraninite [$U(IV)O_2$], and was accompanied by depletion of ^{235}U in the uranium remaining in solution. The resulting fractionation factor, α, was found to be 1.029±0.006.

9.2. Introduction

Isotopic fractionation has been observed for a wide spectrum of elements with multiple naturally occurring isotopes for both biotic and abiotic chemical reactions and processes (§6). This enables the use of specific isotope signatures as markers of many otherwise unobservable (bio)geochemical processes. For example, stable isotope signatures of carbon and nitrogen can be used to reconstruct food chain structure in the environment[1] and, for ancient rocks, iron isotope ratios have been suggested as tracers of early biological activity[2]; more recently chromium isotope fractionation during abiotic chemical reduction has been proposed as a means to assess immobilization of this toxic element in the subsurface[3]. Indeed, with a growing appreciation of the importance of many metals in biological reactions there is significant interest in exploiting isotopic fractionation as an environmental tracer of biological activity. However, it remains unknown to what extent appreciable fractionation occurs for the entire mass spectrum of elements.

Fractionation in the environment is currently believed to be limited to lighter and intermediate mass elements or heavier elements with large isotopic mass differences. In fact, Thallium is the heaviest element for which abiotic fractionation has been observed during adsorption to hydrogenetic Fe-Mn crusts[4] while biological fractionation of heavier metals has only been suggested for ^{122}Te and ^{130}Te, which differ in mass by >6%[5]. Fractionation of uranium, which displays only a small mass difference (~1%) between the two most abundant isotopes ^{235}U and ^{238}U, has thus far only been demonstrated on a large scale in industrial procedures used for nuclear fuel production and in numerous small-scale process, but is not known to occur in the environment. Fuel production is an inefficient and laborious process requiring the enrichment of fissile ^{235}U from natural uranium ore via the lengthy and energy intensive procedures of conversion to a volatile species followed by gas diffusion or centrifugation[6]. Nonetheless, similarities in chemical behavior of iron and uranium during bacterial reduction

and the above observations of heavy element fractionation led us to hypothesize that even uranium isotopes may be subject to appreciable fractionation during bacterial reduction.

9.3. Materials and Methods

To establish whether metal-reducing bacteria can fractionate uranium isotopes, we used a highly controlled kinetic approach (see chapter 9 appendix for further details). Pure cultures of *Shewanella oneidensis* MR-1 were added in a final concentration of ~10^9 cells·mL^{-1} to anaerobic phosphate-free medium containing 1.2 mM soluble uranyl acetate. This material was prepared from National Bureau of Standards (NBS) U_{500} reference material, which consists of the two isotopes ^{238}U and ^{235}U in equal molar amounts*. The concentration of total uranium and of the two isotopes was measured in both the soluble and solid phase to allow calculation of kinetics and mass balance. Total uranium was determined spectrophotometrically using the indicator dye Arsenazo(III)[7] (§7.3.2.1), while isotopic composition was analyzed using an inductively coupled plasma magnetic-sector multiple collector mass spectrometer (MC ICP-MS) (Isoprobe-Micromass) (§7.2.2). Bias in the spectrometric measurement of uranium isotopes due to mass discrimination was corrected by introduction of standards (NBS U_{500} reference material) and randomization of samples. Controls for biological reduction of uranium included medium without cells and with formaldehyde-killed cells. Controls were treated identically except that fewer time points were analyzed for isotopic composition. One prior experiment was carried out similarly (see the chapter 9 appendix for further details).

9.4. Results

Uranium removal from solution in the active (but non-growing) bacterial cultures best fit the previously described first order kinetics[8] (§8) and was observed over a period of 120 hours until ~92% of uranium was precipitated (Figure 9.1). This decrease in soluble uranium was accompanied by accumulation of a dark brown precipitate, which was confirmed by powder x-ray diffraction to be reduced uranium in the form of uraninite (UO_2) (see appendix for further details). Although in the formaldehyde fixed control rapid disappearance of approximately 100 mM uranyl was evident (Figure 9.1) this is attributed to sorption of uranyl ions to phosphate groups on the bacterial surfaces as observed by extended x-ray absorption fine structure spectroscopy (EXAFS) (chapter 8 appendix). Furthermore, x-ray absorption near edge structure (XANES) experiments confirmed previous observations[9],[10] that this behavior did not affect the oxidation state of the uranium.

---

* The starting uranyl acetate was regenerated from uraninite precipitate from previous experiments so that the isotope ratio deviated slightly from unity of the original U_{500} standard material

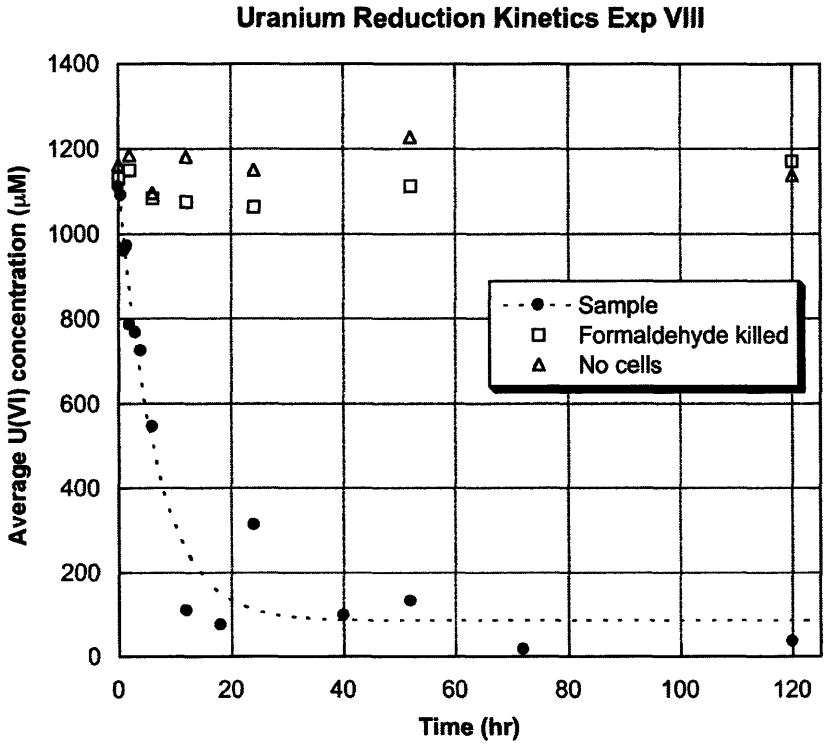

Figure 9.1: Kinetics of uranyl removal from solution by *Shewanella oneidensis* MR-1. •Live cells, ▫ formaldehyde inhibited cells, ▵ no cells.

In the samples containing live bacteria, the composition of the uranium showed a considerable change in isotope ratios with time, following opposite trends in the soluble and solid phases. While the ratios of $^{235}U/^{238}U$ in solution started to decrease from 0.981 at 0 hours to a minimum of 0.960 at 40 hours, they increased in the solid phase relative to the $^{235}U/^{238}U$ ratios in solution indicating preferential removal of the ^{235}U isotope from solution. No substantial change in isotopic ratios was seen in either of the controls, confirming that biologically active cells are necessary for significant fractionation.

A Rayleigh fractionation model[11] was used to determine the fractionation factor (α) for the uranium isotopes and will allow comparison with fractionation of other metals and other uranium isotope separation processes (§6.2).

The experimental data fit the Rayleigh model well, this is an indication that isotope effects during uranium reduction are due to a combination of kinetic and equilibrium effects as the Rayleigh model suggests (Figure 9.2). As expected from a closed system in which an insoluble product is quantitatively formed, the isotope ratio of the reduced precipitate approached the initial isotope ratio of the soluble phase with increasing fraction of total uranium removal from solution (Figure 9.2). The analysis also provides strong confidence in the measurements since the Rayleigh model yielded near inverse relationships for the independently measured isotope composition of the soluble and solid phase uranium, respectively (Figure 9.2).

Isotopic ratio measurements from MC ICP-MS allow for the calculation of δ_{235} according to Eqn. 6.4 where $R_{std} \approx 1$ and R_x = [235]/[238]. Applying Eqn. 6.13 to each time point of the experimental data and solving for α by fitting with Eqn. 6.12 resulted in a fractionation factor for the soluble phase $\alpha_{solution}$=1.029±0.006 (R^2=0.81) and for the solid phase α_{solid}=0.969±0.001 (R^2=0.99) while the controls both had α=1.

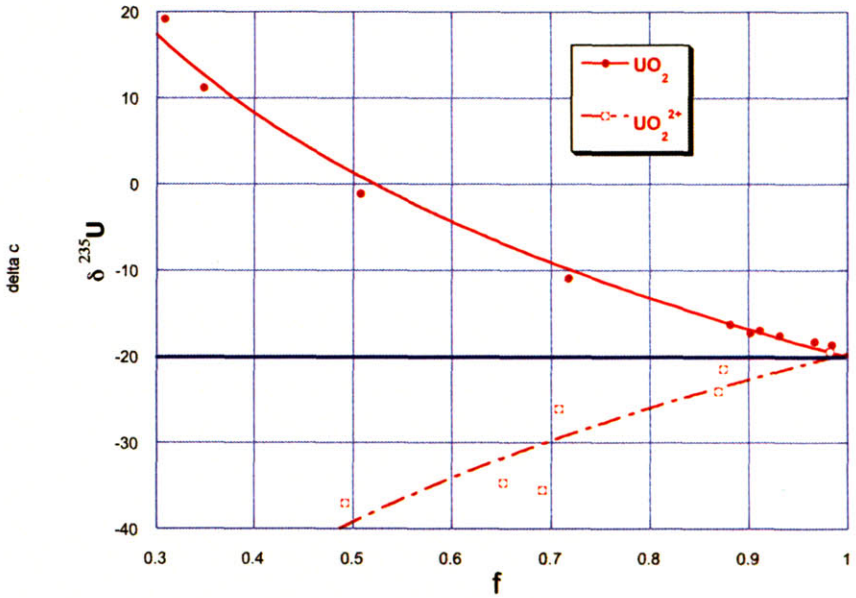

Figure 9.2. Fractionation of uranium isotopes by *Shewanella oneidensis* MR-1 displayed as $\delta^{235}U$ versus f, the fraction of total uranium for the ○ solution phase and ● solid phase. Best fit lines were calculated according to the Rayleigh fractionation model (Eqn. 6.13) yielding near inverse fractionation factors $\alpha_{solution}$=1.029±0.006 (R^2=0.81) and α_{solid}=0.969±0.001 (R^2=0.99), respectively. Values of f below 0.3 were excluded due to high error in the measurement of both f and isotopic ratios at low uranium concentration.

Another way to determine the value of α is to estimate it from the kinetic constants derived for both isotopes using the total uranium concentration (Figure 9.1) and isotope ratios at each time point. These data best fit 1st order kinetics (R^2 = 0.96) allowing the estimation of the rate coefficients k from:

$$[U]_t = [U]_0 e^{-kt} \qquad \text{Equation 9.1}$$

where $[U]_t$ and $[U]_0$ are the solution concentration of the ^{235}U and ^{238}U isotopes at time t and 0, respectively. This resulted in a k_{235} of 0.157±0.027 hr^{-1} and a k_{238} of 0.153±0.027 hr^{-1}, reflecting the slightly faster and more energetically favorable reduction of the lighter uranium isotope. The ratio of the two rate constants k_{235}/k_{238} can be interpreted as a second way to estimate of α, yielding a value of 1.022 and demonstrating good agreement between the two methods based on

calculation of α from kinetic constants and from isotope ratios for each time point.

9.5. Discussion

The observed α of 1.029-1.022 is unexpectedly large considering the relatively small mass difference between uranium isotopes and previously measured fractionation of other metals[3,4,12]. However, these studies described equilibrium effects while the α resulting from kinetic fractionation (both measured and theoretically calculated) of iron and tellurium reduction was on the same order of magnitude as the α for uranium observed here[5,13]. Furthermore, if bacterial uranium reduction proceeds as a multi-step, kinetically driven process, a higher fractionation factor than from a similar single step reaction should be expected. This stems from the slight enrichment occurring in each step of the reaction in conjunction with is overall irreversibility, and gives rise to a larger apparent overall fractionation factor. Indeed, increased isotope fractionation due to a coupled multi-step process is observed for different mechanisms of uranium isotope fractionation for enrichment of fissile ^{235}U from natural ore material. In these, distillation, monothermal chemical exchange, and gaseous diffusion are all single step chemical equilibrium processes and display fractionation factors between 1.0002 and 1.0043[6], comparable to single step equilibrium fractionation of Fe[12], Cr[3] and Tl[4]. In contrast, the gas centrifuge procedure couples kinetic and equilibrium fractionation processes and, with an α of 1.162, leads to even higher fractionation than the bacterial reduction of uranium observed here. While the details of the bacterial reduction mechanism remain speculative, the process is thought to involve several chemical transformations[14] and multiple sites[15] for uranium reduction including reduction of uranium both in the periplasm, as well as on the surface of the cell. Thus it may not be surprising that the α for bacterial uranium reduction appears higher than expected from equilibrium considerations and comparison with other metals.

An important question is whether bacterial activity can lead to uranium isotope fractionation in the environment. Biological uranium reduction has recently been demonstrated in samples from sites contaminated with uranium[16], but natural uranium has an average isotopic ratio of ~0.00705, much less that the 1:1 ratio used in this experiment. Thus, despite the large fractionation associated with the biological reduction demonstrated here, the effect in the environment, if any, should be small. However, small but significant differences in uranium isotope ratios[17] have been noted in the last few years due to an improved ability to reliably measure small-scale isotopic differences at environmentally relevant uranium concentrations[18]. This may mean that with improving technology uranium might be a useful tracer for both recent and ancient anaerobic environments in the Earth's history. Currently, iron isotope signatures are proposed as indicators of anaerobic bacterial respiration in ancient sedimentary rocks[3]. However, iron is redox active in many biological processes while uranium is only known to be biologically active in anaerobic bacterial respiration. Indeed, uranium reduction may be an ancient process since it is wide spread among iron

reducing bacteria and geochemical and phylogenetic evidence suggests that iron-reduction is among the oldest microbial metabolisms on Earth[19]. It will therefore be important to evaluate uranium isotope variation in an environmental and Earth history context, not only that, but uranium isotope ratios could be used to support iron isotope signatures as markers of ancient metabolic activity.

Uranium isotopes and their lead decay products are also central to age estimation of geologically old formations on Earth. In particular, ratios of $^{238}U/^{206}Pb$ and $^{235}U/^{207}Pb$ in zircon and some other igneous minerals have been used for this purpose. However, any isotopic separation of uranium resulting from the bacterial reduction is expected to have relatively little effect on the isotope compositions of these materials because uranium is generally present as uraninite, a highly crystalline reduced mineral form in which the uranium is essentially unavailable to bacteria. Nonetheless, errors in age estimates between $^{238}U/^{206}Pb$ and $^{235}U/^{207}Pb$ have been observed in some cases and have been ascribed to uncertainties in the half-life measurement of the uranium isotopes[20]. Whether a mechanism exists for contribution of bacterial or perhaps chemical fractionation of ^{235}U vs. ^{238}U to such discordant age estimates remains to be determined and could be more pronounced in ancient sedimentary rocks where bacteria had once been active.

9.6. Conclusion

Overall, we conclude that reduction of uranium by the bacterium *S. oneidensis* results in a kinetically driven Rayleigh separation of ^{235}U and ^{238}U with an unexpectedly large fractionation factor α of 1.029-1.022. Because uranium is the heaviest naturally occurring element, the observed bacterial fractionation suggests that all biologically active elements with multiple isotopes can be subject to fractionation, especially if irreversible reactions participate. This significantly expands the list of possible biogeochemical tracers for specific but unobservable biological processes in recent and ancient environments.

9.7. References

[1] **Power, M.E.** (2001) Field Biology, Food Web Models, and Management: Challenges of Context and Scale. Oikos. **94:** 118-129.

[2] **Beard, B. L., C. M. Johnson, L. Cox, H. Sun, K. H. Nealson, C. Aguilar.** (1999) Iron Isotope Biosignatures. Science. **285:**1889-1892.

[3] **Ellis, A. M., T. M. Johnson, T. D. Bullen.** (2002) Chromium Isotopes and the Fate of Hexavalent Chromium in the Environment. Science. **295:**2060-2062.

[4] Rehkämper, M. et al.. (2002) Thallium Isotope Variations in Seawater and Hydrogenetic, Diagenetic, and Hydrothermal Ferromanganese Deposits. Earth. Planet. Sci. Lett. **197**:65-81.

[5] **Smithers, R. M., H. R. Krouse.** (1967) Tellurium Isotope Fractionation Study. Can. J. Chem. **46:**583-591.

[6] **Benedict, M., T. H. Pigford, H. W. Levi** (1981) Nuclear Chemical Engineering 2nd Ed. McGraw Hill Ltd. NY NY. 8

[7] **Savvin, S. B.** (1964) Analytical Applications of Arsenazo III-II, Determination of Thorium, Uranium, Protactinium, Neptunium, Hafnium, and Scandium. Talanta. **11:**1-6.

[8] **Spear, J. L., L. A. Figueroa, B. D. Honeyman.** (2000) Modeling Reduction of Uranium Under Variable Sulfate Concentrations by Sulfate Reducing Bacteria. Appl. Environ. Microbiol. **66:**3711-3721.

[9] **Hu, M. Z.-C., J. M. Norman, B. D. Faison, M. E. Reeves**. (1996) Biosorption of Uranium by *Pseudomonas aeruginosa* Strain CSU: Characterization and Comparison Studies. Biotech. Bioeng. **51:**237-247.

[10] **Kelly, S. D. et al.**. (2002) X-Ray Absorption Fine Structure Determination of pH-Dependent U-Bacterial Cell Wall Interactions. Geochim. Cosmochim. Acta. **66:**3855-3871.

[11] **Kendall, C., J. J. McDonnel eds,** (1998) Isotope Tracers in Catchment Hydrology. Elesevier, N.Y.. 57-70.

[12] **Anbar, A. D., J. E. Roe, J. Barling, K. H. Nealson**. (2000) Nonbiological Fractionation of Iron Isotopes. Science. **288:**126-128.

[13] **Matthews, A., X. Zhu, K. O'Nions.** (2001) Kinetic Iron Stable Isotope Fractionation Between Iron (-II) and (-III) Complexes in Solution. Earth. Planet. Sci. Lett. **192:**81-92.

[14] **Llyod, J. R. et al.** (2002) Reduction of Actinides and Fission Products by Fe(III) Reducing Bacteria. Geomicrobiol. J. **19:**103-120.

[15] **Wall, J. D., L. R. Krumholz.** (2006) Uranium Reduction. Annu. Rev. Microbiol. **60:**149–166.

[16] **Anderson, R. T., et al.** (2003) Stimulating the In Situ Activity of *Geobacter* Species to Remove Uranium from the Groundwater of a Uranium-Contaminated Aquifer. Appl. Envion. Microbiol. **69:**5884-5891.

[17] **Richter, S., A. Alonso, W. De Bolle, R. Wellum, P.D.P Taylor.** (1999) Isotopic "Fingerprints" for Natural Uranium Ore Samples. Int. J. Mass Spec. **193:**9-14.

[18] **Becker, J. S.** (2003) Mass Spectrometry of Long-Lived Radionuclides. Spectrochim. Acta Part B. **58:**1757-1784.

[19] **Vargas, M., K. Kashefi, E. L. Blunt-Harris, D. R. Lovley.** (1998) Microbiological Evidence for Fe(III) Reduction on Early Earth. Nature. **395:**65-67.

[20] **Schön, R., G. Winkler, W. Kutschera.** (2004) A Critical Review of Experiment Data for the Half-Lives of the Uranium Isotopes ^{238}U and ^{235}U. Appl. Radiat. Isot. **60:**263-273.

10. Interactions of Metal Oxidizing Bacteria with Uranium

10.1. Abstract

Here we explore the interactions that iron and manganese oxidizing organisms and their oxidation products have with uranium. It was determined that the manganese oxidizing factor produced by the bacterium *Leptothrix discophora* did not appreciably effect the oxidation of uraninite. However, exposure of uraninite to the oxides produced by *L. discophora* resulted in the production of U(VI) followed by adsorbtion to the manganese oxides. There was no apparent release of uranium into solution. Both U(VI) resulting from the direct addition of uranyl to precipitating biological manganese oxides as well as U(VI) prodiced as a result of the oxidative dissolution of UO_2 resulted in similar uranyl association with the manganese oxide; where the most common mechanism of adsorption was a tridentate U-Mn complex found within the structure of the oxides themselves. Bacterial manganese formation was inhibited by high concentrations of Mn^{2+} as well as U(IV) and U(VI), which may impact the effect that these oxides could have in the environment as adsorbants of uranyl if their formation is inhibited by high contaminant metal concentrations. A general understanding of how different types of bacteria can affect the speciation and, thus, mobility of uranium can be an important step in how we can better understand and predict the mobility of uranium in the environment.

10.2. Introduction

There are many other types of bacteria that can interact with uranium other than sulfate and iron reducing microorganisms. Unlike *S. oneidensis*, metal oxidizing bacteria can both inhibit the transport of uranium, by producing metal-oxides capable of uranyl sorption, or mobilize uranium by the process of oxidative dissolution. One species of bacteria, *Thiobacillus ferrooxidans*, is known to both directly and indirectly oxidize uranium at low pH where U^{4+} can exist in solution. This reaction is highly localized to its specific niches such as mill tailings piles and the bacteria cannot grow by directly catalyzing the oxidation of uranium[1], but nevertheless can lead to the oxidative dissolution of uraninite (UO_2). Although uraninite is generally considered to be a relatively stable uranium mineral under typical environmental conditions, bacteria that are capable of catalyzing uranium oxidation will impact how we understand the effects of long-term storage of UO_2 fuel forms and other UO_2 products (like biologically reduced U) present in the environment. Another species, *Leptothrix discophora* produces manganese oxides, which are powerful environmental oxidants that can also adsorb positively charged metal contaminants like uranyl[2], meaning that this microorganism could alter the chemistry of both U(IV) as well as U(VI). Although the properties of uranium reducing bacteria and their impacts on uranium speciation are more well known, it is also important for us to understand the impacts that other types of

bacteria may have on the chemistry of uranium. The adsorption or oxidation of uranium by metal oxidizing microorganisms may also determine the long-term behavior of uranium in the environments well as how bacteria influence the overall global cycling of uranium. Here we explore the effects that neutrophillic iron and manganese oxidizing microorganisms have on the speciation of uranium.

10.3. Putative Fe Oxidizing Microorganism

Experiments involved an as yet unclassified group of microorganisms that may have anaerobic iron oxidizing properties. Experiments similar to those used to test for growth and iron oxidation were used to test for oxidation using UO_2. These experiments were largely unsuccessful because of many reasons that may have included the low solubility of UO_2* and the extremely slow growth rate of the bacteria. However, such oxidation is at least energetically possible. Another experiment designed to determine preliminary uranium oxidation involved plating the unclassified microorganisms on agar containing UO_2 and looking for the appearance of colonies. Apparent colonies were then examined using fluorescence microscopy. Some types of the bacteria exhibited promising properties, such as a yellowish appearance in the colonies (suggestive of UO_2 oxidation to uranyl) as well as clumping or clustering around what appeared to be oxidized UO_2^{2+}, which is also fluorescent. (Figure 10.1).

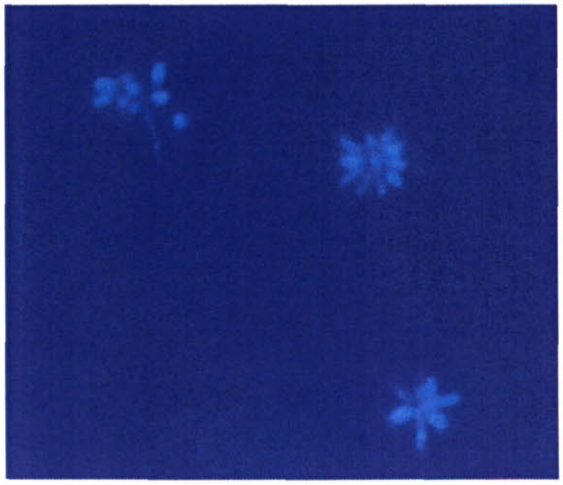

Figure 10.1 A microscopic image of the iron oxidizing bacteria stained with DAPI, which are presumably clustered around oxidized UO_2^{2+}.

This specific experiment was shelved, however, due to communication complications with the WHOI (Woods Hole Oceanographic Institute) group and also because of the difficulty of cultivating these organisms even under optimal conditions, thus other potential candidates were sought out.

---

* At pH 7 the concentration of $Fe(OH)_2^+$ in equilibrium with $Fe(OH)_{3(s)}$ is $\sim 10^{-9}$ M, whereas the concentration of U^{4+} in equilibrium with UO_2 is $\sim 10^{-33}$ M.

10.4. *Leptothrix discophora*

L. discophora is a commonly studied iron and manganese oxidizing organism, usually found in the environment in forest springs, freshwater wetlands, iron springs and upper layers of sediments. They are gram negative strict aerobes and are chemoorganoheterotrops. Cells isolated from the environment will often form exopolymeric manganese oxidizing sheaths, although they frequently lose this ability when cultured. *L. discophora* SS-1 is a sheathless strain which oxidizes manganese in an extracellular matrix; oxidation of manganese will also occur in cell free spent-media.

The production of the Mn oxidizing factor (MOF) is mediated at least in part by a gene designated *mofA*[3]. This gene has moieties similar to a family of proteins known as multicopper oxidases. In general these enzymes have broad substrate specificity and catalyze metal oxidation in a series of one electron transfers, coupling the reduction of O_2 to H_2O. The addition of Cu^{2+} is known to stimulate the manganese oxidation by *L. discophora* when added to cell cultures in stationary phase[4], but not when added to cell-free spent media. It is possible that the addition of Cu^{2+} stimulates the *mof* operon, or that Cu^{2+} can only be incorporated into the MOF as it is produced. The MOF has been shown to consist of at least one 110K, and possibly a second 85K fragment, however neither of these proteins have been purified in such an amount as to be well characterized, and the complete mechanism for microbial manganese oxidation remains unknown. However, two proposed mechanisms for manganese oxidation are given in Figure 10.3.

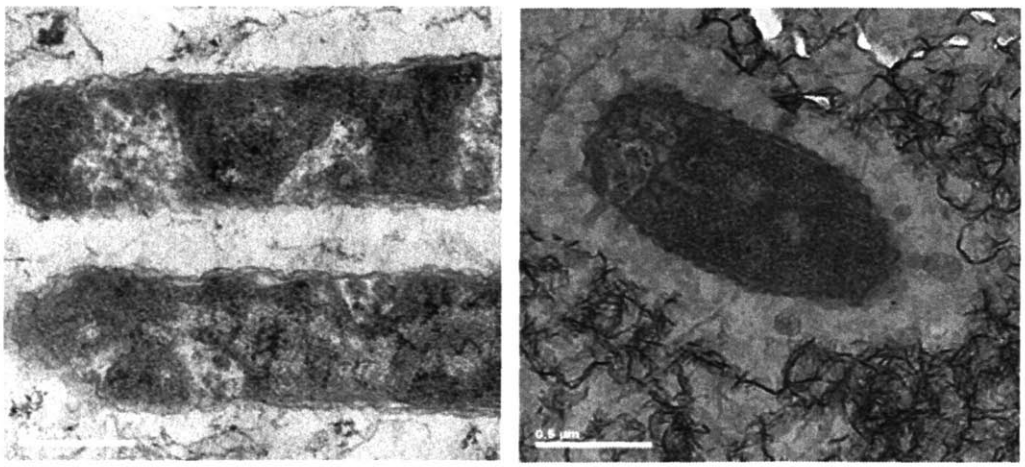

Figure 10.2 TEM images comparing *L. discophora* grown without Mn (left) and with Mn (right). On the right, manganese oxides can be seen in a halo around the cell. Adams and Ghiorse[5] suggested that *L. discophora* secrets the manganese oxidizing proteins by pinching off membraneous blebs, which can be seen in the figure on the right. Bar = 0.5 µM.

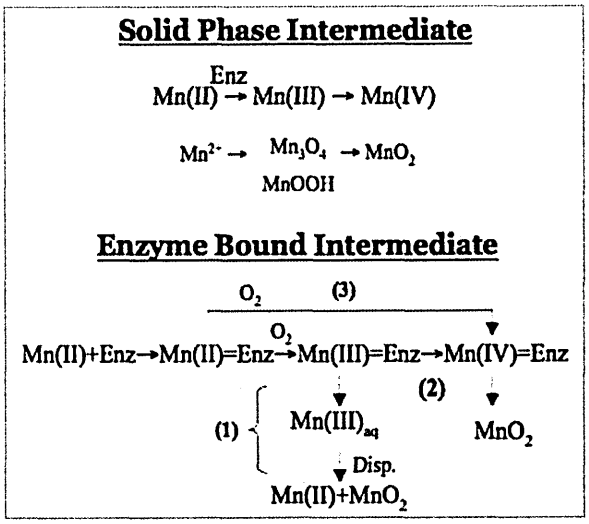

Figure 10.3 Proposed bacterial manganese oxidation pathways[6].

Manganese oxides of biological origin are relatively common in the environment, and in particular, manganese oxides are of interest because they can be powerful environmental oxidants. Not only that, but biological manganese oxides have a high surface area, negative surface charge and an amorphous crystal structure that makes them ideal for sorption of cationic radionuclides[6]. Thus, *L. discophora* has the potential to effect uranium mobilization in the environment in several ways: by direct oxidation of UO_2 by the non-specific MOF, by indirect oxidation of UO_2 by biologically produced manganese oxides, and finally by adsorption of UO_2^{2+}.

Table 10.1 Standard reduction potentials of manganese[13], iron[13] and uranium[7] oxides.

Reaction	E_0 (V)
$O_2 + 4H^+ + 4e^- \Leftrightarrow 2H_2O$	1.23
$MnO_2 + 4H^+ + 2e^- \Leftrightarrow Mn^{2+} + 2H_2O$	1.29
$MnOOH + 3H^+ + e^- \Leftrightarrow Mn^{2+} + 2H_2O$	1.50
$FeOOH + 3H^+ + e^- \Leftrightarrow Fe^{2+} + 2H_2O$	0.670
$UO_2^{2+} + 4H^+ + 2e^- \Leftrightarrow U^{4+} + 2H_2O$	0.273

10.4.1. Direct UO_2 oxidation by MOF

Experiments suggest that the oxidizing protein(s) produced by *L. discophora* is not capable of any significant uranium oxidation. (see the chapter 10 appendix for further information) Most likely this is due to the differences in the chemistry of reduced uranium, which is highly insoluble and reduced manganese, which is readily soluble, which can both sterically and chemically inhibit the

manganese oxidizing factor from interacting with uranium. This further supported by Figure 10.3, which shows the enzyme responsible for oxidation interacting with an ion, rather than a crystalline solid.

10.4.2. Indirect UO_2 oxidation by biological manganese oxides (BMO)

Investigations into the interaction between BMO and reduced uranium did, however, indicate that some UO_2 oxidation occurred when both oxides were contacted with one another in solution. An initial kinetics study was designed to measure the rate of formation of free uranyl when UO_2 was placed in contact with both fresh BMO as well as Mn^{2+} and the oxidizing protein. Filtration of the oxides and measurement of the solution phase for uranyl over time by ICP-AES did not yield any measurable uranium (Figure 10.4). (see appendix for further details) However, this does not necessarily mean that UO_2 is not being oxidized, any free uranyl that may have formed could have sorbed onto the oxide surface[8] and would not have been measured.

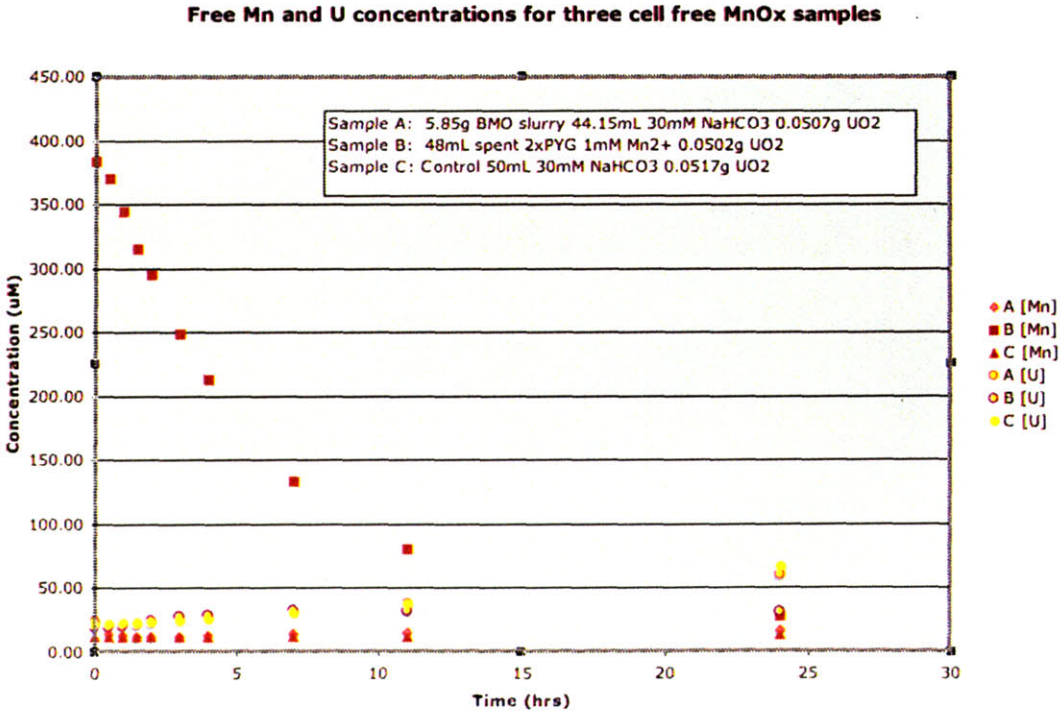

Figure 10.4: Free Mn and U concentrations contacted with BMO. Although concentrations of free uranyl increased slightly with time there was no significant difference in uranyl concentration between the sample and control.

10.4.3. EXAFS study of BMO interactions with UO_2

Samples of BMO formed in the presence of both uranyl and UO_2 were prepared and analyzed using EXAFS, using this method, it is possible to detect oxidized uranyl adsorbed to the surface of biologically produced manganese oxides based on coordination and structural differences between uranium oxidation states that can be seen in the EXAFS spectra. Figure 1.8 shows the deconvoluted fourier transform of the uranium EXAFS spectra for a sample where BMO was contacted with 17 mg of UO_2 (see the chapter 10 appendix for further details). What is interesting about Figure 1.8 is the small shoulder present on the U(IV) peak which indicates that the sample contained both U(IV) and U(VI). In this case, the U(IV) signal overpowered the U(VI) signal, so not much information could be gained about the speciation of U(VI) in this sample. This experiment was repeated (Figure 10.6) and this time every effort was made to remove all of the UO_2 from the BMO sample. Although there was still residual UO_2 (indicated by the small shoulder to the right of the main peak, and the peak corresponding to a U-U interaction at about 3.8 Å), the U(VI) signal is much stronger, allowing for a more detailed examination of the U(VI) BMO interaction. This also gives more evidence for the oxidation of UO_2 by the BMO followed by sorption of uranyl onto the surface of the oxide. Both Figure 1.8 and Figure 10.6 have a smaller peak around 3.1 Å, which is characteristic of a U-Mn interaction, and is similar to studies by Webb et al.[12] who investigated the interaction between uranyl and BMO formed by a *Bacillus sp.*. The U-Mn distance of 3.1 Å also corresponds to a tunnel-like manganese oxide structure, which was shown by Webb et al. [8] to form in the presence of micromolar quantities of uranyl. Unfortunately, the EXAFS technique does not allow for quantification, only estimation of the amount U(VI), which is less than 13% for the sample in Figure 1.8 and 50% for the sample in Figure 10.6.

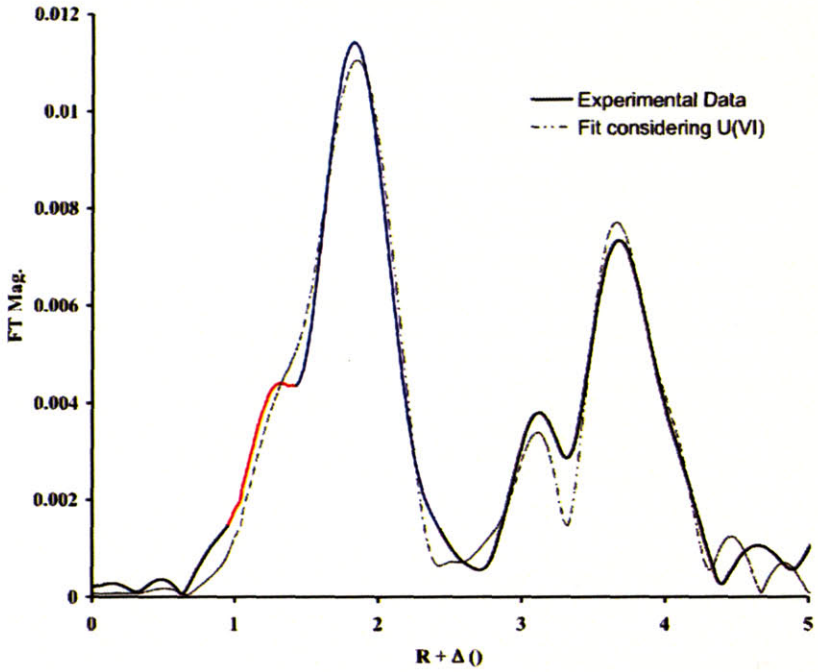

Figure 10.5 The deconvoluted Fourier transform of the uranium EXAFS spectra for a sample where BMO was contacted with 17 mg of UO_2. Both the real data and the experimental fit are shown. The dominant peak here (blue) is due to UO_2 because the measured sample contained both BMO and UO_2, however, the shoulder of this peak (red) is an indication of the presence of U(VI).

Measurement of both the free uranyl in solution and uranyl sorption by EXAFS, laser spectroscopy and IR show that UO_2 is not oxidized above detectable amounts in the presence of biological manganese oxides. Although EXAFS does provide some evidence of oxidative dissolution of UO_2 by the presence of uranyl when contacted with manganese oxide samples, the uranyl is associated with the manganese oxide and not released into solution more than any controls. These studies provide a good indication that although there is some oxidation evident, in the environment it would be unlikely that the contact of uraninite with either *L. discophora* or manganese oxides of biological origin would result in mobilization of uranium.

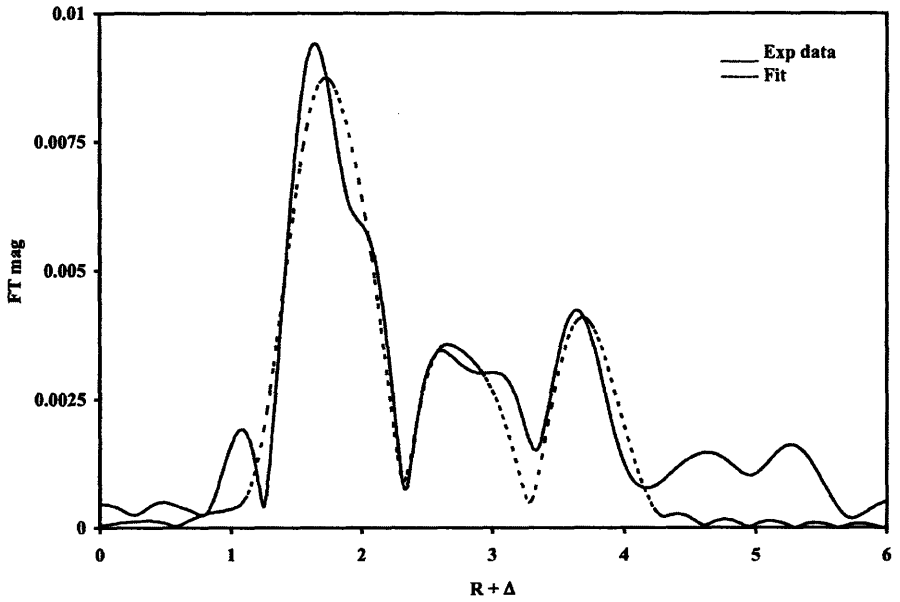

Figure 10.6 The deconvoluted Fourier transform of the uranium EXAFS spectra for a sample of BMO contacted with 50 mg UO_2. In this case as much UO2 was separated from the BMO as possible, revealing a stronger U(VI) signal. Fit considering the presence of U(VI).

10.4.4. Kinetics of BMO formation

Although manganese oxides of biological origin are theoretically capable of uranium oxidation, it is shown that this effect is not large enough to mobilize uranium more so than any aqueous matrix under the conditions examined. On the other hand, these BMO may also have positive effects in the environment, by acting as sorptive agents to immobilize solution phase uranyl.

In a series of several experiments (see appendix for further details) the kinetics of BMO formation with and without uranium are studied. The MOF present in spent MSVP media is inhibited by both high concentrations of Mn^{2+} (> 400 μM) as well as uranium.

Firstly, the BMO formation is studied in the absence of uranium. A Michealis-Menten analysis was obtained by determining the initial (linear) rate of oxide formation as a function of added substrate concentration.

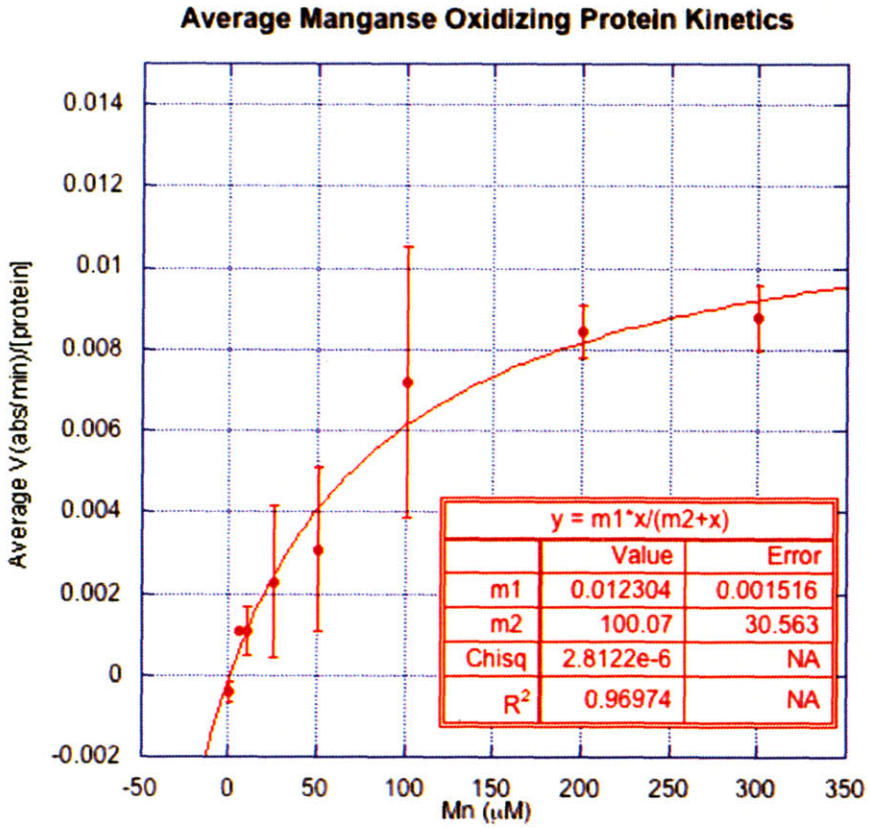

Figure 10.7 Michealis-Menten kinetics of MOF in spent MSVP media.

Data were normalized to protein concentration and averaged. The K_m and V_{max} were found to be 100.07 ± 30.56 μM Mn^{2+} and 0.012 abs/min/μg protein respectively. By converting the V_{max} to concentration by averaging the equilibrium absorbances of the controls, it becomes ~7.2 μM Mn^{2+}/min/μg protein. Tebo et al.[6] reported a K_m of 6 μM Mn^{2+} and V_{max} of 1.0 nM Mn^{2+}/min/μg protein, values significantly lower than described above. A similar experiment by Zhang et al. found a K_m of 5.7 μM Mn^{2+}, however the maximum Mn concentration was only 60 μM. The higher Mn concentrations in Figure 10.7, most likely give rise to the higher K_m found for this data.

It was also noted that in cell free spent media, concentrations of Mn^{2+} (around 400 μM and up) were inhibitory to oxide formation and high enough concentrations of Mn would prohibit oxide formation altogether. These effects have been also been demonstrated when Mn is added to growing cultures of *L. discophora*[9], but the authors did not speculate a reason for the inhibition. BMO formation was also inhibited at higher Mn concentrations by addition of uranyl, with lower concentrations of uranyl required to inhibit oxidation at higher Mn concentrations. This is probably a total metal effect (see chapter 10 appendix),

rather than being strictly caused by uranium, although the input of a non-reactive, but chemically similar metal like uranium could exacerbate the effect.

The kinetics of BMO formation was also inhibited by the presence of UO_2 (Figure 1.7) as indicated by a slower removal of Mn^{2+} from solution relative to a similar sample without UO_2. (see chapter 10 appendix for further details) Because the solubility of UO_2 is so low, the inhibitory effect that solid UO_2 has on BMO formation must be different from the inhibitory effects of uranyl. There is some evidence that the MOF adsorb to the manganese oxides they produce[10]. Boogerd et al. found that after isolating and dissolving precipitated BMO with reducing agent, the manganese oxidizing activity could be partially restored; meaning that there was some attachment of the MOF to the bioprecipitated manganese oxides. Although this effect was not quantified in great detail, adsorption of the MOF to UO_2 could be the reason that manganese oxidation is inhibited in the presence of this solid.

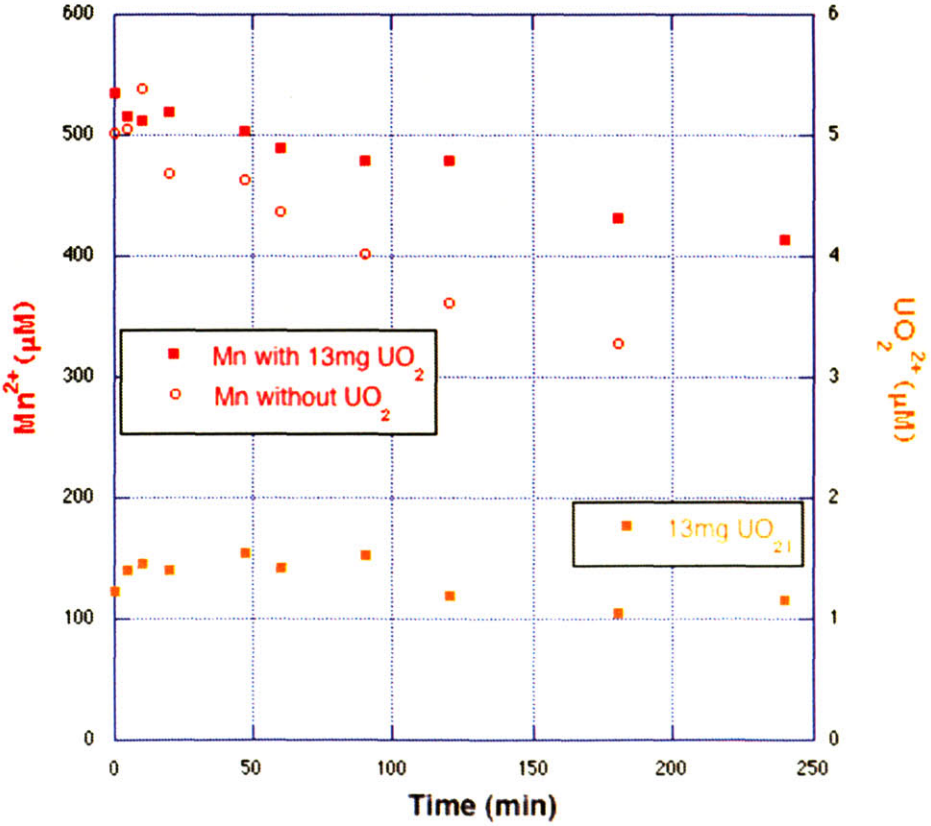

Figure 10.8 Inhibition of BMO formation in the presence of UO_2. Mn^{2+} removal from solution is slower in the presence of UO_2 (closed square) than in the absence of uranium (open circle). Initial Mn^{2+} concentration was 500 µM with a > 30K protein fraction of 0.012 mg/mL. The UO_2^{2+} concentration remains constant (and below the detection limit) throughout the experiment.

It is important to understand how BMO can be formed in the environment and what conditions inhibit their formation, because these oxides may have a large influence on the transport of contaminant trace metals in the environment. Their sorptive abilities may have in fact been underestimated by sorption and transport models which typically utilize abiotically produced oxides in their models[11], a better understanding of the kinetics of BMO formation along with their sorptive capabilities, would enhance the models used to determine transport of metal contaminants in the environment. However, these results show that if growth *L. discophora* could be stimulated in the environment, oxide formation will only occur when contaminant metal concentration is low. This may mean that in highly contaminated areas, decreasing uranium mobility by stimulating metal adsorption to BMO will not be a viable option.

10.4.5. EXAFS study of BMO interactions with UO_2^{2+}

Because of their negative surface charge and high surface area, manganese minerals known to be good absorptive agents for contaminant metals like Cu, Pb, Hg, Pu, and U[6]. Here we examine the speciation of U(VI) in the presence of BMO formed by *L. discophora*.

A sample of spent 2X PYG media containing 1 mM Mn^{2+} was allowed to precipitate overnight in the presence of 20 μM uranyl acetate. The resulting oxides were washed and the samples were prepared for EXAFS. The Uranium L_{III} edge (17.166 keV) x-ray absorption spectra was examined in order to determine the speciation of uranium associated with BMO. Figure 1.9 shows the deconvoluted fourier transform of the uranium EXAFS spectra, where the x-axis corresponds to the average bond distance from uranium. Both the real data and the experimental fit are shown. The first large peak is indicative of the typical U(VI) U=O bond, while the second, smaller peak is due to an association of U(VI) with the MnOx surface.

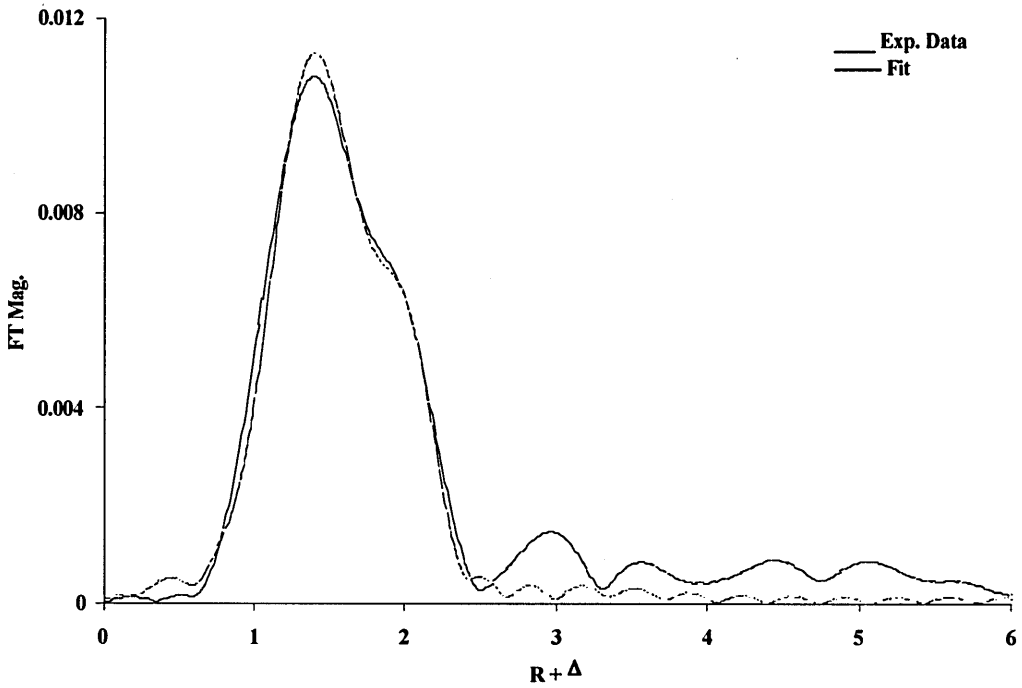

Figure 10.9 The deconvoluted Fourier transform of the uranium EXAFS spectra for a sample where Mn^{2+} was bioprecipitated in the presence of 20 μM U(VI).

The EXAFS spectra is strongly dominated by the U=O and U-Oeq contribution, which contribute to the large peak around 1.5 Å. This indicates that the element closest to uranium is oxygen, and no direct metallic U-Mn bonding can be observed.

The presence of Mn in the Fourier transform (Figure 1.9) may be the peak around 3 Å, but its scattering intensity is low. Then, uranium may be present in form of complex bonded to the surface of MnO_2. From the concentration of uranium used and analogy with literature[12], Webb et al., determined that a majority of the U-Mn interaction at this distance corresponded to the uranium in a tridentate complex occupying a corner within the tunnel structure of MnOx, and to a lesser extent, a bidentate association of uranium with the oxide surface. MnO_2 can present the pseudo-tunnel structure when formed in the presence of 20 μM U and uranyl can adsorb to manganese in a tridentate complex in the Mn tunnel corners along with a bidentate U-Mn surface complex. These data are in good agreement with previous findings by Webb et al.[8,12] who showed similar uranium speciation for samples complexed with manganese oxides produced by spores of *Bacillus sp.* The similarity of uranium interaction with manganese oxides produced

by two different species of bacteria suggests that the mechanisms and product of manganese oxidation by both *Bacillus* and *Leptothrix* are related. Although we have previously shown that U(VI) can inhibit the precipitation of BMO, the incorporation of U(VI) into the structure of the BMO, suggests that oxides formed in the presence of uranyl will be able to adsorb more uranium than pre-existing oxides. Thus, encouraging the growth of manganese oxidizing microorganisms could help to immobilize uranium in areas of low levels of contamination.

10.5. Conclusion

Simple explorative studies into a new species of iron oxidizing microorganism suggest that it may be able to catalyze the dissolution of UO_2. Such a finding warrants further investigation, but also suggests that bacterial oxidative dissolution of uranium is indeed a possibility. On the other hand, investigation into the catalysis of uranium oxidation by another bacteria, showed that the MOF produced by *L. discophora* alone does not appreciably lead to UO_2 oxidation over a short period of time. Not only that but, although EXAFS results suggest the production of some U(VI), BMO precipitation in the presence of UO_2 does not lead to measurable uranium mobilization, but rather U(VI) adsorption to the BMO. Thus, contact of reduced uranium with oxidizing bacteria or their oxide byproducts does not pose a significant source of uranium mobilization into the environment. However, manganese oxides of biological origin can adsorb uranyl at micromolar concentrations. The inhibition of BMO formation at higher concentrations of uranium may rule out the stimulation of *L. discophora* to produce oxides specifically for the sorption of contaminant uranium in environments with significant uranium contamination, although the general prevalence of oxides of biological origin already present in the environment will most likely serve to generally impede the transport of uranium, and BMO precipitated in the presence of low-levels of uranium contamination could lead to further uranium immobilization. The interactions between bacteria and uranium will necessarily be complex, owing to both the diverse nature of bacteria themselves as well as the complex redox and speciation chemistry uranium in the environment. Uranium is of special importance in this instance because it is both a radio and chemically toxic contaminant in the environment. A general understanding of how different types of bacteria can affect the speciation and, thus, mobility of uranium can be an important step in how we can better understand and predict the mobility of uranium in the environment.

10.6. References

[1] **DiSpirito, A. A., O. H. Tuovinen.** (1982) Kinetics of Uranous Ion and Ferrous Iron Oxidation by *Thiobacillus ferrooxidans*. Arch. Microbiol. **133:**33-37

[2] **Banfield, J. F, K. H. Nealson eds.** (1997) Bacterially Mediated Mineral Formation; Insights into Manganese (II) Oxidation from Molecular Genetic and Biochemical Studies. Geomicrobiology; Interactions Between Microbes and Minerals. Mineralogical Society, Washington, D. C. **36:**225-266.

[3] **Corstjens, P. L. A. M. , J. P. M. de Vrind, T. Goosen, E. W. de Vrind- de Jong.** (1997) Identification and Analysis of the *Leptothrix discophora* SS-1 mofA Gene, a Gene Putatively Encoding a Manganese Oxidizing Protein with Copper Domains. Geomicribiol. J. **14:**91-108.

[4] **Brouwers, G. J. et al.** (2000) Stimulation of Mn^{2+} Oxiadtion in *Leptothrix discophora* SS-1 by Cu^{2+} and Sequence Analysis of the Region Flanking the Gene Encoding Putative Multicopper Oxidase MofA.

[5] **Adams, L. F., W. C. Ghiorse.** (1986) Physiology and Ultrastructure of *Leptothrix discophora* SS-1. Arch. Microbiol. **145:**126-135.

[6] **Tebo, B. M. et al.** (2004) Biogenic Manganese Oxides: Properties and Mechanisms of Formation. Annu. Rev. Earth. Planet. Sci. **32:**287-328.

[7] **Harris, D. C.** (1995) Quantitative Chemical Analysis 4th Ed. W. H. Freeman and Co. NY NY. AP32-AP41

[8] **Webb, S. M., J. R. Bargar, B. M. Tebo.** (2005) Determination of Uranyl Incorporation into Biogenic Manganese Oxides Using X-ray Absorption Spectroscopy and Scattering. Phys. Scr. **T115:** 949-952.

[9] **Adams, L. F., Ghiorse.** (1985) Influence of Manganese on Growth of a Sheathless Strain of *Leptothrix discophora*. Appl. Env. Microbiol. **49:**556-562.

[10] **Boogerd, F. C., J. P. M. DeVrind.** (1987) Manganese Oxidation by *Leptothrix discophora*. J. Bacteriol. **169:** 489-494.

[11] **Zhang, J. L. W. Lion, Y. M. Nelson, M. L. Schuler, W. C. Ghiorse.** (2002) Kinetics of Mn(II) oxidation by *Leptothrix discophora* SS1. Geochim. Cosmichim. Acta. **66:**773-781.

[12] **Webb, S. M., C. C. Fuller, B. M. Tebo, J. R. Bargar.** (2006) Determination of Uranyl Incorporation into Biogenic Manganese Oxides Using X-Ray Absorption Spectroscopy and Scattering. Environ. Sci. Technol. **40:**771-777.

11. Future work and Conclusions

Although the results of this thesis provide more insight into the interactions between bacteria and uranium; demonstrating some of the influencing factors affecting the bacterial reduction of uranium, along with uranium isotopic fractionation during this process, as well as describing the effects that microbially produced manganese oxides have on both U(IV) and U(VI), it is ironic that the efforts undertaken to compile and put together a thesis gave the author a lot of ideas for future experiments. There is much work yet to be done before we complete our understanding of how bacteria interact with uranium in the environment, more than likely this information could provide the contents for many more PhD's to come, but the more that we understand how bacteria can affect the speciation and transport of uranium in the environment, the better equipped we will be to handle present and future uranium contamination. Knowing this, there are several experiments that fall directly out of this work, the results of which would necessarily fortify the content of this thesis.

11.1. Future work regarding bacterial reduction of uranium

11.1.1. Uranium reduction kinetics with constant uranium concentration

The kinetic model used in chapter 8 to determine the rate bacterial reduction of uranium predicts that the reduction of uranium will be the fastest at time zero, when the concentration of uranium is at its maximum. This experiment is designed to determine if a maximal reduction rate can be maintained if the concentration of uranium available to the bacteria remains constant. A constant concentration of uranium is sustained in the system by addition of excess uranyl carbonate. The presence of uranyl carbonate precipitate indicates an equilibrium between the solid $UO_2(CO_3)$ and UO_2^{2+} and CO_3^{2-}, as UO_2^{2+} is removed from the system by bacterial reduction, the solid uranyl carbonate will dissolve to maintain equilibrium. The solubility of $UO_2(CO_3)$ is given by:

$$[UO_2^{2+}][CO_3^{2-}]=10^{-14.1}$$

The speciation modeling program CHESS[1] predicts that at a partial pressure of 5% CO_2 and a pH of 6.9 that addition of 2 g/L $UO_2(CO_3)$ leads to a soluble uranyl concentration of approximately 1 mM, with $UO_2(CO_3)$ remaining. This should allow for the maintenance of a constant uranyl concentration of approximately 1 mM, even as uranyl reduced and removed from the system.

11.1.1.1. Materials and Methods

Uranyl carbonate is prepared by adding 6.35 g $UO_2(NO_3)_2$ to 250 mL 0.1 M $NaClO_4$ at pH 4. Figure 11.1 shows that uranyl carbonate will be the dominant uranyl species at 5% CO_2 from pH 3.5-5.5.

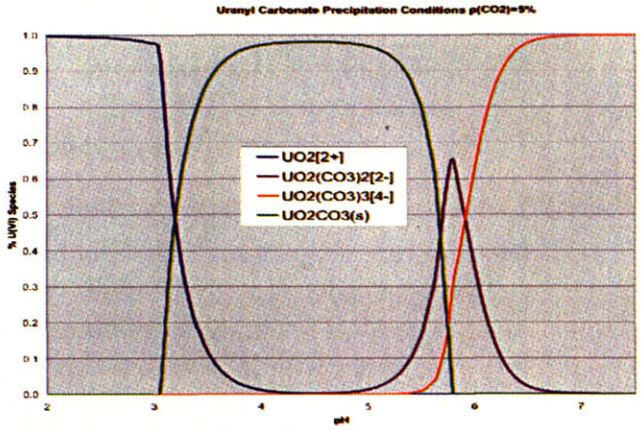

Figure 11.1 Speciation of Uranium at equilibrium in solution with 5% CO_2.

Pure CO_2 is bubbled slowly through the solution of dissolved $UO_2(NO_3)_2$ in a three neck flask for 4-7 days until a whitish-yellow precipitate is formed. The excess CO_2 is out gassed through an additional 250 mL $NaClO_4$. After 4-7 days the solution is removed from the three neck flask and centrifuged for 10 minutes at 3000 rpm. The supernatant is removed and the remaining precipitate is washed twice in $NaClO_4$ equilibrated with CO_2 and placed back into the three neck flask with the remaining $NaClO_4$. This solution is bubbled through slowly with CO_2 for an additional 4-7 days, after which the uranyl carbonate precipitate is collected by centrifugation, rinsed in dIH_2O and dried. The purity of the uranyl carbonate precipitate is verified using IR[2].

Cells grown overnight in 500 mL Tryptic Soy Broth at room temperature can be concentrated and rinsed 3X with $NaHCO_3$ buffer, and resuspended to a final volume of ~20 mL. Cells are split and one half are killed using 10% formaldehyde for the control. Cells will be transferred to a final concentration of approximately 10^9 cells/mL and placed into an anaerobic glovebox under H_2:CO_2:N_2 5:15:balance atmosphere and added to sterile unbuffered anaerobic freshwater medium as described by Kuai et al.[3], which has been brought to equilibrium with the glove box atmosphere and is maintained at a pH of 6.9, with the same exceptions as described previously. Media and cells are then transferred in 3 mL volumes to several glass tubes containing

approximately 6 mg $UO_2(CO_3)$. A cell-free control will consist of lactate media with 2 g/L $UO_2(CO_3)$. At each time point during the course of the experiment one aliquot of the sample and the controls is sacrificed by addition of 10% formaldehyde followed by immediate freezing to cease the reduction reaction.

11.1.1.2. Analysis of the rate of UO_2 formation

In order to asses the rate of uranium reduction at constant concentrations of UO_2^{2+}, the formation of reduced uranium must be measured. Addition of hydrochloric acid to the samples should dissolve $UO_2(CO_3)$ at a rate much faster than UO_2, after exposure to HCl for a certain amount of time, the samples can be filtered, leaving cellular remnants and biogenic UO_2 on the filter. Muffling of the filter (550° C) will burn away both cellular and filter material, remaining uranium can be dissolved in 0.1 M HNO_3 and measured with ICP-AES for concentration.

11.1.2. Discussion

Because the rate of reduction is theoretically greatest at the instantaneous time zero, ie when uranium concentration is at its maximum, the results of this experiment should show an increased rate of formation of biogenic UO_2 when compared to experiments without constant uranyl concentrations. Not only that, but the rate of reduction should also be constant, however, it is more likely that the rate will not remain constant over time due to a decrease in the metabolic activity of *S. oneidensis*. In this manner, it should also be possible to measure the viability of the cells over time and how that relates to the rate of uranium reduction.

Although constant concentrations of uranyl are likely to occur in the environment, especially one that is undergoing pump and treat-types of uranium bioremem diation, the information gained from this experiment can be more directly applied to the optimization of bacterial uranium reduction in a chemostat. Uranium reduction in a bioreactor could be applied to large scale uranium removal from waste sludge or to the industrial production of enriched uranium, although significant research will be required to scale up bacterial uranium reduction to industrial levels.

11.1.3. Other kinetics experiments

There is still much that is unknown about the mechanisms of bacterial uranium reduction, for example, the number of biochemical steps and uranium intermediates involved, how similar these mechanisms are across uranium reducing species of

bacteria, and what are the dominant geochemical forces that can govern bacterial reduction in the environment. The repetition of some of the kinetics experiments described here for different species of uranium reducing bacteria will allow for a comparison of the reduction rate and, at least in part, would differentiate differences in reduction mechanisms.

11.2. Future work regarding the bacterial fractionation of uranium isotopes

Bacterial fractionation of lighter non-metallic isotopes like carbon, nitrogen and oxygen is a fairly well known process, the results of which have numerous bio and geochemical applications, however, biological separation of uranium isotopes is hitherto unknown. While we have demonstrated here that enrichment can be seen using the uranium isotopes ^{235}U and ^{238}U in a 1:1 ratio, it would be more pertinent if bacterial isotopic separation could be demonstrated in samples containing other uranium isotopic rations and even natural uranium, since in theory, the fractionation factor should be independent of the isotopic ratio. Although such experiments would require highly sensitive measurement, if bacterial isotopic separation can be measured at natural uranium isotopic concentrations, it would certainly have an impact on the dating of uranium ores thought to stem from microbial precipitation. Since the results are surprising (in the sense that it is not immediately obvious why or how bacteria are able to measurably separate isotopes that have such small mass differences), support of this experimental data presented here with theoretical modeling is warranted.

Biological separation of uranium also has applications for the safe and cost effective production of enriched uranium for nuclear fuel. Currently, uranium enrichment requires the conversion of uranium to gaseous UF_6, where at high temperature and pressure the miniscule differences in the equilibrium kinetics are harnessed many thousands of times over to achieve isotopic separation. This process is both energy and technology intensive, as well as involving hazardous gaseous fluoride species. Enrichment of uranium by microorganisms on the other hand, can be done without conversion of uranium to UF_6, at room temperatures and pressures, and with minimal technological input. At present, however, such a process is far from achievable and would most likely require extensive basic research as well as significant efforts in order to achieve industrial scale-up.

Although direct biological oxidation of uranium is only currently known for one organism, *Thiobacillus ferrooxidans*, it would certainly be interesting to determine if this bacteria can isotopically separate uranium during oxidation. If so, it would provide yet another strategy for bacterial uranium enrichment, which could even involve a closed loop! Further investigation is warranted not only for the purposes of uranium enrichment, but also to provide insight into the mechanisms of biological fractionation of heavy metals in general.

11.3. Bacterial interactions with other radionuclides

Uranium is indeed a good model element for radionuclide behavior in the environment, and does represent a significant source of radionuclide contamination, however, although other radionuclides may be less prevalent in the environment, they can also be chemically and radiologically harmful. It is also important then, to also understand how bacteria can interact with other radionuclides. *S. oneidensis* is known to reduce Tc, Np and Pu as well as uranium, and in general, reduction does inhibit radionuclide transport in the environment. However, environmental contamination is never limited to a single element, especially in the case of radioactive waste, many contaminant radionuclides can be present at once. Therefore, it would be beneficial to understand how *S. oneidensis* will behave in the presence of several radionuclides of interest; which elements will be reduced first, and how will a change in speciation of one or more elements present effect the rate of reduction and/or speciation of the other elements present? In general, the behavior of uranium reducing bacteria like *S. oneidensis* in mixed wastes will be an important step to our better understanding of how nuclear waste forms will behave in the environment. This can then in turn, allow us to make better choices about how we go about removing radionuclide contaminants from the environment and about the makeup of the fuel forms themselves.

11.4. Conclusions

Here we have described the effects that conditions such as cellular density, electron donor, and pH have on kinetics of uranium reduction by *S. oneidensis*. It was determined that the rate of reduction fit a first-order exponential decay model with a near-linear dependence of the density of cells on the rate of uranium reduction for bacterial concentrations above a minimum threshold density of 1E8 cells/mL, with an optimal cellular density to rate ratio for *in vitro* studies of 1E9 cells/mL. The total uranium solution radioactivity is found to be generally uncorrelated with the reduction rate, although a somewhat faster rate of reduction was observed in samples with greater overall activity. The rate of reduction is slightly dependent on the type of electron donor utilized by the bacteria, and it was found that utilization of lactate as an electron donor for uranium reduction resulted in a rate of reduction that was 34% faster than when compared to H_2. Reduction is also found to be pH dependent, with pH 6.4-6.9 yielding the fastest reduction kinetics. The pH effects both reductive enzyme(s) functionality and uranium speciation dependence, where large changes in pH outside of the optimal pH 6.4-6.9 range lead to no uranium reduction, but smaller changes in pH lead to a decrease in rate associated with the complexation constant of the dominant uranyl carbonate species. Kinetic modeling of uranium reduction should help us to be able to better predict and model how uranium will behave *in situ*, as well as also providing a framework for optimizing bacterial reduction processes *in vitro*.

Not only that, but bacterial uranium reduction resulted in precipitation of solid uraninite accompanied by depletion of ^{235}U in the uranium remaining in solution.

The resulting fractionation factor, α, was found to be 1.029±0.006. The biological isotopic fractionation of uranium has never, until now, been demonstrated. Such results are indeed surprising because they suggest that bacteria could be used to separate ^{235}U from ^{238}U, and could implications for geological analyses which make use of $^{235}U/^{238}U$ isotopic ratios for geologic dating of ancient rocks.

The interactions that iron and manganese oxidizing organisms and their oxidation products have with uranium were also explored. In the environment, iron and manganese oxides of biological origin are of the most prevalent types of iron and manganese minerals found in the environment, thus, their interactions with uranium could have a significant impact on the mobility of uranium in the environment. It was apparent that although bacterial oxidation of uranium is energetically possible, that there is relatively little bacterial interaction, either direct or indirect, with reduced uranium. Although unsurprising, this information offers further support that reduced uranium in the form of UO_2 should be relatively stable in the environment, and that no new assumptions about bacterial oxidative dissolution of UO_2 need to be made at this time. It was determined that the manganese oxidizing factor produced by the bacterium *Leptothrix discophora* did not appreciably effect the oxidation of uraninite. It was also apparent that although bacterial oxidation of uranium is energetically possible, that there is relatively little bacterial interaction, either direct or indirect, with reduced uranium. Although unsurprising, this information offers further support that reduced uranium in the form of UO_2 should be relatively stable in the environment, and that no new assumptions about bacterial oxidative dissolution of UO_2 need to be made at this time. However, exposure of uraninite to the oxides produced by *L. discophora* resulted in the production of U(VI) followed by adsorbtion to the manganese oxides. There was no apparent release of uranium into solution. Both U(VI) resulting from the direct addition of uranyl to precipitating biological manganese oxides as well as U(VI) prodiced as a result of the oxidative dissolution of UO_2 resulted in similar uranyl association with the manganese oxide; where the most common mechanism of adsorption was a tridentate U-Mn complex found within the structure of the oxides themselves. Bacterial manganese formation was inhibited by high concentrations of Mn^{2+} as well as U(IV) and U(VI), which may impact the effect that these oxides could have in the environment as adsorbants of uranyl if their formation is inhibited by high contaminant metal concentrations. It would be interesting to assess the effects that long-term contact that biological manganese oxides have on the speciation, adsorption and possibly oxidation of uranium. Further experimentation is also warranted to determine the kinetics of uranium oxidative dissolution in the presence of bacterially produced manganese oxides. This would be an important step in how we can better understand and predict the effects that these common biologically produced oxides have mobility of uranium in the environment on more relevant time scales.

We are only just beginning to scratch the surface when it comes to our understanding of how microorganisms affect the geochemical cycling and transport of metals in the environment. Uranium and other radionuclides are of

special importance because of current contamination with these metals, but also because of plans to emplace large quantities of nuclear waste in the earth. It is our responsibility to understand the impact that the will have, not only on the environment but for us as well both in the immediate future and in the long term. The efforts described here emphasize that the study of model systems *in vitro* can give us insights into the redox interactions between bacteria and uranium that can be applied to environmental remediation schemes as well as to provide some framework for future improvements to uranium speciation and transport models.

12. Ch 8 Appendix

This appendix will encompass all of the data and detailed methodology for all of the experiments that went into the kinetics modeling for chapter 8.

12.1. Experiment I

12.1.1. Materials and Methods

Cells were grown overnight in 300 mL Tryptic Soy Broth at room temperature. They were then concentrated and rinsed 3X with $NaHCO_3$ buffer, and resuspended to a final volume of ~20 mL. A 5 mL sample of cells were transferred into an anaerobic glovebox under H_2:CO_2:N_2 5:15:80 atmosphere and added to 100 mL sterile anaerobic bicarbonate buffered freshwater medium (unless otherwise specified) as described by Kuai et al.[4], with the following exceptions; phosphate was removed to prevent uranyl precipitation, the carbon source and electron donor was 5mM lactate, and the electron acceptor was ~2 mM uranium. The cell-free control consisted of lactate media with 5ml of bicarbonate buffer. Samples that were 0.9 mL in volume were removed and added to 1.5 mL Eppendorf tubes containing 0.1 mL formaldehyde, were then frozen until analysis. An additional sample was removed at t=0 for cell enumeration by the DAPI method. The final cell concentration was 1.15E8 cells/mL

In order to determine uranium concentration, samples were unfrozen, filtered through 25 mM 0.2 μM syringe filters into 4 mL 0.1 M HNO_3. Samples were then analyzed for soluble uranium concentration with ICP-AES.

12.1.2. Results

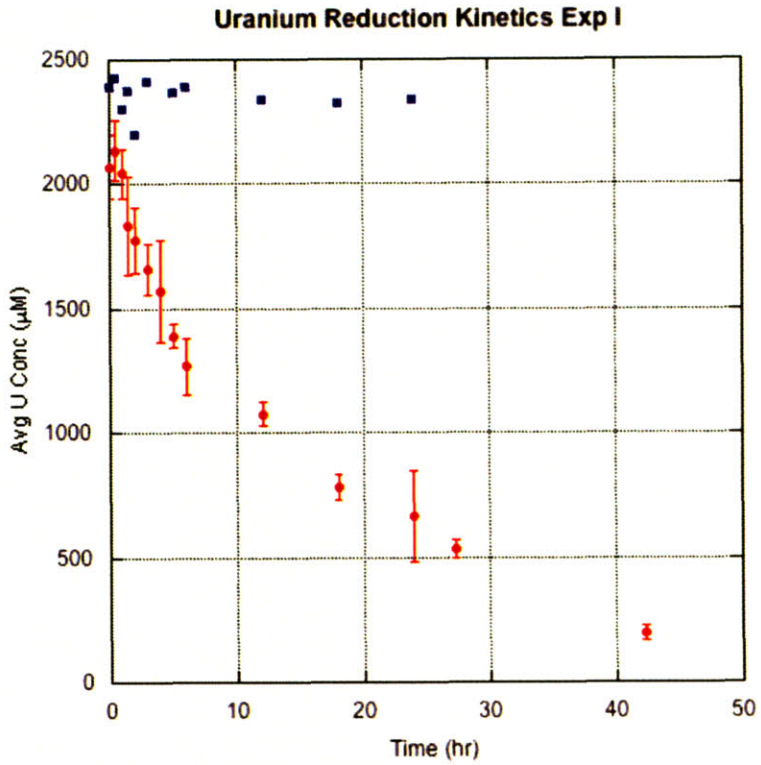

Figure 12.1 Uranium reduction kinetics for experiment I. ● Sample ■ Control. The error bars represent 1 standard deviation in the triplicate ICP-AES measurement.

12.2. Experiment II: Uranium reduction as a function of bacterial density

12.2.1. Materials and Methods

Cells were grown overnight in 1000 mL Tryptic Soy Broth at room temperature. They were then concentrated and rinsed 3X with $NaHCO_3$ buffer, and resuspended in buffer. The concentrated cell concentration was determined using the DAPI method and was found to be 2.66E10 cells/mL. 5mL of cells were transferred into an anaerobic glovebox under H_2:CO_2:N_2 5:15:80 atmosphere and added to 100 mL sterile anaerobic bicarbonate buffered freshwater medium (unless otherwise specified) as described by Kuai et al.[12], with the following exceptions; phosphate was removed to prevent uranyl precipitation, the carbon source and electron donor was 5 mM lactate, and the electron acceptor was ~2 mM uranium. A series of serial dilutions was done to yield cell concentrations of 10^8, 10^7, and 10^6, with the final cell concentration being 1.3Ex where X=9,8,7,6. The cell-free control consisted of lactate media

with 5mL of bicarbonate buffer. Three 1 mL samples were removed and added to 1.5 mL Eppendorf tubes containing 0.1 mL formaldehyde, were then frozen until analysis.

In order to determine uranium concentration, samples were unfrozen, filtered through 25 mM 0.2 μM syringe filters into 4 mL 0.1 M HNO_3. Samples were then analyzed for soluble uranium concentration with ICP-AES.

12.2.2. Results

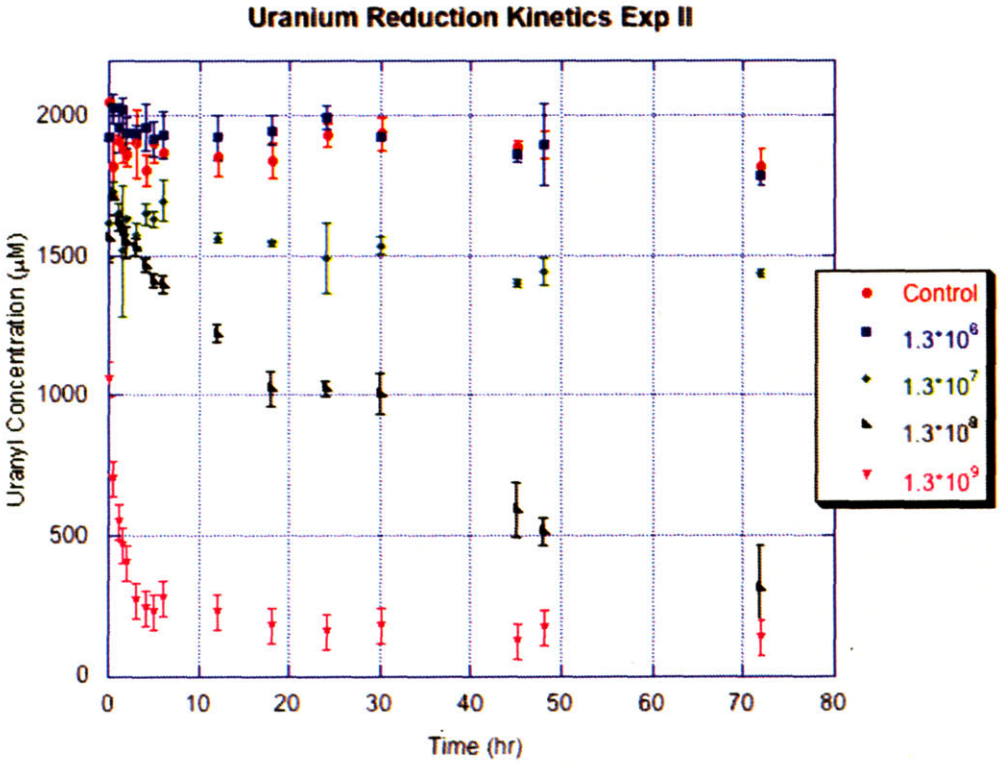

Figure 12.2 Uranium Reduction Kinetics for experiment II. Error bars represent 1 standard deviation from triplicate samples.

12.2.3. U(VI) sorption onto *Shewanella oneidensis*

12.2.3.1. Sample preparation

Samples of the uranium-reducing bacterium *Shewanella oneidensis* in the presence of uranyl acetate were killed with a 10% formaldehyde solution. The sorption of the uranyl onto the bacteria was then examined with EXAFS.

12.2.3.2. Results

For the 22 mM sample, the deconvoluted forurier transformations of the EXAFS spectra (Figure 12.3) only indicate uranyl acetate. Either the high concentration of uranium precluded any cellular interaction, or the high uranyl acetate concentration washed out any signal from uranium in other environments.

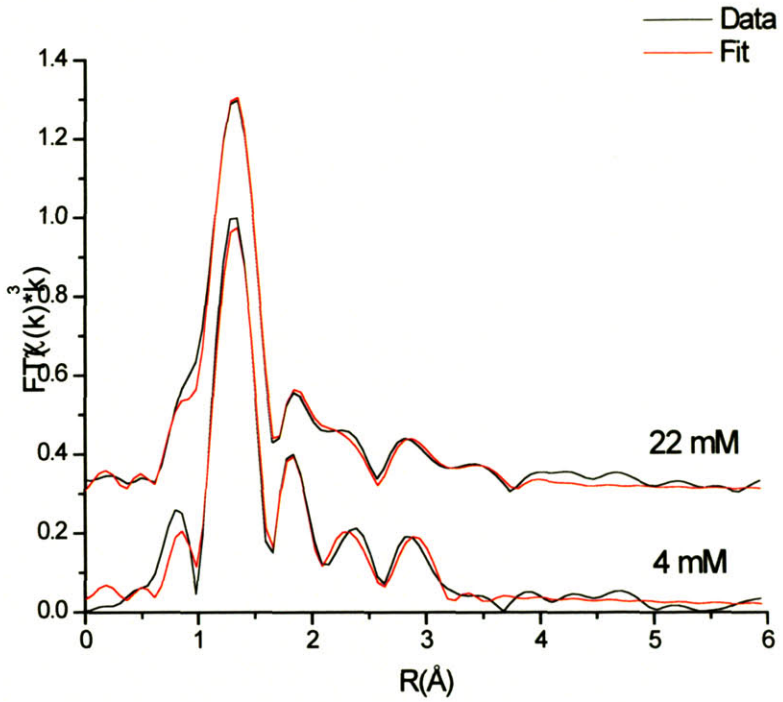

Figure 12.3 : Fourier transforms of uranyl sorption to *Shewanella oneidensis* EXAFS.

The peaks at ~1.2 Å show the presence of U(VI) as uranyl. The data are fit considering uranium associated with phosphate and organic carbon. The 22 mM sample shows a preponderance of uranium associated with organic carbon, most likely acetate, and is primarily due to too high a concentration of uranium. The 4 mM sample, on the other hand, shows both uranyl acetate as well as uranyl phosphate, indicating uranyl sorption to organic phosphate groups. Because the cells were contacted with the uranium for a period of weeks before analysis and the cells may have broken down releasing intercellular phosphate, we cannot determine whether the uranyl is sorbed to phosphate groups present on the cell surface, or phosphate groups that may have leaked out of the cell.

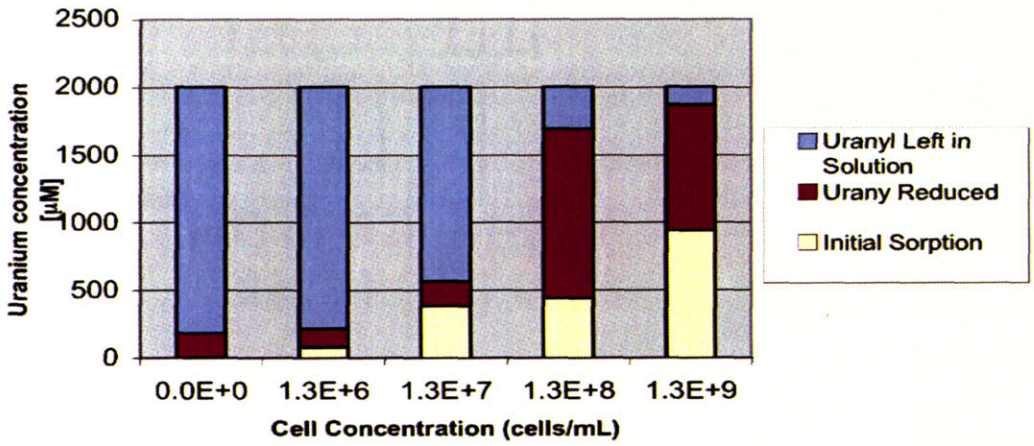

Figure 12.4 Reductive Capacity, illustrating both the total uranium reduced as well as the initial uranium sorption.

Figure 12.4 shows both the total initial sorption as well as the total amount of uranyl reduced as a function of cell number. The trend is towards a greater initial sorption after 30 minutes with larger cell densities, but a maximum total reduction which occurs at a cell density of $1.3*10^8$ cells/mL after which increasing the cell density does not increase the total amount of uranyl reduced in the system.

12.3. Experiment III: Inhibition of uranium reduction by several metabolic inhibitors.

12.3.1. Materials and methods

Cells were grown overnight in 1000 mL Tryptic Soy Broth at room temperature. They were then concentrated and rinsed 3X with $NaHCO_3$ buffer, and resuspended in 20 mL buffer. The concentrated cell concentration was determined using the DAPI method and was found to be 1.27E10 cells/mL. 5 mL of cells were transferred into an anaerobic glovebox under H_2:CO_2:N_2 5:15:80 atmosphere and added to 100 mL sterile anaerobic bicarbonate buffered freshwater medium (unless otherwise specified) as described by Kuai et al.[12], with the following exceptions; phosphate was removed to prevent uranyl precipitation, the carbon source and electron donor was 5 mM lactate, and the electron acceptor was ~2 mM uranium. The final cell concentration was 6.05E8 cells/mL. The controls were as follows: cell-free, formaldehyde killed cells (10% formaldehyde refrigerated for 30 minutes), heat-killed cells (autoclaved 15 minutes), and cells killed

with 0.5 mM cyanide and 10 mM Mo. Three 1 mL samples were removed and added to 1.5 mL Eppendorf tubes containing 0.1 mL formaldehyde, were then frozen until analysis.

In order to determine uranium concentration, samples were unfrozen, filtered through 25 mM 0.2 μM syringe filters into 4 mL 0.1 M HNO_3. Samples were then analyzed for soluble uranium concentration with ICP-AES.

12.3.2. Results

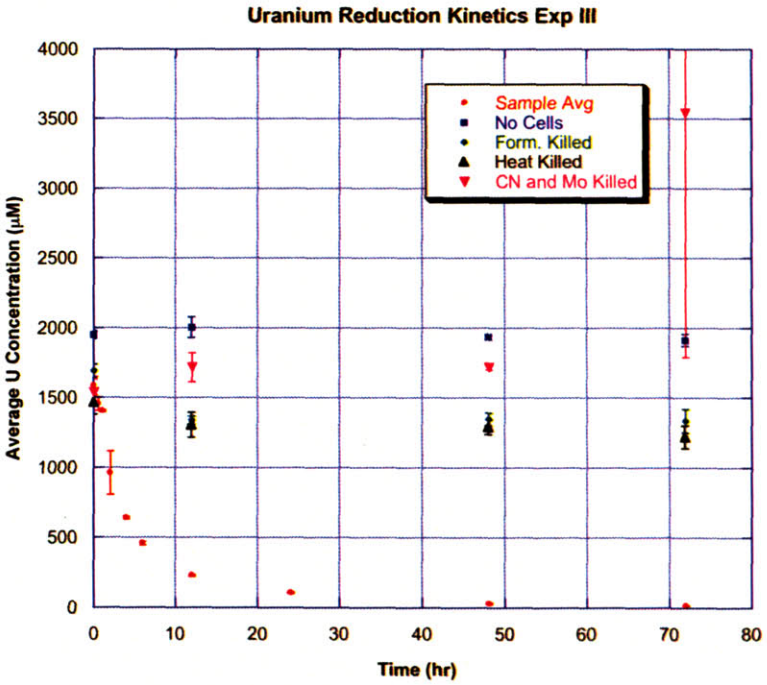

Figure 12.5 Uranium reduction kinetics for experiment III. Error bars represent 1 standard deviation from triplicate samples. The method of killing the cells had no significant effect on the uranium concentration, so formaldehyde was chosen as the preferred method for killing the cells because it took the shortest amount of time and was consistent with using formaldehyde to stop the reduction reaction in the sampling portion of the experiment.

12.4. Experiment V: First fractionation experiment sent to France

12.4.1. Materials and Methods

Cells were grown overnight in 1000 mL Tryptic Soy Broth at room temperature. They were then concentrated and rinsed 3X with $NaHCO_3$ buffer, and resuspended in 20 mL buffer. The

concentrated cell concentration was determined using the DAPI method and was found to be about 10^9 cells/mL.

The uranium reduction medium was equilibrated for 24 hours in an anaerobic glove box under H_2:CO_2:N_2 (5:15:80) atmosphere, after which 100 mL aliquots were dispensed and filter sterilized uranyl acetate solution containing 0.981:1 235U:238U, this material was derived from U500 standard (New Brunswick Laboratories). The uranyl acetate was added to approximately 2 mM, and the pH of the medium adjusted to 7 with NaOH. After 1 hour, washed cells were injected to a final concentration of approximately 1E9 cells/mL and the solutions incubated under constant, gentle stirring. At each time point, three replicates of one mL were withdrawn from the medium, killed by addition of 0.11 mL formaldehyde and stored frozen until further analysis. The two controls were formaldehyde killed cells and no cells and were treated identically. In order to avoid cross contamination during sampling, latex gloves were placed over glovebox gloves and changed frequently, stuffed tips were used and pipettors were acid-wiped after each sampling.

To determine uranium concentration, the three one ml subsamples taken for each time point were filtered through a 25 mM 0.2 μm pore size polycarbonate syringe filters (Whatman) into 5 mL 0.1 M HNO_3 and the samples split for determination of uranium concentration (4 mL) and isotopics (1 mL). Total free uranyl concentration was determined with ICP-AES.

12.4.2. Results

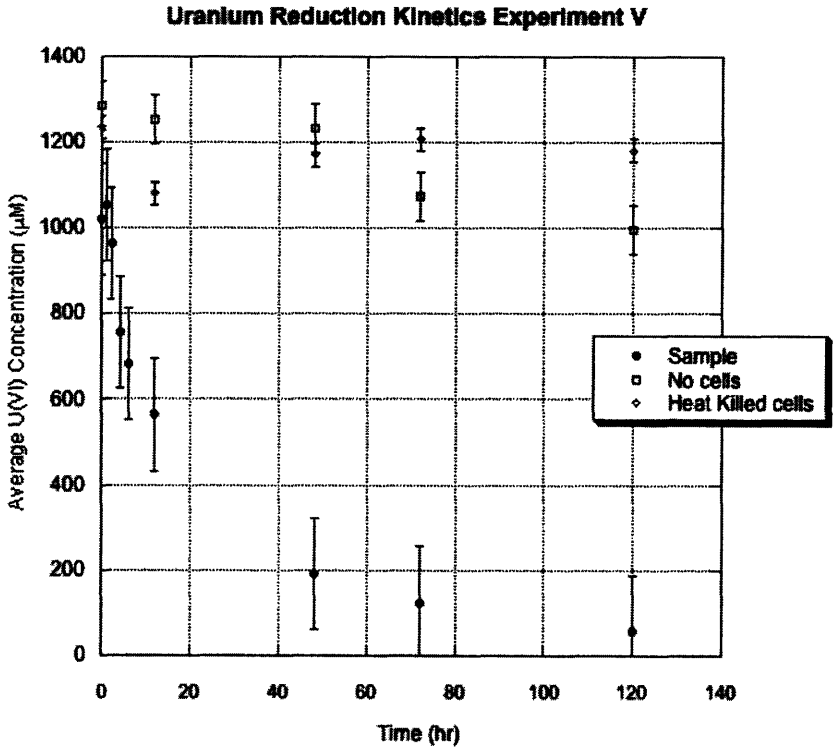

Figure 12.6 Uranium reduction kinetics for experiment V. Error bars represent 1 standard deviation from triplicate samples.

12.5. Experiment VII: Second fractionation experiment, samples sent to UNLV.

12.5.1. Materials and Methods

All reagents were prepared with ultra-pure water (Ultrex II-J.T. Baker) and fresh chemical stocks as well as new plastic containers or acid washed glassware to avoid any potential for contamination from uranium with natural isotopic composition.

The uranium reduction medium was equilibrated for 24 hours in an anaerobic glove box (Coy Laboratories) under H_2:CO_2:N_2 (5:15:80) atmosphere, after which 100 mL aliquots were dispensed and filter sterilized uranyl acetate solution containing 0.981:1 ^{235}U:^{238}U. This material was derived from U500 standard (New Brunswick Laboratories) but deviated from the original 1:1 ratio due to multiple uses in reduction experiments. The uranyl acetate was added to approximately 1.2 mM, and the pH of the medium adjusted to 7 with ultra-pure NaOH. Containers were new, acid

washed 250 mL polypropylene bottles. After 1 hour, washed cells were injected to a final concentration of $9.06x10^8$ mL^{-1} and the solutions incubated under constant, gentle stirring. At each time point, three replicates of one mL were withdrawn from the medium, killed by addition of 0.11 mL formaldehyde and stored frozen until further analysis. The two controls were treated identically except for the following modifications: addition of formaldehyde and no cells added. Additionally two blanks were also utilized: 0.06 mM uranium, and no uranium and were treated identically to experimental samples throughout the experimental processing, blanks were included to serve as an indication of any contamination which might occur during the sample processing. In order to avoid cross contamination during sampling, latex gloves were placed over glovebox gloves and changed frequently, stuffed tips were used and pipettors were acid-wiped after each sampling.

Total Uranium Analysis

To determine uranium concentration and isotopics, the three 1 mL subsamples taken for each time point were combined, and uraninite precipitate and cell material were separated from uranyl acetate remaining in solution by passage through 0.2 μm pore size polycarbonate filters (Whatman) using a new Swinnex syringe filter unit for each sample (Millipore). Carbon was subsequently burned off by muffling for 4 hours at 550° C to control for potential interference of organic matter or filter material in the isotopic analysis. Muffling was done in acid washed beakers to prevent any contamination at this step from residual uranium present on the glassware. Finally, uranium was dissolved in all samples in 5 mL 0.1 M ultrapure HNO_3 and the samples split for determination of uranium concentration (4 mL) and isotopics (1 mL), any remaining undissolved material (carbon) was removed by again passing the sample through a 0.2 μm pore size polycarbonate filters (Whatman). Total free uranyl concentration was determined with ICP-AES.

12.5.2. Results

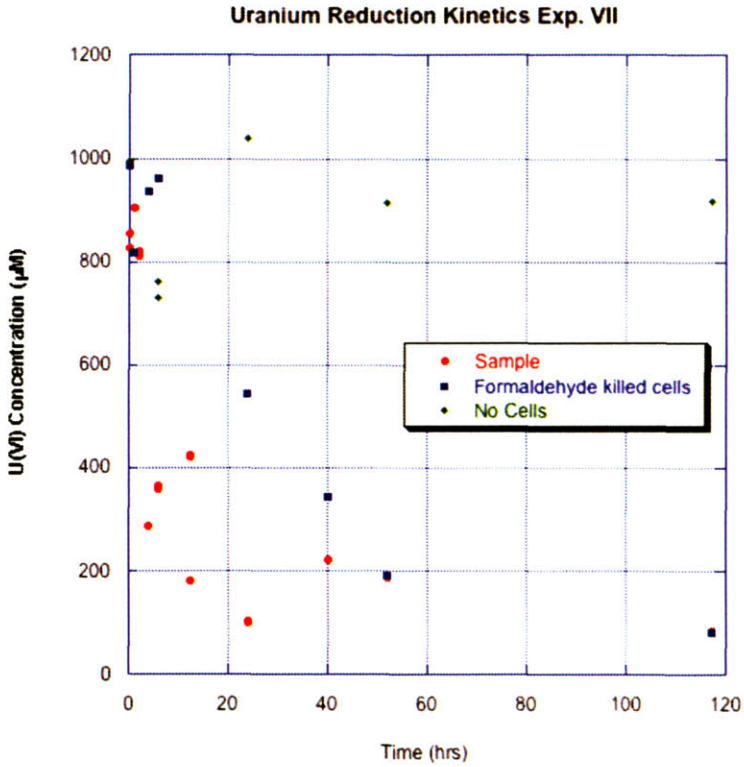

Figure 12.7 Uranium reduction kinetics for experiment VII.

12.6. Experiment VIII: UNLV Experiment II Fractionation

12.6.1. Materials and Methods

All reagents were prepared with ultra-pure water (Ultrex II-J.T. Baker) and fresh chemical stocks as well as new plastic containers or acid washed glassware to avoid any potential for contamination from uranium with natural isotopic composition.

The uranium reduction medium was equilibrated for 24 hours in an anaerobic glove box (Coy Laboratories) under H_2:CO_2:N_2 (5:15:80) atmosphere, after which 100 mL aliquots were dispensed and filter sterilized uranyl acetate solution containing 0.981:1 ^{235}U:^{238}U. This material was derived from U500 standard (New Brunswick Laboratories) . The uranyl acetate was added to approximately 1.2 mM, and the pH of the medium adjusted to 7 with ultra-pure NaOH. Containers were new, acid washed 250 mL polypropylene bottles. After 1 hour, washed cells were injected to a final concentration of 1.03×10^9 mL^{-1} and the solutions incubated

under constant, gentle stirring. At each time point, three replicates of one ml were withdrawn from the medium, killed by addition of 0.11 mL formaldehyde and stored frozen until further analysis. The two controls were treated identically except for the following modifications: addition of formaldehyde and no cells added. Additionally two blanks were also utilized: 0.06 mM uranium, and no uranium and were treated identically to experimental samples throughout the experimental processing, blanks were included to serve as an indication of any contamination which might occur during the sample processing. In order to avoid cross contamination during sampling, latex gloves were placed over glovebox gloves and changed frequently, stuffed tips were used and pipettors were acid-wiped after each sampling.

Total Uranium Analysis

To determine uranium concentration and isotopics, the three 1 mL subsamples taken for each time point were combined, and uraninite precipitate and cell material were separated from uranyl acetate remaining in solution by passage through 0.2 μm pore size polycarbonate filters (Whatman) using a new Swinnex syringe filter unit for each sample (Millipore). Carbon was subsequently burned off by muffling for 4 hours at 550° C to control for potential interference of organic matter or filter material in the isotopic analysis. Muffling was done in acid washed beakers to prevent any contamination at this step from residual uranium present on the glassware. Finally, uranium was dissolved in all samples in 0.1 M ultrapure HNO_3 and the samples split for determination of uranium concentration and isotopics, any remaining undissolved material (carbon) was removed by again passing the sample through a 0.2 μm pore size polycarbonate filters (Whatman).

Uranium concentration was determined spectrophotometrically at 652 nm in a Beckman DU series spectrophotometer with 3 mM Arsenazo III indicator dye (Alpha Aesar). A dilution series of uranium standards was used to correlate sample counts to concentration. To control for variation in measurements, all standards were run at the beginning and end of sample measurements. In addition, every 10 samples two standards were re-measured to check for consistency.

12.6.2. Results

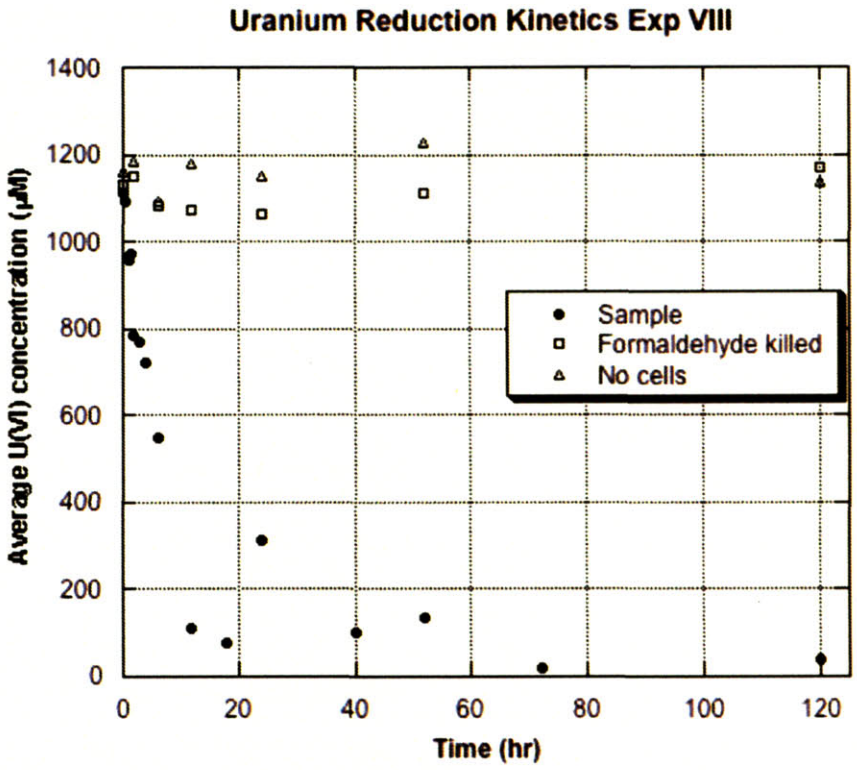

Figure 12.8 Uranium reduction kinetics for experiment VIII.

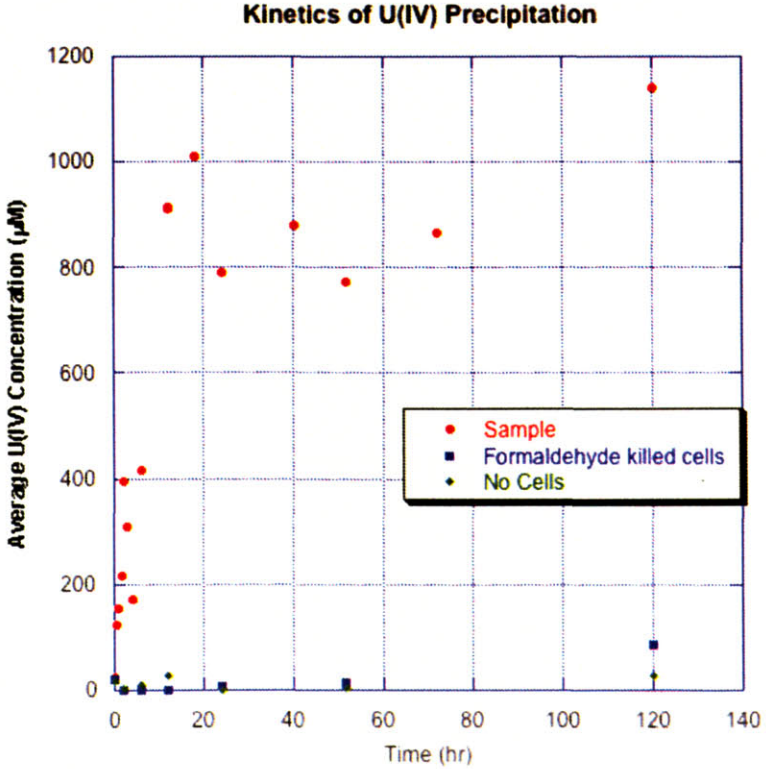

Figure 12.9 Kinetics of $U(IV)O_2$ formation for experiment VIII.

12.7. Experiment IX: First reduction experiment at UNLV

12.7.1. Materials and Methods

Cells were grown overnight in 1000 mL Tryptic Soy Broth at room temperature. They were then concentrated and rinsed 3X with 1 g/L $NaHCO_3$ buffer, and resuspended in buffer. The concentrated cell concentration was determined using the DAPI method and was found to be 3.51E11 cells/mL.

15 mM HEPES buffer was equilibrated for 24 hours in an anaerobic glove box under H_2:Ar (5:95) atmosphere, after which 100 mL aliquots were dispensed and filter sterilized uranyl acetate solution was added to approximately 2 mM, and the pH of the medium adjusted to 6.5-7 with 1 M NaOH; 15 mL concentrated cells were injected to a final concentration of 4.21E10 cells/mL and the solutions incubated under constant, gentle stirring. At each time point, three replicates of 1 mL were withdrawn from the medium, killed by addition of 0.10 mL formaldehyde and stored frozen until further analysis. The two controls were formaldehyde killed cells and no cells and were treated identically.

To determine uranium concentration, the three one ml subsamples taken for each time point were filtered through a 13 mM 0.2 μm pore size polycarbonate syringe filters (Whatman) into 5 mL 0.1 M HNO_3. Total free uranyl concentration was determined with ICP-AES.

12.7.2. Results

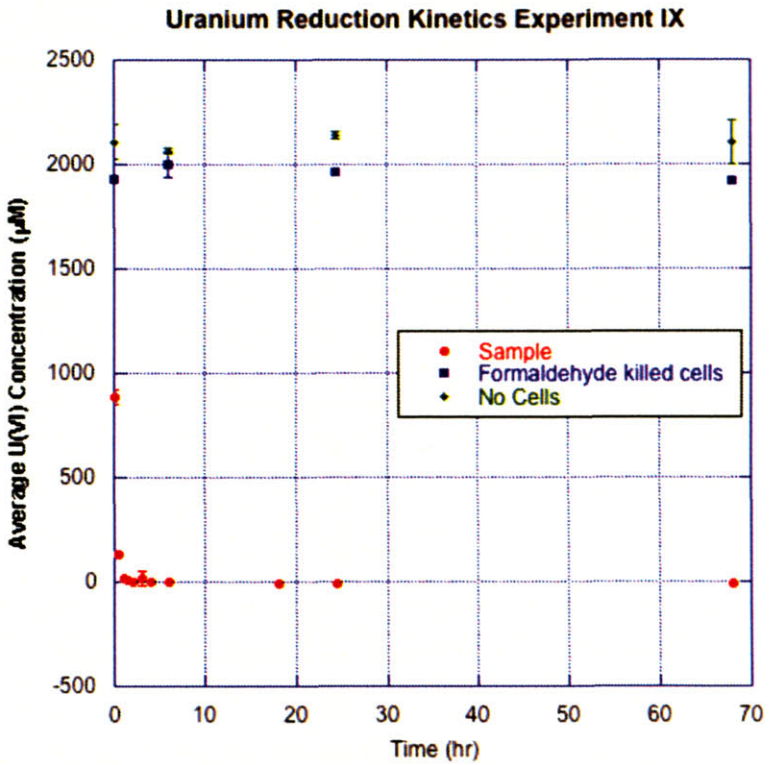

Figure 12.10 Uranium reduction kinetics for experiment IX. Error bars represent 1 standard deviation from triplicate samples.

12.8. Experiment X: Second UNLV Reduction Experiment in HEPES

12.8.1. Materials and Methods

Cells were grown overnight in 1000 mL Tryptic Soy Broth at room temperature. They were then concentrated and rinsed 3X with 15 mM HEPES buffer, and resuspended in ~ 10 mL buffer. The concentrated cell concentration was determined using the DAPI method and was found to be 2.1E11 cells/mL.

The 15 mM HEPES buffer was equilibrated for 24 hours in an anaerobic glove box under H_2:Ar (5:95) atmosphere, after which 100 mL aliquots were dispensed and uranyl acetate solution was added to approximately 2 mM, and the pH of the medium adjusted to 6.5-7 with 1 M NaOH. Concentrated cells were injected to a final concentration of 1.93E9 cells/mL and the solutions incubated under constant, gentle stirring. At each time point, three replicates of 1 mL were withdrawn from the medium, killed by addition of 0.10 mL formaldehyde and stored frozen until further analysis. The

two controls were formaldehyde killed cells and no cells and were treated identically.

To determine uranium concentration, the three one mL subsamples taken for each time point were filtered through a 13 mM 0.45 μm pore size polycarbonate syringe filters (Whatman) into 5 mL 0.1 M HNO_3. Total free uranyl concentration was determined with ICP-AES.

12.8.2. Results

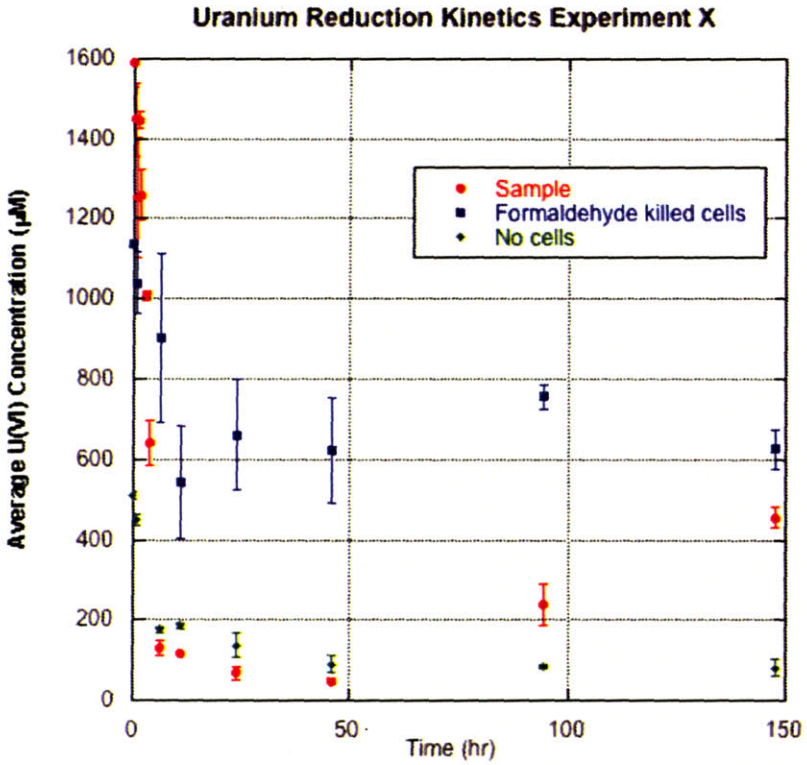

Figure 12.11 Uranium reduction kinetics for experiment X. Error bars represent 1 standard deviation from triplicate samples.

There are several anomalous results that can be seen in this experiment. Firstly, both controls exhibit a significant drop in free uranyl concentration, with the largest decrease in the no cell control. Thus, the decrease in free uranyl cannot be attributed to adsorption to biomass. In both of the controls the decrease in uranyl concentration levels off after about 11hours. This is perhaps due to the formation of uranyl hydroxide. Secondly, after approximately 50 hours in the sample containing live cells, the uranyl concentration is seen to increase, after which the sample also lightened from dark brown to light greenish-yellow. The cause of the late increase in uranyl concentration in the sample is not known.

12.9. Experiment XI: Light v. Dark

This experiment was designed to determine if degradation of the HEPES buffer in the light was the cause of the late increase in uranyl concentration observed in the previous experiment. There was some evidence that exposure of HEPES buffer to light could lead to the production of free-radicals[5,6].

12.9.1. Materials and Methods

Cells were grown overnight in 1000 mL Tryptic Soy Broth at room temperature. They were then concentrated and rinsed 3X with 15 mM HEPES buffer, and resuspended in ~ 12 mL buffer. The concentrated cell concentration was determined using the DAPI method and was found to be 6.19E11 cells/mL.

15 mM HEPES buffer was equilibrated for 24 hours in the dark in an anaerobic glove box under H_2:Ar (5:95) atmosphere, after which 75 mL aliquots were dispensed and uranyl acetate solution was added to approximately 2 mM, and the pH of the medium adjusted to 6.5-7 with 1 M NaOH. Concentrated cells were injected to a final concentration of 1.90E9 cells/mL and the solutions incubated under constant, gentle stirring. At each time point, three replicates of 1 mL were withdrawn from the medium, killed by addition of 0.10 mL formaldehyde and stored frozen until further analysis. There were two samples, treated identically except one was exposed to light and one was darkened. The two controls were formaldehyde killed cells and no cells and were also exposed to light.

To determine uranium concentration, the three one ml subsamples taken for each time point were centrifuged for 5 min at 5000r pm, 20μL supernatant was removed and added to 25 μL 2 mM Arsenazo III in pH 2 buffer to a total volume of 200 μL. Total free uranyl concentration was determined with spectrophotometrically using the Arsenazo III method.

12.9.2. Results

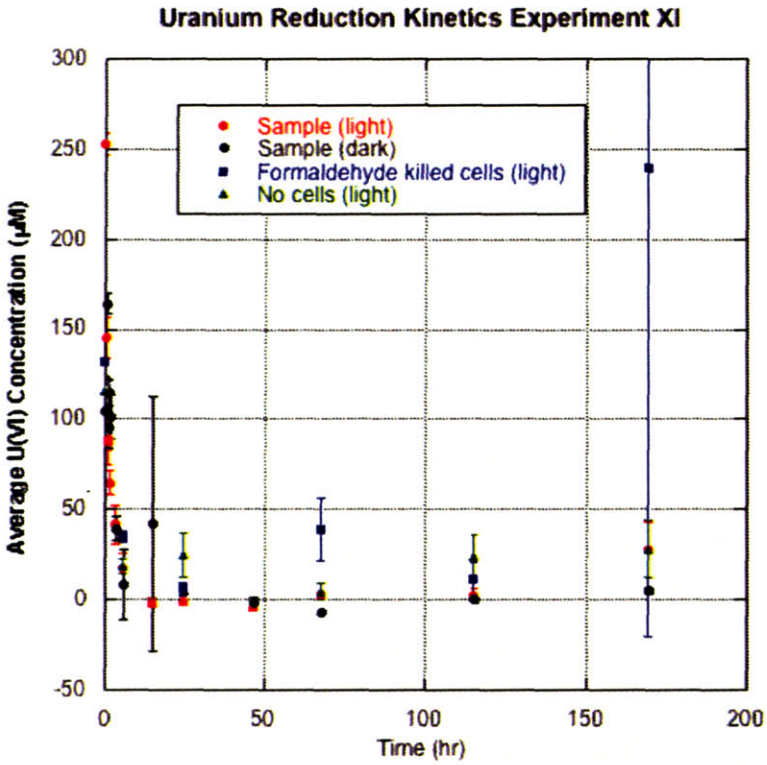

Figure 12.12 Uranium reduction kinetics for experiment XI. Error bars are 1 standard deviation from triplicate samples.

There are several anomalous results that can be seen in this experiment. Again a drop in free uranyl concentration is observed in both controls along with an increase in uranyl concentration after ~50 hours in both of the samples. The method of determining uranium concentration also had significant amounts of error in the measurement. However, the same trends were observed in both the dark and light samples, indicating that any photodegradation of HEPES buffer does not affect the reduction experiment. Because these results were not previously observed in bicarbonate buffered lactate media, it was determined that bicarbonate buffered lactate media was better for subsequent uranium reduction experiments and would eliminate any secondary effects on uranium speciation in HEPES buffer.

12.10. Experiment XII: Final fractionation experiment

12.10.1. Materials and Methods

Cells were grown overnight in 1000 mL Tryptic Soy Broth at room temperature. They were then concentrated and rinsed 3X with 1 g/L $NaHCO_3$ buffer, and resuspended in ~15 mL buffer. The concentrated cell concentration was determined using the DAPI method and was found to be 6.9E10 cells/mL.

The 1 g/L ultrapure $NaHCO_3$ buffer was equilibrated for 24 hours in an anaerobic glove box under H_2:CO_2:N_2 (3:5:92) atmosphere, after which 100 mL aliquots were dispensed and filter sterilized uranyl acetate solution containing ~1:1 235U:238U, this material was derived from equal parts U200 standard and U800 standard(New Brunswick Laboratories). The uranyl acetate was added to approximately 2 mM, and the pH of the medium adjusted to 6.5-7 with 1 M NaOH. Concentrated cells were injected to a final concentration of 1.68E9 cells/mL and the solutions incubated under constant, gentle stirring. At each time point, three replicates of one ml were withdrawn from the medium, killed by addition of 0.10 mL formaldehyde and stored frozen until further analysis. There were two live cell samples, one containing ~2 mM of uranyl with an approximate isotopic ratio of 1:1 235:238, the second contained ~2 mM of uranyl with an approximate isotopic ratio of 1:2 235:238. The two controls were formaldehyde killed cells and no cells both containing ~2 mM of uranyl with an approximate isotopic ratio of 1:1 235:238, and were treated identically. In order to avoid cross contamination during sampling, latex gloves were placed over glovebox gloves and changed frequently, stuffed tips were used and pipettors were acid-wiped after each sampling.

To determine uranium concentration, the three one mL subsamples taken for each time point were filtered through a 13 mM 0.45 μm pore size polycarbonate syringe filters (Whatman) into 5 mL 0.1 M HNO_3 and the samples split for determination of uranium concentration (4 mL) and isotopics (1 mL). Syringe filters were saved in case uranium mass balance was necessary. Total free uranyl concentration was determined spectrophotometrically using Arsenazo III.

12.10.2. Results

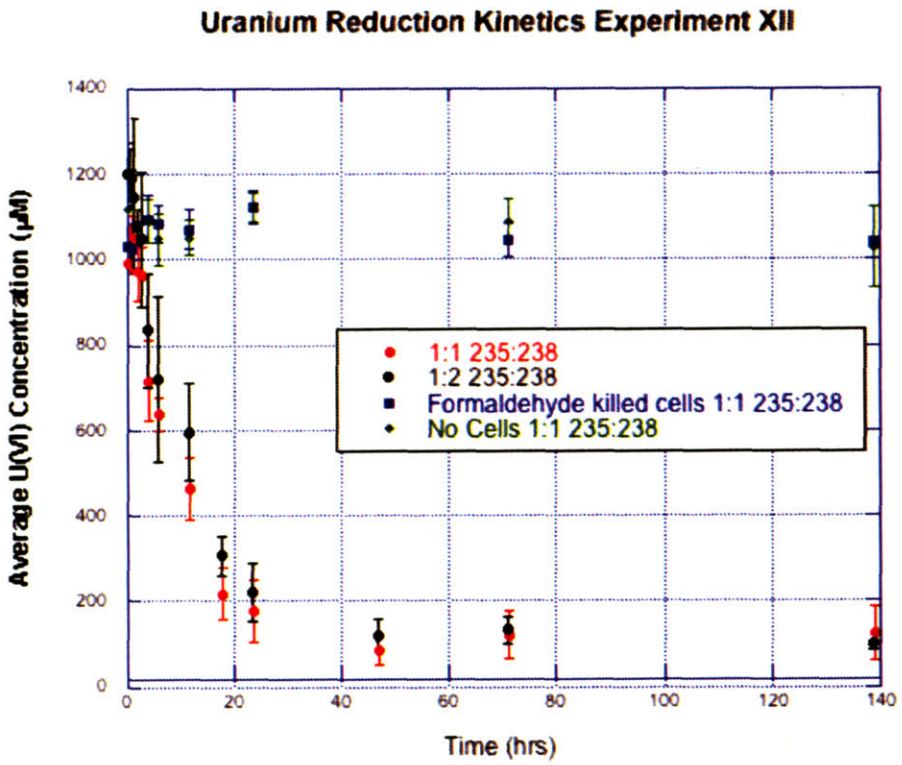

Figure 12.13 Uranium reduction kinetics for experiment XII. Error bars are 1 standard deviation from triplicate samples.

12.11. Experiment XIII: Electron donor dependence

12.11.1. Materials and Methods

Cells were grown overnight in 500 mL Tryptic Soy Broth at room temperature. They were then concentrated and rinsed 3X with 1 g/L $NaHCO_3$ buffer, and resuspended in ~15 mL buffer. The concentrated cell concentration was determined using the DAPI method and was found to be 8.27E10 cells/mL. Cells were transferred into an anaerobic glovebox under H_2:CO_2:N_2 3:5:92 atmosphere and added to 135 mL sterile anaerobic bicarbonate buffered freshwater medium or 1 g/L $NaHCO_3$ buffer. The final cell concentration was 8.7E8 cells/mL. The pH of the medium adjusted to 6.5-7 with 1 M NaOH; and the solutions incubated under constant, gentle stirring. At each time point, three replicates of 1 mL were withdrawn from the medium, killed by addition of 0.10 mL formaldehyde and stored frozen until further analysis.

In order to determine uranium concentration, samples were unfrozen, filtered through 13 mM 0.4 5μM syringe filters into 4

mL 0.1 M HNO_3. Samples were then analyzed for soluble uranium concentration with ICP-AES.

12.11.2. Results

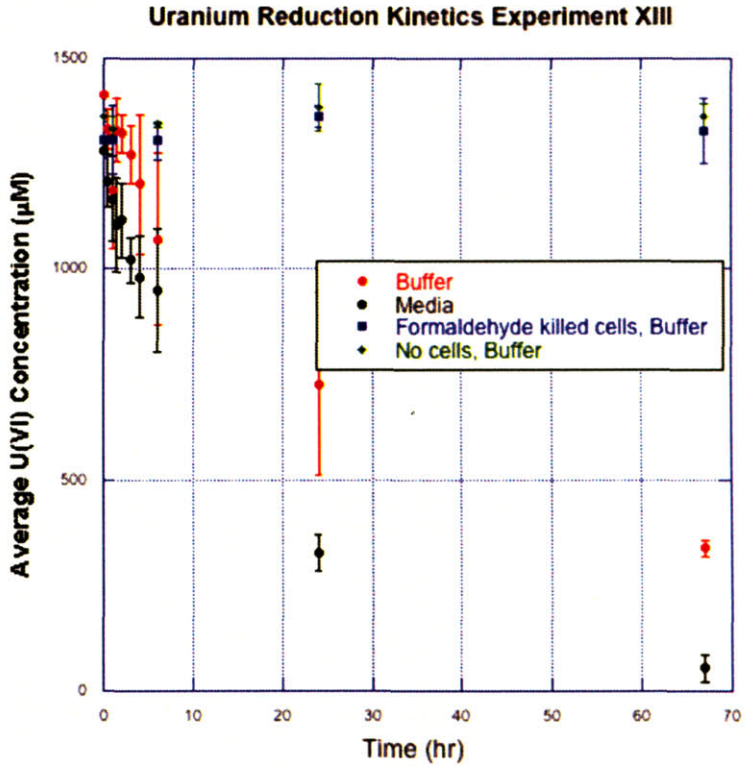

Figure 12.14 Uranium reduction kinetics for experiment XIII. Error bars are 1 standard deviation from triplicate samples.

12.12. Experiments XIV and XV: pH Dependence

12.12.1. Materials and Methods

12.12.1.1. Chess Modeling

Uranium speciation in anaerobic lactate media was modeled using the CHESS[1] algorithm with the following inputs:

Table 12.1 Chess input: species and initial concentrations.

Species and Initial Values		Mol/L
$NH_4^{[+]}$	total concentration	0.005
$Mg^{[2+]}$	total concentration	0.002
$Cl^{[-]}$	total concentration	0.037
$Ca^{[2+]}$	total concentration	0.001
$Na^{[+]}$	total concentration	0.029
$K^{[+]}$	total concentration	0.008
$Acetate^{[-]}$	total concentration	0.004
$HCO3^{[-]}$	total concentration	0.014
$UO_2^{[2+]}$	total concentration	0.002
$H^{[+]}$	activity	1.0E-05

Activity model used: truncated-davies

Interface model used: surface-complexation

12.12.1.2. Experiment XIV

Cells were grown overnight in 700 mL Tryptic Soy Broth at room temperature. They were then concentrated and rinsed 3X with 1 g/L $NaHCO_3$ buffer, and resuspended in ~15 mL buffer. The concentrated cell concentration was determined using the DAPI method and was found to be 1.09E11 cells/mL. Cells were transferred into an anaerobic glovebox under H_2:CO_2:N_2 3:5:92 atmosphere and added to 200 mL sterile anaerobic bicarbonate buffered freshwater medium. The final cell concentration was ~9.75E8 cells/mL. The pH of the medium adjusted with 1 M HCl; and the solutions incubated under constant, gentle stirring. At each time point, three replicates of 1 mL were withdrawn from the medium, killed by addition of 0.10 mL formaldehyde and stored

frozen until further analysis. Two samples containing live cells were adjusted to pH 5.10 and 6.11 and controls containing formaldehyde killed cells were adjusted to pH 5.03 and 6.11, a third control containing no cells was adjusted to pH 5.45.

In order to determine uranium concentration, samples were unfrozen, filtered through 13 mM 0.45 μM syringe filters into 4 mL 0.1 M HNO_3. Samples were then analyzed for soluble uranium concentration with ICP-AES.

12.12.1.3. Experiment XV

Cells were grown overnight in 700 mL Tryptic Soy Broth at room temperature. They were then concentrated and rinsed 3X with 1 g/L $NaHCO_3$ buffer, and resuspended in ~15 mL buffer. The concentrated cell concentration was determined using the DAPI method and was found to be 1.6E11 cells/mL. Cells were transferred into an anaerobic glovebox under H_2:CO_2:N_2 3:5:92 atmosphere and added to 200 mL sterile anaerobic bicarbonate buffered freshwater medium. The final cell concentration was ~9.0E8 cells/mL. The pH of the medium adjusted with 1 M NaOH (and 0.1 M HCL if necessary); and the solutions incubated under constant, gentle stirring. At each time point, three replicates of 1 mL were withdrawn from the medium, killed by addition of 0.10 mL formaldehyde and stored frozen until further analysis. Two samples containing live cells were adjusted to pH 6.9 and 7.5 and controls containing formaldehyde killed cells were adjusted to pH 6.9 and 6.9, a third control containing no cells was adjusted to pH 7.2.

In order to determine uranium concentration, samples were unfrozen, filtered through 13 mM 0.45 μM syringe filters into 4 mL 0.1 M HNO_3. Samples were then analyzed for soluble uranium concentration with ICP-AES.

12.12.2. Results

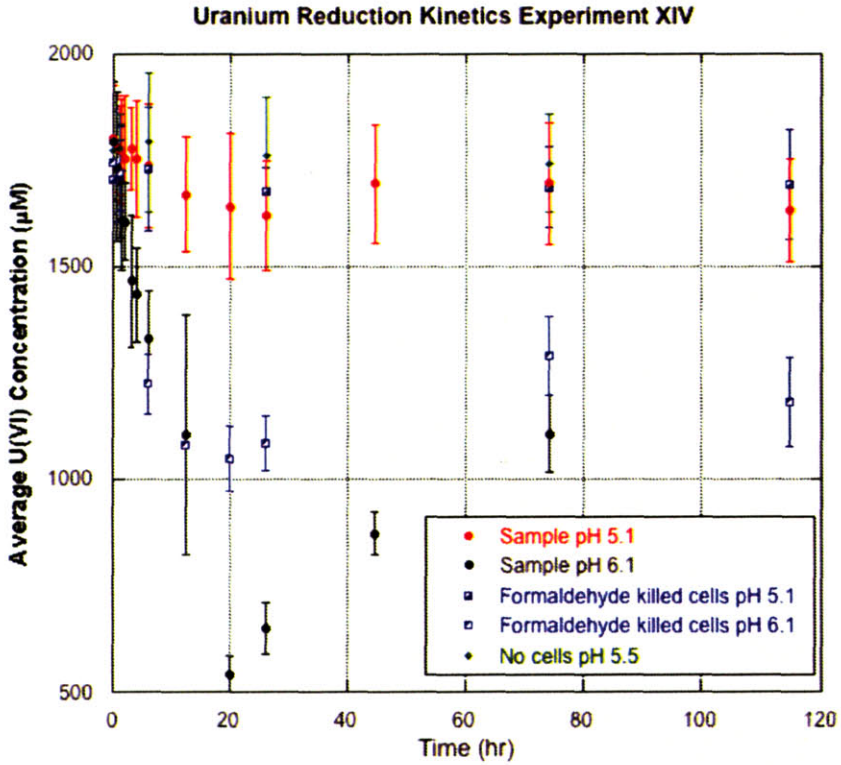

Figure 12.15 Uranium reduction kinetics for experiment XIV. Error bars are 1 standard deviation from triplicate samples.

Table 12.2 pH measurements and adjustments for Exp. XIV.

Time (hr)	S1	S2	C1	C2	C3
-1	6.35	6.38	6.41	6.45	6.44
add 1M HCl	2400 uL	700 uL	2500 uL	700 uL	1000 uL
0	5.10	6.11	5.03	6.11	5.45
1	5.20	6.48	5.15	6.42	5.85
2	5.21	6.54	5.10	6.49	5.91
add 1M HCl	100 uL	500 uL	0 uL	500 uL	100 uL
	5.11	6.11		6.11	5.54
3	5.06	6.22	5.10	6.20	5.56
6	4.98	6.35	4.96	6.25	5.60
12	4.90	6.43	4.95	6.46	5.56
13	5.10	6.40	5.10	6.36	5.57
20	5.11	6.46	5.16	6.50	5.68
26.5	5.10	6.45	5.18	6.47	5.66
74.5	5.13	6.46	5.18	6.54	5.73
115.5	5.23	6.57	5.34	6.55	5.80
Average	5.10	6.38	5.11	6.37	5.66

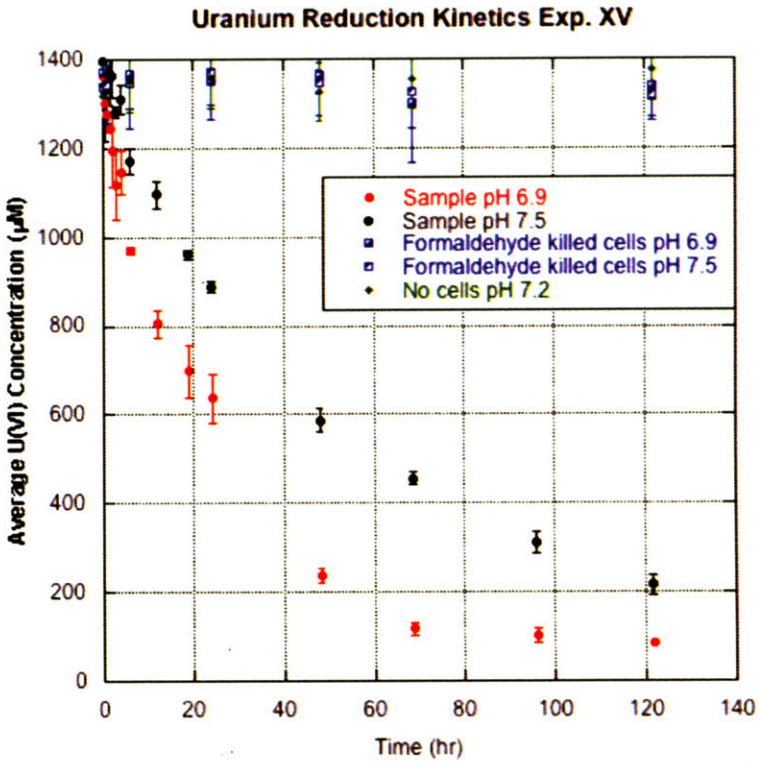

Figure 12.16 Uranium reduction kinetics for experiment XV. Error bars are 1 standard deviation from triplicate samples.

Table 12.3 pH measurements and adjustments for Exp. XV.

Time (hr)	S1	S2	C1	C2	C3
-1	6.401	6.387	6.435	6.416	6.496
0	6.907	7.510	6.898	7.524	7.197
0.5	7.002	7.346	6.971	7.318	7.127
1.5	6.964	7.211	6.922	7.218	7.071
add 0.1 M HCl	1200uL	350uL			300uL
add 1M NaOH		200uL		225uL	100uL
2	6.904	7.507		7.528	7.213
4.5	6.897	7.194	6.888	7.325	7.056
add 0.1 M HCl				75uL	
add 1M NaOH		165uL		175uL	75uL
		7.507		7.566	7.235
6	6.916	7.294	6.881	7.364	7.132
add 0.1 M HCl					
add 1M NaOH		100uL		100uL	35uL
		7.516		7.530	7.197
13	6.942	7.286	6.890	7.185	7.003
add 0.1 M HCl				1850uL	
add 1M NaOH		125uL		500uL	100uL
		7.485		7.575	7.213
19	6.986	7.285	6.879	7.346	7.081
add 0.1 M HCl	700uL				
add 1M NaOH		150uL		125uL	75uL

	6.893	7.521		7.496	7.222
24	6.944	7.325	6.892	7.286	7.113
add 0.1 M HCl					
add 1M NaOH		100uL		140uL	50uL
		7.510		7.505	7.216
45	6.961	7.304	6.846	7.298	7.081
add 0.1 M HCl					
add 1M NaOH		125uL		125uL	60uL
		7.483		7.510	7.196
68.5	6.999	7.362	6.878	7.327	7.143
add 0.1 M HCl	700uL				
add 1M NaOH		75uL		105uL	
	6.918	7.478		7.510	
94	6.962	7.340	6.901	7.362	7.125
add 0.1 M HCl					
add 1M NaOH		100uL		100uL	50uL
		7.495		7.506	7.217
122	6.929	7.328	6.872	7.320	7.144
Average	6.942	7.395	6.893	7.409	7.149
Stdev	0.036	0.111	0.031	0.121	0.067

12.13. References

[1] **van der Lee, J., L. De Windt.** (2000) JCHESS v. 2.5. CIG-École des Mines de Paris.

[2] **Chernorukov, N. G., A. V. Knyazeva, I. V. Sergacheva.** (2002) Synthesis, Structure, and Physicochemical Characteristics of Rutherfordite and Tetrasodium Uranyl Tricarbonate. Raciochemistry. **44:**212-215.

[3] **Kuai, L., A. A. Nair, M. F. Polz.** (2001) Rapid and Simple Method for the Most-Probable-Number Estimation of Arsenic-Reducing Bacteria. Appl. Environ. Microbiol. **67:**3168-3173.

[4] **Kuai, L., A. A. Nair, M. F. Polz.** (2001) Rapid and Simple Method for the Most-Probable-Number Estimation of Arsenic-Reducing Bacteria. Appl. Environ. Microbiol. **67:**3168-3173.

[5] **Zigler, J. S., J. L. Lepe-Zunga, B. Vistica, I. Gery.** (1985) Analysis of the Cytotoxic Effects of Light-Exposed HEPES-containing Culture Medium. Lab. Vis. Res. **21:**282-287.

[6] **Zeiger, M. A., D. J. Glofcheski, J. R Lepock, J. Kruuv.** (1991) Factors Influencing Survival of Mamalian Cells Exposed to Hypothermia. V. Effects of Hepes, Free Radicals, and H_2O_2 Under Light and Dark Conditions. Cryobiol. **28:**8-17.

13. Chapter 9 Appendix

13.1. Overview

Two independent experiments were carried out. In the first (preliminary) experiment, uranium fractionation was determined by incubating and sacrificing replicate tubes of uranium-reduction medium. Total uranium was measured for the solution and solid phase but isotopes were determined for the solution phase only. The results (Figure 13.1 and Table 13.6) suggested extensive fractionation; however, variation among the tubes sacrificed at the specific time points was large and we thus decided to design a second experiment in which one batch system would be subsampled. Moreover, in the second (main) experiment total uranium and the two isotopes were measured for both the solution and solid phase in order to allow mass balance and thus exclude with authority the potential that contamination with uranium from natural sources might have caused the observed isotopic variation in the first experiment. Natural uranium has an extremely skewed ratio of isotopes in favor of ^{238}U so that even small amounts of contamination of the solution phase might yield appearance of fractionation in the solution phase of the experiment. This is, however, not the case for the solid phase where ^{235}U is expected to be enriched.

13.2. Material and Methods

13.2.1. Bacterial strain and culture conditions

To generate sufficient biomass for the fractionation experiments, *Shewanella oneidensis* MR-1 (ATTC 7005500) was grown for approximately 24 h at room temperature in tryptic soy broth (Difco) under aerobic conditions. Cells were harvested in mid-exponential phase by centrifugation and washed three times with anaerobic $NaHCO_3$ (2 g/L) buffer made with ultrapure water (Sigma) before transfer to the fractionation medium.

13.2.2. Uranium.

In both experiments, enriched uranium was obtained from an initial stock of an NBS certified U500 uranium standard (49.383 weight

percent ^{235}U and 50.029 weight percent ^{238}U). Because the material was regenerated from solid precipitate from previous experiments, the ratio deviated slightly from the initial value in the final experiment.

13.2.3. Uranium reduction medium.

For all anaerobic uranium reduction experiments, a bicarbonate buffered freshwater medium was prepared as described by Kuai *et al.*[1] except that phosphate salts were omitted to avoid precipitation of uranyl phosphate and that the carbon source was 5 mM lactate.

13.3. Uranium fractionation experiments

13.3.1. First (preliminary) experiment

Uranium reduction medium was prepared to a volume of 250 mL and U500 uranyl acetate was added to a final concentration of 2 mM. The pH was determined to be 6.27. Replicate test tubes were filled with 10 mL of the enriched uranium medium and purged with 20% CO_2 and 80% N_2 for 3 minutes each.

To each experimental and control tube, bacteria were added to a final concentration of approximately 10^9 cells/mL. The tubes were then pressurized with approximately 30 mL of 100% H_2 and incubated at room temperature with gentle shaking until sacrificing entire tubes at specific time points by addition of 1 mL of 100% ethanol. This was done to one control and two replicate experimental tubes at 0, 4, 8, 11, 24, 48.5, 72, 120, and 170 hours.

13.3.1.1. Total Uranium Analysis

Samples were transferred into 15 mL polypropylene centrifuge cones and centrifuged for 30 minutes at 3,700 rpm. The supernatant was filtered through 0.2 μm filters to remove any particles. 4.75 mL of the filtrate was amended with 0.25 mL of concentrated HNO_3. Total uranium was measured by Inductively Coupled Plasma-Atomic Emission Spectroscopy (ICP-AES; Spectroflame ICP-D).

13.3.1.2. Uranium Isotopic Analysis

Uranium isotopic composition of both phases was determined by ICP magnetic-sector multiple collector mass spectrometer (Isoprobe – Micromass). Samples were introduced into the plasma with a peristaltic pump, a micronebulizer and a water-cooled cyclonic spray chamber. The National Bureau of Standard (NBS) SRMs U-500 reference material was selected to correct for bias due to mass differences. These standards were prepared with high purity water and 60% nitric acid (Normatom I, Prolabo) resulting in solutions with concentration from 50 to 500 ppb.

In order to obtain precise measurements, standards and samples were arranged in the sequence standard-sample-standard. Samples included filtrates, filters, controls and blanks. The measured $^{235}U/^{238}U$ ratio for samples was corrected with a correction factor F calculated as:

F = (NBS certified ratio)/(mean of the measured ratio of standard 1 and 2)

where standard 1 and 2 are the SRM U500 standard, and $(^{235}U/^{238}U)_{certified}$ = 0.999698 x 0.142 analyzed before and after the sample, respectively.

The ratio was then calculated as follows:

$$(^{235}U/^{238}U)_{real} = (^{235}U/^{238}U)_{measured} \times F$$

To guarantee the accuracy of results, two other standards (SRM U750 and SRM U200) were introduced in one run. The accuracy was defined by:

$$Accuracy(\%)=(^{235}U/^{238}U)_{measured\ and\ corrected}-(^{235}U/^{238}U_{certified})*100/(^{235}U/^{238}U_{certified})$$

13.3.2. Second (main) experiment.

All reagents were prepared with ultra-pure water (Ultrex II-J.T. Baker) and fresh chemical stocks as well as new plastic containers or acid washed glassware to avoid any potential for contamination from uranium with natural isotopic composition.

The uranium reduction medium was equilibrated for 24 h in an anaerobic glove box (Coy Laboratories) under H_2:CO_2:N_2 (5:15:balance) atmosphere, after which 100 ml aliquots were dispensed and filter sterilized uranyl acetate solution containing 0.981:1 ^{235}U:^{238}U. This material was derived from U500 standard (New Brunswick Laboratories) but deviated from the original 1:1

ratio due to multiple uses in reduction experiments. The uranyl acetate was added to approximately 1.2 mM, and the pH of the medium adjusted to 7 with ultra-pure NaOH. Containers were new, acid washed 250 mL polypropylene bottles. After 1 h, washed cells were injected to a final concentration of $1x10^9$ ml^{-1} and the solutions incubated under constant, gentle stirring. At each time point, three replicates of one ml were withdrawn from the medium, killed by addition of 0.11 ml formaldehyde and stored frozen until further analysis. The two controls were treated identically except for the following modifications: addition of formaldehyde and no cells added. Additionally two blanks were also utilized: 0.06 mM uranium, and no uranium and were treated identically to experimental samples throughout the experimental processing, blanks were included to serve as an indication of any contamination which might occur during the sample processing. In order to avoid cross contamination during sampling, latex gloves were placed over glovebox gloves and changed frequently, stuffed tips were used and pipettors were acid-wiped after each sampling.

13.3.2.1. Total Uranium Analysis

To determine uranium concentration and isotopics, the three 1ml subsamples taken for each time point were combined, and uraninite precipitate and cell material were separated from uranyl acetate remaining in solution by passage through 0.2 μm pore size polycarbonate filters (Whatman) using a new Swinnex syringe filter unit for each sample (Millipore). Carbon was subsequently burned off by muffling for 4 h at 550°C to control for potential interference of organic matter or filter material in the isotopic analysis. Muffling was done in acid washed beakers to prevent any contamination at this step from residual uranium present on the glassware. Finally, uranium was dissolved in all samples in 0.1 M ultrapure HNO_3 and the samples split for determination of uranium concentration and isotopics, any remaining undissolved material (carbon) was removed by again passing the sample through a 0.2 μm pore size polycarbonate filters (Whatman).

Uranium concentration was determined spectrophotometrically at 652 nm in a Beckman DU series spectrophotometer with 3mM Arsenazo III indicator dye (Alpha Aesar). A dilution series of uranium standards was used to correlate sample counts to concentration. To control for variation in measurements, all standards were run at the beginning and end of sample measurements. In addition, every 10 samples two standards were re-measured to check for consistency.

13.3.2.2. Isotopic Analysis:

Isotopic measurements were made with an Axiom, a magnetic sector instrument equipped with a multiple faraday detector array (Thermo Elemental, San Jose, CA, USA) operated under the conditions summarized in Table 13.1. The sample introduction system (CPI International, Santa Rosa, CA, USA) consisted of a PFA μflow nebulizer, a water-cooled PFA spray chamber (Scott type) and a sapphire injector tube. Samples were diluted, if necessary, with ultrapure 1% HNO_3 (acid: Seastar, Seattle, WA, USA; water: 18.2 MΩ) to the faraday detector's working range of about 10^6 to 10^8 cps. The axial channel and H3 detectors were used to measure the ^{235}U and ^{238}U signals, respectively. The detectors amplifier gains were calibrated and varied less than 10 ppm for 5 replicate scans. U isotopes were determined with the Axiom using the same standard-sample-standard and mass bias correction scheme as described earlier.

Table 13.1 MC-ICP-MS instrumental and operating parameters

Rf power	1250 W
Plasma gas flow rate	14.0 L/min
Auxiliary gas flow rate	1.00 L/min
Nebulizer gas flow rate	0.91 L/min
Points per peak	10
No. of scans per run	1
No. of runs	3
Resolution setting	Low (R~420)
Solution uptake	~200 μL/min

13.3.3. Other Uranium Analyses:

13.3.3.1. EXAFS

Uranyl interactions with the bacterial cell surface were analyzed using EXAFS techniques similar to those described in Curran et al.[2]

13.3.3.2. XRD

The bacteria and uraninite pellets from the 170-hour preliminary experiment sample were dried in an oven set at 80° C at atmospheric pressure. Several drops of collodion were mixed in with the solids and allowed to dry on a glass sample holder. The XRD spectrum was taken with a Rigaku RU300 with a 185 mm diffractometer. The scan settings were as follows : 2θ/θ reflexion, continous scan, 0.02° sampling interval with a starting angle of 10° and finishing angle of 100°, and a scan speed of 1° per minute.

13.4. Supplementary results

Table 13.2 Solution phase concentration of total uranium and the two isotopes, and the ratio of isotopes at the different time points for the second (main) experiment.

Time (hr)	235/238	[U] (μM)	[^{238}U]	[^{235}U]	f	δ^{235}U
0.0	0.981	1110.792	560.720	550.072	1.000	-18.991
0.5	0.980	1091.913	551.337	540.575	0.983	-19.520
1.0	0.976	966.073	488.928	477.145	0.870	-24.100
1.5	0.979	971.357	490.956	480.401	0.874	-21.500
2.0	0.974	786.367	398.382	387.984	0.708	-26.100
3.0	0.964	768.196	391.045	377.151	0.692	-35.532
4.0	0.965	724.213	368.500	355.713	0.652	-34.700
6.0	0.963	546.520	278.419	268.100	0.492	-37.063
12.0	0.966	108.711	55.310	53.401	0.098	-34.500
18.0	0.962	75.492	38.472	37.020	0.068	-37.745
24.0	0.961	313.560	159.908	153.652	0.282	-39.126
40.0	0.960	98.077	50.028	48.048	0.088	-39.576
52.0	0.961	131.657	67.130	64.527	0.119	-38.776
72.0	0.961	16.961	8.650	8.311	0.015	-39.121
120.0	0.962	36.515	18.616	17.899	0.033	-38.500

Table 13.3 Solid phase concentration of total uranium and the two isotopes, and the ratio of isotopes at the different time points for the second (main) experiment.

Time (hr)	235/238	[U] (μM)	[^{238}U]	[^{235}U]	f	δ^{235}U
0.0	---	1.428	---	---	0.001	---
0.5	1.012	93.642	46.539	47.102	0.084	12.095
1.0	1.016	120.748	59.901	60.847	0.109	15.803
1.5	0.999	181.177	90.649	90.528	0.163	-1.334
2.0	0.998	309.001	154.620	154.381	0.278	-1.545
3.0	1.019	268.636	133.045	135.591	0.242	19.131
4.0	1.011	152.660	75.908	76.752	0.137	11.124
6.0	0.999	389.576	194.902	194.674	0.351	-1.167
12.0	0.983	863.494	435.513	427.981	0.777	-17.294
18.0	0.982	895.453	451.704	443.750	0.806	-17.609
24.0	0.989	737.655	370.859	366.795	0.664	-10.958
40.0	0.983	752.925	379.685	373.240	0.678	-16.974
52.0	0.984	655.243	330.314	324.930	0.590	-16.300
72.0	0.981	755.889	381.507	374.382	0.680	-18.676
120.0	0.982	1159.027	584.871	574.156	1.043	-18.321

Table 13.4 Raw data for the main experiment of the solution phase of the formaldehyde inhibited control.

Time (hr)	235/238	[U] (μM)	[^{238}U]	[^{235}U]	f	δ^{235}U
2.0	0.981	1151.063	581.052	570.012	1.017	-19.000
6.0	0.981	1084.889	547.647	537.242	0.959	-19.000
24.0	0.981	1063.368	536.784	526.585	0.940	-19.000
52.0	0.981	1113.038	561.857	551.181	0.983	-19.000
120.0	0.981	1171.501	591.369	580.133	1.035	-19.000

Table 13.5 Raw data for the main experiment of the solution phase of the no cell control.

Time (hr)	235/238	[U] (μM)	[^{238}U]	[^{235}U]	f	δ^{235}U
0.0	0.981	1162.790	586.971	575.819	1.000	-19.000
2.0	0.981	1185.149	598.258	586.891	1.019	-19.000
6.0	0.981	1095.843	553.177	542.666	0.942	-19.000
12.0	0.981	1180.703	596.013	584.689	1.015	-19.000
24.0	0.981	1151.192	581.117	570.075	0.990	-19.000
120.0	0.981	1137.056	573.981	563.075	0.978	-19.000

Table 13.6 Raw data for the first (preliminary) experiment of the solution phase U(VI)[3].

Time (hr)	235/238	[U] (μM)	[^{238}U]	[^{235}U]	f	δ^{235}U
0.0	0.991	854.980	429.400	425.400	1.000	-9.333
4.0	0.973	534.080	270.700	263.300	0.625	-27.137
8.0	0.928	23.460	12.160	11.290	0.027	-71.936
11.0	0.913	42.050	21.970	20.070	0.049	-86.680
24.0	0.958	110.910	56.630	54.270	0.130	-41.611
48.5	0.953	22.350	11.440	10.900	0.026	-46.545
72.0	0.935	21.570	11.149	10.420	0.025	-65.440
120.0	0.942	285.410	146.900	138.400	0.334	-58.114
170.0	0.994	573.610	287.600	285.900	0.671	-5.851

Table 13.7 Raw data for the initial experiment of the solution phase of the heat killed controls[3].

Time (hr)	235/238	[U] (μM)	[^{238}U]	[^{235}U]	f	δ^{235}U
0.0	0.995	1030.190	516.386	513.804	1.000	-5.000
4.0	0.995	1148.880	575.880	573.000	1.115	-5.000
8.0	0.992	1126.960	565.743	561.217	1.094	-8.000
11.0	0.994	1080.890	542.071	538.819	1.049	-6.000
24.0	0.994	1181.320	592.437	588.883	1.147	-6.000
48.5	0.995	1020.870	511.714	509.156	0.991	-5.000
72.0	0.996	1049.290	525.696	523.594	1.019	-4.000
120.0	0.996	1064.770	533.452	531.318	1.034	-4.000
170.0	0.994	1144.700	574.072	570.628	1.111	-6.000

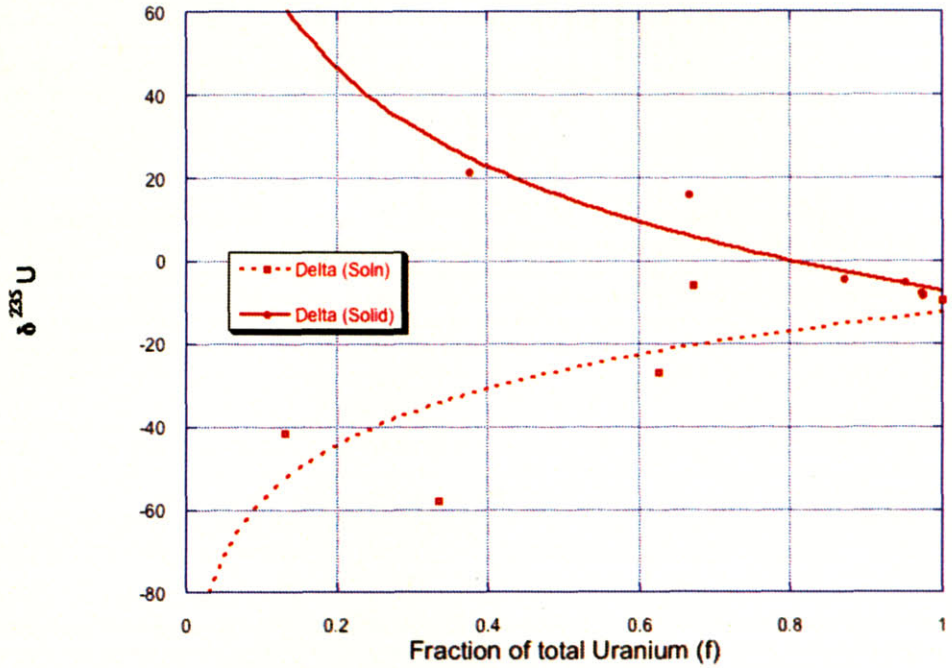

Figure 13.1 $\delta^{235}U$ vs. f for the preliminary experiment fit with the same Rayleigh fractionation model as in the primary data[3]. The solution phaseis indicated by the dashed line. From this model the calculated values of α are remarkably similar to the main experiment: $\alpha_{soln}=1.02$ ($R^2=0.513$).

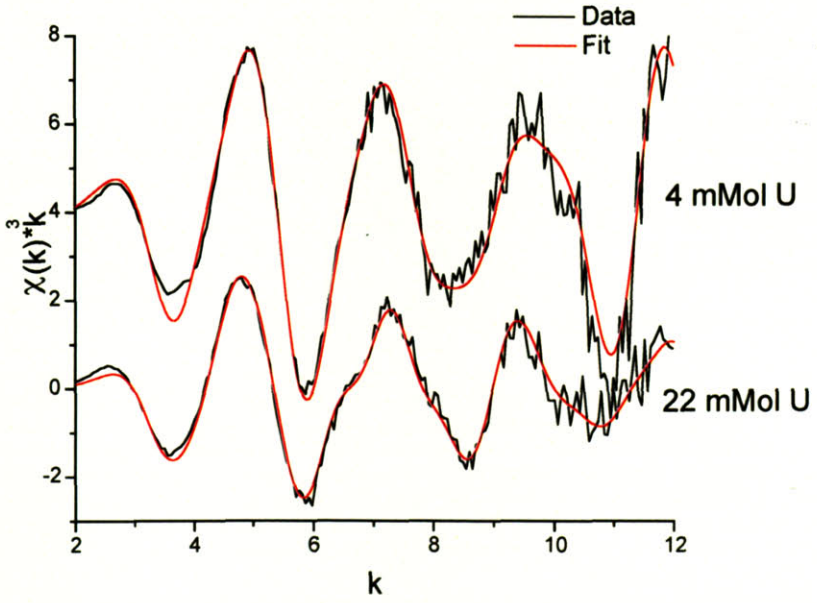

Figure 13.2[4] Uranium L_3 edge EXAFS spectra of bacteria samples and corresponding fits. The 4 mM sample is a good example of uranyl phosphate, the 22 mM sample is a

mixture of uranyl phosphate and uranium in an organic carbon structure, most likely uranyl acetate which was the form of U(VI) used for this experiment.

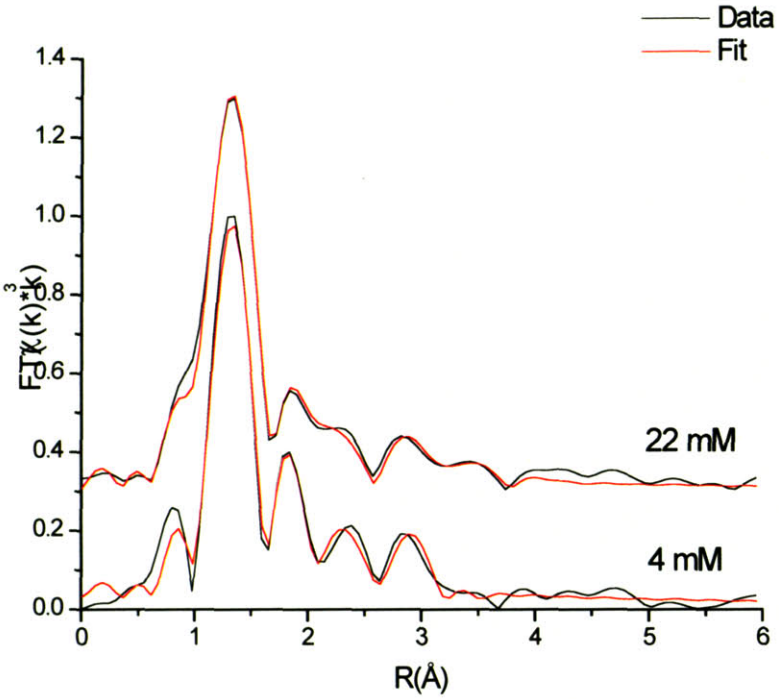

Figure 13.3[4] Fourier transforms of bacteria EXAFS, further emphasizing differences in the uranium environment.

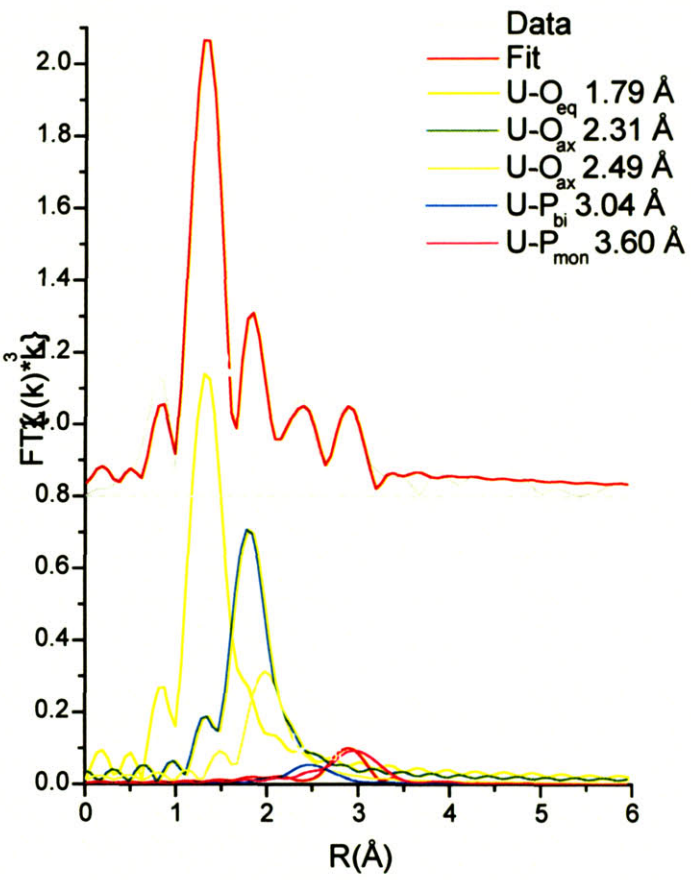

Figure 13.4[4]. Deconvolution of 4 mM fit, showing the contribution of each shell to the total Fourier transform. The method of interaction between the uranium and bacterium is through attachment to a phosphate group. However, it is possible that because the samples were kept at room temperature for over a week before scanning, this could be the inorganic phosphate released following cell lysis. All of the uranium was present as U(VI) and was not reduced as a result of sorption.

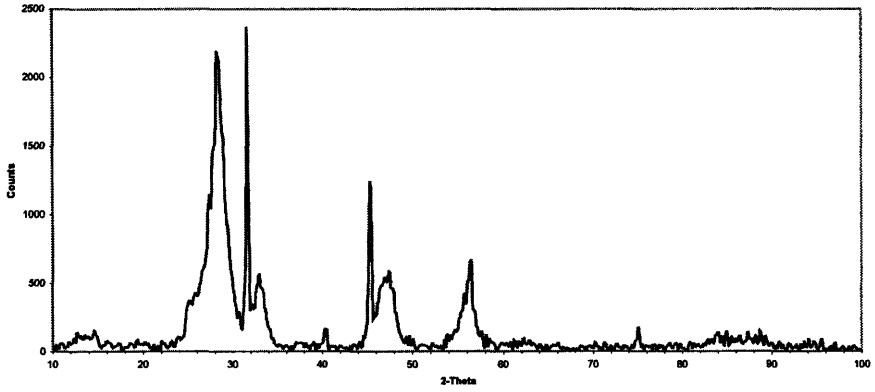

Figure 13.5[3]. XRD spectra of precipitate produced with decreased bacteria concentration and incubated for two months. This spectra matches well with that of UO_2.

13.5. Acknowledgements

The Author would like to thank Cristophe Moulin of DEN/DPC/SECR Laboratoire de Spéciation des Radionucléides et des Molécules CEA-Saclay France, Virginia Curran and Randi Cohen both of the Department of Nuclear Engineering, Massachusetts Institute of Technology, Vanja Klepac-Ceraj and Chanathip Pharino both of the Department of Civil and Environmental Engineering, Massachusetts Institute of Technology, and Jim Cizdziel at the University of Nevada Las Vegas, for their contributions to the data and methodology presented in the supplementary material.

13.6. References

[1] **Kuai, L., A. A. Nair, M. F. Polz.** (2001) Rapid and Simple Method for the Most-Probable-Number Estimation of Arsenic-Reducing Bacteria. Appl. Environ. Microbiol. **67**:3168-3173.

[2] **Curran, G., Y. Sevestre, W. Rattray. P. Allen, K. R. Czerwinski.** (2003) Characterization of Zirconia-Thoria-Urania Ceramics by X-ray and Electron Interactions. *J. Nuc. Mat.* **323**:41-48.

[3] **Cohen, R.** (2001) Bacterial Reduction of Uranium and Plutonium. S.M. Thesis. Massachusetts Institute of Technology.

[4] **Curran, V.** (2003) X-Ray Absorption Spectroscopy of Actinide Speciation in Solid Solutions. PhD Thesis. Massachusetts Institute of Technology.

14. Chapter 10 Appendix

14.1. Bacterial strain and culture conditions

Leptothrix discophora (ATCC 43182) was maintained at 26° C in the rich medium 2X PYG medium[1] at pH 7.3. This media, however, contains yeast extract and peptone, which interfere with the quantification of manganese oxidizing protein produced by the bacteria. HEPES at concentrations greater than 1 mM will also interfere with the Lowry-protein assay[2] (§ 7.3.2.2). Thus, for some experiments *L. discophora* is also grown in minimal MSVP media[3] at 26° C and pH 7.3. Alternately, $NaHCO_3$ can be used as a substitute buffer, but prevents the precipitation of BMO, bacteria can also be grown in MSVP media without buffer. It was experimentally determined that the minimum OD_{600} for manganese oxidation in cell-free spent media was 0.4, bacterial density less than this value resulted in no measurable oxidation of manganese. Boogerd suggests that in batch culture, *L. discophora* will only produce MOF after the cells have reached stationary phase.[4]

14.2. Protein isolation and concentration determination

Determination of the concentration of oxidizing protein(s) produced by *L. discophora* will give a relationship between cellular density and the total oxidizing potential of the protein(s) present.

Because the concentration of oxidizing protein produced by *L. discophora* is typically very low, the protein must first be concentrated from a solution of spent media, before it can be assayed.

Bacteria are removed from MSVP media by vacuum filtration through a 0.2 μM filter (VWR # 87006-064). Spent media is added to a volume of 3 mL to a 30 KD molecular weight cut off Microsep centrifugal device (Pall # OD030C41) and centrifuged at 4186xg for 50 minutes. The liquid remaining unfiltered contains the concentrated manganese oxidizing protein(s), Mn^{2+} added to filtrate did not oxidize Mn, addition of Mn^{2+} to the unfiltered portion, results in the formation of BMO. Although it may contain other proteins, the >30 KD size fraction is a quick and easy way to obtain a maximum estimate of the amount of oxidizing potential in a sample of spent media.

The >30 KD size fraction is collected and diluted in DIH_2O to a final volume of 200 μL. Standards of 0, 0.01, 0.05, 0.1, 0.25, 0.5, 0.75, and 1.5 mg/mL are prepared from a stock solution of 2 mg/mL Bovine Serum Albumin (Pierce biosciences Product #23210). Samples and standards measured for protein concentration according to the protocol for the Lowry Protein Assay Kit (Pierce Biosciences Product #23240).

14.3. Test for oxidative dissolution of UO_2 by Spent media and BMO

14.3.1. UO_2 oxidation by spent media

14.3.1.1. Methods

L. discophora is grown 48 hours in 1 or 2X PYG media, with or without manganese. Approximately 0.1 g UO_2 is added to 15 mL of the following samples: filtered 2XPYG spent media + Mn, filtered 1XPYG spent media - Mn, and unfiltered 2XPYG media - Mn. Samples are shaken at 170 rmp for the duration of the experiment. At several time intervals 1 mL is removed from each sample and centrifuged for 1 minute at 5000 rpm, 900 μL supernatant is removed and added to 9 mL 0.1 M HNO_3 for measurement of uranium concentration with ICP-AES.

14.3.1.2. Results

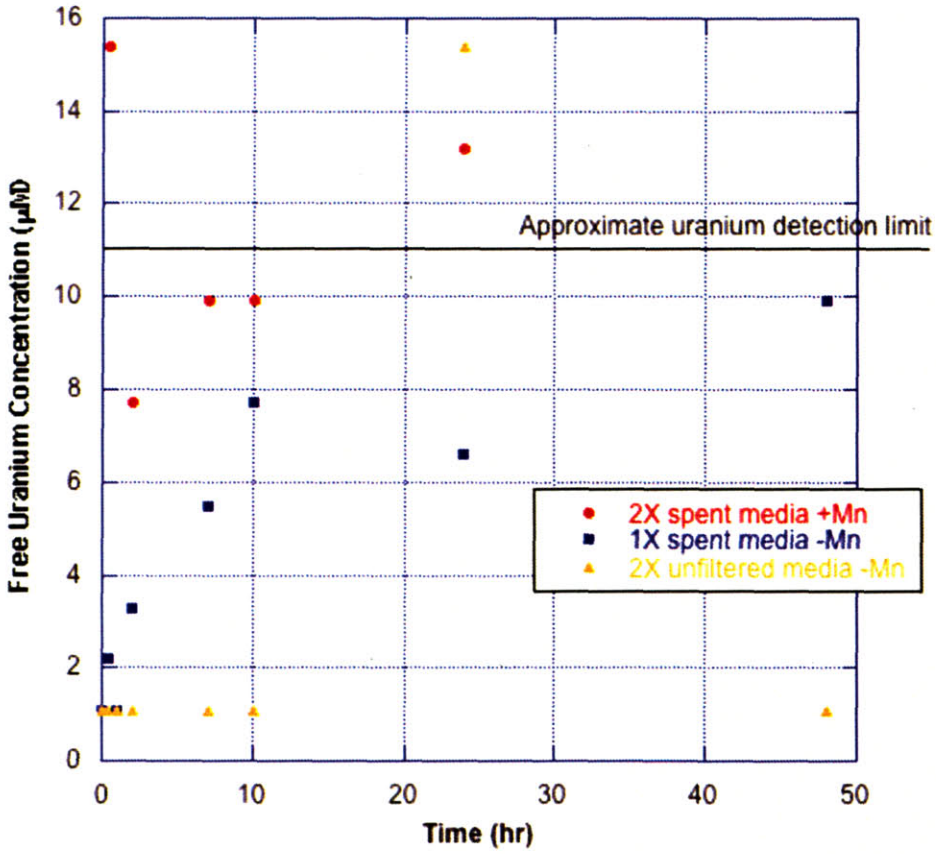

Figure 14.1 Free uranium concentration over time contacted with *L. discophora* media. Nearly all measured values were below the uranium detection limit, thus it was determined that within 48 hours contact of UO_2 with MOF did not result in any significant uranium dissolution.

14.3.2. UO_2 oxidation by BMO

14.3.2.1. Methods

L. discophora is grown 48 hours in 1 L 2XPYG media to an OD_{600} of 0.539 and filtered through a 0.2 μM pore size filter. Approximately 387 μL of 1M $MnCl_2$ is added to 387 mL spent media, and manganese oxides are allowed to precipitate overnight, then rinsed 2X in DIH_2O. Oxides are concentrated by centrifugation and 5.85 g of concentrated MnOx slurry is added to 44.15 mL of 30 mM $NaHCO_3$ and 0.0507 g UO_2 and comprise sample A. In the second sample (B), manganese oxides are

precipitated in the presence of UO_2, a final concentration of 1 mM Mn^{2+} is added to 48 mL spent media and 0.0502 g UO_2. The control (C) consisted of 50 mL 30 mM $NaHCO_3$ and 0.0517 g UO_2. At several time points 2 mL of each sample was removed and filtered through a a 0.2 μM pore size filter into 4 mL 0.1 M HNO_3. Samples were then measured using ICP-AES for free Mn^{2+} and UO_2^{2+}.

14.3.2.2. Results

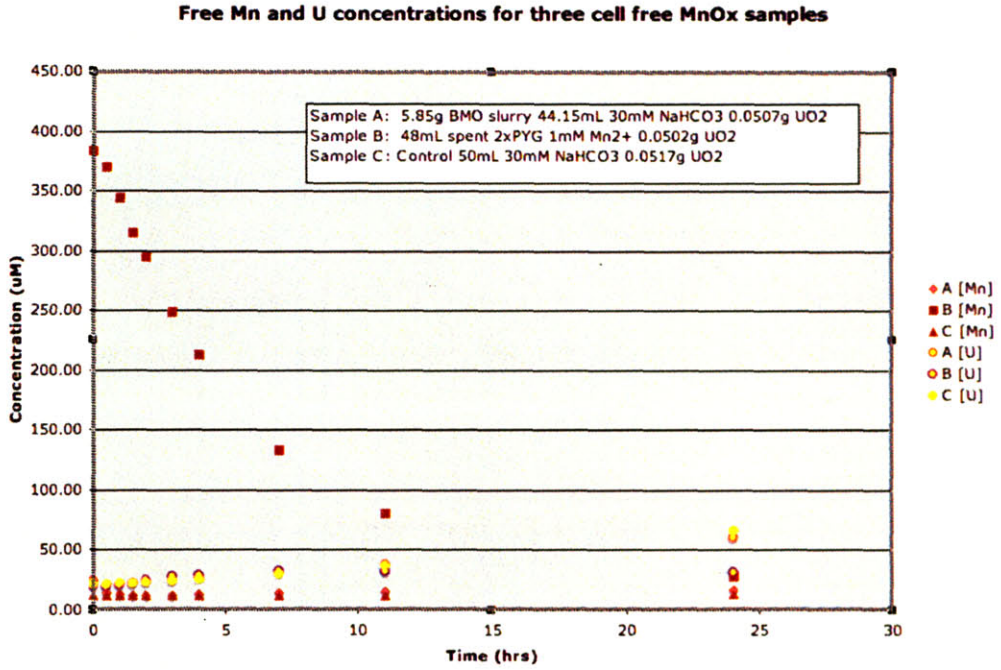

Figure 14.2 Free Mn and U concentrations contacted with BMO. Although concentrations of free uranyl increased slightly with time there was no significant difference in uranyl concentration between the sample and control.

14.4. Preparation of samples for EXAFS analysis

Three samples were prepared for two different EXAFS analyses.

14.4.1. BMO and UO_2

The first sample was prepared by addition of 1 mM (final concentration) Mn^{2+} to cell-free spent 2X PYG media. A 3 mL subsample of spent media was set aside for determination of protein concentration. The protein concentration was found to be 0.012 mg/mL > 30K size fraction. Manganese oxides were allowed to precipitate overnight and then 0.0166 g < 100 mesh UO_2 was

added. The manganese oxides and UO_2 were shaken gently together for approximately 13 hours. In order to remove salt and any residual Mn^{2+} from the sample, the oxides are collected by centrifugation (10 minutes at 4000 rpm) and added to dialysis tubing with a 7K MWCO (Pierce Biosciences Product #68700) which is placed in 4 L DIH_2O for 3 days. The oxides are then dried at 40° C. The uranium concentration is estimated to be ~76%.

14.4.2. BMO and UO_2^{2+}

This sample was prepared by addition of 1 mM Mn^{2+} and 20 μM Uranyl acetate to cell-free spent 2X PYG media. A 3 mL subsample of spent media was set aside for determination of protein concentration. The protein concentration was found to be 0.012 mg/mL > 30K size fraction. The manganese oxides were precipitated overnight in the presence of uranyl. In order to remove salt and any residual Mn^{2+} from the sample, the oxides are collected by centrifugation (10 minutes at 4000 rpm) and added to dialysis tubing with a 7K MWCO (Pierce Biosciences Product #68700) which is placed in 4 L DIH_2O for 3 days to unbound U and Mn. The oxides are then dried at 40° C. The uranium concentration is estimated to be ~25%.

14.4.3. BMO and UO_2, second sample.

This sample was prepared by addition of 1 mM (final concentration) Mn^{2+} to cell-free spent 2X PYG media. Manganese oxides were allowed to precipitate overnight and then 0.0502 g < 100 mesh UO_2 was added. The manganese oxides and UO_2 were shaken gently together overnight. In order to remove salt and any residual Mn^{2+} from the sample, the oxides are collected by centrifugation (5 minutes at 10,000 rpm). The oxides are washed three times with DIH_2O and separated as much as possible from the denser UO_2 phases which collect at the bottom and sides of the centrifuge tubes. The oxides are then dried at 40° C. The uranium concentration is estimated to be <1%.

14.4.4. Preparation and EXAFS analysis

Samples were prepared by dilution of compound in BN (0.5% - 1% mass). Uranium L_{III} edge(17.166 keV) X-Ray absorption spectra were collected at the Advanced Photon Source (APS) using a Si (1,1,1) double crystal monochromator. Spectra were recorded in transmission geometry using Ar filled ionization chamber and in

fluorescence using a 13 element detector. Energy calibration was done using an Yttrium foils (K edge = 17.038 keV).

For each sample, several EXAFS spectra were recorded [0 - 13] $Å^{-1}$ and averaged. The background contribution was removed using Autobk software and data analysis was performed using WINXAS. For the fitting procedure, amplitude and phase shift function were calculated by FEFF8.2. The feff.inp files were generated by ATOMS using crystallographic structures taken from literature.

The adjustments of EXAFS spectra were performed under the constraints $S_0^2 = 0.9$, a single value of energy shift ΔE_0 was used for all scattering. The uncertainty on the coordination number (C.N) is 20%, the uncertainty on the distance (R) is 0.02 Å.

14.4.5. Results

14.4.5.1. BMO and UO_2

The EXAFS averaged spectra was k^2 -weighted, the Fourier transform performed between 2.5^{-1} and 11.4 $Å^{-1}$. The fitting was done in 2 steps:

- Considering presence of only UO_2.
- Considering presence of UO_2 and U(VI) that can result from oxidation of UO_2.

Considering only U(IV), the phase and amplitude function were calculated using the UO_2 referenced. The following conditions were used for the fitting: the coordination numbers were correlated to those in UO_2, and distance and σ^2 were not correlated.

The results are presented in Table 14.1, fourier transform in Figure 14.3 and k^2 - EXAFS spectra in Figure 14.4.

Table 14.1 Structural parameters of the BMO and UO_2 sample considering only the presence of U(IV).

BMO and UO_2	Structural parameter			
Scattering	C.N	R Å	σ^2	Eo eV
U-O 1 shell	8	2.35	0.0083	3
U-U	12	3.87	0.0041	3
U-O 2d shell	24	4.46	0.0059	3
Residual		11 %		

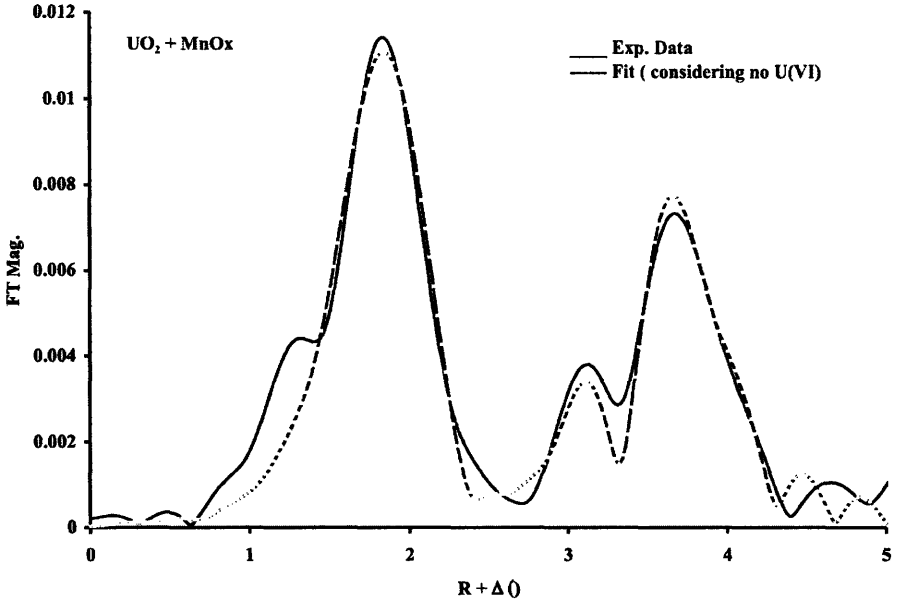

Figure 14.3 Fourier transform of the k^2 - EXAFS spectra. Fit not considering the presence of U(VI).

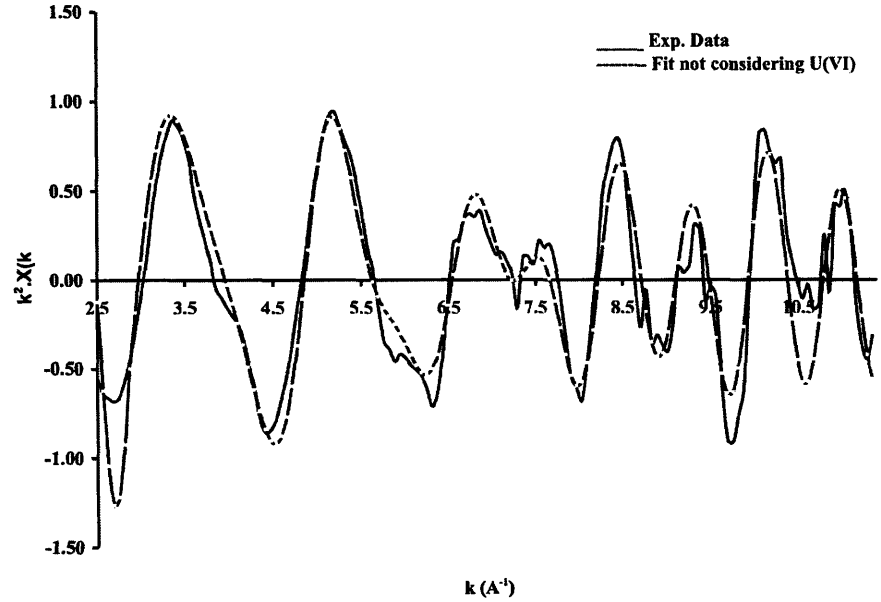

Figure 14.4 k^2 – EXAFS spectra. Fit not considering the presence of U(VI).

Considering presence of UO_2 and U(VI), EXAFS averaged spectra was k^2 -weighted and the Fourier transform performed between 2.4 $Å^{-1}$ and 11.4 $Å^{-1}$.

The phase and amplitude function were calculated using of the UO_2 and uranium hydroxide referenced. The following conditions were used for the fitting: the single scattering U=O calculated in uranium hydroxide was used, σ^2 was fixed to 0.001, and the single scattering calculated for UO_2 were used with the same conditions as previously.

The results are presented in Table 14.2, Fourier transform in Figure 14.5 and k^2 - EXAFS spectra in Figure 14.6.

Table 14.2 Structural parameters of the BMO and UO_2 sample considering the presence of both U(IV) and U(VI).

BMO and UO_2	Structural parameter			
Scattering	C.N	R Å	σ^2	Eo eV
U=O	0.28	1.73	0.001	
U-O 1 st shell	8	2.35	0.0083	7.21
U-U	12	3.87	0.0041	7.21
U-O ^{2d} shell	24	4.46	0.0059	7.21
Residual		12 %		

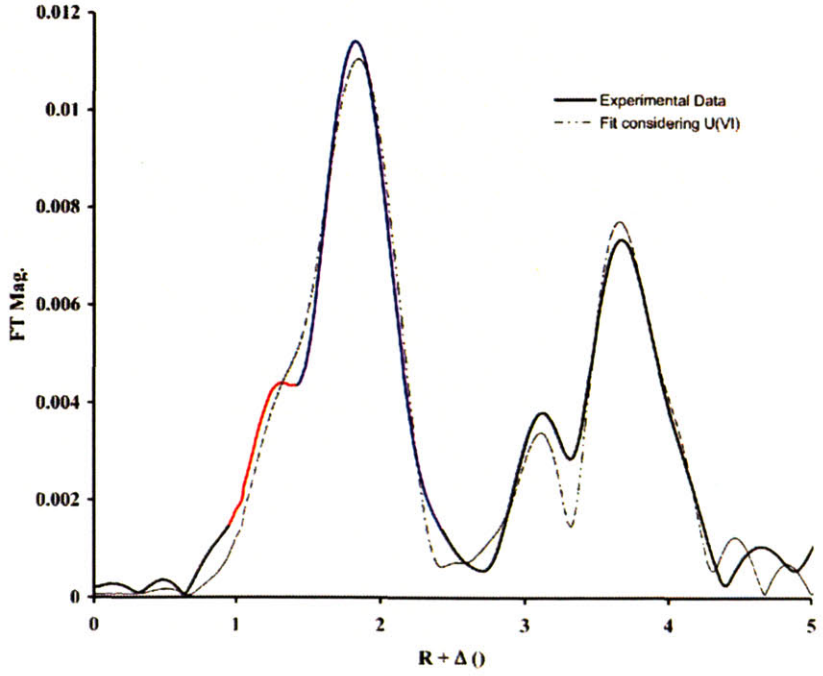

Figure 14.5 Fourier transform of the k^2 - EXAFS spectra. Fit considering the presence of U(VI).

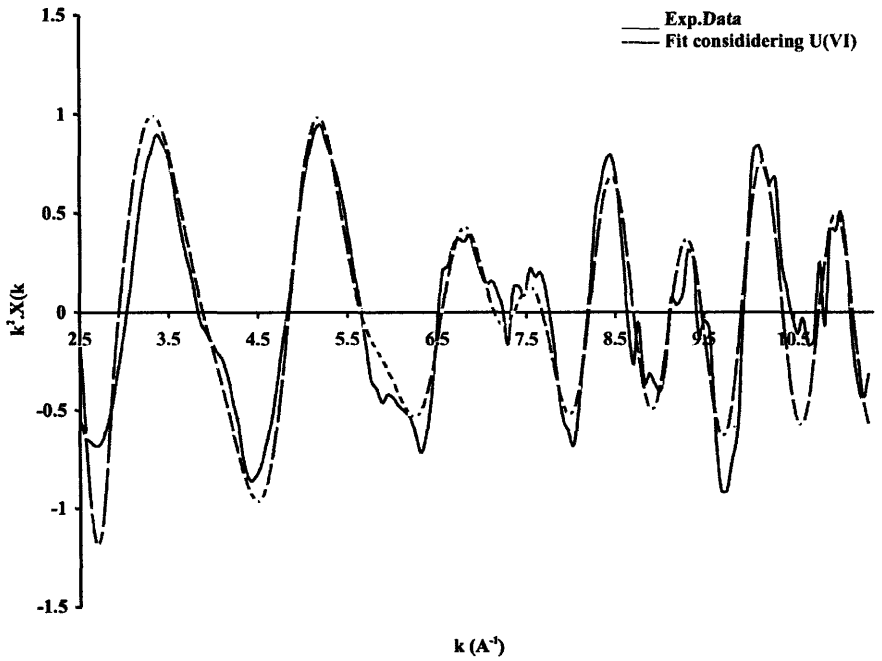

Figure 14.6 k^2 – EXAFS spectra. Fit considering the presence of U(VI).

Preliminary EXAFS Analysis on compound UO_2 + MnO_x reveals that UO_2 is the preponderant compound. EXAFS adjustment done with absence and presence of U(VI) does not present a significant difference on the residual (1%). Nevertheless, if U(VI) is present in the sample it represent not more than 13 % of the total uranium.

14.4.5.2. BMO and UO_2^{2+}

The EXAFS averaged spectra was k^2 -weighted, the Fourier transform performed between 2 $Å^{-1}$and 11$Å^{-1}$. The spectra was first fitted using the single scattering U=O and U-Oeq calculated in the uranium hydroxide compound. The C.N of U=O was fixed to 2. Results are presented in Table 14.1, Figure 14.7, and Figure 14.8.

Table 14.3 Structural parameters of the BMO and 20 μM UO_2^{2+} sample.

BMO and UO_2^{2+}	Structural parameter			
Scattering	C.N	R Å	σ^2	Eo eV
U=O	2	1.796	0.0013	5.38
U-O eq	4.27	2.375	0.0077	5.38
Residual		7 %		

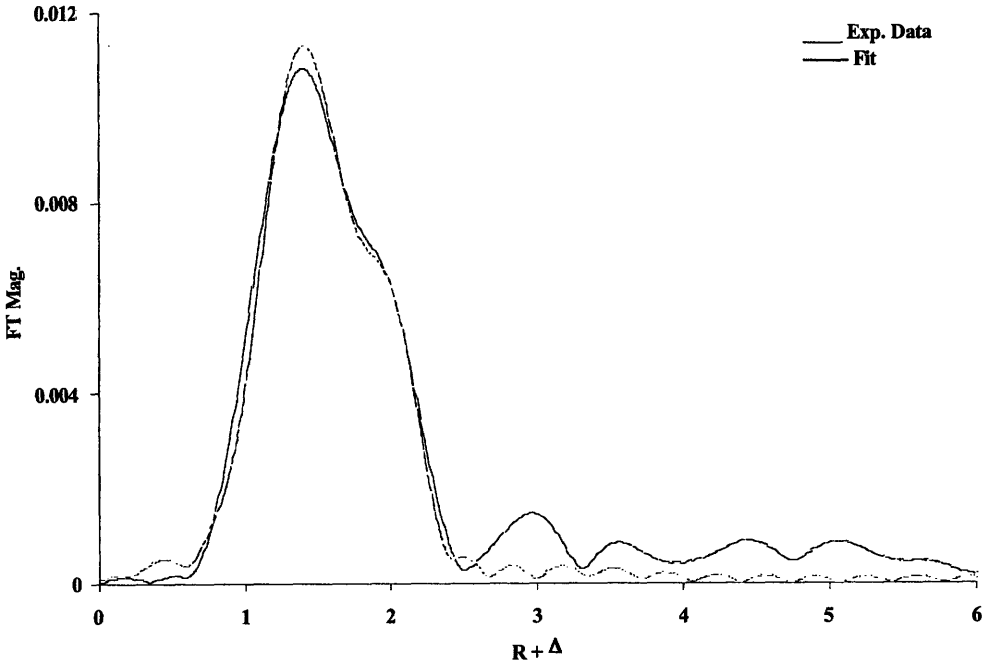

Figure 14.7 Fourier transform of the k^2 - EXAFS spectra.

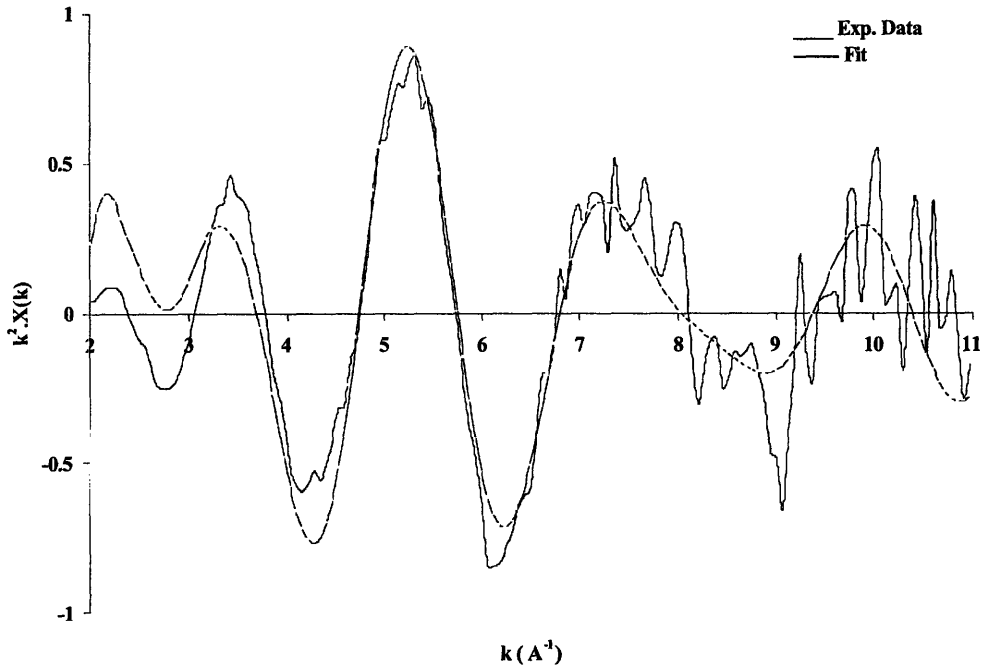

Figure 14.8 k^2 – EXAFS spectra.

The EXAFS spectra is strongly dominated by the U=O and U-Oeq contribution. The first shell around U is composed by O atoms: no metallic bonding U-Mn can be observed.

The presence of Mn in the FT may be the peak around 3 Å, but its scattering intensity is low. Then, Uranium may be present in form of complex bonded to the surface of MnO_2. From the concentration of U used and analogy with literature[5], MnO_2 can present the pseudo- tunnel structure. In the pseudo tunnel structure it was shown that U is present in as a tridentate complex.

14.4.6. BMO and UO_2, Second Sample Results.

Table 14.4 Structural parameters of the BMO precipitated in the presence of UO_2 with as much removal of UO_2 as possible. Considering the presence of both U(IV) and U(VI).

BMO and UO_2 II	Structural parameter			
Scattering	C.N	R Å	s^2	Eo eV
U-Mn	1.289	3.131	0.003	3.973
U(IV)-O	4.905	2.287	0.012	3.973
U(IV)-U(IV)	5.801	3.832	0.007	3.973
U(VI)=O	0.921	1.883	0.001	3.973
U(VI)-O	2	2.399	0.004	3.973

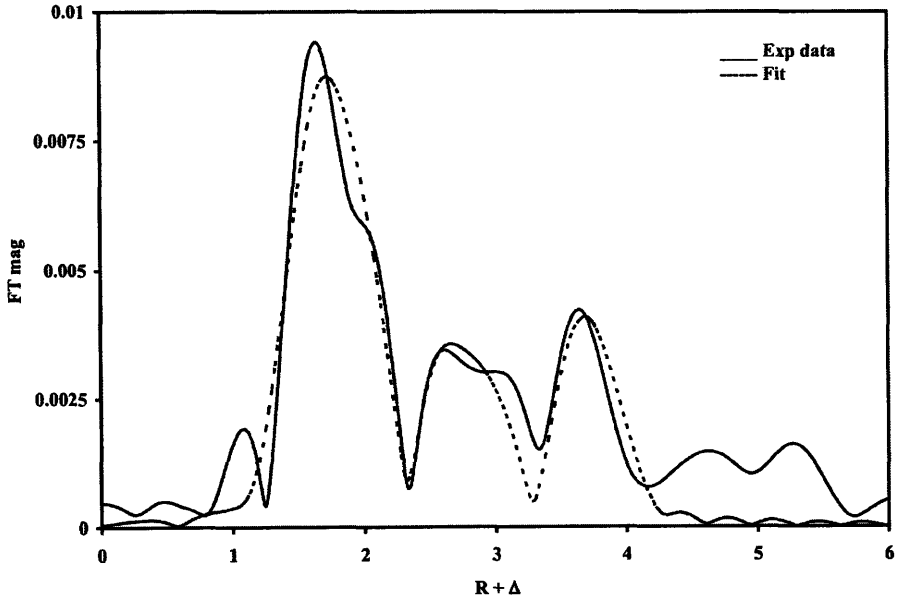

Figure 14.9 Fourier transform of the k^2 - EXAFS spectra of a sample of BMO contacted with UO_2. In this case as much UO_2 was separated from the BMO as possible, revealing a stronger U(VI) signal. Fit considering the presence of U(VI).

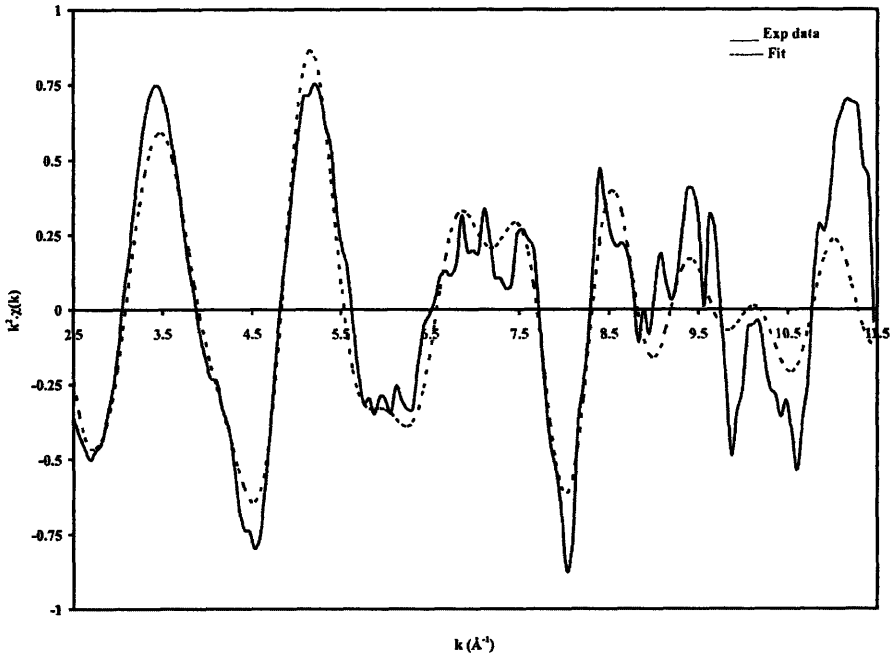

Figure 14.10 k^2 – EXAFS spectra.

14.5. Kinetics of BMO formation

The kinetics of bacterial manganese oxide formation in the presence of uranium are studied. *Leptothrix discophora* is grown to an $OD_{600} > 0.4$ in MSVP media at room temperature (or 26° C), spent media is then filtered and assayed for protein concentration.

14.5.1. Experiment I

In the initial experiment, varying concentrations of Mn^{2+} and U(VI) are added to 1mL volumes of spent MSVP medium after growing with *L. discophora* for 96 hrs. The OD_{600} was 0.644 with a >30K protein concentration of 3 μg/mL. Kinetics of BMO formation are measured spectophotometrically with UV/VIS at 400 nm. Standards are prepared by adding known quantities of Mn^{2+} to spent media and relating the maximum absorbance to BMO concentration. Figure 14.11 is an example of kinetics scan, each line represents the absorption at three minute intervals, and shows the formation of the BMO over time from 380-750 nm, the right graph shows the absorbance at 400 nm over time.

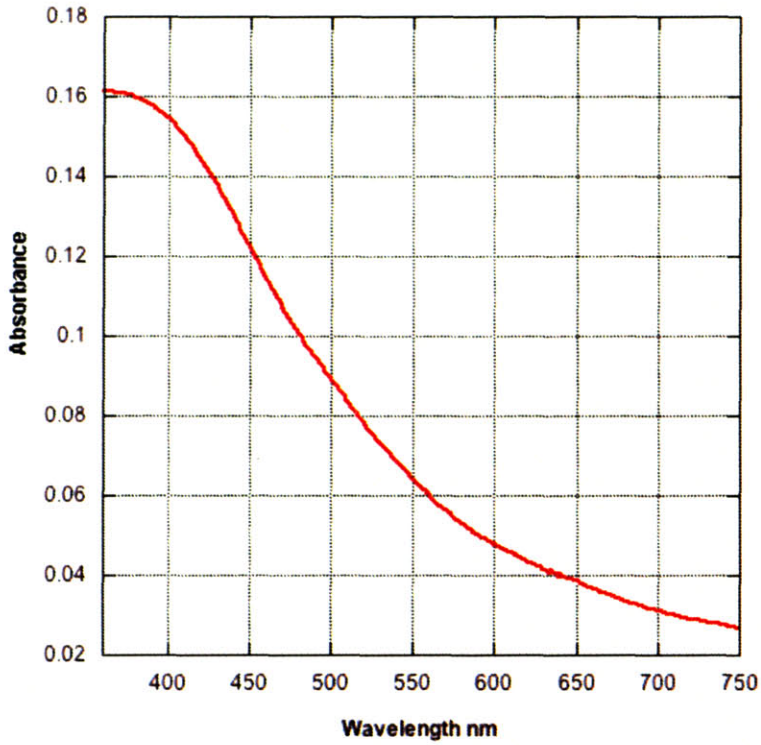

Figure 14.11 An absorbance scan of BMO precipitate. For kinetics scans, absorbance was measured at λ=400 nm.

Samples were analyzed over a period of several days, and as the sample aged, the protein activity diminished. This was demonstrated by a decrease in the oxidation kinetics for older samples containing the same concentration of Mn^{2+}. Thus, samples were normalized each day to a control containing Mn and no uranium.

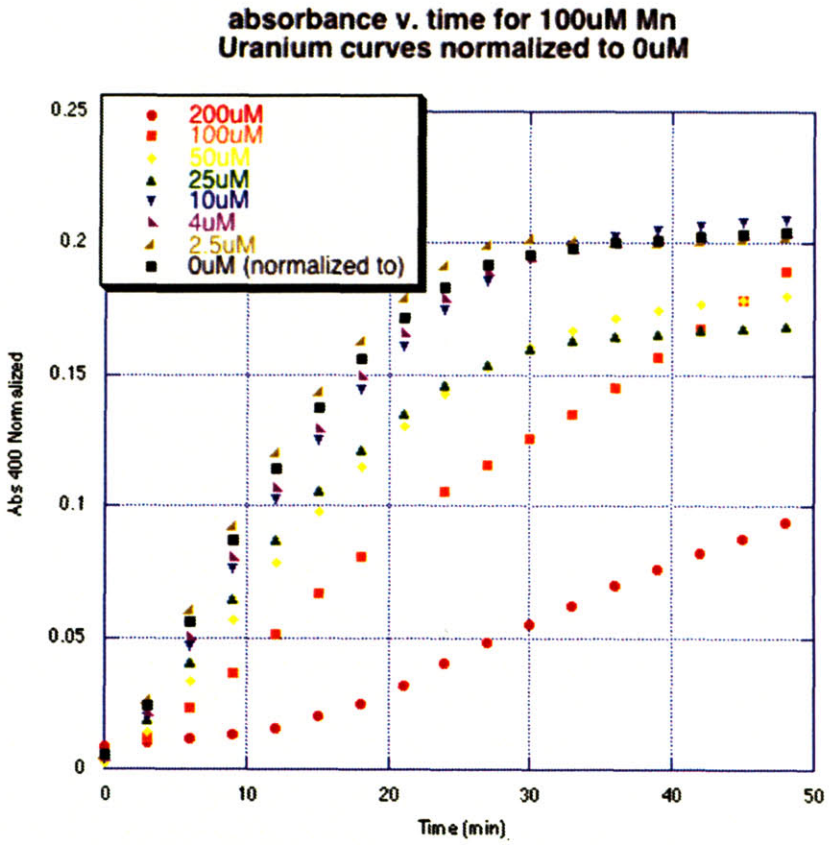

Figure 14.12 Kinetics of manganese oxide formation in spent MSVP media (*L. discophora* grown 96 hours) with 100 μM Mn2+ and varying concentrations of U(VI) (inset). Normalized to 100 μM Mn2+ samples without U(VI). The general trend here is that increasing the amount of U(VI) present slows down the formation of the MnOx as well as decreases the total amount of oxide formed. One interesting exception to this trend is with 2.5 μM U(VI), here the formation of the oxide was slightly faster.

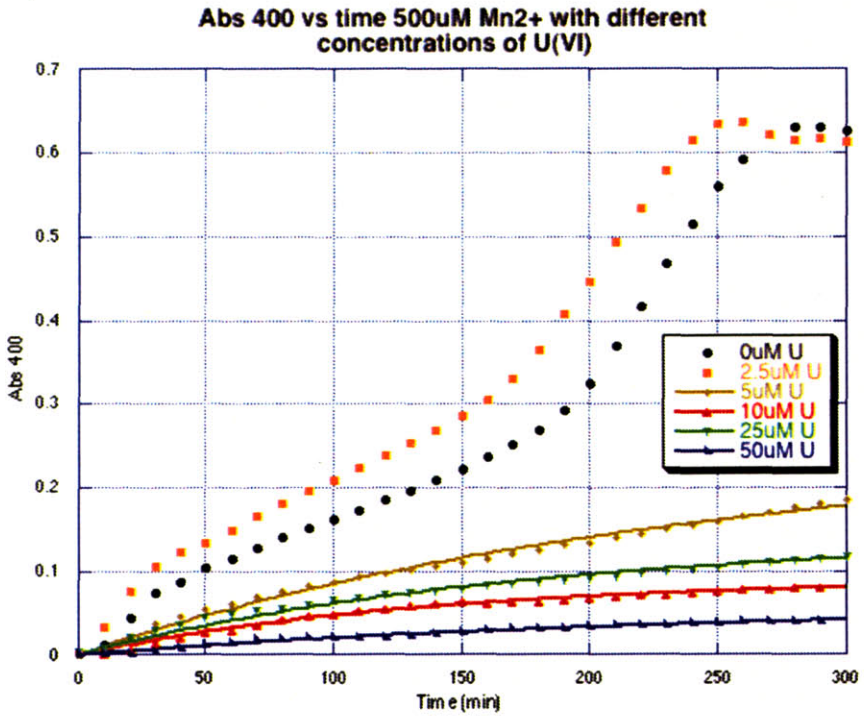

Figure 14.13 Kinetics of manganese oxide formation in spent MSVP media (*L. discophora* grown 96 hours) with 500 μM Mn^{2+} and varying concentrations of U(VI) (inset). Because of too few 500 μM scans without U(VI) these results are unnormalized. The trends here are the same as with the 100 μM Mn samples, however one interesting thing to note is that it actually takes much *less* U(VI) to inhibit the oxide formation, and in fact almost no oxide was formed when 100 μM U(VI) was added. The "synergistic" effect upon addition of small amounts of U(VI) is more apparent in this case.

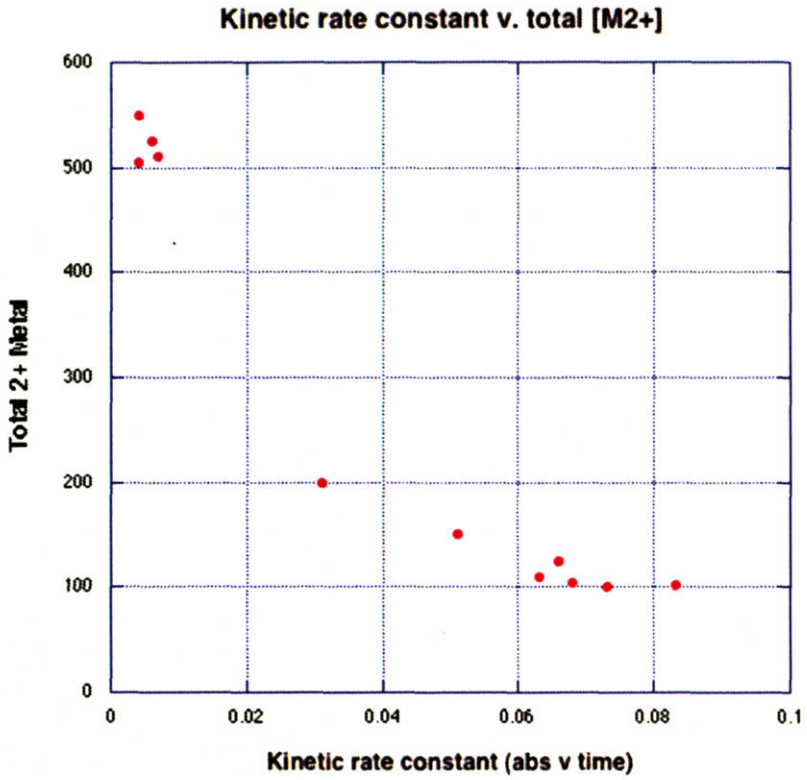

Figure 14.14 The kinetic rate constant (obtained from the fits) of the MnOx formation vs total metal ([Mn]+[U]).

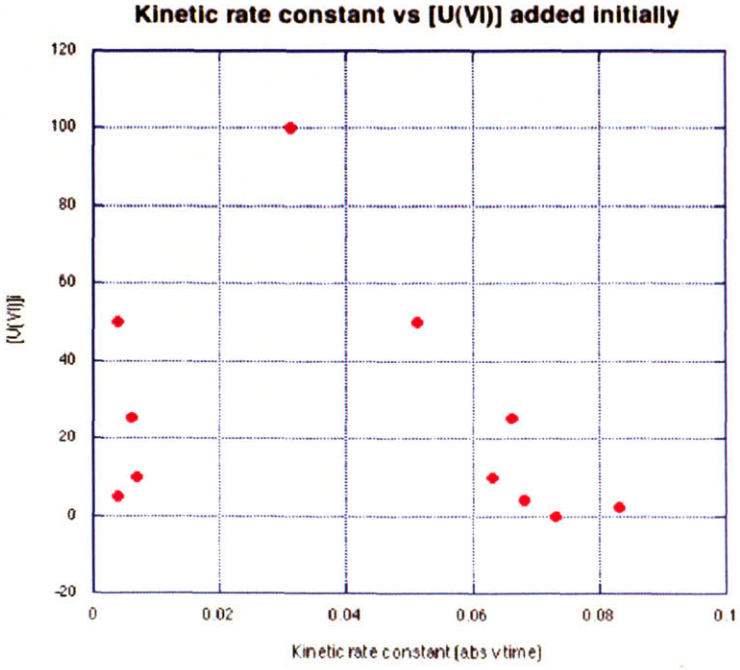

Figure 14.15 The kinetic rate constant (obtained from the fits) of the MnOx formation vs initial amount of U(VI) added. As you can see this data correlates less well with the rate constant than the total metal in Figure 14.14.

14.5.2. Experiment II

The sample was prepared according to § 14.4.1, and the control (no UO_2) was prepared from the same batch of spent media with the same amount of added Mn^{2+} (500 μM). At set time intervals 1 mL of sample and control were removed from the batch experiments and filtered through a 13 mM 0.45 μm pore size syringe filter into 5 mL 0.1 M HNO_3. Samples were analyzed using ICP-AES for free Mn^{2+} and UO_2^{2+}. No significant production of UO_2^{2+} was observed.

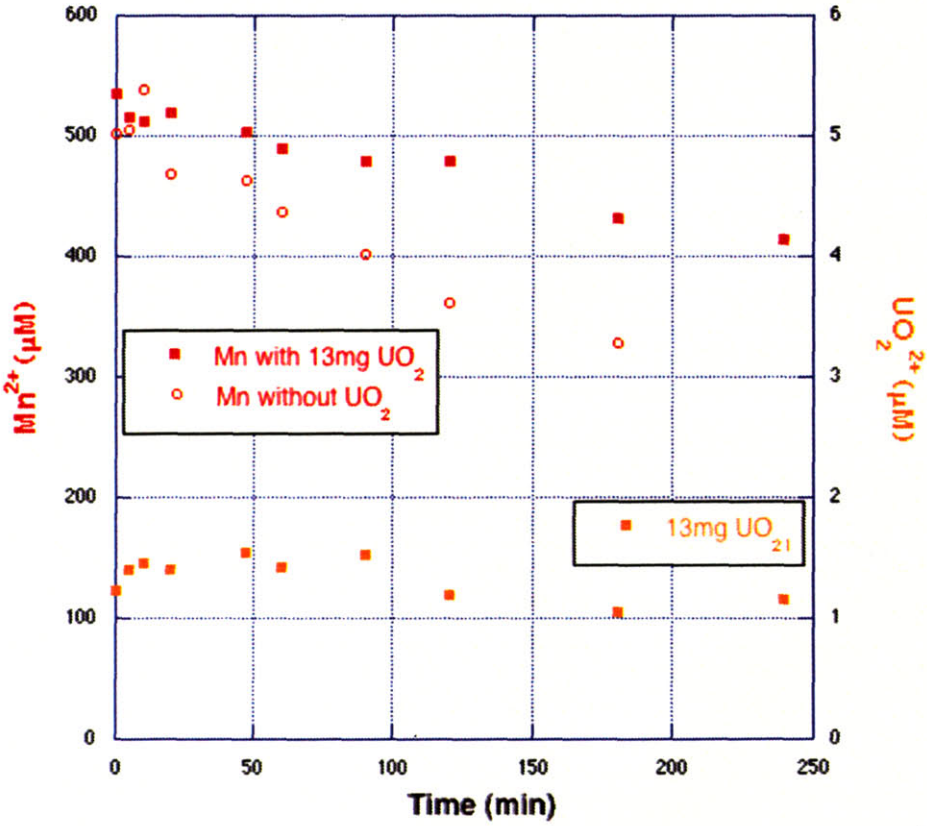

Figure 14.16 Inhibition of BMO formation in the presence of UO_2. Mn^{2+} removal from solution is slower in the presence of UO_2 (closed square) than in the absence of uranium (open circle).

14.5.3. Experiment III

In order to further examine the effects of uranium concentration on the kinetics of BMO formation, several more experiments were done. This time 200 μL of sample was used and samples were measured concurrently using a 96 well plate-reading UV/VIS, so no normalization is necessary.

L. discophora is grown in MSVP media 72 hours to an OD_{600}=0.402, with a >30K protein concentration of 1.3 μg/mL. After filling a 96 well plate according to Table 14.5 200 μL of spent media are added to each well, kinetics of BMO formation are measured at 400 nm in 30 second intervals for the first 30 minutes and then 3 minute intervals after that for 6 hours.

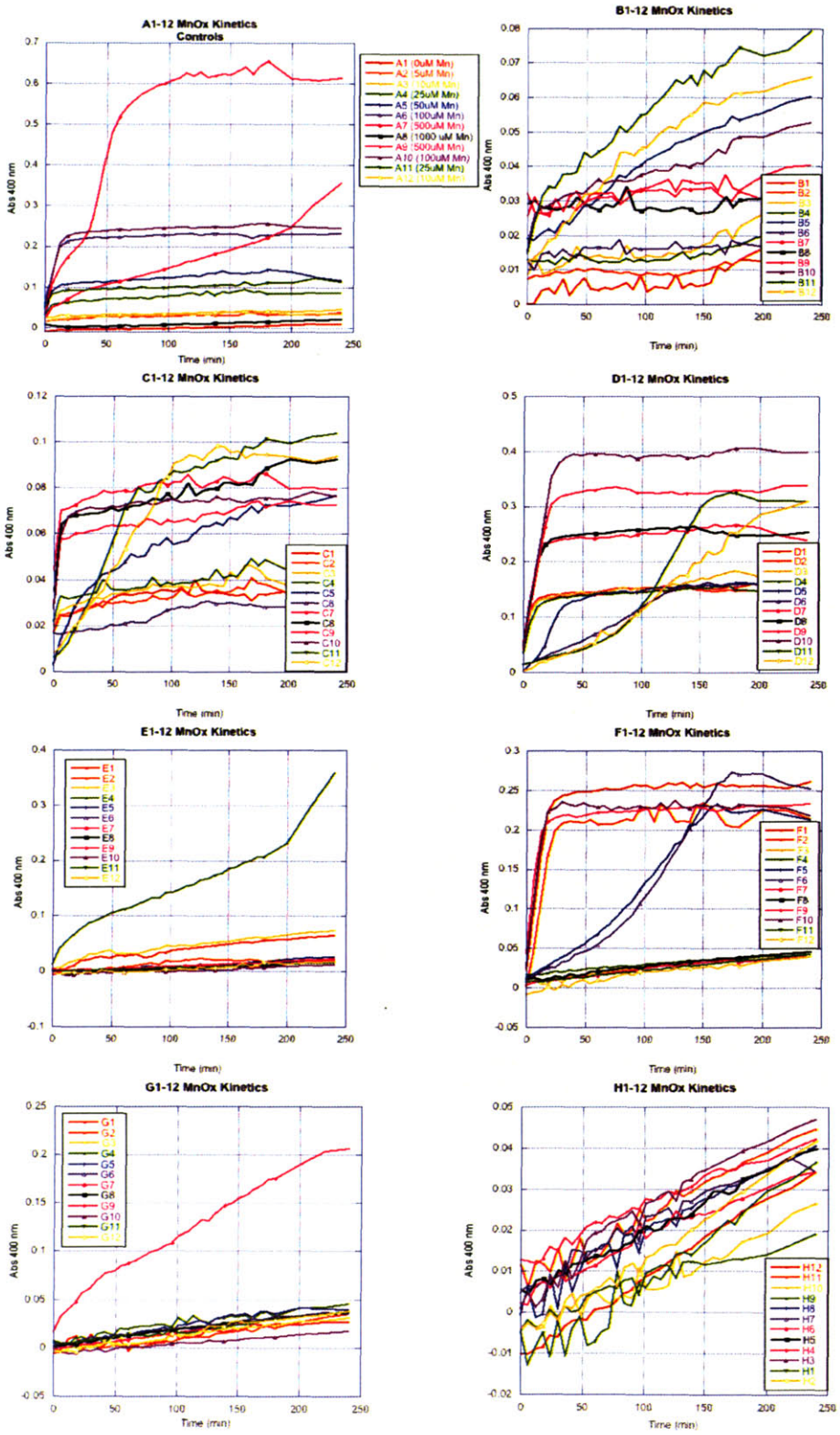

Figure 14.17 Kinetics of BMO formation with varying concentrations of U and Cu according to Table 14.5. Absorbances greater than 0.5 are considered positive for manganese oxidation.

Table 14.5 Mn, U and Cu concentrations for each sample well in Experiment II.

Well	[Mn] (uM)	[U] (uM)	[Cu] (uM)	Well	[Mn] (uM)	[U] (uM)	[Cu] (uM)	Well	[Mn] (uM)	[U] (uM)	[Cu] (uM)
A1	0	0	0	B1	.0	0	0	C1	10	0	0
A2	5	0	0	B2	0	1	0	C2	10	1	0
A3	10	0	0	B3	0	5	0	C3	10	5	0
A4	25	0	0	B4	0	10	0	C4	10	10	0
A5	50	0	0	B5	0	25	0	C5	10	25	0
A6	100	0	0	B6	0	50	0	C6	10	50	0
A7	500	0	0	B7	5	0	0	C7	25	0	0
A8	1000	0	0	B8	5	1	0	C8	25	1	0
A9	500	0	0	B9	5	5	0	C9	25	5	0
A10	100	0	0	B10	5	10	0	C10	25	10	0
A11	225	0	0	B11	5	25	0	C11	25	25	0
A12	10	0	0	B12	5	50	0	C12	25	50	0
D1	50	0	0	E1	500	0	0	F1	100	10	1
D2	50	1	0	E2	500	1	0	F2	100	10	10
D3	50	5	0	E3	500	5	0	F3	100	10	50
D4	50	10	0	E4	500	10	0	F4	100	10	100
D5	50	25	0	E5	500	25	0	F5	100	50	1
D6	50	50	0	E6	500	50	0	F6	100	50	10
D7	100	0	0	E7	1000	0	0	F7	100	50	50
D8	100	1	0	E8	1000	1	0	F8	100	50	100
D9	100	5	0	E9	1000	5	0	F9	100	1	1
D10	100	10	0	E10	1000	10	0	F10	100	1	10
D11	100	25	0	E11	1000	25	0	F11	100	1	50
D12	100	50	0	E12	1000	50	0	F12	100	1	100
G1	500	10	1	H1	1000	10	1				
G2	500	10	10	H2	1000	10	10				
G3	500	10	50	H3	1000	10	50				
G4	500	10	100	H4	1000	10	100				
G5	500	50	1	H5	1000	50	1				
G6	500	50	10	H6	1000	50	10				
G7	500	50	50	H7	1000	50	50				
G8	500	50	100	H8	1000	50	100				
G9	500	1	1	H9	1000	1	1				
G10	500	1	10	H10	1000	1	10				
G11	500	1	50	H11	1000	1	50				
G12	500	1	100	H12	1000	1	100				

14.5.4. Experiment IV

After determining which samples oxidized manganese and which did not, a second experiment was done to further explore the oxidation kinetics under different metal concentrations. Again, 200 μL of sample was used and samples were measured concurrently using a 96 well plate-reading UV/VIS, so no normalization is necessary.

L. discophora is grown in MSVP media 72 hours to an OD_{600}=0.747, with a >30K protein concentration of 4.1 μg/mL. After filling a 96 well plate according to Table 14.6 200 μL of spent media are added to each well, kinetics of BMO formation are measured at 400 nm in 30 second intervals for the first 30 minutes and then 3 minute intervals after that for 6 hours.

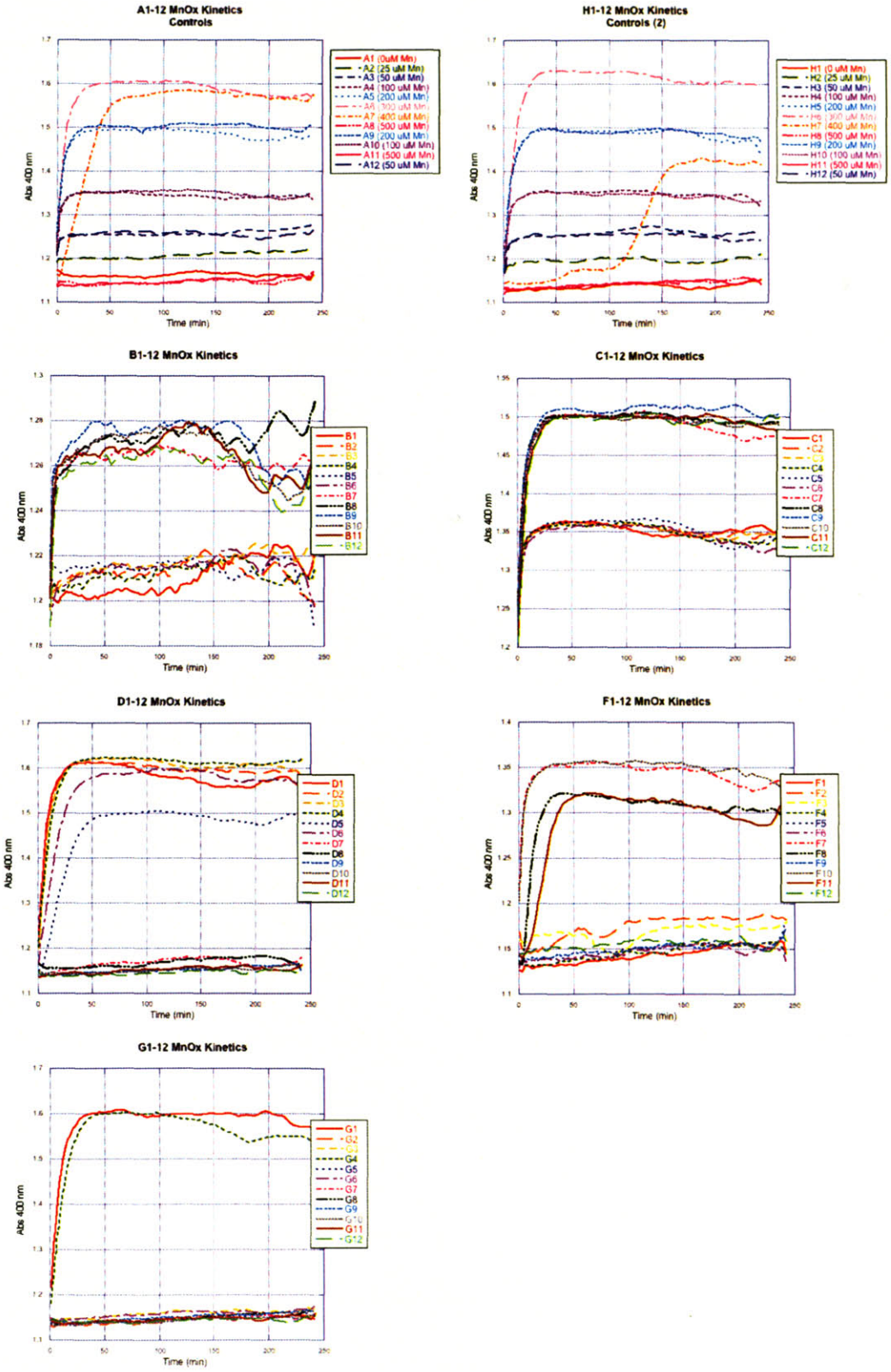

Figure 14.18 Kinetics of BMO formation with varying concentrations of U and Cu according to Table 14.6. Absorbances greater than 0.5 are considered positive for manganese oxidation.

Table 14.6 Mn, U and Cu concentrations for each sample well in Experiment II.

Well	[Mn] (uM)	[U] (uM)	[Cu] (uM)	Well	[Mn] (uM)	[U] (uM)	[Cu] (uM)	Well	[Mn] (uM)	[U] (uM)	[Cu] (uM)
A1	0	0	0	B1	25	0	0	C1	100	0	0
A2	25	0	0	B2	25	1	0	C2	100	1	0
A3	50	0	0	B3	25	5	0	C3	100	5	0
A4	100	0	0	B4	25	10	0	C4	100	10	0
A5	200	0	0	B5	25	25	0	C5	100	25	0
A6	300	0	0	B6	25	50	0	C6	100	50	0
A7	400	0	0	B7	50	0	0	C7	200	0	0
A8	500	0	0	B8	50	1	0	C8	200	1	0
A9	200	0	0	B9	50	5	0	C9	200	5	0
A10	100	0	0	B10	50	10	0	C10	200	10	0
A11	500	0	0	B11	50	25	0	C11	200	25	0
A12	50	0	0	B12	50	50	0	C12	200	50	0
D1	300	0	0	E1	500	0	0	G1	300	10	1
D2	300	1	0	E2	500	1	0	G2	300	10	10
D3	300	5	0	E3	500	5	0	G3	300	10	50
D4	300	10	0	E4	500	10	0	G4	300	50	1
D5	300	25	0	E5	500	25	0	G5	300	50	10
D6	300	50	0	E6	500	50	0	G6	300	50	50
D7	400	0	0	E7	100	10	1	G7	500	10	1
D8	400	1	0	E8	100	10	10	G8	500	10	10
D9	400	5	0	E9	100	10	50	G9	500	10	50
D10	400	10	0	E10	100	50	1	G10	500	50	1
D11	400	25	0	E11	100	50	10	G11	500	50	10
D12	400	50	0	E12	100	50	50	G12	500	50	50
H1	0	0	0								
H2	25	0	0								
H3	50	0	0								
H4	100	0	0								
H5	200	0	0								
H6	300	0	0								
H7	400	0	0								
H8	500	0	0								
H9	200	0	0								
H10	100	0	0								
H11	500	0	0								
H12	50	0	0								

14.6. References

[1] http://atcc.org/common/documents/mediapdfs/1503.pdf
[2] Modified Lowry Protein Assay Kit documentation. (2005) http://www.piercenet.com/files/0389dh4.pdf
[3] http://atcc.org/common/documents/mediapdfs/1917.pdf
[4] **Boogerd, F. C., J. P. M. de Vrind.** (1987) Manganese Oxidation by *Leptothrix discophora*. J. Bacteriol. **169:**489-494.
[5] **Webb, S. M., J. R. Bargar, B. M. Tebo.** (2005) Determination of Uranyl Incorporation into Biogenic Manganese Oxides Using X-ray Absorption Spectroscopy and Scattering. Phys. Scr. **T115:** 949-952.

15. Master Reference List

Papers

Abedoulas, A., W. Lutze, H. E. Nuttal. (1996) Uranium Contamination in the Subsurface: Characterization and Remediation. Uranium: Mineralogy, Geochemistry and the Environment. Mineralogical Society of America, Washington D.C..
Adams, L. F., Ghiorse. (1985) Influence of Manganese on Growth of a Sheathless Strain of *Leptothrix discophora*. Appl. Env. Microbiol. **49:**556-562.
Adams, L. F., W. C. Ghiorse. (1986) Physiology and Ultrastructure of *Leptothrix discophora* SS-1. Arch. Microbiol. **145:**126-135.
Advanced Light Source, http://www-als.lbl.gov/als/quickguide/viewstouse.pdf
Amend, J. P., E. L. Shock. (2001) Energetics of Overall Metabolic Reactions of Thermophillic and Hyperthermophillic Archea and Bacteria. FEMS Microbiol. Rev. **25:**175-243.
Anbar, A. D., J. E. Roe, J. Barling, K. H. Nealson. (2000) Nonbiological Fractionation of Iron Isotopes. Science. **288:**126-128.
Anderson, R. T., D. R. Lovley. (2002) Microbial interactions with Uranium: An Environmental Perspective. Interactions of Microorganisms with Radionuclides. Elsevier Science Ltd.
Anderson, R. T., et al. (2003) Stimulating the *In Situ* Activity of *Geobacter* Species to Remove Uranium from the Groundwater of a Uranium-Contaminated Aquifer. Appl. Environ. Microbiol. **69:** 5884-5891.
Anderson, V. K. (2002) The Effect of Carbonate Concentration on Uranium Oxide Dissolution Kinetics. M.S. Thesis, Massachusetts Institute of Technology.
Banaszak, J. E., B. E. Rittmann, D. T. Reed. (1999) Subsurface interactions of actinide species and microorganisms: Implications for the bioremediation of actinide-organic mixtures. J. Radioanal. Nuc. Chem. **241:**385-435.
Banaszak, J. E., D. T. Reed, B. E. Rittmann. (1999) Reduction and Precipitation of Neptunium(V) by Sulfate-Reducing Bacteria. Migration 1999 Conference Proceedings, Lake Tahoe Nv.
Banfield, J. F, K. H. Nealson eds. (1997) Bacterially Mediated Mineral Formation; Insights into Manganese (II) Oxidation from Molecular Genetic and Biochemical Studies. Geomicrobiology; Interactions Between Microbes and Minerals. Mineralogical Society, Washington, D. C. **36:**225-266.
Barton, L. L., K. Choudhury, B. M. Thomson, K. Steenhoudt, A. R. Groffman. (1996) Bacterial Reduction of Uranium: The First Step of *In Situ* Immobilization of Uranium. Rad. Waste. Manage. Environ. Rest.
Beard, B. L., C. M. Johnson, L. Cox, H. Sun, K. H. Nealson, C. Aguilar. (1999) Iron Isotope Biosignatures. Science. **285:**1889-1892.
Becker, J. S. (2003) Mass Spectrometry of Long-Lived Radionuclides. Spectrochim. Acta Part B. **58:**1757-1784.
Benedict, M., T. H. Pigford, H. W. Levi (1981) Nuclear Chemical Engineering 2nd Ed. McGraw Hill Ltd. NY NY. 8.

Boogerd, F. C., J. P. M. de Vrind. (1987) Manganese Oxidation by *Leptothrix discophora*. J. Bacteriol. **169:**489-494.
Brainard, J. R., B. A. Strietelmeier, P. H. Smith, P. J. Langston-Unkefer, M. E. Barr, R. R. Ryan. (1992) Actinide Binding and Solubilization by Microbial Siderophores. Radiochim. Acta. **58/59**: 357-363.
Brantley, S. L., L. Liermann, T. D. Bullen. (2001) Fractionation of Fe Isotopes by Soil Microbes and Organic Acids. Geology. **29:**535-538.
Brar, S. K. et al. (2006) Bioremediation of Hazardous Wastes – A Review. Pract. Periodical of Haz., Toxic, and Radioactive Waste Mgmt. **10:**59-72.
Brooks, S. C., et al.. (2003) Inhibition of Bacterial U(VI) Reduction by Calcium. Environ. Sci. Technol. **37:**1850-1858.
Brouwers, G. J. et al. (2000) Stimulation of Mn^{2+} Oxiadtion in *Leptothrix discophora* SS-1 by Cu^{2+} and Sequence Analysis of the Region Flanking the Gene Encoding Putative Multicopper Oxidase MofA.
Carder, E. A., A. Galy, J. A. McKenzie, C. Vasconcelos, H. Elderfield. (2005) Magnesium Isotopic Evidence for Widespread Microbial Dolomite Precipitation in the Geological Record. American Geophysical Union Fall Meeting.
Chernorukov, N. G., A. V. Knyazeva, I. V. Sergacheva. (2002) Synthesis, Structure, and Physicochemical Characteristics of Rutherfordite and Tetrasodium Uranyl Tricarbonate. Raciochemistry. **44:**212-215.
Clark, D. L., D. E. Hobart, M. P. Neu. (1995). Actinide Carbonate Complexes and Their Importance in Actinide Environmental Chemistry. Chem. Rev. **95:**25-48.
Cohen, R. (2001) Bacterial Reduction of Uranium and Plutonium. S.M. Thesis. Massachusetts Institute of Technology.
Cook, J.R. (2005) Estimated All Pathways and Inadvertent Intruder Doses
Copeland, A. et al., (2005) Complete sequence of *Desulfovibrio desulfuricans G20*. US DOE Joint Genome Institute. Genbank ID: CP000112.
Corstjens, P. L. A. M. , J. P. M. de Vrind, T. Goosen, E. W. de Vrind- de Jong. (1997) Identification and Analysis of the *Leptothrix discophora* SS-1 mofA Gene, a Gene Putatively Encoding a Manganese Oxidizing Protein with Copper Domains. Geomicribiol. J. **14:**91-108.
Curran, G., Y. Sevestre, W. Rattray. P. Allen, K. R. Czerwinski. (2003) Characterization of Zirconia-Thoria-Urania Ceramics by X-ray and Electron Interactions. *J. Nuc. Mat.* **323:**41-48.
Curran, V. (2003) X-Ray Absorption Spectroscopy of Actinide Speciation in Solid Solutions. PhD Thesis. Massachusetts Institute of Technology.
DiSpirito, A. A., O. H. Tuovinen. (1982) Kinetics of Uranous Ion and Ferrous Iron Oxidation by *Thiobacillus ferrooxidans*. Arch. Microbiol. **133:**33-37.
Ellis, A. M., T. M. Johnson, T. D. Bullen. (2002) Chromium Isotopes and the Fate of Hexavalent Chromium in the Environment. Science. **295:**2060-2062.
Ellis, A. S., T. M. Johnson, M. J. Herbel, T. D. Bullen. (2003) Stable Isotope Fractionation of Selenium by Natural Microbial Consortia. Chem. Geol. **195:**119-129.
Fanghanel, T., V. Neck. (2002) Aquatic Chemistry and Solubility Phenomena of Actinide Oxides/Hydroxides. Pure. Appl. Chem. **74:**1895-1907.

Finneran, K. T., R. T. Anderson, K. P. Nevin, D. R. Lovley. (2002) Potential for Bioremediation of Uranium-Contaminated Aquifers with Microbial U(VI) Reduction. Soil. Sed. Contam. **11:**339-357.
Francis, A. J., (1994) Microbial Transformations of Radioactive Wastes and Environmental Restoration Through Bioremediation. J. Alloys. Compd. **213:** 226-231. from Saltstone Disposal Using Updated Salt Waste Compositions.
Fuller, C. C., J. R. Bargar, J. A. Davis, J. Piana. (2002). Mechanisms of Uranium Interactions with Hydroxyapatite: Implications for Groundwater Remediation. Enviorn. Sci. Tech. **36:**158-165.
Gong, C. (2006) Personal correspondence.
Gram, HC. (1884) Über die isolierte Färbung der Schizomyceten in Schnitt- und Trockenpräparaten. Fortschritte der Medizin **2:**185-89.
Haas, J. R., A. Northup. (2004) Effects of Aqueous Complexation on Reductive Precipitation of Uranium by *Shewanella putrefaciens*. Geochem. Trans. **5:**41-48.
Haas, J. R., T. J. Dichristina, R. Wade Jr.. (2001) Thermodynamics of U(VI) sorption onto *Shewanella putrefaciens*. Chem. Geol. **180:**33-54.
Harris, D. C. (1995) Quantitative Chemical Analysis 4th Ed. W. H. Freeman and Co. NY NY. AP32-AP41.
Hayat, M. A. (2000) Principles and Techniques of Electron Microscopy: Biological Applications. 299, 342-343.
Herbel, M. J., T. M. Johnson, R. S. Oremland, T. D. Bullen. (2000) Fractionation of Selenium Isotopes During Bacterial Respriatory Reduction of Selenium Oxyanions. Geochim. Cosmichim. Acta. **64:**3701-3709.
Hoefs, J. (1997) Stable Isotope Geochemistry. Springer-Verlag, Berlin. 7-8.
Holmes, D. E., K. T. Finneran, R. A. O'Neil, D. R. Lovley. (2002) Enrichment of Members of the Family *Geobacteraceae* Associated with Stimulation of Dissimilatory Metal Reduction in Uranium-Contaminated Aquifer Sediments. Appl. Environ. Microbiol. **68:** 2300-2306.
Honeyman, B. (2005) Understanding of Hanford Tank Wastes. Presentation to the Committee on the Management of Certain Radioactive Waste
Hu, M. Z.-C., J. M. Norman, B. D. Faison, M. E. Reeves. (1996) Biosorption of Uranium by *Pseudomonas aeruginosa* Strain CSU: Characterization and Comparison Studies. Biotech. Bioeng. **51:**237-247.
Ishida, T. (2002) Isotope Effect and Isotope Separation: A Chemist's View. J. Nuc. Sci. Technol. **39:** 407-412.
Jensen, M. L., (1958) Sulfur Isotopes and the Origin of Sandstone-Type Uranium Deposits. Econ. Geol. **53:**598-616.
Johnson, T. M. (2004) A Review of Mass-Dependent Fractionation of Selenium Isotopes and Implications for Other Heavy Stable Isotopes. Chem. Geol. **204:**201-214.
Keith-Roach, M. J., F. R. Livens eds. (2002) Microbial Interactions with Metals/Radionuclides: The Basis of Bioremediation. Interactions of Microorganisms with Radionuclides. Elsevier Science Ltd, Oxford UK. 179-203.
Kelly, S. D. et al.. (2002) X-Ray Absorption Fine Structure Determination of pH-Dependent U-Bacterial Cell Wall Interactions. Geochim. Cosmochim. Acta. **66:**3855-3871.

Kendall, C., J. J. McDonnel eds, (1998) Isotope Tracers in Catchment Hydrology. Elesevier, N.Y.. 60-70.
Kharaka, Y.K. , A.S. Maest eds. (1992). Tracing watershed weathering reactions with $\delta^{13}C$. Water- Rock Interaction, Proceedings of the 7th International Symposium, Park City, Utah, 13-18 July 1993, Balkema, Rotterdam, pp. 569-572.
Kim, J. I., K. R. Czerwinski. (1996) Complexation of Metal Ions with Humic Acid: Metal Ion Charge Neutralization Model. Radiochim. Acta. **73:**5-10.
Konhauser et al. (2002) Could bacteria have formed the Precambrian banded iron formations? *Geology*. **30:**1079-1082.
Kritee, K., B. Klaue, J. D. Blum, T. Barkay. (2004) Mercury Stable Isotope Fractionation During Bacterial Reduction Of Hg(II) to Hg^0. 7th International Conference on Mercury as a Global Pollutant. Ljubljana, Slovenia. (poster). http://aesop.rutgers.edu/~barkay/Goldschmidt05Final.ppt
Kuai, L., A. A. Nair, M. F. Polz. (2001) Rapid and Simple Method for the Most-Probable-Number Estimation of Arsenic-Reducing Bacteria. Appl. Environ. Microbiol. **67:**3168-3173.
Kuai, L., A. A. Nair, M. F. Polz. (2001) Rapid and Simple Method for the Most-Probable-Number Estimation of Arsenic-Reducing Bacteria. Appl. Environ. Microbiol. **67:**3168-3173.
Lajtha, K., R. H. Michener eds. (1994) Tracing the Diets of Fossil Animals Using Stable Isotopes. Stable Isotopes in Ecology and Environmental Science. 63-92.
Lewis, M. (2000) M.S. The Behavior or Uranium in the Environment: Bacterial Reduction of an Aqueous Uranium Species Thesis, Massachusetts Institute of Technology.
Liu, C., Y. A. Gorby, J. M. Zachara, J. K. Fredrickson, C. F. Brown. (2002) Reduction Kinetics of Fe(III), Co(III), U(VI), Cr(VI), and Tc(VII) in Cultures of Dissimilatory Metal-Reducing Bacteria. Biotechnol. Bioeng. **80:**637-649.
Lloyd, J. R., P. Yong, L. E. Macaskie. (2000) Biological Reduction and Removal of Np(V) by Two Microorganisms. Environ. Sci. Technol. **34:**1297-1301.
Lloyd, J. R., V. A. Sole, C. V. G. Van Praagh, D. R. Lovley. (2000) Direct and Fe(II)-Mediated Reduction of Technetium by Fe(III)-Reducing Bacteria. Appl. Environ. Microbiol. **66:**3743-3749.
Lloyd, J. R. et al. (2002) Reduction of Actinides and Fission Products by Fe(III) Reducing Bacteria. Geomicrobiol. J. **19:**103-120.
Londry K. L., D. J. Des Marais. (2003) Stable Carbon Isotope Fractionation by Sulfate-Reducing Bacteria. Appl. Env. Microbiol. **69:**2942.
Lovley, D. R. (1993) Dissimilatory Metal Reduction. Annu. Rev. Microbiol. **47:**263-290.
Lovley, D. R. (1993) Dissimilatory Metal Reduction. Annu. Rev. Microbiol. **47:**263-290.
Lovley, D. R., E. J. P. Phillips, Y. A. Gorby, E. R. Landa. (1991) Microbial Reduction of Uranium. Nature. **350:**413-415.
Lovley, D. R., J. R. Lloyd. (2000) Microbes With a Mettle for Bioremediation. Nat. Biotechnol. **18:** 600-601
Lovley, D. R., P. K. Widman, J. C. Woodward, E. J. Phillips. (1993) Reduction of Uranium by Cytochrome c_3 of *Desulfovibrio vulgaris*. Appl. Environ. Microbiol. **59:**3572-3576.

Lovley, D.R., E. J. P. Phillips, Y. A. Gorby, E. R. Landa. (1991) Microbial Reduction of Uranium. Nature. 350:413-415.
Lowry, O.H., et al. (1951.) Protein Measurement with the Folin Phenol Reagent. J. Biol. Chem. **193**:265-275.
Macaskie, L. E., R. M. Empson, F. Lin, M. R. Tolley. (1995) Enzymatically-Mediated Uranium Accumulation and Uranium Recovery Using; a *Citrobacter* sp. Immobilised as a Biofilm Within a Plug-Flow Reactor. J . Chem. Tech. Biotechnol. **63:**1-16.
Madigan, M. T., J. M. Martinko, J. Parker eds. (2003) Brock Biology of Microorganisms 10^{th} ed. 148.
Madsen, E. L. (1998) Epistemology of Environmental Microbiology. Env Sci Tech. **32:** 429-439.
Matthews, A., X. Zhu, K. O'Nions. (2001) Kinetic Iron Stable Isotope Fractionation Between Iron (-II) and (-III) Complexes in Solution. Earth. Planet. Sci. Lett. **192:**81-92.
McKay, D. S., et al. (1996). Search for Past Life on Mars: Possible Relic Biogenic Activity in Martian Meteorite ALH84001. Science. **273:**924-930.
Miller, C. J., J. R. Del Mastro. (1994) The Use of Selective Extraction Chromatographic Columns as an Alternative to Solvent Extraction for the Separation of Uranium Followed by the Use of Arsenazo III as a Colormetric Reagent for Uranium Determination. INEL http://www.osti.gov/bridge/servlets/purl/10183134-g0un6c/webviewable/10183134.pdf.
Morrison, S. J., P. S. Mushovic, P. L. Neisen. (2006) Early Breakthrough of Molybdenum and Uranium in a Permeable Reactive Barrier. Environ. Sci. Technol. **40:**2018-2024.
Mullen, L., C. Gong, K. Czerwinski. Complexation of Uranium(VI) with the Siderophore Desferrioaxamine B. in press.
Nakashima, S., J. R. Disnar, A. Perruchot. (1999) Precipitation Kinetics of Uranium by Sedimentary Organic Matter Under Diagenetic and Hydrothermal Conditions. Econ. Geol. **94:**993-1006.
Nelson, D.M., and K.A. Orlandini. (1986) Source effects of metal movement in groundwater. Argonne National Laboratory Report ANL 86-15.
Mohaghegi, A., D. M. Updegraff, M. B. Goldhaber. (1985) The Role of Sulfate Reducing Bacteria in the Deposition of Sedimentary Uranium Ores. Geomicrobiol. J. **4:**153-173
Neu, M. P., G. A. Icopini, H. Boukhalifa. (2005) Plutonium Speciation Affected by Environmental Bacteria. Raciochim. Acta. **93:**705-714.
Nevin, K. P., D. R. Lovley. (2000) Potential for Nonenzymatic Reduction of Fe(III) During Microbial Oxidation of Organic Matter Coupled to Fe(III) Reduction. Env. Sci. Technol. **34:**2472-2478.
Newville, M. (2004) Fundamentals of XAFS. Consortium for Advanced Radiation Sources. University of Chicago. Chicago, Il.
Paustian, T. (1999) Microbiology and Baceteriology: The World of Microbes. Section 2-25 The cell wall surrounds and holds in the microbe. http://www.bact.wisc.edu/Microtextbook/index.php?module=Book&func=displayarticle&art_id=60
Peters, K. E., C. C. Walters, J. M. Moldowan. (2005). The Biomarker Guide Second Edition, I. Biomarkers and Isotopes in the Environment and Human History. P.138-139.

Poole, R. K. ed., (1999) Fungal Production of Citric and Oxalic Acid: Importance in Metal Speciation, Physiology and Biogeochemical Processes. Advances in Microbial Physiology. Academic Press, San Diego, Ca. **41:** 47-79.
Power, M.E. (2001) Field Biology, Food Web Models, and Management: Challenges of Context and Scale. Oikos. **94:** 118-129.
Rehkämper, M. et al. (2002) Thallium Isotope Variations in Seawater and Hydrogenetic, Diagenetic, and Hydrothermal Ferromanganese Deposits. Earth. Planet. Sci. Lett. **197**:65-81.
Ribet, I., C. J. Ptacek, D. W. Blowes, J. L. Jambor. (1995) The Potential for Metal Release by Reductive Dissolution of Weathered Mine Tailings. J. Contam. Hydrol. **17:**239-273.
Richter, S., A. Alonso, W. De Bolle, R. Wellum, P.D.P Taylor. (1999) Isotopic "Fingerprints" for Natural Uranium Ore Samples. Int. J. Mass Spec. **193:**9-14.
Riordan, C., M. Bustard, R. Putt, A. P. McHale. (1997) Removal of Uranium from Solution Using Residual Brewery Yeast: Combined Biosorption and Bioprecipitation. Biotechnol. Lett. **19:**385-387.
Ruggerio, C. E., M. P. Neu, J. H. Matonic, S. D. Reilly. (2000) Interactions of Pu with Desferrioaxime Siderophores can Affect Bioavailability and Mobility. Actinide. Res. Q. **2000:**16-18.
Rusin, P. A., et al., (1994) Solubilization of Plutonium Hydrous Oxide by Iron-Reducing Bacteria. Environ. Sci Technol. **28:**1686-1690.
Savvin, S. B. (1964) Analytical Applications of Arsenazo III-II, Determination of Thorium, Uranium, Protactinium, Neptunium, Hafnium, and Scandium. Talanta. **11:**1-6.
Schidlowski, M. (1988) A 3,800-Million-Year Isotopic Record of Life from Carbon in Sedimentary Rocks. Nature. **333:**313-318.
Schön, R., G. Winkler, W. Kutschera. (2004) A Critical Review of Experiment Data for the Half-Lives of the Uranium Isotopes ^{238}U and ^{235}U. Appl. Radiat. Isot. **60:**263-273.
Shanbahg, P.M., G. R. Choppin. (1981) Binding of Uranyl by Humic Acid. J. Inorg. Nucl. Chem. **43:**3369-3372.
Smithers, R. M., H. R. Krouse. (1967) Tellurium Isotope Fractionation Study. Can. J. Chem. **46:**583-591.
Spear, J. L., L. A. Figueroa, B. D. Honeyman. (1999) Modeling the Removal of Uranium U(VI) from Aqueous Solutions in the Presence of Sulfate Reducing Bacteria. Environ. Sci. and Technol. **33:**2667-2675.
Spear, J. L., L. A. Figueroa, B. D. Honeyman. (2000) Modeling Reduction of Uranium Under Variable Sulfate Concentrations by Sulfate Reducing Bacteria. Appl. Environ. Microbiol. **66:**3711-3721.
Szymanski, W. N. (1994) Uranium In Situ Leach Mining in the United States. Uranium Industry Annual 1993. Energy Information Administration. Washington, D.C. ix-xxv. DOE/EIA-0478(93).
Tebo, B. M. et al. (2004) Biogenic Manganese Oxides: Properties and Mechanisms of Formation. Annu. Rev. Earth. Planet. Sci. **32:**287-328.
Tebo, B. M., A. B. Obraztsova. (1998) Sulfate-reducing Bacterium Grows with Cr(VI), U(VI), Mn(IV), and Fe(III) as Electron Acceptors. FEMS Microbiol. Lett. **162:**193-198.

Thomas, R. (2001) Beginner's Guide to ICP-MS Part III: The Plasma Source. Spectroscopy. **16(6):**26-30.
Thomas, R. (2001) Beginner's Guide to ICP-MS Part VI – The Mass Analyzer. Spectroscopy. **16(10):**44-48.
Thomas, R. (2001) Beginner's Guide to ICP-MS Part VII – Mass Separation Devices – Double Focusing Magnetic Sector Technology. Spectroscopy. **16(11):**22-27.
Valley J. W., D. R. Cole, eds. (2001) Reviews in Mineralogy and Geochemistry: Stable Isotope Geochemistry. **43.**
Valley J. W., D. R. Cole, eds. (2001) Equilibrium Oxygen, Hydrogen and Carbon Isotope Fractionation Factors Applicable to Geologic Systems: Reviews in Mineralogy and Geochemistry: Stable Isotope Geochemistry. **43:**3-6.
Valley J. W., D. R. Cole, eds. (2001) Isotopic Evolution of the Biogeochemical Carbon Cycle During the Precambrian. Reviews in Mineralogy and Geochemistry: Stable Isotope Geochemistry. **43:**555.
Valley, J. W., H. P. Taylor, J. R. O'Neil eds. (1986) Theoretical and Experimental Aspects of Isotopic Fractionation. Reviews in Mineralogy: Stable Isotopes in High Temperature Geological Processes. **16:**1-40.
Valls M., S. Atrian, V. De Lorenzo, L. A. Fernandez. (2000) Engineering a Mouse Metallothionen on the Cell Surface of *Ralstonia eutrophia* CH34 for Immobilization of Heavy Metals in Soil. Nat. Biotechnol. **18:**661-665.
Vargas, M., K. Kashefi, E. L. Blunt-Harris, D. R. Lovley. (1998) Microbiological Evidence for Fe(III) Reduction on Early Earth. Nature. **395:**65-67.
Wall, J. D., L. R. Krumholz. (2006) Uranium Reduction. Annu. Rev. Microbiol. **60:**149–166.
Webb, S. M., C. C. Fuller, B. M. Tebo, J. R. Bargar. (2006) Determination of Uranyl Incorporation into Biogenic Manganese Oxides Using X-Ray Absorption Spectroscopy and Scattering. Environ. Sci. Technol. **40:**771-777.
Webb, S. M., J. R. Bargar, B. M. Tebo. (2005) Determination of Uranyl Incorporation into Biogenic Manganese Oxides Using X-ray Absorption Spectroscopy and Scattering. Phys. Scr. **T115:** 949-952.
Wood, S.A. (1996) The Role of Humic Substances in the Transport and Fixation of Metals of Economic Interest (Au, Pt, Pd, U, V). Ore. Geol. Rev. **11:**1-31.
Zeh, P., K.R. Czerwinski, J.I. Kim (1997) Speciation of Uranium in Gorleben Groundwaters. Radiochim. Acta. **76**: 37-44.
Zeiger, M. A., D. J. Glofcheski, J. R Lepock, J. Kruuv. (1991) Factors Influencing Survival of Mamalian Cells Exposed to Hypothermia. V. Effects of Hepes, Free Radicals, and H_2O_2 Under Light and Dark Conditions. Cryobiol. **28:**8-17.
Zhang, J. L. W. Lion, Y. M. Nelson, M. L. Schuler, W. C. Ghiorse. (2002) Kinetics of Mn(II) oxidation by *Leptothrix discophora* SS1. Geochim. Cosmichim. Acta. **66:**773-781.
Zhang, J., P. D. Quay, D. O. Wilbur. (1995). Carbon Isotope Fractionation During Gas-Water Exchange and Dissolution of CO_2. Geochim. Cosmichim. Acta. **59:**107-114.
Zhu, X. K., et al. (2002) Mass Fractionation Processes of Transition Metal Isotopes. Earth. Planet. Sci. Lett. **200:**47-62.

Zigler, J. S., J. L. Lepe-Zunga, B. Vistica, I. Gery. (1985) Analysis of the Cytotoxic Effects of Light-Exposed HEPES-containing Culture Medium. Lab. Vis. Res. **21**:282-287.

Pdf files, documents and programs

2XPYG Media http://atcc.org/common/documents/mediapdfs/1503.pdf

Advanced Light Source, http://www-als.lbl.gov/als/quickguide/viewstouse.pdf

Department of Energy, Richland Office FY04 progress report.
http://www.hanford.gov/rl/uploadfiles/10025_pie.pdf

Modified Lowry Protein Assay Kit documentation. (2005)
http://www.piercenet.com/files/0389dh4.pdf

MSVP Media http://atcc.org/common/documents/mediapdfs/1917.pdf

Pierce Protein Assay Technical Handbook.
http://www.piercenet.com/files/1601325%20ProteinAssay.pdf

Resources on Isotopes: Carbon. http://wwwrcamnl.wr.usgs.gov/isoig/period/c_iig.html
Spectro Analytical Instruments Ciros Vision ICP-AES Brocure.

Selinummi, J., S Hautaniemi. (2004) CellStats. http://www.cs.tut.fi/sgn/csb/cellstats/

Tank Waste Retrieval, Processing and On-site Disposal at Three Department of Energy Sites: Final Report. (2006) http://www.nap.edu/catalog.11618.html. 13-33.

Uranium Location Database Compilation. (2006). EPA Document ID 402-R-05-009.

van der Lee, J., L. De Windt. (2000) JCHESS v. 2.5. CIG-École des Mines de Paris.

Wolery, T. (1992) Eq3/6: A Software Package Designed for Geochemical Modelling of Aqueous Systems: A Package Overview and Installation Guide (Version 7). (UCL-MA-110662 PT I ed.). Lawrence Livermore National Laboratory.

URL's

http://biology.uwsp.edu/faculty/TBarta/dilPlating/DilutionSeries.html
http://cp.chem.agilent.com/cag/other/icp-ms.jpg
http://elchem.kaist.ac.kr/vt/chem-ed/spec/uv-vis/graphics/uv-vis-1.gif
http://en.wikipedia.org/wiki/DAPI
http://en.wikipedia.org/wiki/Image:Microscope_diag.PNG
http://en.wikipedia.org/wiki/Uranium_mining#Open_pit

http://nobelprize.org/educational_games/physics/microscopes/tem/index.html
http://www.agroeco.nl/~wise/439-440/image/leaching.gif
http://www.biologycorner.com/resources/gram_bacteria.jpg
http://www.goldsim.com/images/Yucca2.gif
http://www.nrc.gov/materials/fuel-cycle-fac/ur-milling.html
http://www.world-nuclear.org/info/inf27.htm
http://www.wwnorton.com/college/anthro/bioanth/ch12/O-isotope2.gif

FINIS CORONAT OPUS